The thesis title: Ice and conical structure interactions	Date: 10-6-2010 Number of pages (including Appendix): 257			
	Master Thesis	X	Project Work	
Name: Wenjun Lu				
Teacher / supervisor: Prof. Sveinung Løset				
Other external professional contacts / supervisors: Prof. Jørgen Amdahl				

Abstract:

The pursuit of energy in Arctic waters drives people to design ocean structures applying new concepts. Conical structures which shift the ice failure mode from crushing to bending could reduce the total ice load. Moreover, its symmetric geometry naturally achieves the requirement of ice-vaning and reduces the risk of possible large ice loads induced by the failure of ice-vaning that might be encountered by other shapes of floaters. The thesis is based on the model test results of a group of conical structures in different ice conditions. All the tests were conducted in the Hamburg Ship Model Basin (HSVA) in Germany.

The thesis comprises two parts. In the first part, the ice basin test results of the SEVAN FPU-Ice Buoy were analyzed. Based on the test data, the structure's responses and load transferring characteristics were examined using the computer software Diadem. And the hydrodynamic and hydro-static characteristics were calculated by using Hydro-D. Then this dynamic system was analyzed in the surge direction. Based on the calculation results, explanations concerning the dominant pitch response coinciding with the pitch natural frequency were given in a descriptive way. Furthermore, a low-frequency ice accumulation volume was visually observed. This was thought to be the cause of the dominant low frequency surge displacement. The relationships between different structural responses with different ice load components were also identified. It was pointed out that the surge displacement was mainly influenced by the ice sliding load while pitch displacement was mainly influenced by the ice rotating load. According to the analysis of this system in surge direction, it was further found that the mooring force was mainly to counterbalance the ice sliding load while the ice rotating load was mainly counterbalanced by the inertia force and mooring force.

Furthermore, based on a discussion about level ice-conical structure interaction processes, a numerical model concerning the *level ice and moored structure interaction* was developed using MATLAB in the first part of this thesis. The calculation results were compared with the test data. It is found that this numerical model gives good predictions of the surge and heave displacements. And it was also found that the ice accumulation load (a part of ice sliding load) and ventilation load (a part of ice rotating load) are two major contributors to the total ice load.

In the second part, the analysis was based on the test data of five conical structures designed by AkerSolutions. Both moored and fixed structures with different geometries were tested in different ice conditions (level ice, managed ice, and ice ridges) with different ice speeds (0.1 m/s, 0.5 m/s and 1 m/s

at full-scale). Extensive comparisons of the test results in different ice conditions with different ice speeds are discussed in Part II of my thesis.

In conclusion, the thesis discusses the *ice-conical structure interaction* processes, loading characteristics, and response characteristics, based on which a numerical model was developed. Furthermore the influences of the geometry of the structure, different ice conditions, and different ice speed were also discussed based on experiment data and theoretical analysis.

Stikkord:

1. Ice loads
2. Level ice
3. Moored conical structures
4. Fixed conical structures

_____

(sign.)

NTNU
Faculty of Engineering Science and Technology
Department of Civil and Transport Engineering

Date: feb. 9

MASTER THESIS

TBA4920 Marine Civil Engineering, master thesis

Spring 2010

for

Wenjun Lu

English title

Ice and conical structure interactions

Norwegian title

Is og konisk struktur interaksjoner

BACKGROUND

The large energy reserve in the Arctic area stimulates exploration in this harsh environment to satisfy the energy hunger of the world. Different new concepts of ocean structures have be designed in order to operate in different ice conditions.

Comparing with a vertical structure, the conical structure can largely reduce the ice load by shifting the ice failure mode from crushing to bending failure mode. Moreover, its symmetric shape allows the structure to be totally independent of ice-vaning. This can reduce the risk of large ice load induced by the possibility of not being able to follow the ice drift direction that other unsymmetrical structures may encounter.

The thesis is based on the test data of a group of conical structures. All these tests were conducted in the Hamburg Ship Model Basin (HSVA). These test results include the tested model's response and load histories under different ice conditions (level ice, managed ice, ice ridge).These valuable test data supplied the author with great opportunities to look into the

characteristics of ice and conical structure interactions.

The thesis comprises two parts. Part I is based on the test results of SEVAN FPU-Ice Buoy. This buoy is designed to be working in both open water and icy waters. The focus will be put on the buoy's behaviour in level ice and ice ridges. The level ice and conical structure interaction processes and characteristics will be investigated in this part. Part II of the thesis is based on the test results of a group of conical structures designed by AkerSolutions. These structures are of different geometries, two of which are moored structures while the other three are fixed models. They were tested in different ice conditions with different ice speed (0.1 m/s, 0.5 m/s and 1 m/s at full-scale). Based on the test results, especially the horizontal ice load, extensive comparisons are made so as to identify the influence of different factors during the ice and conical structure interactions.

TASK DESCRIPTION

Description of task

In Part I of the thesis, the SEVAN FPU-Ice Buoy's responses in different tests shall be analyzed. At first, three sets of responses (surge, heave and pitch) in level ice shall be transformed into the frequency domain so as to identify the response characteristics of the structure (dominant vibration period is each direction). Then these responses' normalized correlation coefficients shall be calculated to investigate the relationships of different responses based on which the ice load transferring paths and relationships between the ice load and buoy's responses shall be discussed. Based on the observations and discussions and also previous level ice-ship interaction researches, the level ice and conical structure interaction processes are discussed. The involved ice load components are identified and the calculation method of which are also discussed. Afterwards, the numerical model regarding the "level ice and moored conical structure interaction" is developed so as to verify the previous discussions and also supply a numerical method to predict the moored conical structure's response histories and ice load histories in level ice.

In Part II of the thesis, with all the test data concerning all five different conical structures designed by AkerSolutions, extensive comparisons shall be made. The comparisons are primarily made based on the frequency domain analysis results and statistical information of the horizontal ice load. The influences from different ice conditions, different ice speeds, and different geometries are investigated in this part.

Aims and purpose

The aims of the thesis is to investigate the ice and conical structures' interacting processes,

interacting characteristics which include the relationship between different structural responses, the relationship between different ice load components and the structural responses, the characteristics of the dynamic properties of a moored conical structure in level ice.

Based on the above investigations, a numerical model of *level ice and moored conical structure interaction* should be developed so as to quantify the importance of different factors in the interaction processes and also supply a numerical method to predict the moored conical structure's behaviours in level ice.

Furthermore, based on the comparisons made in Part II of the thesis, the influence of different ice conditions, different ice speeds, and different structural geometries should be identified which will be useful as future design guide.

Subtasks and research questions

1. What is the relationship between the surge, heave and pitch response for a moored structure in level ice?
2. What are the ice load transferring paths when the ice is interacting with the conical structure?
3. What is the relationship between different load components (ice breaking load, ice rotating load and ice sliding load) with different structural responses (surge, heave and pitch)
4. What is the influence of ice ridges with different characteristics (boundary conditions, mean cross-sectional area, and ice management behind the ridge)?
5. What is the interaction processes and involved ice load components when level ice interacting with conical structures?
6. How to calculate different load components?
7. For moored structure, when taking into consideration of the structural responses' influence on the intact ice, how the structural responses, ice load and ice breaking characteristics will be like?
8. Quantitatively, how much influence of ice drift speed, different ice conditions and structure's geometries could have on the ice load?
9. What are the possible stories behind the peak ice load?

GENERAL ABOUT CONTENT, WORK AND PRESENTATION

The task description for the master thesis is meant as a framework for the work of the candidate. Adjustments might be done as the work progresses. Tentative changes must be

done in cooperation and agreement with the supervisor and professor in charge at the Department. (Also including external cooperative partners where this is applicable).
In the evaluation thoroughness in the work will be emphasized, as will be documentation of independence in assessments and conclusions. Furthermore the presentation (report) should be well organized and edited; providing clear, precise and orderly descriptions without being unnecessary voluminous.

The report shall include: (templates are found on http://www.ntnu.no/bat/skjemabank)

- Standard report front page.
- Title page with abstract and keywords (signed by the student).
- Summary and acknowledgement. Table of content including list of figures, tables and enclosures. If useful and applicable a list of important terms and abbreviations should be included.
- The main text.
- Clear and complete references to material used, both in text and figures/tables. This also applies for personal and/or oral communication and information.
- Text of the Thesis (these pages) signed by the professor in charge.
- The report must have a complete page numbering.
- The thesis may possibly be written as a scientific article. The report must come with report front and title pages and, if necessary, with appendices that document the work performed in the process of writing of the article.

Submission procedure

- The complete, original report (un-bounded).
- Two copies (bounded).
- If applicable: X additional copies if agreed upon for instance with external partner (to be paid for by the Department or the external partner)
- CD with the complete report (pdf-format) and all assisting or underlying material.
- A brief (one to two A4 pages including possible illustrations) popular science summary of the work, aiming at publication on the Department's web-site. Include a copy of this html document on the CD. Template is found on: http://www.ntnu.no/bat/skjemabank

The summary shall include the objectives of the work, explain how the work has been conducted, present the main results achieved and give the main conclusions of the work.
Advice and guidelines for writing of the report is given in: "Writing Reports" by Øivind Arntsen. Additional information on report writing is found in "Råd og retningslinjer for rapportskriving ved prosjekt og masteroppgave ved Institutt for bygg, anlegg og transport" (In Norwegian). Both are posted on http://www.ntnu.no/bat/skjemabank

Documentation collected during the work, with support from the Department, shall be handed in to the Department together with the report.

According to the current laws and regulations at NTNU, the report is the property of NTNU. The report and associated results can only be used following approval from NTNU (and external cooperation partner if applicable). The Department has the right to make use of the results from the work as if conducted by a Department employee, as long as other arrangements are not agreed upon beforehand.

Tentative agreement on external supervision, work outside NTNU, economic support etc
Separate description to be developed, if and when applicable.

Health, safety and environment (HSE)
The health, safety and environmental (HSE) work at NTNU shall constitute continuous and systematic efforts that are integrated into the primary activities. NTNU emphasizes the safety for the individual employee and student. The individual safety shall be in the forefront and no one shall take unnecessary chances in carrying out the work. Information in English on HSE is given on: http://www.ntnu.no/hse. In particular, if the student is to participate in field work, visits, field courses, excursions etc. during the Master Thesis work, he/she shall make himself/herself familiar with the ***Fieldwork HSE Guidelines*** http://www.ntnu.no/hms/retningslinjer/HMSR07E.doc. General HSE provisions that apply in all laboratories and workshops are given on: http://www.ntnu.no/hse/labhandbook.

The students do not have a full insurance coverage as a student at NTNU. If a student wants the same insurance coverage as the employees at the university, he/she must establish an individual travel and personal injury insurance. More information about students and insurance is found on the faculty HSE page on: http://www.ntnu.no/ivt/adm/hms/. (Documents are in Norwegian only, ask the supervisor to explain).

Start and submission deadlines

The work on the Master Thesis starts on **February 8th, 2010**

The thesis report original (not bounded) and 2 bounded copies and the CD as described above shall be submitted at the latest on **July 5th, 2010 at 1500 hrs**.

Professor in charge: Sveinung Løset

Other supervisors: Sveinung Løset

Department of Civil and Transport Engineering, NTNU

Date: Feb.9th, 2010

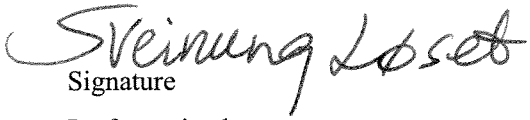

Signature

Professor in charge

Preface and acknowledgments

Born in a subtropical area, I first saw *ice* when I was about 3 years old. I was fascinated by this cold, transparent and fragile “glass”. Now, it is becoming one of the most important things in my life. It is where my career is.

I would like to express my sincere thanks to the Erasmus Mundus programme of European Union without whose financial support I won’t have such a wonderful encounter with the *ice world.*

Then I would like to give my best gratitude to Professor Sveinung Løset who has given me so many precious opportunities. In the winter holiday of 2009, I was given the chance to program the *ice action calculations* based on ISO/DIS (2009). This program was extensively used in Part II of the thesis. In the summer holiday of 2009, he again gave me a summer job in which, I had my first contact with “*ice and moored conical structure interactions*”. This summer job largely increased my understanding about the interaction between ice and conical structures. In February of 2010, with all these valuable data supplied by Professor Løset, I started my working on this thesis. During the whole process, his guidance was of great help. Besides the knowledge I have learned from him, I was also deeply influenced by his enormous encouragements, his precision, and his kindness.

Then my thank goes to Mr. Raed Lubbad and Mr. Oddgeir Dalane. They also offered me huge help on my way to the *ice world*. Based on Raed’s *ice action calculation* script, I effectively learned how to make my own script. Raed also gave me lots of suggestions concerning the level ice-ship interactions. Most of the work in Part II of this thesis is based on Mr. Dalane’s previous analysis. He also helped me a lot in the frequency domain analysis of the time signals.

Finally, I would like to thank my parents far in China. I miss you!

May 31, 2010
Trondheim, Norway
Wenjun Lu

Thesis summary

The thesis is primarily focused on the ice and conical structure interactions based on the test data of a group of conical structures in various ice conditions conducted in the Hamburg Ship Model Basin (HSVA).

In the first part of the thesis, the investigations are based on the test results of SEVAN-FPU-Ice Buoy. The test results include the buoy's responses and mooring force histories in different directions. In the beginning of Part I, some introductions regarding the test set-up and the geometries of the structure were given. Then the analysis starts based on the test data supplied by HSVA.

At first, the structural responses (surge, heave and pitch) were analyzed in the frequency domain by calculating the Power Spectrum Density (PSD) of each response's time record. Based on this, the characteristics of the structural responses in different directions were explored together with the dynamic properties of the structure (Natural frequencies in each direction). It is found that there is a dominant low frequency component in the surge response. The cause of this was suggested to be the slow varying ice accumulation load and it was confirmed in one of the test by checking the test video. It was also found that the dominant pitch responses are always around its natural frequency. Possible reasons to explain this phenomenon was also given in the thesis. For heave, it seems to be influenced by both the surge and pitch responses. The PSD of heave is spreading in a wide range of the frequency domain and it is not as concentrated as the surge and heave responses.

Then the influences from the ridges on the responses of the structure were studied. The SEVAN FPU-Ice Buoy was tested under different types of ridges. The investigations were primarily based on the maximum surge displacement appeared during the ridge and structure interactions. It is found that the ice management behind the ridge, ridges with unbounded boundary conditions and ridges with smaller mean cross-sectional area are all able to reduce the surge displacement. One common place of all these situations (ice management behind the ridge; unbounded ridges; and smaller mean cross-sectional area) is that they reduce the amount of ice rubbles that are required to be mobilized during the ridge and structure interactions.

Afterwards, the normalized correlation coefficients of different responses in different ice conditions were calculated so as to find some similarities between different responses. Based on this the ice load transferring paths were discussed. It was found that the surge response is mainly influenced by the ice sliding load (mainly ice accumulation load), the pitch response is mainly influenced by the ice rotating load (mainly ventilation load), and the heave response is influenced by both of them. A simple example was used to verify this founding.

In the next, the SEVAN FPU-Ice Buoy's governing dynamic equation in surge direction was written based on all the hydrodynamic and hydrostatic coefficients calculated using Hydro-D. The ice load history was back calculated according to this governing dynamic equation and each term in the equation was further explored so as to identify the role of the inertia force during the interaction process and also the relationship between different ice load component inputs and the counteracting force from the structure. It is found that the inertia force behaves like a double-edged blade due to its continuous direction changes. Sometime it is helping to break the ice thus reducing the mooring force, while some other time it goes in the same direction as the ice drift hence leading to a much larger mooring force than the ice load. It was also found that the ice sliding load is mainly counterbalanced by the mooring force; and the ice breaking and ice rotating load are mainly counterbalanced by the inertia force and mooring force.

Based on the previous investigations and discussions, and also an introduction about level ice and ship interactions, it becomes possible to define the ice and conical interaction processes and the involved load components together with their calculation methods. Based on all this, a numerical model was developed and coded in MATLAB so as to verify all the assumptions and methods that have been used by comparing the calculation results with the measured data. This also supplies a possibility to predict the response of the moored conical structure in level ice by numerical simulations.

In Part II of the thesis, five conical structures designed by AkerSolutions were tested in different ice conditions with different ice speeds. Three of them are fixed models and the other two are moored models. In the beginning of Part II, some introductions about the test programme and the geometries of all the tested structures were given. Then based on all the recorded data, especially the horizontal ice load, extensive comparisons were made among different ice speeds, different ice conditions, and different structures.

It was found that the ice load's speed dependency is not consistent for all the structures. Usually the ventilation load is not sensitive to the ice speed. For structures with good ice

clearing ability regardless of ice speed changes, the average ice load is increasing with ice speed. However, for other structures, it was found that the ice accumulation load decrease with increasing ice speed, meaning that as the ice speed increases, their ice clearing ability improves. Under such circumstances, the average ice load does not have an obvious ice speed dependency since they have a decreased ice accumulation load with increased ice speed to offset other load components that are increasing with ice speed.

However, the ice speed has influences on the dominant ice load frequencies and the estimated ice breaking length. As the ice speed increases, the dominant ice load frequencies also increase while the estimated ice breaking length decreases.

Regarding the managed ice, the average ice load could be largely reduced in managed ice than in level ice (only half of the ice load as in level ice conditions). This has been explained as the consequences of the largely reduced two major contributors (ventilation load and ice accumulation load) to the total ice load. The ice load (both amplitude and frequency)'s speed dependency was similar as mentioned above for level ice conditions.

Concerning the ice ridges, in this test campaign, a fixed model was tested in a multi-year ice ridge which was constructed by a layering technique. It was found that the maximum ridge load encountered by the fixed model in a multi-year ice ridge was mainly attribute to the ice breaking and ice rotating load. Although a large ice accumulation volume was observed in the test video, it seems they are not a major contributor to the maximum ice load. For moored models, they were tested in two different first-year ice ridges with different keel width. Again it was found that ridges with larger mean cross-sectional area lead to larger ice load.

In terms of the geometry influences on the ice load, it was found that the waterline diameter and the "neck" size of the structure have strong effects on the ice clearing ability which will in turn have influences on the ice load.

Moreover, the theoretical ice loads on these conical structures in both level ice and ice ridge were calculated based on ISO/FDIS (2009) and compared with the measured maximum values. It was found that the code tends to give relatively lower values than the measured ones. In the end, most of these measured peak values were further studied based on the video. The stories behind these peak loads were given in Appendix A of Part II.

Based on all the observations, calculations, discussions, and conclusions, our understanding towards ice and conical structure interactions have been improved. However, it also brought

lots of problems in different aspects of this topic that worth continuing exploration!

Table of content

List of abbreviations

COG	Centre of Gravitation
DOF	Degree of freedom
FFT	Fast Fourier Transform
FPU	Floating Production Unit
HSVA	Hamburg Ship Model Basin
JIP	Joint Industry Project
NTNU	Norwegian University of Science and Technology
ODE	Ordinary Differential Equation
PDE	Partial Differential Equation
PSD	Power Spectrum Density
2D	Two dimensional
3D	Three dimentional

List of frequently used symbols

Roman symbols	Meanings
A_{cusp}	The area of the broken ice cusp
A_{slope}	The area of the conical hull
$A_{vertical}$	The area of the vertical part (neck) of the hull
C_d	Drag coefficient
D	Cusp depth
E	Young's module of ice
$F_{mooring}$	The mooring force in the horizontal direction
F_{tot}	The total ice resistance
F_c	The ice resistance from crushing;
F_b	Ice resistance from bending
F_s	Ice resistance from submergence of the broken ice pieces
F_{drag_Normal}	Viscous drag force normal to the contact surface of the structure
$F_{inertia,hrizontal}$	Horizontal inertia load
f	Friction force
g	Gravitational acceleration
H	Horizontal force
h	Thickness of the level ice
I	Moment of inertia of the ice beam's cross section
K_{surge}	Hydrostatic stiffness in surge direction
K_{heave}^{up}	Hydrostatic stiffness in heave direction
r	The radius of the waterline area
L	The length of 'ice beam' in the calculation;
L_{break}	Ice breaking length in the bow region
Δl	Length step (element length) during the calculation using FEM
M	Moment within the ice beam
N	Total number of a signal series

N_N	Normal force on conical hull;
N_H	Normal force induced horizontal force;
N_V	Normal force induced vertical force;
N_A	The axial force of the ice beam [N];
P	Pressure;
r_w	The radius of the waterline area
T_{surge}	Natural period in surge direction
T_{heave}	Natural period in heave direction
T_{pitch}	Natural period in pitch direction
t	Time
Δt	Time step during the calculation of the ODE
w	Cusp width
w_b	Width of the ice beam
V	Vertical force
V_{ice_volume}	Ice accumulation volume
v_h	The relative velocity between level ice and moored structure
Δv	Relative velocity change between the moored conical structure and level ice
y	The vertical displacement of the beam;

Greek symbols	**Meanings**
α	Angle of the rotating ice with water plane [^{o}];
α_{water_in}	the angle when water starting to flush into the ventilated area;
β	Parameter to describe the velocity change effect on ice accumulation volume [-];
ε_{water_in}	A reduction number between *(0,1]*
$\varepsilon_{water\ flush\ speed}$	A parameter to describe the water flush-in speed
η	Displacement in surge direction
$\dot{\eta}$	Velocity in surge direction
$\ddot{\eta}$	Acceleration in surge direction
θ	The angle of the conical hull

μ	The friction coefficient
ξ	Damping ratio
ρ_{xy}	The normalized cross correlation coefficient
ρ_{ice}	The density of ice;
ρ_w	The density of sea water;
σ	Standard deviation
σ_f	Flexural strength of ice;
ω_d	Damped natural frequency of the structure
ω_N	Natural frequency of the structure

Matrix and vectors	**Meanings**
A	Added mass of the structure
B	Added damping
C	Hydrostatic stiffness of the structure
K	Stiffness of the structure
M	Mass of the structure/moment
$\mathbf{N_s}$	shape function in FEM
v	Nodal displacements of the beam
V	Nodal velocity of the beam
ω	Test function in Galerkin's method

Superscripts	**Meanings**
$(\dot{})$	Deviation with time;
$(\acute{})$	Deviation with space;
$(\bar{})$	Averaging

Subscripts	**Meanings**
max	maximum

Part I

LEVEL ICE AND MOORED CONICAL STRUCTURE INTERACTION BASED ON SEVAN FPU-ICE BUOY

Table of content for Part I

List of figures for Part I

List of tables for Part I

1 Introduction

The large energy reserve in the arctic region stimulates exploration in this harsh environment to satisfy the energy hunger of the world. A relatively few arctic-offshore structures have been constructed and operated in these ice conditions. For example, in the shallow water (less than 20 m) of the Canadian Beaufort Sea, man-made islands have been successfully used for exploration (Federking and Schwarz, 1982). As the exploration intrudes deeper water, floating structure would be more applicable and structure with sloping face could effectively reduce the ice load by shifting the ice failure mode from crushing to flexural failure. For example, a cable moored platform of sloping face in the waterline, 'Kulluk' operated with success in the Beaufort Sea (Nixon and Ettema, 1987).

Nowadays, the SEVAN FPU-Ice[1] Buoy was proposed as a new concept that operates both in open water and ice conditions with different drafts. This moored conical structure could reduce the ice load by bending the incoming ice; and its symmetric shape could also naturally satisfy the ice-vaning requirement. The model of SEVAN FPU-Ice was tested in the spring 2008 in the large ice tank at the Hamburg Ship Model Basin (HSVA). In Chapter 2, some introduction about the geometries of the structure and the test set up will be given.

The measured data concerning the buoy's responses (displacement, velocity, and acceleration in all six degrees of freedoms-6DOFs) in different ice conditions are available. The mooring forces in all 3 directions are also recorded. Based on the recorded data, the structural responses will be first analyzed in the frequency domain and then the correlation of different responses will be calculated. According to the calculation results, some structural responses' characteristics will be discussed in Chapter 3. The discussion also covers the relationship between different responses and ice load transferring processes.

In Chapter 4, the structure was considered as a dynamic system. The ice load is the input to this system and responses are the outputs. The hydrodynamic and hydrostatic characteristics of the SEVAN FPU-Ice Buoy were calculated in this chapter so as to construct the governing dynamic equation. Then each term of the governing equation in surge direction was studied in both time domain and frequency domain so as to identify some characteristics of this dynamic

[1] FPU represents Floating, Production Unit; and "ice" means this structure is able to operate in ice conditions.

system.

Different from a fixed structure, the ice load will be further complicated by the response (surge, heave, pitch etc) of the floating structure. The structural responses will pose different initial and boundary conditions to the next round of ice-structure interaction. Due to the limited data and observations, few numerical models are available in this respect. Accordingly, a numerical model concerning the interaction between the moored structure and level ice would be of interests. Based on the available data, and discussion in terms of level ice-ship interactions, Chapter 5 of this master thesis will engage in constructing such a numerical model taking into consideration the major processes during the level ice and moored conical structure interactions. The calculation results will be compared with the test results so as to verify some preliminary assumptions regarding different load components' contributions to the total structural responses.

2 Experiment Set-up

Before presenting the analysis, the experiment set-up of the SEVAN FPU-Ice in various ice conditions will first be briefly introduced. The tests are scaled according to Froude law with a scale ratio of 1:40 ($\lambda = 40$). The scaling relations are listed in Table 2.1

Table 2.1 Scale factors

Parameters	Scaling factor
Length	λ
Time	$\lambda^{0.5}$
Speed	$\lambda^{0.5}$
Acceleration	1
Force	λ^3
Moment	λ^4
Mass	λ^3
Angle	1
Angular velocity	$\lambda^{-0.5}$
Flexural strength	λ
Crushing strength	λ
Modules of Elasticity	λ
Coefficient of friction	1

All the numbers presented in the following will be in full-scale.

2.1 Main dimensions of SEVAN FPU-Ice

The geometries of the SEVAN FPU-Ice are shown in the following figure and table.

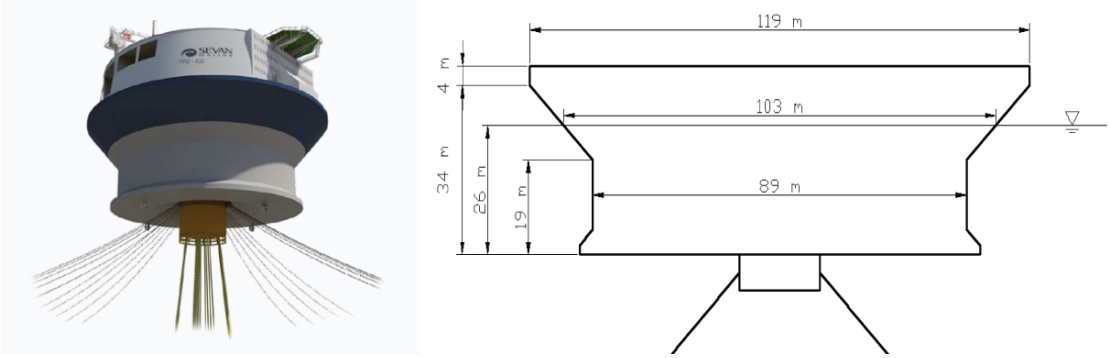

Figure 2.1 Main geometries of SEVAN FPU-Ice (Løset and Aarsnes, 2009)

The SEVAN FPU-Ice Buoy is intending to operate in both open water and ice conditions with two different ice drafts. The main characteristics are shown in the following table.

Table 2.2 Main characteristics of the structure (Løset and Aarsnes, 2009)

Parameter	Dimensions
Open Water Draft	
Draft	15.0 m
Displacement	91940 mT
Freeboard to main deck	15.0 m
Freeboard to process deck	19.0 m
VCG	31.8 m
GM0 (dry)	6.8 m
GM (incl. free Surf. Corr.)	5.7 m
Ice Condition Draft	
Draft	26.0 m
Displacement	172700 mT
Freeboard to main deck	4.0 m
Freeboard to process deck	8.0 m
VCG	21.7 m
GM0 (dry)	25.8 m
GM (incl. free Surf. Corr.)	25.3 m

The model was tested in both open water (Trondheim) and in various ice conditions (HSVA). This thesis will only focus on the test results in various ice conditions which will be introduced in the following sections.

2.2 Test programmes

The structure was towed through four ice sheets with prescribed speed simulating the ice drift speed in different ice conditions. There are four major test series with different ridge conditions. The ice conditions and test details in each series are shown in the following figures and tables.

The recorded results are fitted to the coordinate system as shown in Figure 2.2. The *X* axis is in the water level. The positive directions are shown in the figure. Although only a 2 dimensional figure is shown here, it can be easily generalized to a 3 dimensional coordinate system for 6 DOFs (surge, heave, pitch; sway, roll, yaw) according to right hand law.

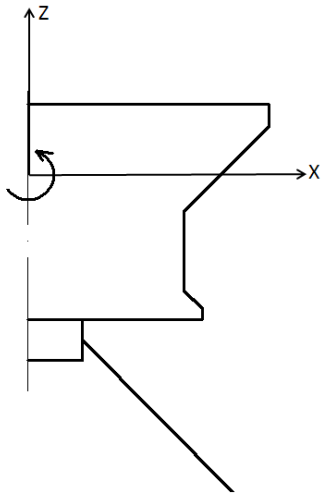

Figure 2.2 Coordinate system of the test results

In the above coordinate system, x represents the direction of surge, z represents the direction of heave, and the rotating arrow represents the direction of pitch.

2.2.1 Test conditions for Test #1000 series

The structure was towed through level ice with an imbedded *severe ridge*. The ice ridge is partly consolidated. The main characteristics of the test conditions are shown in the following table.

Table 2.3 Ice conditions for Test #1000 series

#1000 series – Level ice, severe ridge	
Ice drift speed:	0.5 m/s
Level ice thickness:	1.96 m
Average ice strength:	540 / 1240 kPa
Max ridge keel depth + sail height:	17.8 m + 3.8 m
Ridge consolidation:	~ 2.5 – 3 m
Ridge cross-sectional area	863 m2
Structure trim	3o forward
1110 – Breaking level ice	
1120 – Penetrating ice ridge	
1130 – Breaking level ice – Ice transport observation	

The arrangement of the level ice together with the ridge is shown in the following figure:

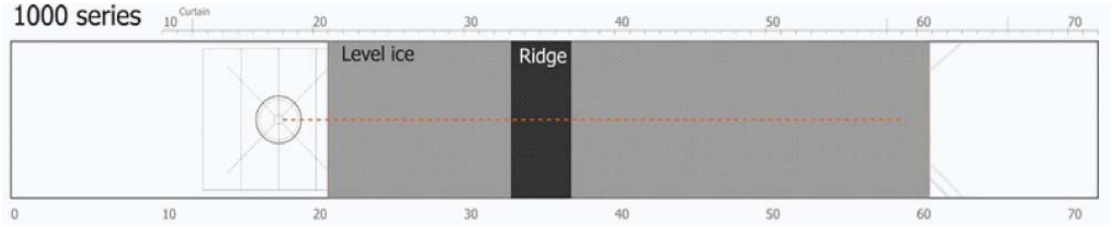

Figure 2.3 Schematic view of the Test #1000 in level ice and ice ridge

2.2.2 Test conditions for Test #2000 series

In Test #2000, the structure was towed through the level ice with the presence of an *extreme design ridge*. The main characteristics of the level ice and ridge are shown in the following table. It can be seen that the cross-sectional area of the extreme design ridge (1267 m^2), compare with the severe design ridge in Test #1000 (863 m^2) is much larger.

Besides, the structure was further towed through the broken ice field as shown in the following figure. However, the test results in managed ice will not be fully covered in Part I of this thesis. There will be more discussions about managed ice in Part II of this thesis.

Table 2.4 Ice conditions for Test #2000 series

#2000 series – Level ice, extreme design ridge	
Ice drift speed:	0.5/1 m/s
Level ice thickness:	1.92 m
Average ice strength:	720 kPa
Max ridge keel depth + sail height:	22.8 m + 4.8 m
Ridge consolidation:	~ 2-3 m
Ridge cross-sectional area	1267 m2
Structure trim	3o forward
Rubble field thickness	10 m
2110 – Breaking level ice	
2120 – Breaking ice ridge, full confined (infinite length)	
2130 – Breaking level ice – Ice transport observation	
2200 _ Advancing rubble field / tight ice	

The following two figures shows the test arrangement of level ice, ice ridge and managed ice in Test #2000.

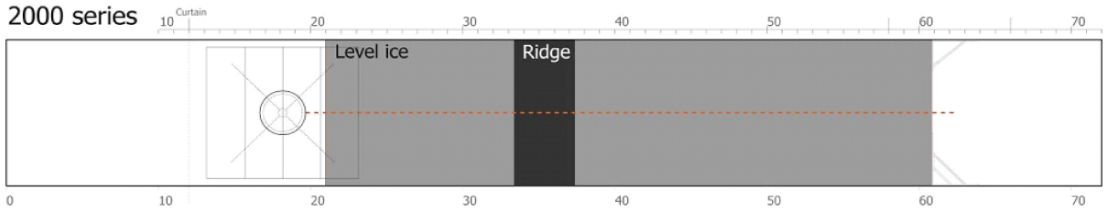

Figure 2.4 Schematic view of the Test #2000 in level ice and ice ridge

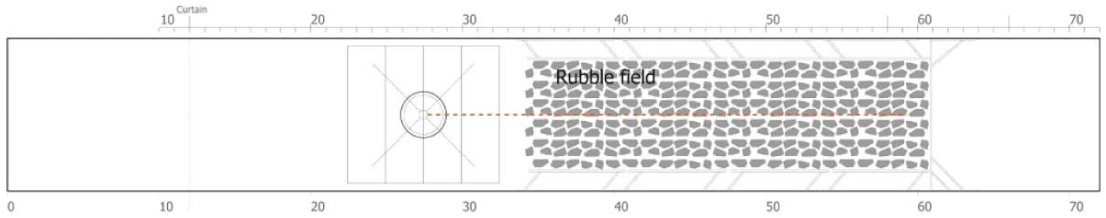

Figure 2.5 Schematic view of the Test #2000 in managed ice

2.2.3 Test conditions for Test #3000 series

Different from the previous two test programmes, in Test #3000, the successive ice ridges were set up in the test. As can be seen from the following figure, the first ridge is of finite length (unconfined) while the second one is in a confined situation simulating an infinitely long ice ridge. The detailed parameters for the level ice and two different ice ridges are shown in the following table.

Table 2.5 Ice conditions for Test #3000 series

#3000 series – Level ice, extreme design ridge		
Ice drift speed:	0.5 m/s	
Level ice thickness:	1.84 m	
Average ice strength:	580/1600 kPa	
	Ridge 1	Ridge 2
Max ridge keel depth + sail height:	22.8 m + 4.8 m	21.2 m + 4.8 m
Ridge consolidation:	~ 2-3 m	~ 2-3 m
Ridge cross-sectional area	1138 m2	1249 m2
Structure trim	3o forward	3o forward
Ridge length	320 m	Confined (infinite)
3110 – Breaking level ice		
3120 – Breaking ice ridge 1, non-confined (length: 320 m)		
3130 – Breaking level ice		
3140 _ Breaking ice ridge 2, confined		

The arrangement of the level ice and ice ridge are shown in the following figure.

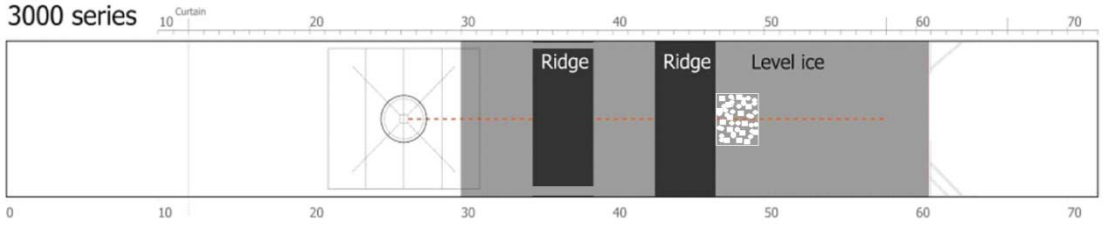

Figure 2.6 Schematic view of the Test #3000 in level ice and ice ridge[2]

[2] The location number in this figure may not be correct. It is mainly to show the general arrangement of the level ice, different ice ridges and the managed ice. So it is put here without further investigation about the specific location.

2.2.4 Test conditions for Test #4000 series

In Test #4000, two unbounded successive ice ridges were imbedded in level ice. The structure was towed through the ice sheet as shown in the following figure. The parameters of the level ice and ridges are shown in the following table.

Table 2.6 Ice conditions for Test #4000 series

#4000 series – Level ice, extreme design ridge		
Ice drift speed:	0.5 m/s	
Level ice thickness:	1.84 m	
Average ice strength:	850 kPa	
	Ridge 1	Ridge 2
Max ridge keel depth + sail height:	18.8 m + 6.8 m	20.8 m + 4.8 m
Ridge consolidation:	~ 2-3 m	~ 2-3 m
Ridge cross-sectional area	1270 m2	1103 m2
Structure trim	3o forward	3o forward
Ridge length	320 m	320 m
4110 – Breaking level ice		
4120 – Breaking ice ridge 1, non-confined (length: 320 m)		
4130 – Breaking level ice		
4140 _ Breaking ice ridge 2, non-confined (length: 320 m)		
4200 _ Advancing rubble field/tight ice		

The general arrangements of level ice and ice ridges are shown in the following figure. Similary as for Test #3000, the precise location of the ridges in the figure may not be correct. However, in the current situation, a general arrangement of the level ice and different ice ridges are illustrative.

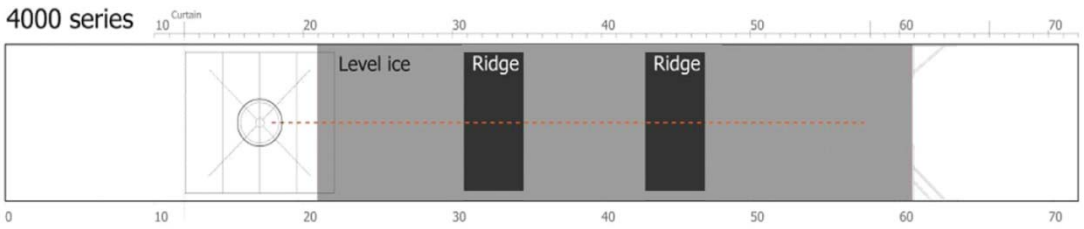

Figure 2.7 Schematic view of the Test #4000 in level ice and ice ridge

The structure was also tested in managed ice as shown in the following figure.

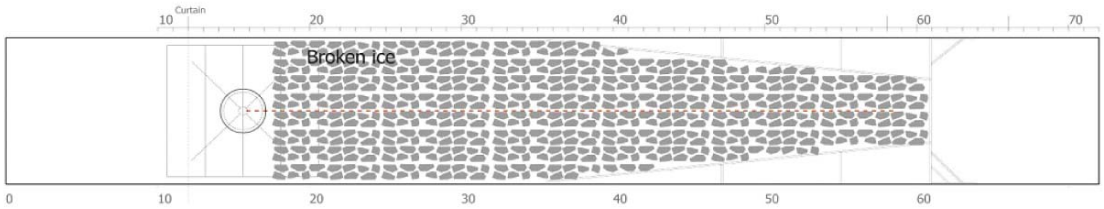

Figure 2.8 Schematic view of the test 42000 in managed ice

2.2.5 Discussions about the test programmes and the thesis work

As we can see from the previous test program's introductions, the SEVAN FPU-Ice model was tested in different ice conditions. Lots of useful information regarding the structure's performances in different ice conditions could be obtained from the test results.

However, in Part I of this thesis, the attention mainly focus on the *level ice and moored conical structure interactions*. Based on the test data in level ice, the structure's responses, ice load transferring processes, and characteristics of different ice load components will be addressed. According to all these discussions, a numerical model of *level ice and moored conical structure interactions* is developed.

The comparisons of different ice ridge actions are discussed briefly according to the structure's surge responses.

Other valuable test data, such as the structure's response, mooring load histories in ice ridge and managed ice still need further investigation.

3 Ice and moored conical structure interactions based on experimental data

3.1 Introduction

SEVAN FPU-Ice, with two different drafts, is capable of operating in both ice free and ice infested environments (Løset and Aarsnes,2009). The structure has a downward facing conical hull that ensures the ice to break in the bending failure mode which effectively reduces the ice load compared with ice breaking in the crushing failure mode. Furthermore, this structure is completely independent of ice-vaning. This will reduce the risk of not being able to follow the ice drift direction which will lead to large ice loads that other unsymmetrical structures may encounter in the ice infested waters.

Model tests of this structure have been conducted in HSVA in 2008. The available data include the moored structure's responses and mooring forces in various ice conditions. In these tests, ice breaking patterns and breaking properties are documented; maximum structural responses and mooring loads in different ice condition have been identified.

However, in this master thesis, a more general interest is focused on the level ice and moored conical structure interactions. These test videos and data supplied the author with great opportunities to look into the interaction processes and structural responses' properties.

Firstly, the structure's responses in all 6DOFs are studied in level ice by transferring the time domain records into the frequency domain. The Power Spectrum Density (PSD) and the dominant frequency for each response are calculated and identified.

Secondly, in order to obtain some insights about the structure's responses in ice ridge, *normalized cross correlation* is calculated to quantify the relationships between the structural responses in different ice conditions. Mainly two sets of structure's responses (surge, pitch and heave; sway, roll and yaw) are calculated in both level ice and ice ridge.

Thirdly, the structure alone was taken as a dynamic system with the ice load as inputs and

structural responses as outputs. The hydrodynamic and hydrostatic coefficients of the structure are calculated. Afterwards, the governing dynamic equation in surge direction was constructed. Each term within this governing dynamic equation is further explored. The ice load is back-calculated in the time domain and compared with mooring force so as to identify the role of inertia force in ice breaking processes. Furthermore, the ice load, mooring force and the inertia force is studied in the frequency domain to get some insights about how the involved forces in this dynamic system counterbalancing each other.

3.2 Frequency domain analysis of different responses

With the recorded structure's responses, it is possible to use the Fast Fourier Transform (FFT) method to obtain the PSD in the frequency domain. Consequently the dominant vibration frequency in each of the 3DOFs (surge, heave and pitch) can be identified.

3.2.1 Calculation method

Prior to the calculation, the time series had been processed to eliminate the weak ice influence in the transition from open water to level ice. Approximately 5 m (Model scale) of the recorded values have been deleted from the beginning of the time history to skip the *run in time* and also a portion of the tank that has *temperate ice*, the remaining of which are left for analysis as shown in Figure 3.1. Calculations are conducted for different ice conditions. The signal selections for all the tests are shown in Appendix A.

Based on the selected signals, the Welch's method was used to obtain the PSD. The Welch's method is based on the FFT method. The selected time series as shown in Figure 3.1 and Appendix A are first processed by applying the "Detrend" command in MATLAB so as to remove the mean value or linear trend before the FFT processing. The basic theory of FFT and the Welch's algorithm are illustrated in Appendix B.

The above two procedures (Signal selection and Welch's method) are accomplished by using the software DIADEM and MATLAB respectively.

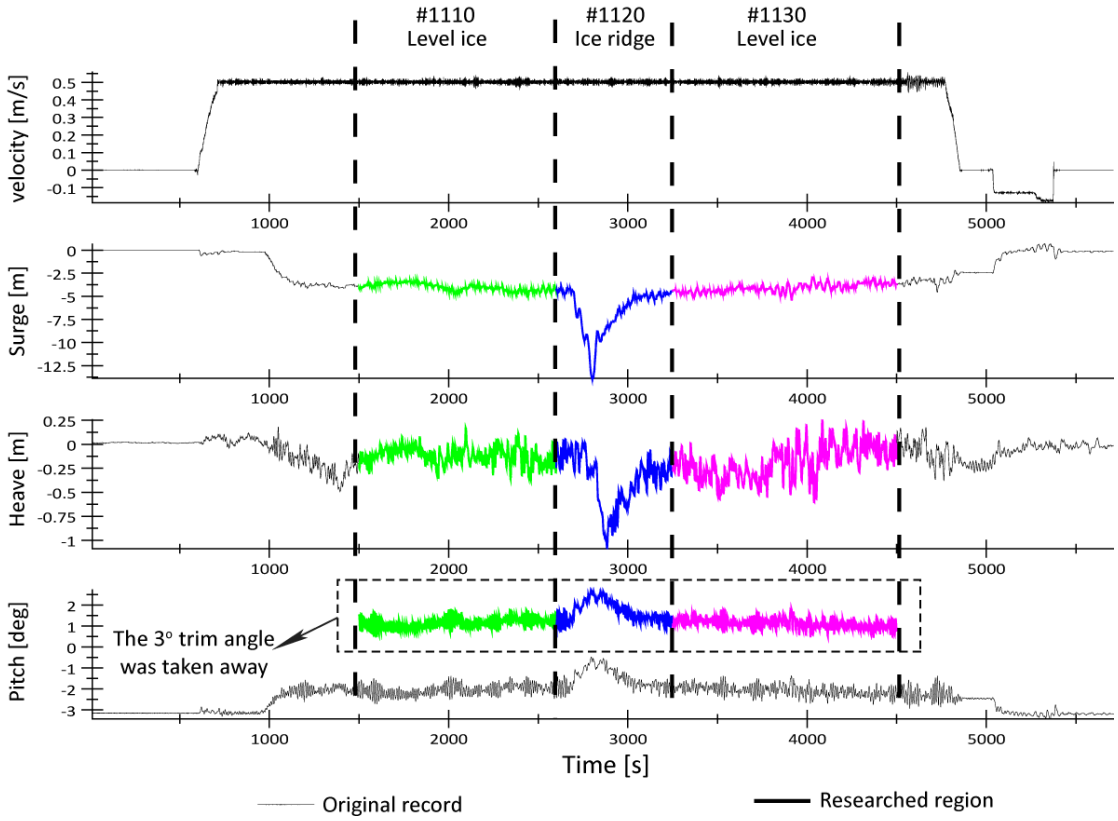

Figure 3.1 Illustration of signal selection

3.2.2 Calculation results

Before going into the detailed test results, the general information regarding the SEVAN FPU-Ice's natural frequencies/periods in each direction are first estimated here by a simple "uncoupled" calculation. When estimating the natural frequency of the structure, the following assumptions have been made:

- The system is linear, the stiffness in each direction can be assumed to be constant;
- The hydrodynamic effect from the water is excluded. Only the structure's mass in each direction is considered; no added mass was considered in the calculation;
- The influence from ice is not considered; (e.g. ice accumulation may increase the mass of the structure)
- The responses of the structure in each direction are thought to be uncoupled;

Regarding the first assumption, since very small variation amplitudes of the structural responses are found in the tests results. For example, in level ice, for surge, the variation of the amplitude is around 1 m with its mean 4 m; for heave, the variation is around 0.5 m; and the pitch variation is about 1^{o}. This can be seen in Figure 3.1. All of these variations are very

small comparing with the geometry of the structure as shown in Figure 2.1. So a linear structure assumption will not induce large errors.

In terms of the second assumption, as will be shown in the later sections, the hydrodynamic effects are comparatively small comparing with the static characteristic of the structure. In detail, the added mass is much smaller than the actual mass of the structure and the static stiffness of the structure is very large. Accordingly, the error induced by this assumption will not be very large.

Concerning the third assumptions, in the current analysis, the ice will only be treated as loadings instead of becoming a part of the structure. But in reality, the existence of ice (broken ice) may change the structural characteristics (e.g. hydrostatic stiffness and mass) and also the hydrodynamic characteristics of the structure. These influences being excluded here can only be viewed as an expedient.

At last, an uncoupled situation was assumed. The coordinate system of the recorded responses is shown in Figure 2.2. From the figure it can be seen that this coordinate system reduced the coupling possibilities of different responses comparing with other often-use coordinate systems such as making the Centre of Gravity (COG) as the origin of the coordinate system in solid mechanics. For the current rough estimation of the structure's natural frequencies, this uncoupled assumption is applicable.

Based on the above assumptions, a very simple calculation method could be adopted to estimate the natural frequency/period of the structure in the following 3 directions with the known stiffness[3] of the structure.

According to the calculations, it is found that the natural period of the SEVAN FPU-Ice Buoy is

$$T_{surge} = \frac{2\pi}{\omega} = 2\pi/\sqrt{\frac{K_{11}}{m}} = 2\pi/\sqrt{\frac{3.2\times10^6}{172.7\times10^6}} = 46 \text{ s}$$

$$T_{heave} = \frac{2\pi}{\omega} = 2\pi/\sqrt{\frac{K_{33}}{I}} = 2\pi/\sqrt{\frac{85.4\times10^6}{172.7\times10^6}} = 9 \text{ s}$$

$$T_{pitch} = \frac{2\pi}{\omega} = 2\pi/\sqrt{\frac{K_{55}}{I}} = 2\pi/\sqrt{\frac{4.37\times10^{10}}{14.2\times10^{10}}} = 11.33 \text{ s}$$

[3] The mooring stiffness in surge direction is back-calculated based on the mean value of the measured surge displacement and horizontal mooring force as 3.2 MN/m. The calculated value is very close to the design value 3.48 MN/m. The hydrostatic stiffness of the structure in heave and pitch directions are calculated with Hydro-D.

These estimated natural periods will give some insight when comparing with the structure's responses characteristics which will be detailed in the following sections.

The calculated PSD for each structure's response in different ice conditions are shown in the following figures followed by the identified dominant vibration frequencies and period in the tables.

3.2.2.1 Test #1000 series-Level ice

The PSD in Test #1000 series in level ice is shown in Figure 3.2 and the identified dominant frequencies are listed in Table 3.1.

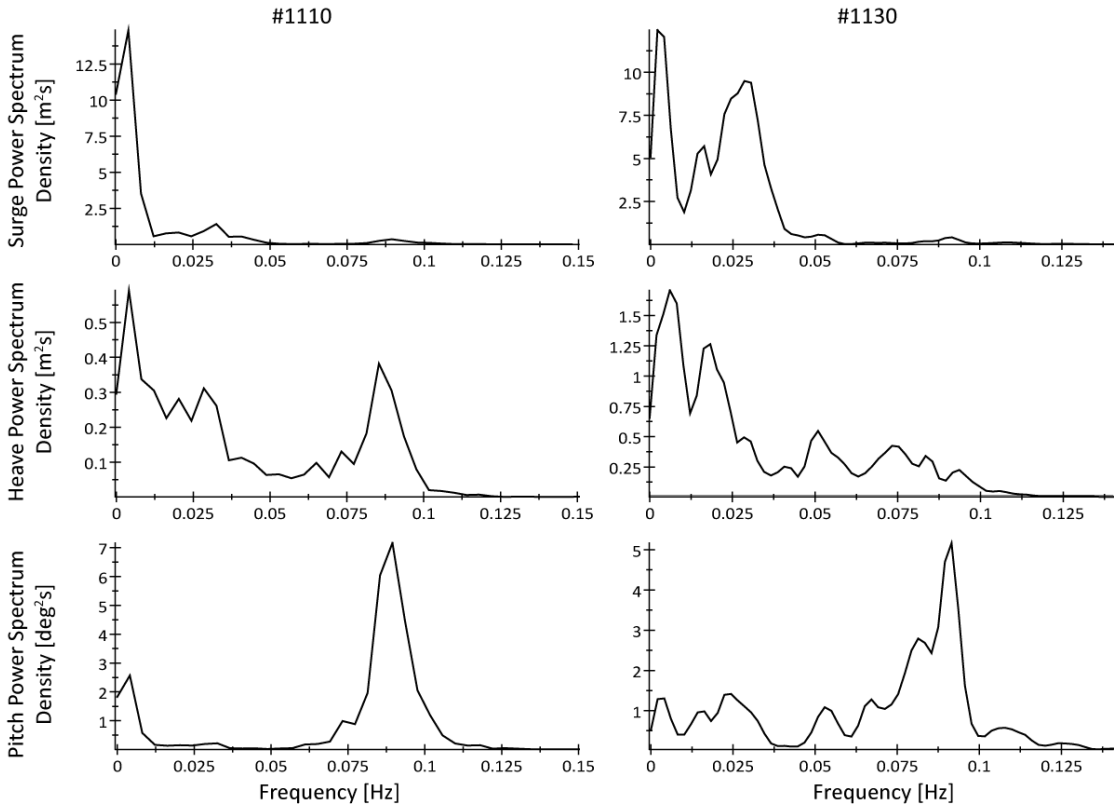

Figure 3.2 PSD of structural responses in Test #1000-Level ice

As we can see from the above figure that the surge displacement has a very low dominant frequency, and the pitch displacement has a dominant frequency around its natural frequency. For heave response, its dominant vibration seems to be influenced by both the surge and pitch responses meaning it has dominant vibrations around both the low frequency band as surge and around the high frequency band as pitch.

Table 3.1 Dominant frequency/period of structural responses in Test #1000 level ice

Test Series	#1110		#1130	
	Dominant frequency [Hz]	Dominant period [s]	Dominant frequency [Hz]	Dominant period [s]
Surge	0.00407	245.70	0.00204	490.20
Heave	0.00407	245.70	0.00610	163.93
Pitch	0.08950	11.17	0.09160	10.92

Based on the above figure and table, a very long dominant period of variation was observed for surge and heave. The recorded surge, heave and pitch responses in time domain are shown in the following figure for Test #1110 so as to illustrate the possible cause of such low frequency (long period) responses.

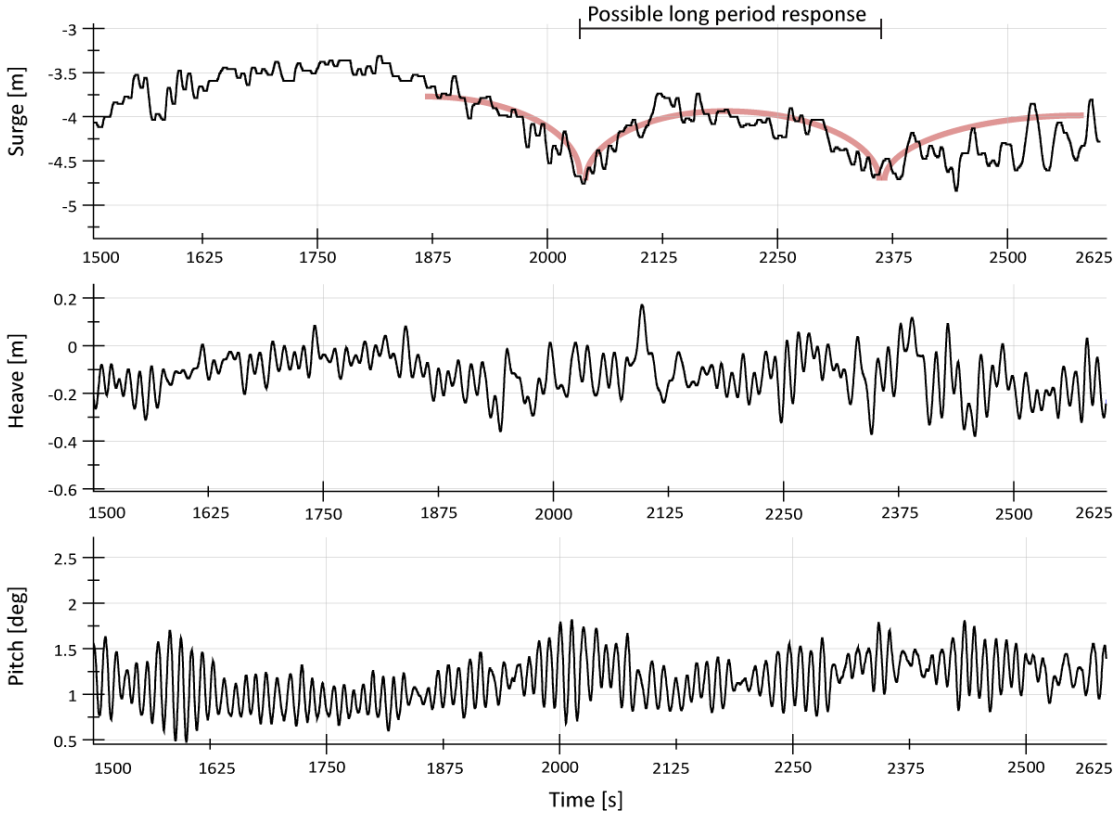

Figure 3.3 Illustration of the time series together with the possible long period response

This low frequency (long period) variation is believed to be induced by ice accumulation which is not only relevant to the geometry of the structure but also relevant to the responses (e.g. velocity and displacement) of the structure. As can be seen from Figure 3.3, the possible long period response was estimated based on the frequency domain analysis.

Furthermore, a scrutiny of the video concerning the ice accumulation volume change with

time was conducted. The following figures (see Figure 3.4) are obtained when the ice accumulation volume reaches the maximum[4] during a period. This video is recorded in Test #1110 and the time shown in the figure is in model scale. It can be seen that the intervals of these "peaks" are 37 s, 42 s, and 33 s respectively. In full-scale, they are

$$37\ \text{s} \times \sqrt{40} = 234\ \text{s}$$
$$42\ \text{s} \times \sqrt{40} = 265\ \text{s}$$
$$33\ \text{s} \times \sqrt{40} = 208\ \text{s}$$

These values are quite close to the calculated dominant period of surge 245.7 s which was shown in Table 3.1. This further confirms the assumption that the low frequency response has strong relationship with ice accumulation variations.

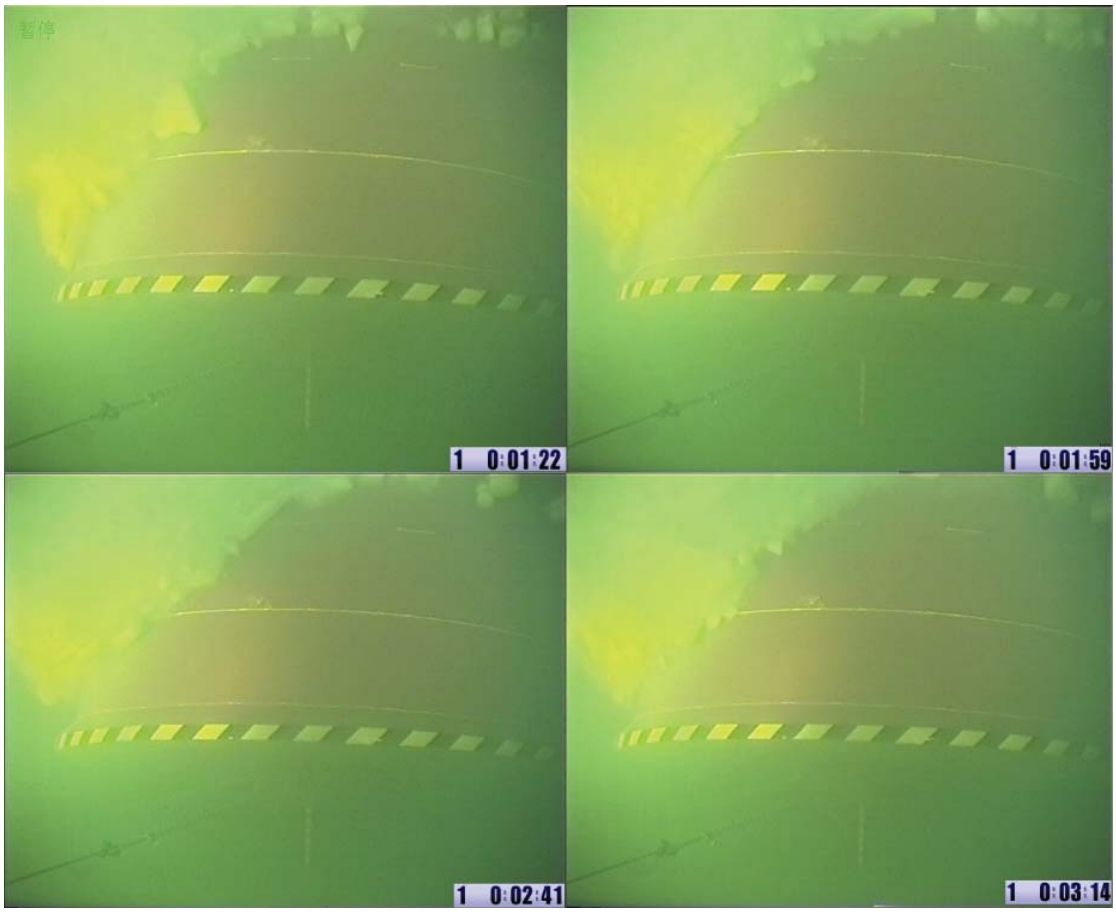

Figure 3.4 Illustration of peak ice accumulation volume together with time in the video (Model Scale)

From Figure 3.2 and Table 3.1 we can further compare the differences of the responses in level ice before and after the ice ridge.

For pitch displacement, the dominant vibration period remains more or less the same before

[4] Here the maximum ice accumulation volume was determined visually from the under-water video. It was chosen at the moment of the increasing ice accumulation volume suddenly start to decrease.

and after the ridge. From the video, it also can be seen that generally the ice breaks in accordance with the structure's pitch responses. This means within one period of the structure's pitch movement, that an obvious ice breaking and rotating phase is completed in the bow region of the structure[5]. This phenomenon will be explained at a later stage.

For surge and heave displacements, generally the responses' characteristics in the frequency domain are more or less the same. However, it seems that after the structure exiting the *severe ridge*, the PSD for surge and heave are not as 'concentrated' as before entering the *severe ridge*.

3.2.2.2 Test #2000 series-Level ice

Similarly, the PSD for the responses in level ice of Test #2000 are shown in the following figure. A major part of the surge response resides in the low frequency band. And pitch displacement has a large portion of the PSD around its pitch natural frequency (with period 11.33 s).

Comparing the PSD in level ice before and after the *extreme design ridge* it can be seen that for heave and pitch displacement, a major part of the responses in the low frequency band become more dominant after exiting the *extreme design ridge* than before entering it. For surge displacement, after exiting the ridge, its PSD is not as concentrated as before entering the ridge.

[5] Due to the large size of this structure, non-simultaneous breaking of ice around the structure is a more general case. Here only the bow-region ice breaking frequency was compared with the structure's pitch frequency.

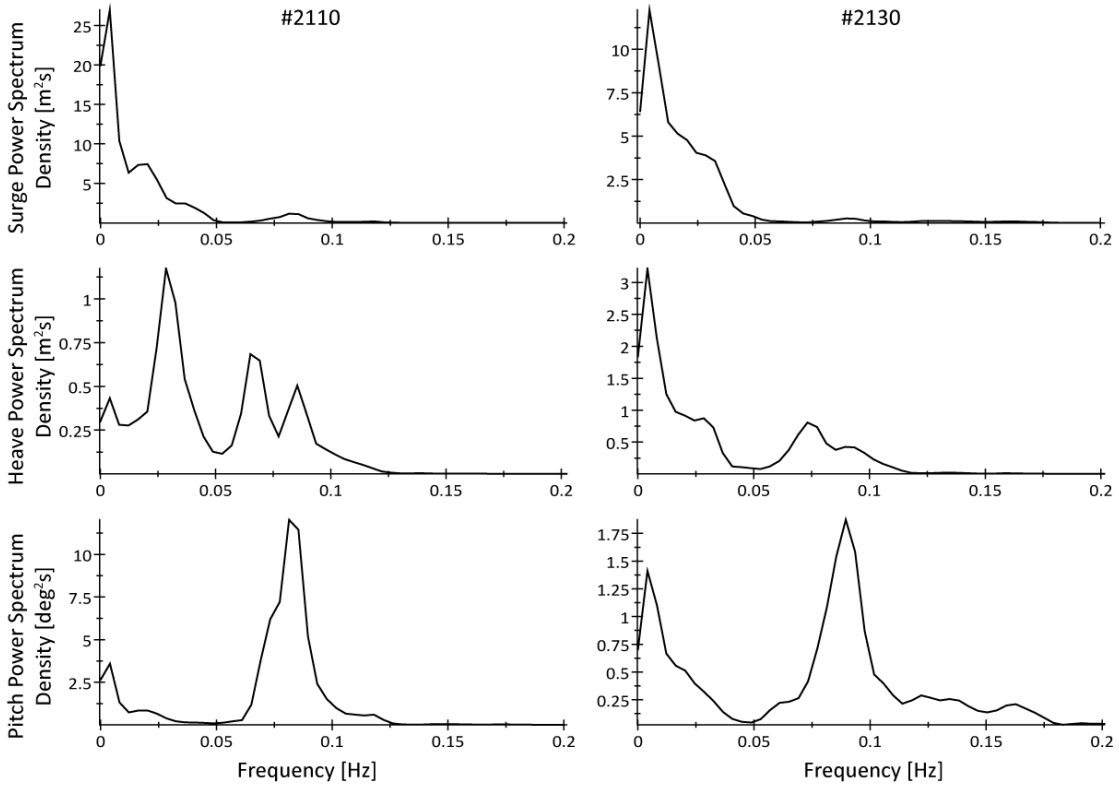

Figure 3.5 PSD of structural responses in Test #2000-Level ice

Another different place in these two test conditions is the ice speed. In Test #2110 (left) the ice speed is about 0.5 m/s while in Test #2130 (right) the ice speed is about 1 m/s. Generally, with a higher ice speed, a higher ice load frequency is expected. However, it seems the dominant response frequency of the structure did not become larger in this case. On the contrary, the low frequency became more dominant. From this phenomenon it can be further inferred that after the structure exiting an ice ridge, lots of ice rubbles accumulated in front of the structure. The ice accumulation becomes the dominant contributor to the total ice load comparing with other load contributors such as *ice breaking* and *ice rotating loads*[6]. However, as will be pointed out later that the pitch response of the structure is relatively more sensitive to the *ice rotating load*, hence from Figure 3.5 a relatively larger portion of the responses in the high frequency band (around 0.15 Hz) becomes more dominant after the structure exited the *extreme design ridge* with a speed of 1 m/s.

The detailed dominant frequencies/periods are shown in the following table. Similarly the large surge and heave periods are thought to be induced by the ice accumulation variations. And the pitch response's dominant periods are remaining more or less the same around its natural period.

[6] The precise definition of these load components will be given in Chapter 5. Here only a literal meaning should be sufficient to understand the descriptive reasoning.

Table 3.2 Dominant frequency/period of structural responses in Test #2000 level ice condition

Test Series	#2110		#2130	
	Dominant frequency [Hz]	Dominant period [s]	Dominant frequency [Hz]	Dominant period [s]
Surge	0.00407	245.70	0.00407	245.70
Heave	0.02850	35.09	0.00407	245.70
Pitch	0.08140	12.29	0.08950	11.17

3.2.2.3 Test #3000 series-Level ice and managed ice

The PSD of the structural responses in different ice conditions (level ice and managed ice) are shown in three columns in the following figure. In Test #3110 (left column), the structure was tested in level ice before entering the *extreme design ridge*. In Test #3130 (middle column), the structure was tested in level ice after exiting the *extreme design ridge* with finite length. For Test #3150 (right column), the structure is advancing in managed ice just after exiting another *extreme design ridge* with infinite length. In all cases, the ice speed is 0.5 m/s.

See from the first row of the following figure, the surge displacement has a low frequency response in Test #3130. However, when the structure exited the ridge and entered level ice again, the dominant surge period becomes more or less around its natural period (43 s). For heave and pitch displacements, comparisons between Test #3110 and Test #3130 show that a low frequency became more dominant after exiting the ridge. For all three responses in managed ice just after exiting the ridge, the PSD is not as concentrated as before.

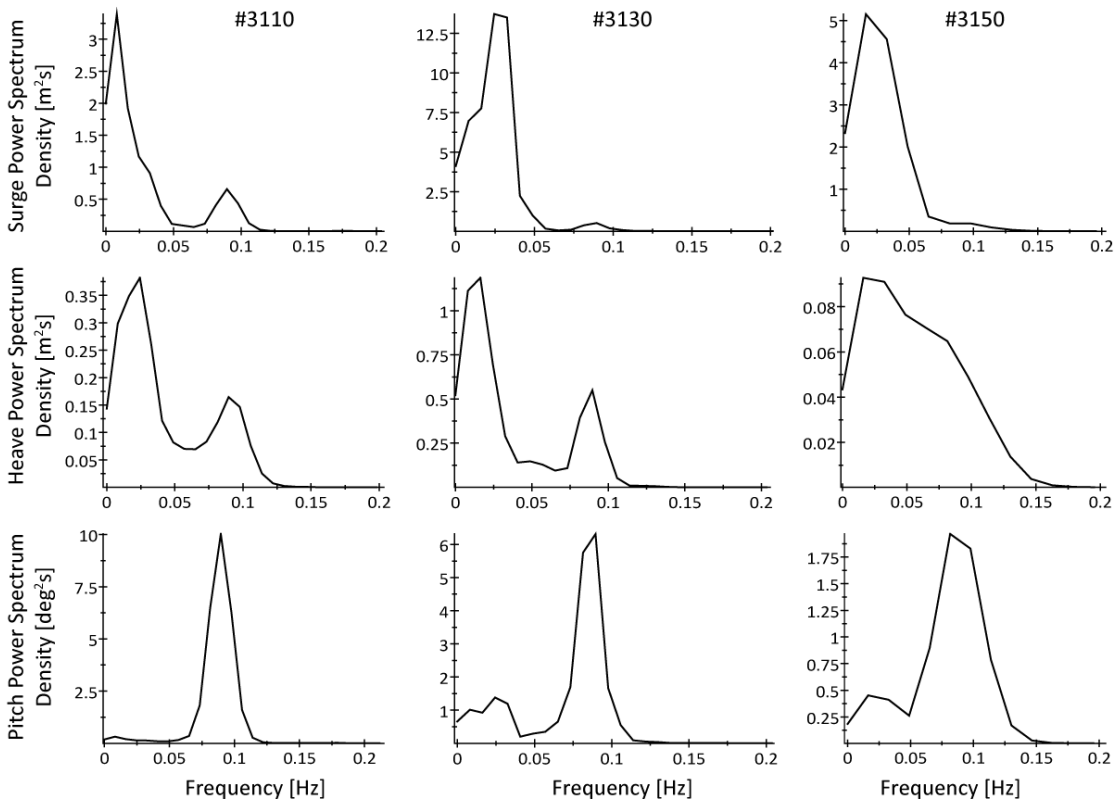

Figure 3.6 PSD of structural responses in Test #3000-Level ice

The detailed dominant response frequencies and periods are shown in the following table. Similarly, the much longer response period of surge and heave are thought to be induced by the ice accumulation effects. And dominant pitch response periods are all around its natural period.

Table 3.3 Dominant frequency/period of structural responses in Test #3000 level ice condition

Test Series	#3110		#3130		#3150	
	Dominant frequency [Hz]	Dominant period [s]	Dominant frequency [Hz]	Dominant period [s]	Dominant frequency [Hz]	Dominant period [s]
Surge	0.00814	122.85	0.0244	40.98	0.0163	61.35
Heave	0.02440	40.98	0.0163	61.35	0.0163	61.35
Pitch	0.08950	11.17	0.0895	11.17	0.0814	12.29

3.2.2.4 Test #4000 series-Level ice

The PSD of the structural responses in Test #4000 are shown in the following figures. All the tests (#4110, #4130 and #4150) are in level ice before or after the ridges. Two continuous ridges are imbedded in level ice. Both of them are of finite length. See from the comparisons of different columns in the following figure, it is found from the first two columns that after exiting the ridge, the PSD of surge and pitch responses are not as concentrated as before. For pitch displacement, in all cases, it has a dominant response period around its natural period.

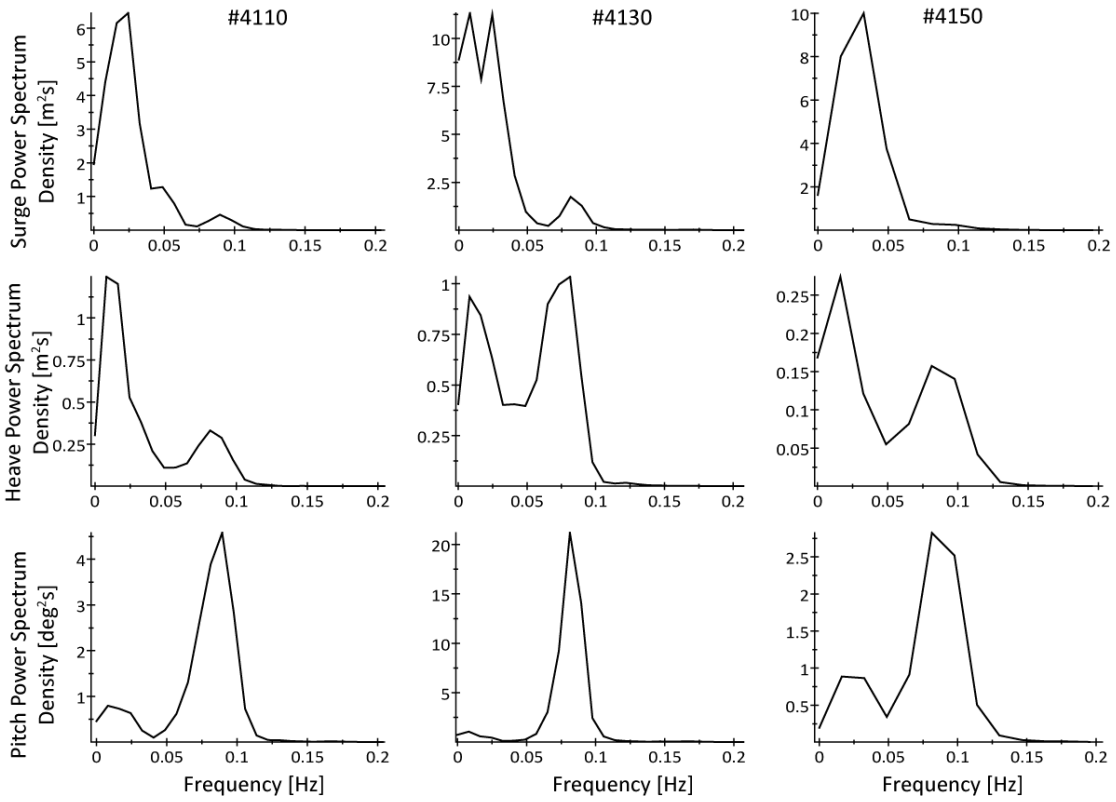

Figure3.7 PSD of structural responses in Test #4000-Level ice

The detailed dominant response frequencies and periods are shown in the following table.

Table 3.4 Dominant frequency/period of structural responses in Test #4000 level ice condition

Test Series	#4110		#4130		#4150	
	Dominant frequency [Hz]	Dominant period [s]	Dominant frequency [Hz]	Dominant period [s]	Dominant frequency [Hz]	Dominant period [s]
Surge	0.0244	40.98	0.00814	122.85	0.0326	30.67
Heave	0.00814	122.85	0.0814	12.29	0.0163	61.35
Pitch	0.0895	11.17	0.0814	12.29	0.0814	12.29

3.2.3 Discussion about the frequency domain analysis

Based on the previous PSD analysis concerning different responses in different level ice conditions (different ice speeds; before or after the ice ridge), the following general phenomena have been observed.

- The dominant pitch responses are always around its natural frequency;
- Usually, a very low frequency response is dominant in both surge and heave directions;
- In Test #3130 and #4140, the surge displacement's dominant frequency is very close to its natural frequency;
- Generally, after exiting the ice ridge, the PSD of the structure's responses became not as concentrated as before entering the ridge.
- In most cases, after exiting the ice ridge, a low frequency response became more dominant in the structural responses.

The explanations to these observed phenomena will be given in the following:

3.2.3.1 Ice-accumulation-induced low frequency responses

As has been shown in the test results of Test #1000, a dominant low frequency response was identified in the PSD of surge displacement (see Figure 3.2). The possible long period vibration track was also suggested in the time history of surge displacement as shown in Figure 3.3. It was believed this low frequency response is induced by ice accumulation which was further confirmed by the recorded video.

In the later frequency domain analysis, it was further found that basically in the entire surge, and heave responses' PSD figures, dominant low frequency responses could be identified. And the dominant periods of these responses are about 120 s and 240 s. As we have already found in the video for Test #1000 the possible ice accumulation period is around 200 s. These periods are almost in a same scale. Accordingly, a reasonable inductive conclusion[7] could be made here that all these low frequencies are expected to be induced by the *ice accumulation load* which is believed to be a low frequency, high amplitude load.

[7] Here the inductive conclusion is based only on the video record of test #1000 and theoretical reasoning. For future work, it is expected some ***image analysis*** of the recorded video is required to quantitatively demonstrate the variation frequency of the ice accumulation volume in each test so as to further confirm this conclusion.

Theoretically, it also makes sense. The ice accumulation volume is not only relevant to the geometry of the structure, but also relevant to the responses of the structure. All these factors acting together may lead to an *ice accumulation load* component with relatively very low frequency. This also implies that the major cause of surge displacement is due to *ice accumulation load* as will be further discussed in the upcoming sections.

However, as can be seen from Table 3.3 and Table 3.4, in Test #3130 (level ice after an extreme design ridge) and Test #4110 (level ice before ridge), the dominant surge response period are around its natural period. This is quite different from the usual cases that the dominant surge responses are in low frequency band.

Based on the recorded video, when the structure was advancing in level ice (as shown in Figure 3.8), a very huge radial crack in level ice was observed in both tests. Seen from the video, it can be sensed that with the presence of this obvious radial crack, the broken ice pieces become relatively larger comparing with in intact level ice.

Figure 3.8 The observed huge radial cracks in Test #3130 (left) and #4110 (right)

The presence of relatively larger ice breaking sizes could be indicated by the variation of pitch responses. As can be seen from Table 3.3 and Table 3.4, the dominant pitch response period increased from 11.17 s in Test #3130 (intact level ice) to 12.29 s in Test # 3150 (level ice with cracks); and from 11.17 s in Test #4110 (intact level ice) to 12.29 s in Test #4130 (level ice with cracks). It will be explained later that the pitch response frequency is most relevant to the ice breaking frequency. An increased dominant pitch response period, with the same ice drift speed, means a longer ice breaking length.

Theoretically, this can also be explained based on *Energy conservation*. And it could be useful to explain the occurrence of larger ice broken pieces with the presence of large radial cracks.

Because the explanation could be generalized to *managed ice* where lots of "cracks" are present.

Assuming the structure is the considered system, the energy input into the system is from the kinetic energy of the incoming ice. This amount of the input energy is only relevant to the mass and velocity of the incoming level ice and it could be assumed to be constant regardless of the presence of cracks.

The output of the energy includes the energy which is damped away by the hydrodynamic effect of the water and the energy required to break, rotate and clear the broken ice pieces. As will be pointed out in the upcoming sections, the added damping of the structure is comparatively small and will be neglected here. The major part of the input energy is spent on breaking, rotating and clearing the broken ice pieces. Since the total volume of the broken ice pieces are the same regardless of the presence of the cracks, the energy required to clear the broken ice pieces can also assumed to be constant.

Then the remaining energy is spent on ice breaking and ice rotating. The influence of cracks on these two energy consumers will be discussed separately in the following:

- Energy required to rotate the ice

With the presence of a huge crack, the *ventilation effects*[8] could be comparatively reduced since the water has an easy "path" (the crack) to flush into the void space above the broken ice pieces. Due to the influence of this reduced ventilation effect, the energy required to rotate the broken ice is expected to decrease. However, it should be noted that the total ice rotating energy is relevant to both the ventilation effect and the ice breaking size. According to the less variation of pitch frequencies, the ice breaking sizes' variations are thought to be not significant enough to increase to required energy to rotate the broken ice pieces even under the absent of less ventilation effect. So a reduced ice rotating energy is the most likely result in the current case.

- Ice breaking energy

From the *Energy conservation*'s point of view, reduced energy consumption in ice rotating means that more energy is used to break the ice. Here, it is assumed that the newly broken ice piece's perimeter is proportional to the ice breaking energy. Since there is a very large crack, even with the unchanged ice breaking energy input, relatively larger broken ice pieces could

[8] Ventilation effect means when the broken ice pieces are rotated by the structure, due to the inability of water to (fully) flush in the void space above the broken ice pieces, huge pressure difference could be induced above and below the broken ice pieces. This huge pressure difference will be transferred to the structure and hence induce large ice load in the ice rotating phase.

be expected especially for those pieces neighbouring the crack. This large crack will save some of the energy input which could be used somewhere else to form a longer broken ice perimeter (larger ice pieces). So, the increased ice breaking energy will tend to break even larger ice floes. Here one may argue that why not the increased ice breaking energy lead to smaller broken ice pieces since the overall perimeter of these smaller broken pieces are larger than a single large floe. However, this *much smaller broken ice pieces* assumption is in contradictory with the less-varying pitch frequency which is a sensitive indicator of ice breaking sizes. So, in general, a relatively larger ice breaking size is expected with the presence of cracks.

Comparing with smaller broken ice pieces, it will be easier for the larger broken ice pieces to be cleared away. This is because for the smaller broken ice pieces, an “inter-lock” situation is common among ice pieces. Furthermore, the accumulated volume of the smaller ice pieces appears to be a “smooth body” experiencing less fluid influence (less turbulence). On the contrary, the accumulated volume for larger ice pieces can be view as a “blunt body” under larger influences from the flow around the structure, leading to more effective ice clearing processes. These two differences are illustrated in Figure 3.9 with exaggeration.

As pointed out before, the energy used to clear the ice was assumed to remain more or less constant. This assumption was based on a full contact between ice rubbles and the structure in both small broken ices piece and large broken ice pieces cases. This means in both cases, the contact areas are assumed to be the same, the total volume of broken ice pieces are the same. However, in large broken ice pieces situations, a more effective ice clearing process is going on. This means that the accumulated volume in the situation with large broken ice pieces changes very fast and hence an *ice accumulation load* with relatively higher frequency is expected. And the dominant ice accumulation load period could be expected to improve from more than 120 s/ 240 s to about 40 s which is around the natural period of surge.

The above reasoning process linked the presence of a relatively high surge frequency with the presence of the large crack in level ice in a qualitative way. Since it is a very long reasoning process, the whole reasoning route is further illustrated in Figure 3.10.

In terms of future work in this part, there may be:

- Modeling the ice breaking characteristics with the presence of pre-breaking cracks to confirm the above expectation of a larger size broken ice pieces;
- Modeling the ice clearing process with different broken ice piece size, different arrangements, and different ice drift speeds. More interests could be put on the

turbulence formation and effects in clearing the broken ice pieces.

- The above descriptive analysis amplified the ice accumulation's influence on improving the dominant surge frequency from 120 s/240 s to only 40 s. During this process, some other influences may also present which still need further consideration. But this does not influence the current conclusion about the ice accumulation's large influence on the surge response.

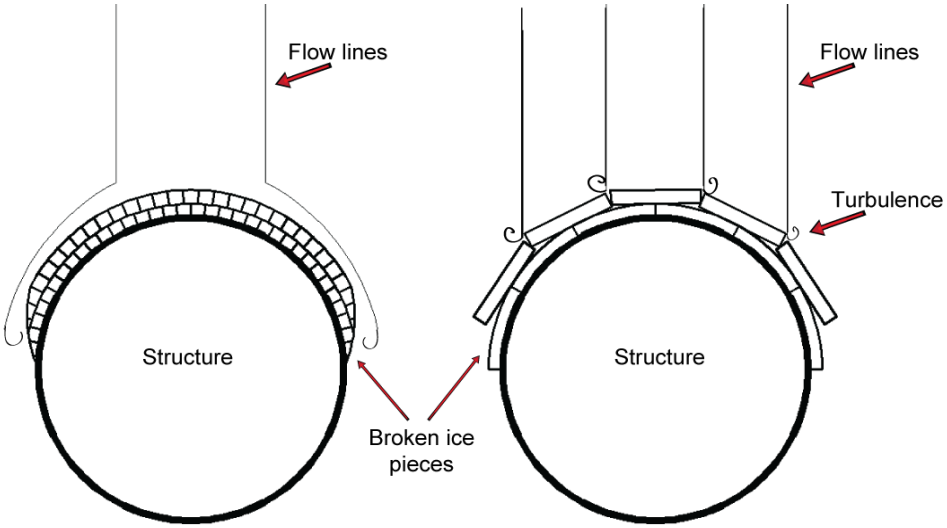

Figure 3.9 Illustration of ice clearing with different broken ice size (bird view; with exaggeration)

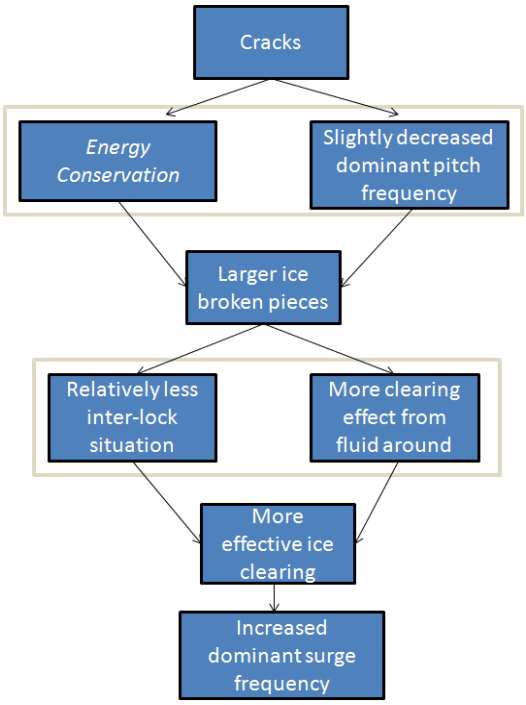

Figure 3.10 Reasoning route of cracks lead to increased surge frequency

3.2.3.2 Pitch response and ice breaking

As pointed out before, in all the tests, the structure mainly pitched around its natural frequency. Different from surge displacement where the ice accumulation is the major contributor, the major cause for pitch displacement is the ice rotating load. This can be proved by examining the time history of pitch response whose mean value is around 1^o while its variation range is between 0^o~2^o. This means that the mean contribution[9] from the low frequency ice accumulation load (nearly constant value) is not as large as the variation induced by the high frequency ice breaking (possible) and rotating load. Based on this, the following two explanations are given concerning the structure's dominant pitch frequency is around its natural frequency.

- **First explanation: Focusing on the frequency of the excitation force**

It is suggested the ice breaking length is about 3.5 times the thickness of the ice for the plate mode of bending failure (Li et al. 2003). Based on this, the ice breaking length is expected to be about 7 m in the current tests. Considering the ice drift speed to be 0.5 m/s, the duration of ice rotating phase is about 7/0.5 = 14 s. This loading period is very close to the natural period of pitch which is estimated to be 11.33 s. The frequency ratio in this case is about 0.81. According to Chopra (2005), the response factor's relationship with the frequency ratio could be shown in Figure 3.11.

[9] Since the ice accumulation load is of very low frequency, the relevant response of the structure is close to the static response. So the mean value was checked to get a feeling about the amplitude of ice accumulation influence to pitch displacement.

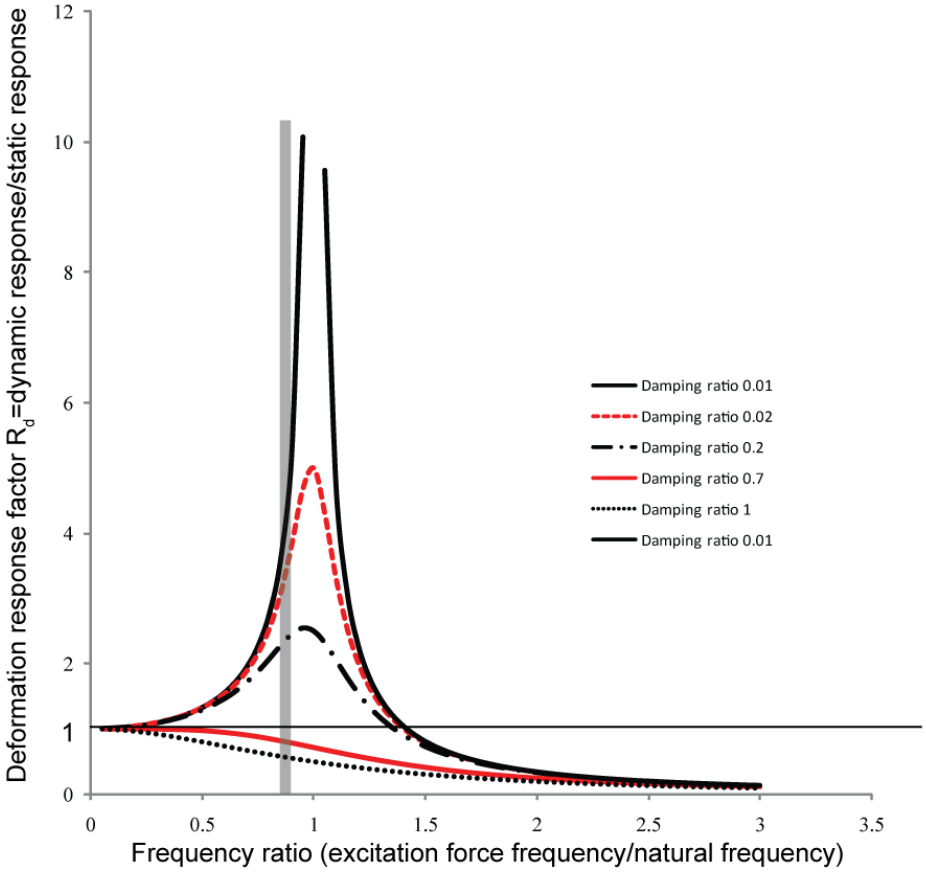

Figure 3.11 Illustration of ice rotating load frequency together with possible pitch response

The shaded area is in accordance with the current tests. The horizontal axis represents the frequency ratio which is around 0.81 in the current tests. And the vertical axis represents the dynamic pitch response over the static response. As will be shown later, the added damping in pitch direction is comparatively small and a large Moment of Inertia is available in the pitch direction. Hence a very small damping ratio is expected. Hence the observed large pitch responses around its natural frequency are explained by a possible excitation force with frequencies around the structure's natural frequency[10] of pitch.

- **Second explanation: Focusing on the influence of pitch response on ice load frequency**

The above explanation is from the perspective of the external force's frequency. Another explanation can be from the perspective of the pitch response's influence on ice loads. It

[10] More precisely, the structure vibrates around its damped frequency $\omega_d = \omega_N\sqrt{1-\xi^2}$ where ω_d is the damped frequency of the structure; ω_N is the natural frequency of the structure; and ξ is the damping ratio which is estimated to be very small in the current case. So, the difference between ω_d and ω_N is not large, these two frequencies will not be discriminated and will be written as *around the natural frequency* of the structure in the following analysis.

appeared that the pitch frequency tends to "converge" to its natural frequency. As will be illustrated in the following chapter that the surge and pitch responses are highly correlated with time lag 0. It can also be observed in the previous PSD figures for the surge response that there will always be a "small" peak around the frequency where the dominant pitch frequency is observed. This means that a high frequency variation (about 0.1 Hz) component exists in the structure's surge displacement. Besides, the major pitch response is in phase with this "small-peak" surge response component. In a descriptive way, based on the coordinate system shown in Figure 2.2, this means that when the structure has positive pitch movement (pitch back), the structure also has a surge component in the negative direction (surge back); when the structure has a negative pitch movement (pitch forward), the structure also has a positive surge movement (surge forward). This description can be useful to explain why the dominant frequency of pitch response tends to "converge" to its natural frequency.

As will be shown, the *relative velocity* between the incoming ice and the structure influences the ice breaking length. Generally, if there is a larger *relative velocity* between the structure and the incoming ice, there tends to be shorter ice breaking lengths. On the contrary, when there is a smaller *relative velocity* between the structure and the incoming ice, the ice breaking length is expected to be longer.

When the structure is pitching forward[11], the structure is also surging forward. In this situation, the *relative velocity* between the ice and the structure is very large, so a shorter ice breaking length is expected. However, such a short ice breaking length means less ice breaking resistance and less ice rotating resistance to force the structure pitching back again. Instead, this short ice breaking phenomenon may only slow down the forward speed of surge and pitch (to "brake" the structure's movements). When the *relative velocity* between the structure and the incoming ice was reduced, in a new round of ice-structure interaction, a relatively long ice breaking length was expected. Under such long broken ice pieces, the ice rotating load's amplitude and duration both become very large. This relatively long duration ice rotating load will also force the structure to pitch and surge backward. However, at certain degree, water will flush into the void space above the broken ice pieces and the ice rotating load will decrease instantly. At this stage, the structure could be viewed as been "released" from external excitation and will "vibrate freely" according to its own natural frequency. And it will pitch forward for another new round of ice-structure interaction. Then three possibilities

[11] The term forward and backward is used here to gain an intuitive feeling of the structural responses. Forward means the forward direction of the structure and is opposite to the ice drift direction. Backward means the backward direction of the structure and is in a same direction of the ice drift direction. Based on the coordinate system shown in Figure 2.2, the strict definitions of *forward* and *backward* are: Pitch forward/backward=negative/positive pitch; Surge forward/backward=positive/negative surge.

can be identified:

- Possibility 1:

(See (a) of Figure 3.16 and Figure 3.12 for the possible loading history)

The previous ice breaking length is too long that when the structure "freely" vibrates forward, it meets no new ice. In this case, the structure will continue pitching according to its natural frequency. And eventually it will have a new contact with the incoming ice with the following possibilities (2 or 3) as shown in the following. But in this case, the dominant pitch response frequency is expected to be its natural frequency.

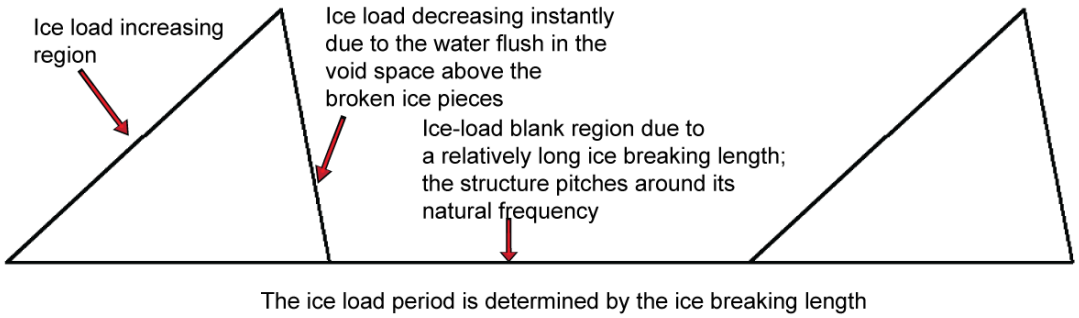

Figure 3.12 Typical loading history of Possibility 1

(Note: only the ice rotating load was shown in the above figure)

- Possibility 2:

(see (b) of Figure 3.16)

When the structure pitches forward and has a new round contact with the incoming ice with a large *relative velocity*. Two sub-cases could be identified.

Case 1: (see Figure 3.13 for the typical loading history)

The *relative velocity* is so large that the ice breaking length is very short. Then the induced ice rotating resistance is expected to be very low. And it is possible that such low ice load cannot "turn" the structure back (force the structure pitch back). Accordingly, the only effect of such small broken ice pieces is to slow down the forward speed of pitch and surge. This may lengthen the pitching period to be a little bit larger than the original natural period, but due to the small size of the broken ice pieces, the structure's pitching period will still remain around its natural period. When the next round of interaction starts, the *relative velocity* has been reduced. The interaction process will shift to possibility 3 as shown in (c) of Figure 3.16.

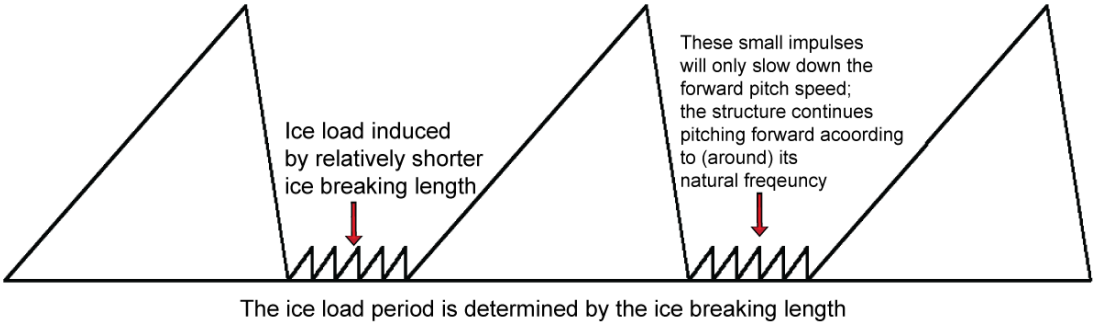

Figure 3.13 Typical loading history of Case 1 of Possibility 2

(Note: only the ice rotating load was shown in the above figure)

Case 2: (see Figure 3.13 for the typical loading history)

The *relative velocity* is so large that a small ice breaking length is expected. But different from Case 1, it is possible that even such small size ice breaking length may have sufficient resistance force to "turn" the structure back in a frequency which is relevant to the size of the broken ice pieces. This is because both the ice rotating load's amplitude and frequency are dependent on the size of the broken ice pieces as will be shown at a later stage by a numerical model. In this case, the structure's pitch response frequency will totally be determined by the external force's frequency not its natural frequency. This needs a relatively lower speed compared with the speed in Case 1.

But in the current test campaign, as mentioned before, the typical ice breaking length is about 7 m based on Li's recommendation (Li et al. 2003) with a typical load period of 14 s which is quite close to the natural period of the pitch response of the structure 11.33 s. Accordingly, for the current structure, even in this case, it will also pitch around its natural frequency.

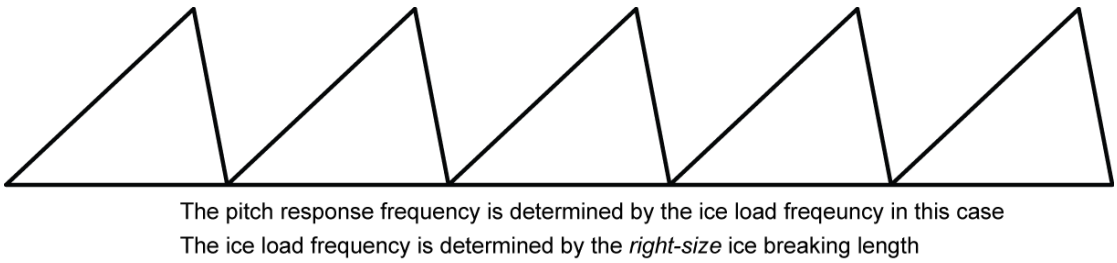

Figure 3.14 Typical loading history of Case 2 of Possibility 2

(Note: only the ice rotating load was shown in the above figure)

From the discussion for possibility 2, it can also explain why in a higher ice drift speed, the dominant pitch response was also around its natural frequency. In Test #2130 with an

ice speed of 1 m/s, the structure also pitched around its natural frequency. This is because under higher ice drift velocity, there will be a much higher chance for the response of the structure to fall in Case 1 of possibility 2 in which the structures was mainly vibrating around its natural frequency.

- Possibility 3 (see (c) of Figure 3.16 and Figure 3.15 for the typical loading history)

When the structure pitches forward and has a new round contact with the incoming ice with a small relative velocity as shown in (c) of Figure 3.16. A relatively longer ice breaking length was expected and hence large ice rotating force with a longer period. Then the structure was forced to pitch back. When the ice load (ice rotating load) decreased instantly due to water flush into the void space above the broken ice pieces, the "released" structure will pitch forward according to its natural frequency and has a new round of contact which could fall into any of the above 3 mentioned possibilities. Except in Case 2 of possibility 2, all other Cases have a very high chance to lead to dominant pitch responses of the structure around their natural frequencies.

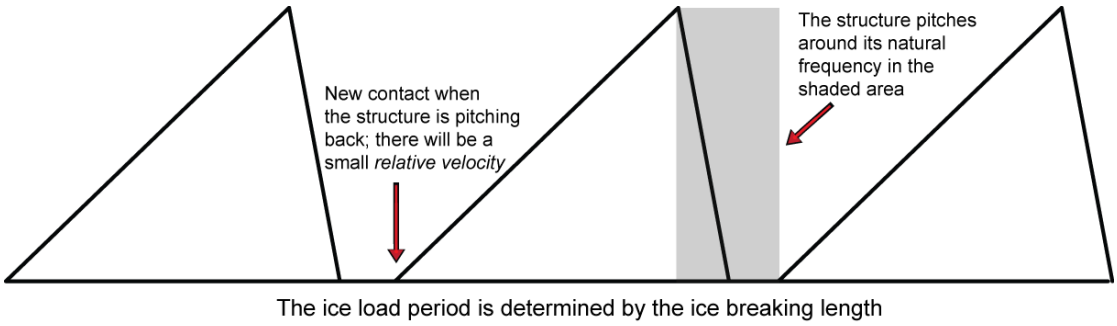

Figure 3.15 Typical loading history of Possibility 3

(Note: only the ice rotating load was shown in the above figure)

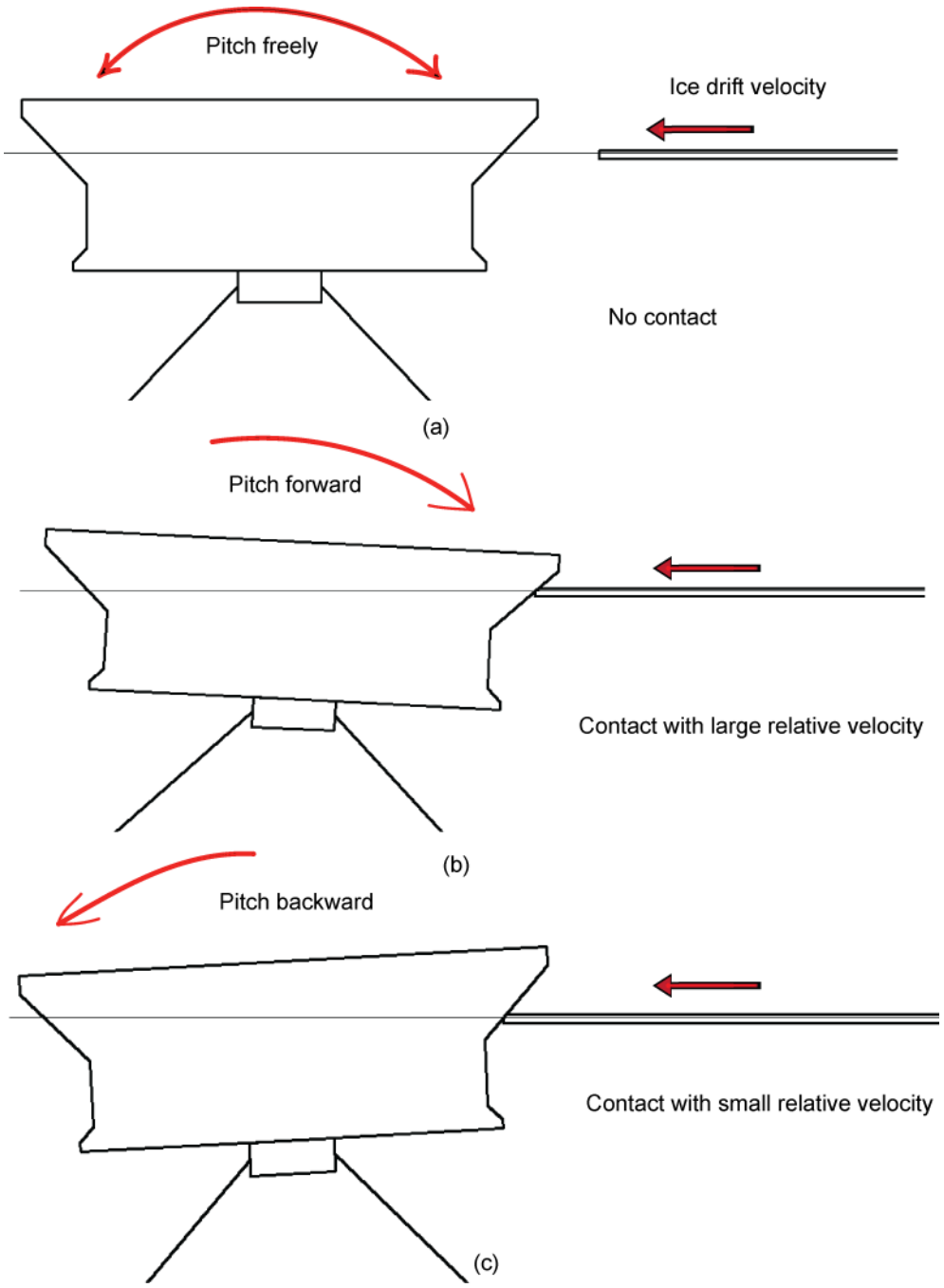

Figure 3.16 Illustration of the possibilities of structural pitch response with ice drift

(*Upper*: possibility 1; *middle*: possibility 2; *lower*: possibility 2)

Different from a fixed structure, for a moored structure, its response influences the dominant loading frequency. Based on the previous discussion, the following two implications could be obtained:

- For an already constructed moored structure whose dominant pitch frequency is fixed. In order to avoid resonant in its pitch response, the best working environment for this structure is not under very high ice drift speed nor very low ice drift speed,

but a speed that can produce the *right-size* broken ice pieces providing sufficient large ice load to control the pitch response of the structure following the frequency of the ice load which is relevant to the broken ice size. And the estimated loading frequency should be away from the structure's natural frequency.

- For an already known ice condition, to construct a moored structure working in such environment, the structure's natural frequency should be considered to be away from the possible dominant ice rotating load frequencies. Furthermore, the natural frequency of pitch, if possible, should be designed as low as possible, then no matter at high ice drift speed or low ice drift speed, the ice load frequency can be considered relatively large. Then the frequency ratio will be relatively large, according to Figure 3.11, the surge response will be reduced even comparing with a static loading case.

(Note: the above two implications concerns only the pitch response. In reality, many other structural responses should also be taken into consideration. In the coming sections, based on the investigation regarding surge, heave and pitch responses, different loading components, and their relationship with different loading processes, a more detailed suggestion regarding the target design frequency of the structure will be suggested.)

From two perspectives, the above discussion qualitatively explained why the dominant pitch response's frequency is always around its natural frequency even for different ice speeds. Further quantitative work is required to find the borderline between Case 1 and Case 2 of possibility 2. It is expected that an *Energy Conservation*'s point of view could be adopted to identify the *right-size* of the broken ice pieces which not just slow down the broken ice pieces but also are able to force the structure to pitch backward to certain degree. During the whole process the structure will be forced to pitch according to the ice load's frequency which is expected to be much higher than the designed pitch natural frequency.

After identifying the right-size of the broken ice pieces, the optimum working environment for such a moored structure could also be suggested.

3.2.3.3 Ridge's influence on the structure's responses

The ridge's influence on the structure's response starts when the structure is entering the ridge and will last further after the structure exits the ridge. In this section, the ridge's influence on

the structure's response will be treated in the following two different cases. The first is when the structure was advancing inside the ridge. In this case, the time history of the response will be required for comparisons. The second is after the structure exits the ridge condition. Some differences can be identified from the previous PSD figures as will be discussed later.

- Structure's responses in ridge condition

The comparisons are made based in Figure 3.1, Figure A 1, Figure A 2, and Figure A 3. In different test series, the ridge conditions are different. In total, 6 ridges were tested. The characteristics of these ridges were listed in Table 2.3, Table 2.4, Table 2.5, and Table 2.6. The major differences between these ridges are "*mean cross-sectional area*", "*Boundary condition (finite or infinite ridge)*", and "*ridge with/without ice management behind*". Here, the surge displacement will mainly be used to quantify the influence from ridge. Because the *ice accumulation* is very dominant during the ridge and structure interactions and the surge displacement could be viewed as the major indicator of the *ice accumulation load*.

Table 3.5 Surge responses in different ridge conditions

Test	#1120	#2120	#3120	#3140	#4120	#4140
Cross sectional area [m2]	863	1267	1138	1249	1270	1103
Max- surge displacement [m]	-13.87	-49.31	-32.93	-19.25	-41.51	-36.03
Boundary condition	Confined		Unconfined	Confined	Unconfined	

➢ Comparisons of maximum surge displacements with different cross-sectional area

When comparing the surge displacement between Test #1120 and Test #2120 in confined ridge conditions, it can be seen that a larger cross sectional area of the ridge leads to larger responses of the surge displacement.

Comparing the surge displacements among Test #3120, Test #4120 and Test #4140 in unconfined conditions, similar results can be obtained. The surge displacements of Test #4140 and Test #3120 are more or less the same since they have similar cross sectional area. But the surge displacement is much larger in Test #4120 since a much larger cross-sectional area was found in this test.

➢ Maximum surge comparisons with different boundary condition

Ridges in Test #2120 and Test #4120 have almost the same cross-sectional area, but different boundary conditions. We see from the maximum surge response, that the unconfined ridge induced less surge displacement compared with the confined ridge.

- The effect of ice management behind the ridge

The ridge in Test #3140 was specially treated by applying ice management behind the ridge. The cross-sectional area of the ridge in Test #3140 is very close to that of Test #2120, and they both have the same confined boundary condition. However, the maximum surge displacement in Test #3140 was reduced. The interaction process is shown in the following figures:

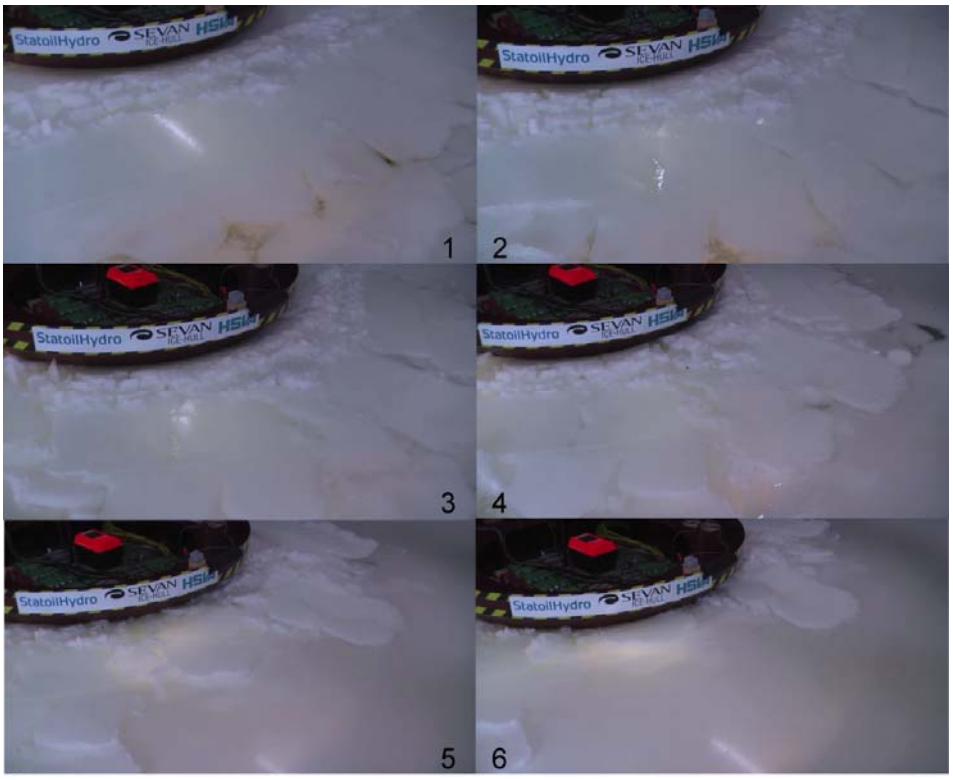

Figure 3.17 Illustration of structure interacting with ridge with ice management behind the ridge

As we can see from the above figure that when the structure enters the ridge, due to the ice management behind it, the ridge started to be deflected in a relatively easier way. The broken ice pieces behind the ridge were easily pushed forward and some even being pushed above the following intact level ice (rafting).

The explanation to all the previous observations is the same. In order to reduce the ridge influence on the structure's response, reducing the volume of the ice pieces that are needed to be cleared away is crucial. A confined ridge means a long ridge (the length is thought here to be perpendicular to the ice drift direction). When the structure is advancing through such a ridge, lots of ice pieces need to be mobilized. Similarly larger mean cross-sectional area means that a larger amount of broken ice pieces are required to be cleared away. Ice management, as shown in the table and the figure, can reduce the surge displacement. This is because the boundary condition behind the ridge has been changed. In this case, less

broken ice pieces are needed to be mobilized to make a path for the structure.

- Structure's responses in level ice after the ridge

Based on the previous observations, after exiting the ridge, the PSDs of all the responses become not as concentrated as before entering the ridge. This means that after exiting the ridge, the ice load has more components that are spreading in a wider range of the frequency domain. Moreover, in several cases as in Test #2130 (see Figure 3.5) and Test #3130 (see Figure 3.6), a comparatively more significant low frequency component has been observed in level ice after the structure exiting the ridge. This can be explained as after exiting the ridge, large amount of ice rubbles are accumulated around the structure. It takes a longer time to clear away such a huge amount of ice accumulation which cannot happen in common level ice. This will induce a relatively low frequency component in the structure's responses. In terms of the ice load components spreading in a wide range of the frequency domain, this may be induced by the fact that with the huge amount of ice accumulation just after exiting the ridge, the whole ice breaking, ice rotating, and ice clearing phase becomes more complicate. There is a larger "interface" with intact level ice and more other interaction processes (e.g. interactions between broken ice pieces) involved after exiting the ridge advancing in level ice. That might be the reason why more load components that are appearing in a wider frequency range.

3.3 Correlations between the structure's responses

In the previous Section 3.2, the emphasis was mainly put on the structure's response in level ice. The ridge condition was only slightly touched upon at the end of that section. Due to the short duration and less variation of the structural response in ridge condition, it seems not very suitable to do some frequency domain analysis. Instead, in this section, the correlations between the structure's responses will be calculated in different ice conditions to get some insights about the structure's response in different ice conditions.

3.3.1 Calculation method

The Normalized cross correlation is calculated between structural responses to quantify the similarity between different structure's response history.

$$\rho_{xy}(\tau) = \frac{1}{N}\sum \frac{[x(\tau)-\overline{x}][y(\tau+t)-\overline{y}]}{\sigma_x \sigma_y} \tag{3.1}$$

in which,

$\rho_{xy}(\tau)$	is the normalized cross correlation of the x and y series;
N	is the number of the discrete numbers in the x and y series;
$x(\tau)$ and $y(\tau)$	are the value of the x and y series;
τ	is the time lag between x series and y series, with different time lag τ, different normalized cross correlation will be calculated, the largest one of which describes how similar and with how much time lag these two series are;
$\overline{x}$ and $\overline{y}$	are average values of the x and y series.

The following two sets of correlation are to be calculated in this chapter

Set 1: *Cov<surge, pitch>;*
Cov<surge, heave>;
Cove<pitch and heave>

Set 2: *Cov<sway, roll>;*
Cov<sway, yaw>;
Cov<roll, yaw>;

The time series have been processed to eliminate the weak ice influence in the transition from open water to level ice. Approximately 5 m (Model scale) of the recorded values have been deleted from the beginning of the time history to skip the *run in time* and also a portion of the tank that has *temperate ice*, the remaining of which are left for analysis as shown in Figure 3.1. Calculations will be conducted in different ice conditions. The signal selections for all the tests are shown in Appendix A.

The software 'DIADEM' was used to calculate the normalized cross correlation of structural responses in various ice conditions according to the above mentioned methods. The calculation results and discussions will be presented in the following.

3.3.2 Calculation results

After calculating the afore-mentioned six pairs of normalized cross correlation in various

ice conditions with different time lag, the largest cross correlation values are identified together with the time lag. The results are presented in the following tables and figures.

- Surge and pitch responses

  The results are shown in the following table and figure:

Table 3.6 Normalized cross correlation of surge and pitch

Test	Test #1000	Test #2000	Test #3000	Test #4000
Level ice_1	-0.632	-0.56	-0.51	-0.444
Ice ridge_2	-0.884	-0.865	-0.901	-0.888
Level ice_3	-0.628	-0.73	-0.554	-0.426
Ice ridge_4			-0.893	-0.925
Level ice_5			-0.518	-0.596

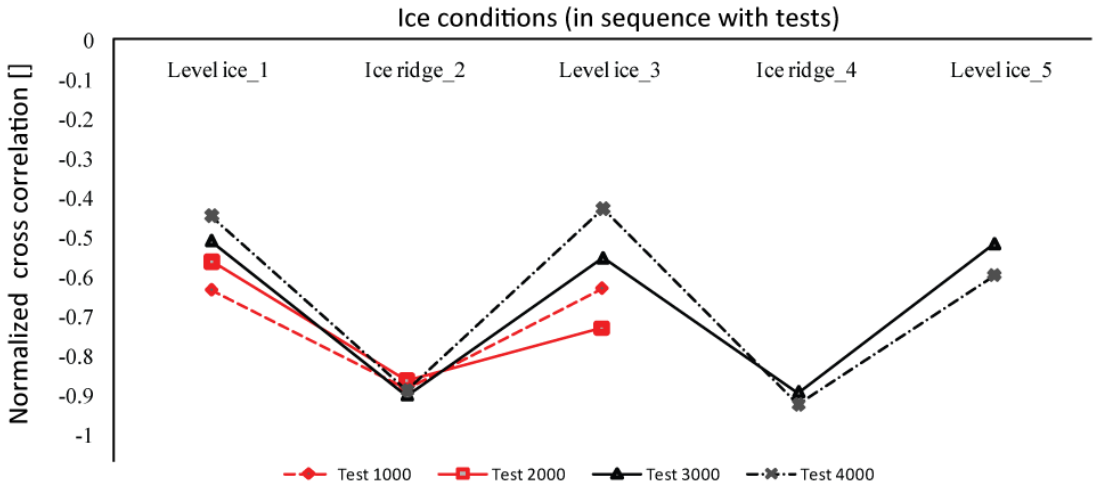

Figure 3.18 Normalized cross correlation of surge and pitch in various ice conditions

Table 3.6 and Figure 3.18 show that *Cov<Surge, Pitch>* are highly correlated. The time lag is 0 according to the calculation. They are negatively correlated since the positive surge direction is opposite to the structure's actual surge displacement in the test[12].

Furthermore, it can be seen in Figure 3.18 that *Cov<Surge, Pitch>* are larger in ice ridges than in level ice. The correlation coefficient is around -0.9 in an ice ridge and around -0.5 in level ice.

[12] see Figure 2.2 for the defined coordinate system for the test

- Surge and heave responses

The results are shown in the following table and figure:

Table 3.7 Normalized cross correlation of surge and heave

Test	Test # 1000	Test # 2000	Test # 3000	Test # 4000
Level ice_1	-0.32	-0.391	-0.368	-0.201
Ice ridge_2	-0.56	-0.753	-0.704	-0.706
Level ice_3	0.406	0.461	-0.223	0.343
Ice ridge_4			-0.419	-0.574
Level ice_5			0.535	0.479

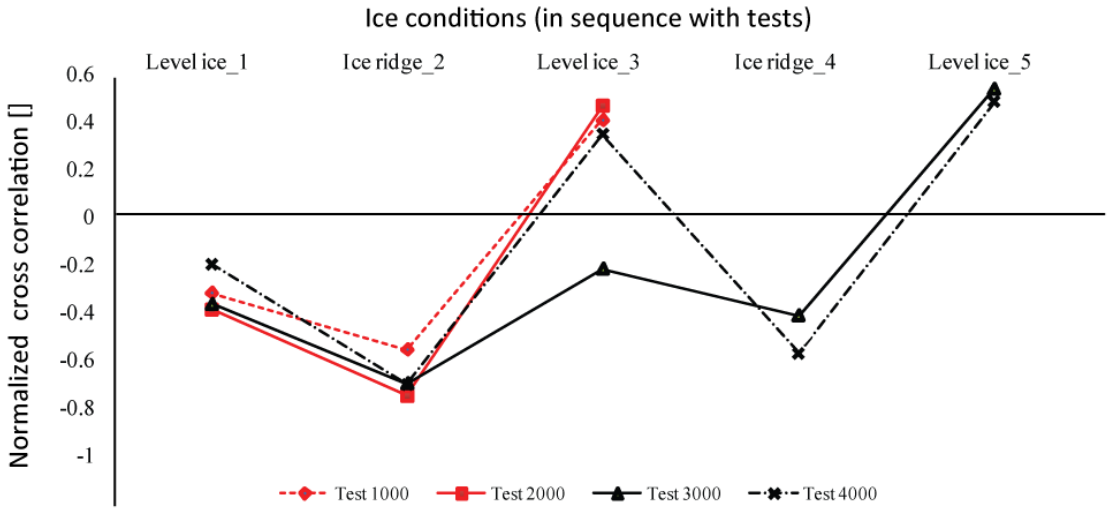

Figure 3.19 Normalized cross correlation of surge and heave in various ice conditions

The absolute values of the normalized cross correlation coefficient of <*Surge*, *Heave*> in level ice situations are around 0.5. And they are either positively correlated or negatively correlated. They are not as highly correlated as surge and pitch. In ice ridge, the correlation coefficients are higher, and they are negatively correlated with a correlation coefficient around -0.7.

- Pitch and heave responses

The results are shown in the following table and figure:

Table 3.8 Normalized cross correlation of pitch and heave

Test	Test # 1000	Test # 2000	Test # 3000	Test # 4000
Level ice_1	-0.39	0.32	0.27	-0.269
Ice ridge_2	0.582	0.818	0.713	0.767
Level ice_3	-0.348	-0.424	-0.329	0.464
Ice ridge_4			0.43	0.621
Level ice_5			-0.309	-0.389

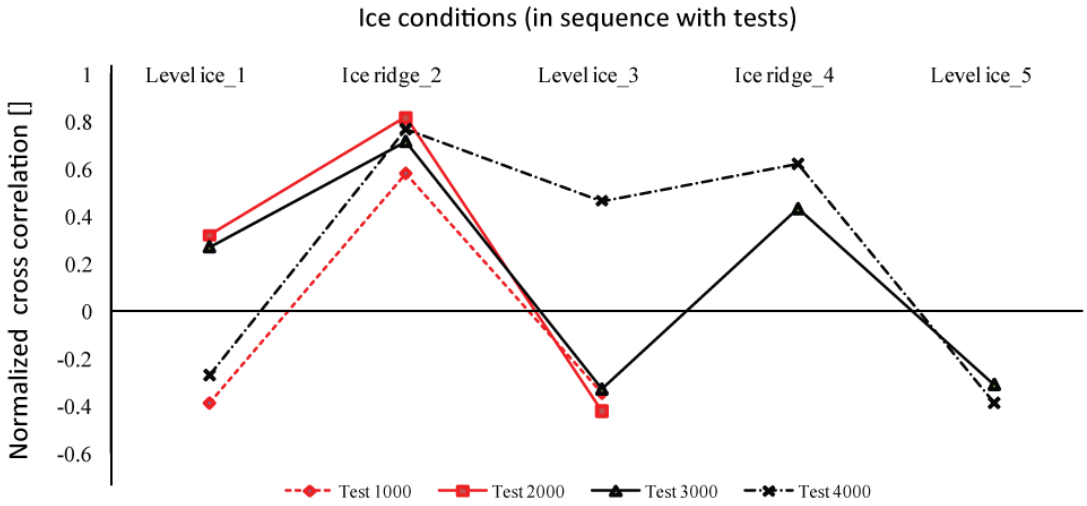

Figure 3.20 Normalized cross correlation of pitch and heave in various ice conditions

Similarly, <*Pitch, Heave*> are weakly correlated in level ice. The correlation coefficient is sometime positive, sometime negative with an absolute value around 0.4. However, in the ice ridge case, comparing with the level ice situation, pitch and heave are highly correlated with correlation coefficients between 0.5-0.8.

- Normalized correlation coefficient for sway, roll and yaw

The normalized correlation coefficients for sway, roll and yaw have no consistent trend being observed. The calculation results were shown in Appendix C with tables and figures. The discussions concerning these three responses will be given later.

3.3.3 Discussions

Based on the previous calculation results and comparisons in different ice conditions, the

observations are concluded here:

- In level ice, *Cov<Surge, Pitch>*, *Cov<Surge, Heave>*, and *Cov<Pitch, heave>* are not 100% correlated with each other. All three pairs of normalized correlation coefficients are around 0.4~0.5 in level ice.
- For all the above three pairs of normalized correlation coefficients among surge, heave and pitch, they are larger in ice ridge than in level ice. They are in the range of 0.6~0.9.
- For the other three pairs of normalized correlation coefficients among sway, roll and yaw, no obvious consistent trend was identified.

In order to explain the above calculation results, the ice load components and ice load transferring processes will be discussed in the following.

3.3.3.1 The ice load transferring processes

Before presenting the physical explanations of the above observations, a simple case with harmonic contact force $Nsin(\omega t)$ acting on the conical hull of the structure will first be discussed. This harmonic load can be viewed as a highly idealized periodic *ice breaking and ice rotating load*. This simple case is illustrated in the following

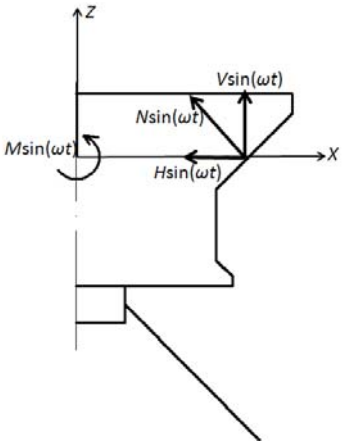

Figure 3.21 An illustration of external force in different direction[13]

In Figure 3.21, $Nsin(\omega t)$ *i*s the normal harmonic force, $Vsin(\omega t)$, $Hsin(\omega t)$ and $Msin(\omega t)$ are vertical, horizontal, and moment loadings decomposed from the normal force having the same frequency. The coordinate system has been shown in Figure 3.21 and a system with uncoupled mass and stiffness is assumed in this simple case. When taking into consideration of a constant hydrodynamic effect (added mass and added damping) of the system, the dynamic equation of the above system could be written as:

[13] This coordinate system is different from the one used to record the test results.

$$\begin{pmatrix} M & 0 & 0 \\ 0 & M & 0 \\ 0 & 0 & I \end{pmatrix}\begin{pmatrix} \ddot{x} \\ \ddot{z} \\ \ddot{\theta} \end{pmatrix}+\begin{pmatrix} B_{11} & B_{13} & B_{15} \\ B_{31} & B_{33} & B_{35} \\ B_{51} & B_{53} & B_{55} \end{pmatrix}\begin{pmatrix} \dot{x} \\ \dot{z} \\ \dot{\theta} \end{pmatrix}+\begin{pmatrix} K_{11} & 0 & 0 \\ 0 & K_{33} & 0 \\ 0 & 0 & K_{55} \end{pmatrix}\begin{pmatrix} x \\ z \\ \theta \end{pmatrix}=\begin{pmatrix} H\sin(\omega t) \\ V\sin(\omega t) \\ M\sin(\omega t) \end{pmatrix} \quad (3.2)$$

With the applied the harmonic load, solving this governing dynamic equation, the structure's responses are composed of two parts which are the *transient part* and the *steady state* (Chopra, 2005). The *transient responses* have the same frequency as the natural frequency[14] but this response will be dissipated away due to the damping effect. In the *steady state*, the responses of the structure have the same frequency as the external excitation force. In the current simple example, all three responses are suffering from the same loading frequency in their respective directions and they should have the same response frequencies. Then the correlation coefficients among all these three responses should be highly correlated[15]. However, the reality is far from this simple case.

Here the processes of ice loads' transferring to the structure will be discussed. Usually, between the interface of two objects, in the current case the ice and the structure, it is mainly the *normal contact force* and *shear force* that are transferred from one object to another. Usually the *shear force* (e.g. friction) has some relationship with the *normal force*, hence they can be assumed to be in same loading frequencies. Due to the different geometry of the interface, the amplitudes of the decomposed load components in different direction are different. For the current SEVAN FPU-Ice, two kinds of interface could be identified. These are the conical hull[16] (underwater part) and the vertical hull (the neck part) of the structure. The influences of ice loads on the structural responses will be introduced separately in the following:

[14] More precisely, the transit parts' frequencies are the damped frequencies. Since the damping ratio in different directions are different, so the transient response' frequencies are different in different directions. But this difference can be neglected here since the damping ratios are expected to be very small in all three directions as will be shown later.

[15] Attention: the response amplitude doesn't affect the correlation between two time series, eg, $A_1 sin(\omega t)$ and $A_2 sin(\omega t + \phi)$'s correlation is $cos\ (\phi)$, regardless of the difference between A_1 and A_2

[16] In the following discussion, the term conical hull means the underwater part of the overall conical hull.

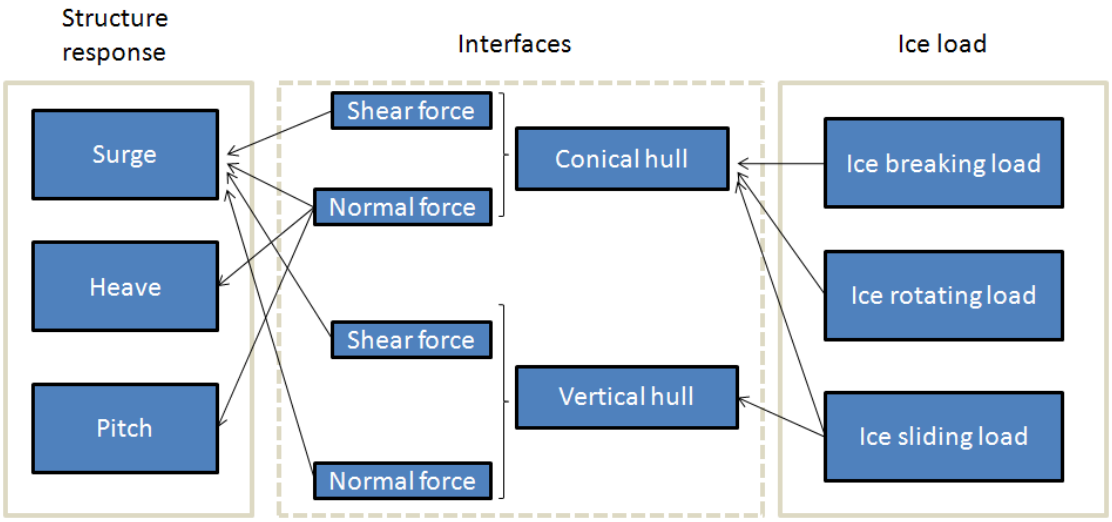

Figure 3.22 Flow chart of load transferring processes (from right to left)

- Influence on surge displacement

Since the most significant relative movement between the structure and ice is in the direction of ice drift, it is reasonable to assume that the major part of the *shear force* is acting horizontally, and the total effect of which is in the same direction as the ice drift. As shown in Figure 3.22, most of the shear forces are inducing the surge displacement.

The normal contact force acting on the 45° conical hull will be decomposed in surge, heave and pitch directions.

The total normal contact force acting on the vertical hull will only be acting in the surge direction. As shown in Figure 3.22, loads transferred by the vertical hull will induce mainly the surge displacement.

- Influences on heave and pitch displacements

As can be seen in Figure 3.22, the major load contributors to the heave and pitch displacements are normal forces transferred by the conical hull. Such normal forces have two major sources. One is from the *ice breaking and ice rotating load* and the other is from *ice sliding load*.

Concerning the *ice breaking and ice rotating load*, they are mainly acting on *half* of the 45° conical hull (only the bow region). After decomposition, they can be effectively transferred in horizontal, vertical and rotational directions. And these load components could reserve the original normal loads' frequencies.

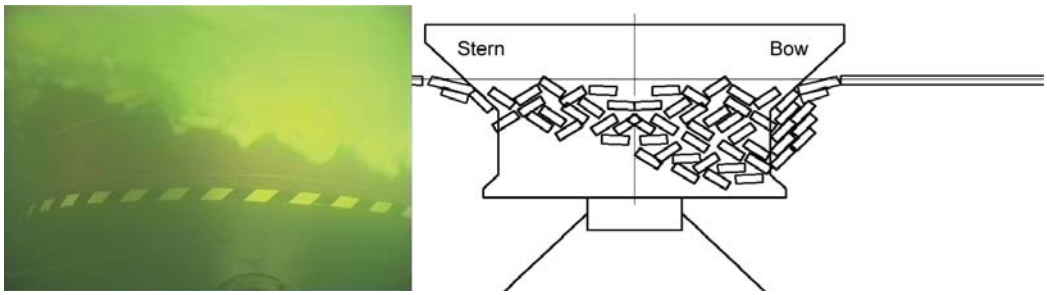

Figure 3.23 Illustration of ice accumulation based on the video of Test #1000

However, for the *ice sliding load*, it is acting nearly on the *whole* conical hull (both the stern and bow region of the structure, see Figure 3.23). This means that the *ice sliding load* can be effectively transferred in the vertical direction. In the rotational direction, certain portion of the broken ice pieces is accumulating in the "stern" of the structure. These *stern accumulated broken ice pieces* will offset the pitch moment induced by the *bow accumulated ice pieces.* Thus the *ice sliding load* is less effectively transferred as pitch moment. And the pitch moment reserves less frequency characteristics of the *ice sliding load*.

As will be pointed out in Chapter 5, two major contributors of the total ice load are the *ice rotating load* and the *ice sliding load.* Generally, the *ice rotating load* has a higher dominant frequency than the *ice sliding load*. Based on the above ice load transferring processes, it can be found that:

- The surge response is influenced mostly by the *ice sliding load* (from both vertical and conical hull; both normal force and shear force). And the *ice rotating load* also has some influence on the surge displacement. This is in agreement with the previous observation that the surge displacement has a relatively significant low frequency component around the structure's pitch natural frequency region
- The pitch displacement is mainly influenced by the *ice rotating load*. Another major contributor, the *ice sliding load,* becomes less dominant due to the *self-balance* phenomena as shown in Figure 3.23. This also explained why the dominant pitch response frequency has stronger relationship with the *ice rotating frequency*[17].
- The heave response is influenced by both the ice rotating load and ice sliding load. This explains why in the previous frequency domain analysis, on both high and low frequency, there are more or less similar PSD values in both low and high frequency bands.

It should be noted that the above discussions and conclusions have been highly idealized

[17] For detailed pitch response frequency discussion, please refer to the previous chapter.

so as to highlight the major contributors to different structural responses. In reality, they are interacting with each other, meaning the load transferring paths can connect any two items shown in Figure 3.22.

3.3.3.2 Discussion about the correlations between different structural responses

Based on the previous theoretical discussion about load transferring processes, it is found that the surge response is mainly influenced by the *ice sling load* and a small portion of *ice rotating load*; pitch response is mainly induced by the *ice rotating load*; heave response is influenced by both *ice sliding* and *ice rotating load.*

In level ice, as will be pointed out later, the *ice rotating load* and *ice sliding load* are the two major contributors of the total ice load. So, in level ice, each structural response has its own dominant loading source with different dominant frequencies. Furthermore, there is a certain portion of the ice load being transferred by the conical hull which brings some similarities in each of the structural response. This explained why the normalized correlation coefficients between different responses are neither 1 nor 0. In the following, a simple example will be utilized to verify the above reasoning and also get a possible quantitative feeling about the ice load components' influences.

- **A simple example to illustrate the influence of the idealized *ice sliding load* and *ice rotating load*.**

This example is based on Figure 3.2, the frequency domain analysis of Test #1000. The assumption behind this analysis is that:

- It is mainly the *ice sliding load* and *ice rotating load* influencing the structure's responses;
- Different responses have different major contributors from the total ice load. In brief, surge is mainly influenced by *ice sliding force*; pitch is mainly influenced by *ice rotating load*; and heave is influenced by both; hence the dominant frequency of surge will be viewed as the dominant frequency for *ice sliding force* and the dominant frequency of pitch response will be viewed as the dominant frequency for *ice rotating load*;
- The *ice sliding load* and *ice rotating load* will be assumed to be harmonic load in this example. Accordingly, the responses of the structure will be treated as harmonic responses;
- The amplitude of the response is assumed to equal to the *square root* of their maximum

PSD respectively.

Based on the above assumptions, the following procedures are adopted to construct the *harmonic* responses of the structure.

- Identify the *ice sliding load* frequency and *ice rotating load* frequency based on the dominant surge frequency and pitch frequency respectively;
- Extract the maximum PSD of each response in the above two frequency band;
- Based on the above available amplitudes and frequency, creating 1000 s long signals representing the surge, heave and pitch responses respectively.
- Calculating the normalized cross correlation of the above artificially constructed responses series and comparing with the actual value in Test #1000 and give comments.

The results are shown in the following table and figures:

Table 3.9 Amplitude and dominant frequency extracted from Figure 3.2

	Ice sliding load			Ice rotating load		
	PSD_max	Amplitude	Frequency	PSD_max	Amplitude	Frequency
Surge	14.84 m2s	3.85 m	0.004 Hz	0.357 m2s	0.60 m	0.09 Hz
Heave	0.592 m2s	0.77 m	0.004 Hz	0.382 m2s	0.62 m	0.09 Hz
Pitch	2.57 deg2s	1.6	0.004 Hz	7.16 deg2s	2.68	0.09 Hz

Based on the information in the above table, the *idealized* surge, pitch and heave displacement could be constructed by the following equations:

$$surge = 3.85\sin(2\pi \times 0.004x) + 0.6\sin(2\pi \times 0.09x) \tag{3.3}$$

$$heave = 0.77\sin(2\pi \times 0.004x) + 0.62\sin(2\pi \times 0.09x) \tag{3.4}$$

$$pitch = 1.6\sin(2\pi \times 0.004x) + 2.68\sin(2\pi \times 0.09x) \tag{3.5}$$

In the above equations, on the right-hand side of the equation, the first term represents the low frequency part induced by the *ice sliding load*; the second term represents the high frequency part induced by *ice rotating load*. The parameter in front of each of the *sine* term represents the contribution from each frequency. As can be seen from the equation for surge displacement, more contributions are from the low frequency part. Similarly, for heave, the contributions from both frequencies are very close; for pitch, more contributions are from the high frequency part. Based on these equations, the artificial responses are shown in the following figure:

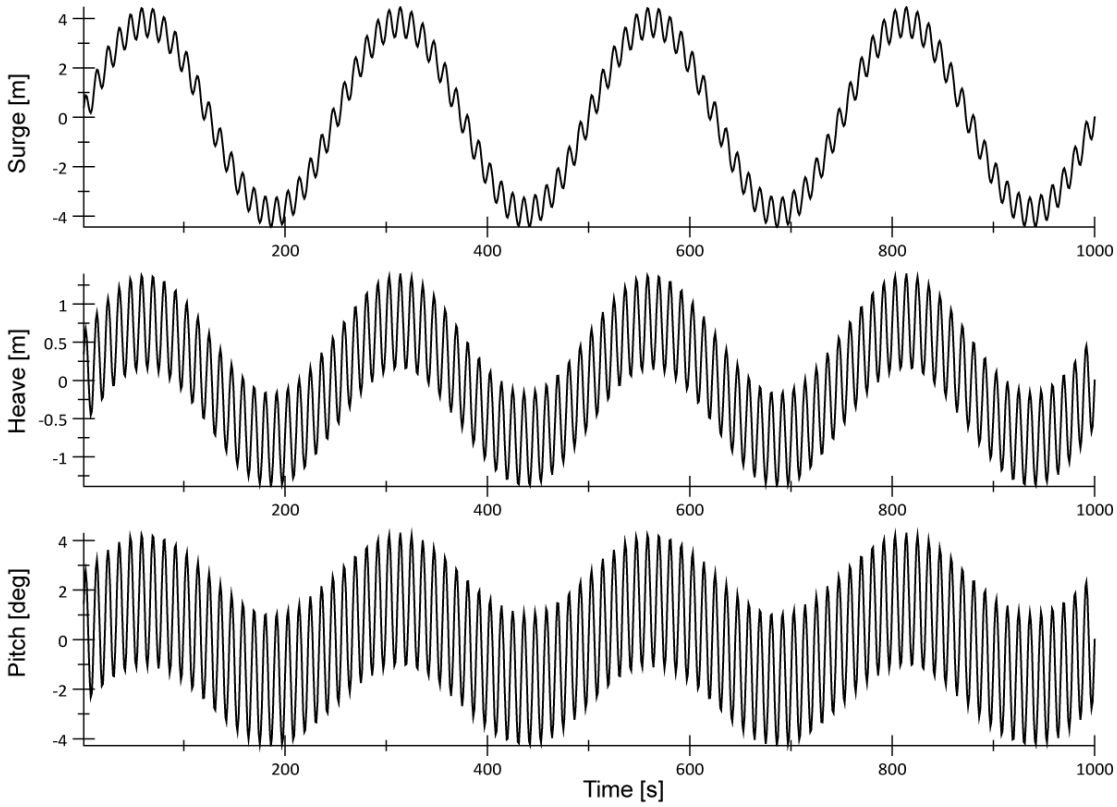

Figure 3.24 The idealized harmonic responses of the structure

Then calculating the normalized cross correlation of the above artificial responses and comparing with the actual values. The comparisons are shown in the following table:

Table 3.10 Comparisons of normalized cross correlation between the artificial response and actual responses

	Artificial value	Actual value
Cov <Surge Pitch>	0.639	0.632
Cov <Surge Heave>	0.866	0.32
Cov <Pitch Heave>	0.938	0.39

Table 3.10 shows that very good agreements were found for *Cov<Surge, Pitch>*. The other two correlations are not well predicted. This may due to an inappropriate estimation of the heave response by the previous Equation(3.4). As we can see from the PSD distribution of these responses in Figure 3.2, surge and pitch have relatively more concentrated PSD, hence they can be represented by the dominant frequency part better than the heave response whose PSD is spreading in a wider range. This may be because the *ice sliding load* and *ice rotating load* in the heave direction are on a same level, which may further complicate the ice load frequencies by interacting with each other. So, we can assume that Equation(3.3) and

Equation(3.5) are reliable and the normalized cross correlation between surge and pitch is also reliable.

Based on comparisons of the above results, especially the good agreement of *Cov<Surge, Pitch>*, and also the discussions about the reliability of the results, the previous conclusions are further verified and extended in the following:

- The main reason for the normalized correlation coefficients in level ice are in the range of 0.4~0.5 are because different responses are induced by different dominant load contributors who are of different dominant frequencies;
- For surge, it is mainly influenced by the low frequency *ice accumulation load*;
- For pitch, it is mainly influenced by the relatively high frequency *ice rotating load*;
- For heave, it is influenced by both *ice accumulation load* and *ice rotating load*. However, these two loads are on the same scale in level ice, they may interact with each other in a more complicated way. Then we can expect that the heave responses cover a relatively wide range.

- **Structural responses' correlations in different ice conditions**

As pointed out before, the normalized correlation coefficients for surge, heave and pitch in ridge condition are larger than in level ice. They are in the range of 0.6~0.9.

Based on the previous discussion about the ice load transferring processes and also the simple example which was used for level ice case verification, the above observation can be easily explained here. In level ice, the *ice sliding load* and *ice rotating load* are the dominant load components. However, in ice ridge, it is mainly the *ice sliding load* that is dominant. This means that all three responses are mainly influenced by the *ice sliding load*. Then it is natural to expect that all three responses have similar dominant frequencies and hence a larger correlation could be found among surge, heave and pitch in ice ridge.

- **Normalized cross correlation coefficient for sway, roll and yaw**

For the *<sway roll>*, *<sway yaw>* and *<roll yaw>* correlation values, no obvious relationships have been identified. This might due to the randomness of these responses. For a symmetric structure as in the current case, when suffering from symmetric loads, there will be no sway, roll and yaw responses at all. In reality, the structure is also suffering from some random ice loads that are induced by the inhomogeneous ice strength in different directions; uneven distributions of the submerged broken ice and pressure difference in the wake area. The sway, roll and yaw responses are mainly induced by these

random ice loads. Accordingly, it is difficult to identify obvious relationship between the structures' sway, roll and yaw displacements.

In the previous two chapters, the focus was put on the structure's responses. The recorded responses, especially the surge, heave and pitch displacements in *level ice* were analyzed in the frequency domain in Chapter 2. Then in Chapter 3, these responses are further compared in *different ice conditions* by calculating the normalized cross correlation coefficients. Based on the previous two chapters' analysis, a very general ice structure interaction processes has been identified. This includes the ice loads transferring processes; the relationship between different structural responses and different ice load components.

In the next chapter, the emphasis will be put on the dynamic system of the moored structure in level ice. The moored structure's hydro-dynamic characteristics, hydro-static characteristic, mooring load and ice load will be further investigated.

4 Dynamic characteristics of the SEVAN FPU-Ice Buoy

In relation to ice interaction the dynamic characteristics of the moored conical structures are of great interests in comparison with fixed structures. The major difference between static and dynamic problems is the presence of inertia force. One major question in the beginning of this chapter would be what kind of role is the inertia force playing in the interaction processes? The answer to this question would especially of great interest for the gigantic SEVAN FPU-Ice Buoy which has a large mass of up to about 172700 mT (metric ton) in ice draft conditions.

For simplicity reasons, all the analysis in this chapter will be made in the surge direction only. The results of which will be generalized to other degree of freedoms. Calculation in the surge direction will be conducted to answer the above questions. With the known governing dynamic equation in the surge direction as Equation(4.1), different terms in this equation will further be analyzed.

$$(M+A_{11})\ddot{\eta}+B_{11}\dot{\eta}+C_{11}\eta+F_{mooring}=F_{ice} \tag{4.1}$$

In which

M	is the mass of the structure, which is 172700000 kg;
A_{11}	is the added mass in surge direction;
B_{11}	is the added damping in surge direction;
C_{11}	is the hydrostatic stiffness in surge direction, which can be treated as 0;
η, $\dot{\eta}$, and $\ddot{\eta}$	are the displacement, velocity and acceleration in surge direction;
$F_{mooring}$	is the mooring force in the horizontal direction;
F_{ice}	is the total ice load in the horizontal direction;

As can be seen from the above equation, for the moored structure working in icy waters, the hydrodynamic effects are important during the interaction process. So in the first section of this chapter, the hydrodynamic coefficients will be calculated.

4.1 The buoy's hydrodynamic and hydrostatic properties

At first, the buoy's added mass, added damping and hydrostatic stiffness are calculated using HYDRO-D. The models are shown in Figure 4.1.

Here, in order to show the hydrodynamic effects of the bilge, two models (model with/without bilge) are built in the HYDRO-D and the results are shown in Figure 4.1 and Figure 4.2.

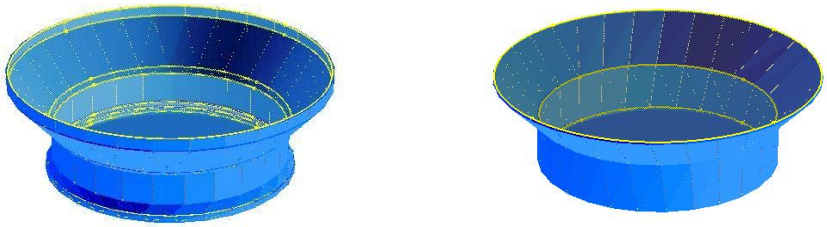

Figure 4.1. The model of the SEVAN FPU-Ice in HYDRO-D

(*left:* with bilge; *right*: without bilge)

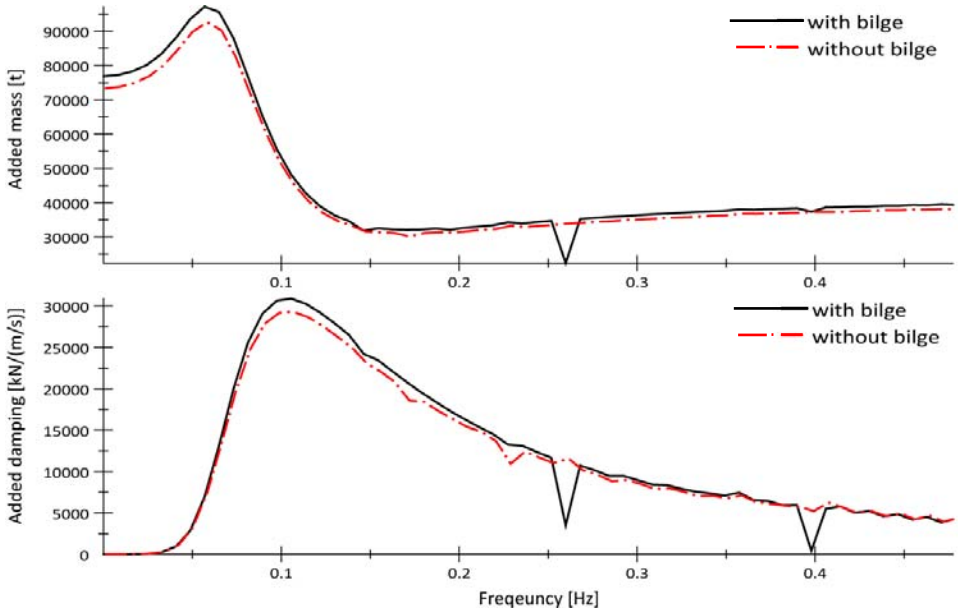

Figure 4.2. The hydrodynamic properties of two different models in surge direction

As can be seen from the above two figures, the hydrodynamic coefficients of these two models are generally similar except that for the model with bilge, several sudden changes are observed. These sudden changes are thought to be induced by the bilge. In Figure 4.2, only the *added mass* and *added damping* in surge directions are shown. Actually all the

hydrodynamic coefficients in all 6 DOFs were calculated and 3 of them (surge, heave and pitch directions) together with the calculated hydrostatic stiffness are listed in Appendix D.

These calculated values will be used in the numerical model which will be constructed in Section 5.3.2.

In this chapter, again for simplicity reasons, the added mass and added damping will be treated as constant values. Based on the previous analysis, the dominant surge response frequency is about 0.004 Hz. The added mass is about 77000 t and the added damping is very small (around 0.5 kN/(m/s)). So in the forthcoming calculation, the added damping part will be neglected, and the added mass will be taken as 77000 t.

4.2 Analysis of the dynamic forces

Within dynamic Equation(4.1), except the ice load, all the other terms are already known. Based on the already known surge acceleration history, surge displacement history, mooring force history, and the already known coefficients as shown below, the ice load history could also be back calculated.

The values of the coefficients are

$A_{11} = 77000\,000$ kg

$B_{11} = 500$ N/(m/s) and will be treated as 0

$M + A_{11} = 172700000 + 77000000 = 249700000$ kg

$C_{11} = 0$ N/m

The mooring force history and structural response history will be chosen based on Test #1000. The ice load will be calculated according to Equation(4.1), and then the mooring force and ice load are depicted together in Figure 4.3. From the upper figure, it can be seen that the mooring force does not always equal the ice load; and the ice load varies at a much faster pace than the mooring force.

In level ice (middle part of Figure 4.3), the ice load has larger variation amplitudes than the mooring force. From the value it can be seen that sometime the ice load is larger than the mooring force and sometime it is smaller than the mooring force. The difference between the mooring force and ice load is due to the influence of the inertia force.

In ice ridges (lower part of Figure 4.3), the mooring force varies much slower than it used to

be in level ice. At the peak of the mooring force, it seems to have same values with the ice load, meaning at this time point the inertia force is around 0 and there is less dynamic effect when the peak ridge load was encountered. Similarly, the difference between the mooring force and ice load is due to the influence of inertia force.

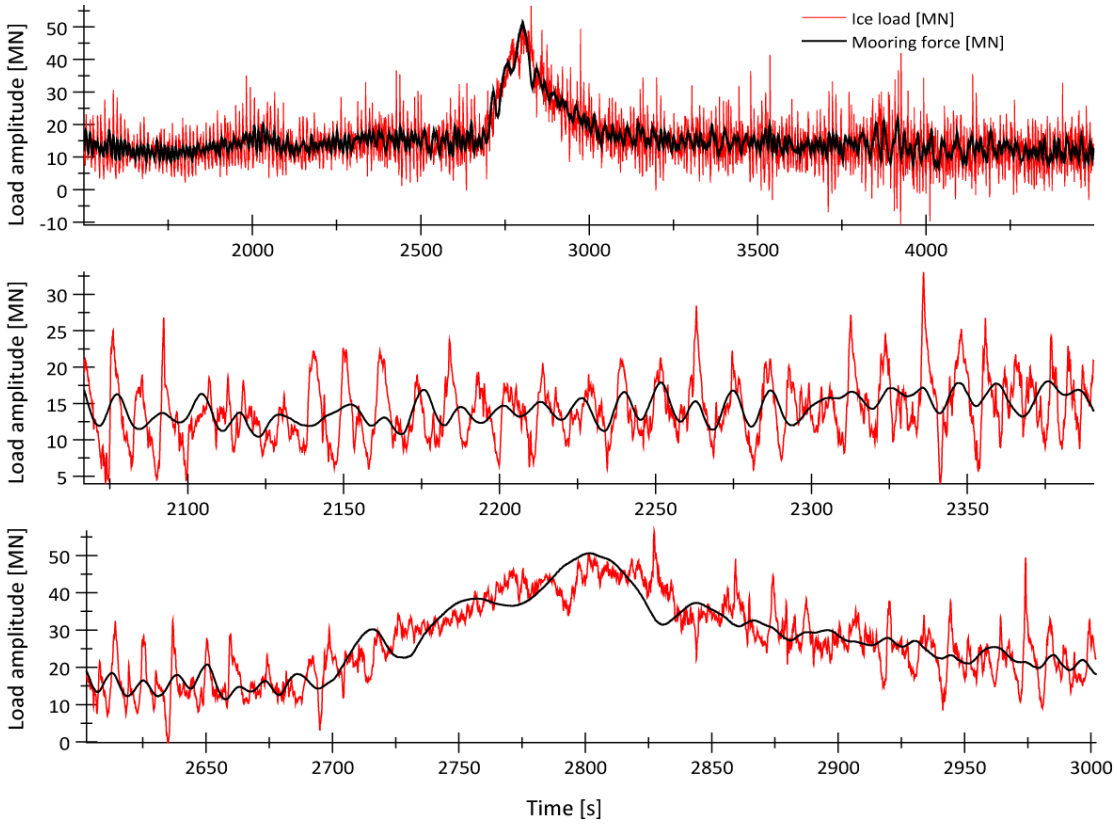

Figure 4.3 Mooring force comparing with ice load based on Test #1000

(*Upper:* overall time history comparison; *Middle:* comparison in level ice; *Lower:* comparisons in ice ridge)

One striking observation in both level ice and ice ridge is that the mooring force is not always larger than the ice load nor the ice load is always larger than the mooring force.

In order to get a clearer understanding about the ice load, mooring force and inertia load, the results of which in level ice of Test #1000 were further transformed in the frequency domain as shown in Figure 4.4 together with their time domain records.

From the PSD figure of these forces, it is found that for all three loads, there is a large PSD value around the frequency 0.09 Hz (11.11 s). This value is very close to the dominant pitch response frequency and also was assumed to be the *ice rotating* frequency. For mooring forces, it has a low dominant frequency 0.004 Hz (250 s) which is the same as the dominant surge response frequency and was thought to be induced by *ice sliding load*.

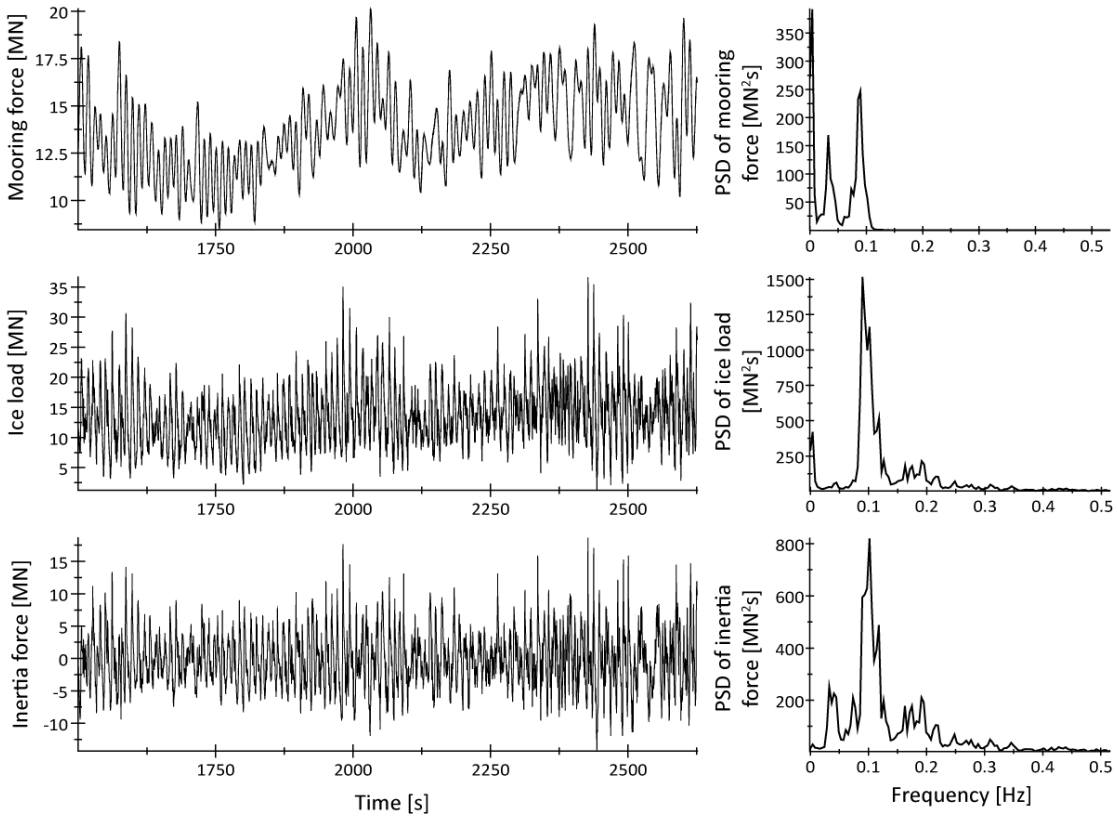

Figure 4.4 Frequency domain comparisons of mooring force, ice load and inertia force based on Test #1000 in level ice

4.3 Discussions about different dynamic forces

Based on the previous analysis of mooring force, ice load and inertia force in both time domain and frequency domain, the important observations are listed here:

- In both level ice and ice ridges, the mooring force is not always larger than the ice load nor is the ice load always larger than the mooring force.
- Two major frequency bands that have dominant PSD values for the ice load were identified from Figure 4.4. The lower one is the same as the surge dominant frequency (0.004 Hz); another is the same as the pitch dominant frequency (0.09 Hz). Moreover, the inertia load's dominant frequency is also 0.09 Hz and mooring force's dominant frequency is 0.004 Hz.

The first observation actually tells the influence of the inertia force during the ice breaking processes. The difference of mooring force and ice load is the inertia force based on Equation(4.1). The inconsistent relationship between the mooring force and ice load is because the inertia force's direction is always changing during the interaction processes.

The inertia load could be viewed as a double-edged term in ice breaking. When it is acting against the ice drift direction, it is helping to break the ice and hence the mooring force was expected to be lower than the ice load; on the other hand, when it is acting towards the ice drift direction, larger mooring force is expected. This explains the question posed in the beginning of this chapter.

The second observation in the loading analysis could be discussed together with the previous response analysis. This will give a much clearer relationship between different load components and also the responses. Concerning the dynamic load frequency analysis part, as can be seen from Figure 4.4, the high frequency part of the ice load was counterbalanced by both the mooring force and the inertia force, and the low frequency part of the ice load was mainly counterbalanced by the mooring force part. As pointed out before in the structural response analysis, the high frequency (0.09 Hz) part of the ice load is due to *ice rotating load*, and the low frequency (0.004 Hz) part is due to *ice sliding load*. It can be further inferred that: the *mooring force* is crucial to offset the *ice sliding load*; the *mooring force* and *inertia force* are crucial to offset the *ice rotating load*. The relationship between the ice load components and structural force terms are generalized in the following

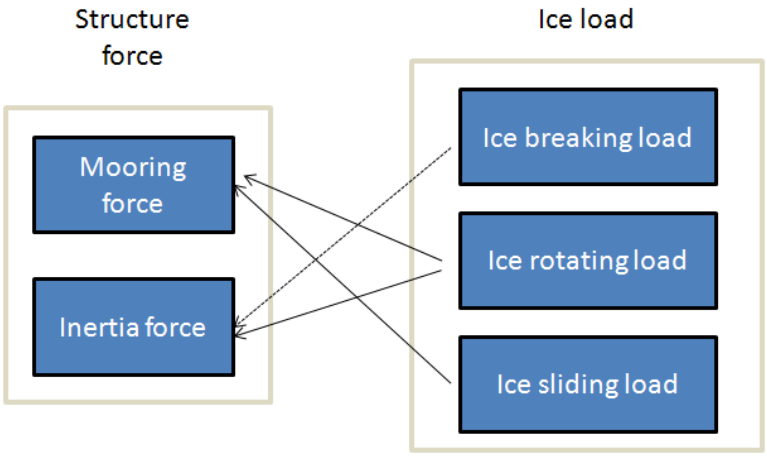

Figure 4.5 The major offset relationship between the ice load and structural force[18]

In the previous Chapter 3 and Chapter 4, the analyses were mainly based on the model tests data. Based on the analysis, different ice load components' characteristics were given; the interaction processes of ice and structure was also covered; and the relationship between different ice load components and different structure's reacting forces was also discussed. All of these analyses together would draw a much clearer picture about the ice and conical

[18] Currently, there is no data for ice breaking load. Since the ice breaking load has a very short duration, appearing like an impulse, it is estimated to be mainly counterbalanced by the inertia force of the structure. Since no data is available, then the arrow pointing to inertia force was drawn in *dashed* arrow line.

interaction processes. In the next chapter, we will go one step further to reconstruct the above process (level ice and moored conical structure) in a numerical model. This would bring us much more quantitative understanding about the whole level ice and moored conical structure interactions.

5 A numerical model of the level ice and moored conical structure interaction

5.1 Introduction

Different from a fixed conical structure, for a moored model, when interacting with ice, its relatively large response will further complicate the interaction processes. In order to predict the responses of the structure and also its influence on ice actions, a numerical model was developed in this chapter.

In the beginning of this chapter, some historical review about level ice-ship interaction processes will be given. Then some useful knowledge will be borrowed from this area based on which new level ice and conical structure interaction will be discussed. Afterwards, the level ice-moored conical structure interaction processes will be programmed using MATLAB. The output of this numerical model will be the ice load history and structural responses' histories which will be compared with the test results.

5.2 Theories

In the beginning of this section, some historical review about the level ice-ship interaction results will be given. Then the level ice-conical structure interaction theories will be given based on the borrowed knowledge from and comparisons with level ice-ship interactions.

5.2.1 Level ice-ship interactions

5.2.1.1 General introductions

The ice load a ship encountered could be estimated from similar shape ship and similar ice conditions; or from model tests; or from analytical model. The ice load mainly depends on the hull geometry, ice thickness, ice strength, dynamic friction of ice-hull interface, and the speed of the ship (Løset, 1995).

Enkvist (1983) estimated the total ice load by the following formula:

$$F_{tot} = (F_c + F_b)(1+1.4\frac{v}{\sqrt{gh}}) + F_s(1+9.4\frac{v}{\sqrt{gL}}) \quad (5.1)$$

In which the speed dependence was considered, and three different contributions to the total ice load were identified:

F_{tot} is the total ice load;

F_c is the ice load from crushing;

F_b is the ice load from bending;

F_s is the ice load from submergence of the broken ice pieces.

From this formula it also be seen that the Froud number is very important during the ice-ship interaction processes.

5.2.1.2 Level ice-ship interaction processes and load components calculation method based on Kotras (1983)

Kotras (1983) developed a numerical model to calculate different load components of the total ice load for a ship advancing in level ice. In the description of his model, he identified the following processes of level ice-ship interactions (see Figure 5.1).

- In the initial contact, the intact level ice start to crush slightly;
- And the level ice was also deflected by the advancing ship while the crushing continues;
- At certain point when the internal stress of the level ice exceeds its flexural strength, it breaks; In Kotras's paper (1983), the ice breaking pattern was assumed to be cusps and wedges breakings.
- When the broken ice pieces are rotating downwards by the ship, a void space may appear above the broken ice pieces due to the inability of water flushing in the void space immediately; During the rotating of the broken ice pieces, the ventilation also increases;
- When the broken ice pieces become parallel to the ship hull, and a new intact level ice having the initial contact with the ship, the above mentioned whole processes begin anew.

During the whole processes, three load components of the total ice load were identified:

- Breaking of ice;
- Turing of broken ice floes;
- Submergence of broken ice floes;

These loads were acting on the ship in a form of both normal and frictional force. In detail, during the whole process, the force involved include *the force generated by crushing of the ice sheet, ventilation above the broken ice floe, buoyancy of the ice pieces, viscous drag of the ice floes, and acceleration of the broken ice masses*. These forces were written explicitly in Kotras's numerical model.

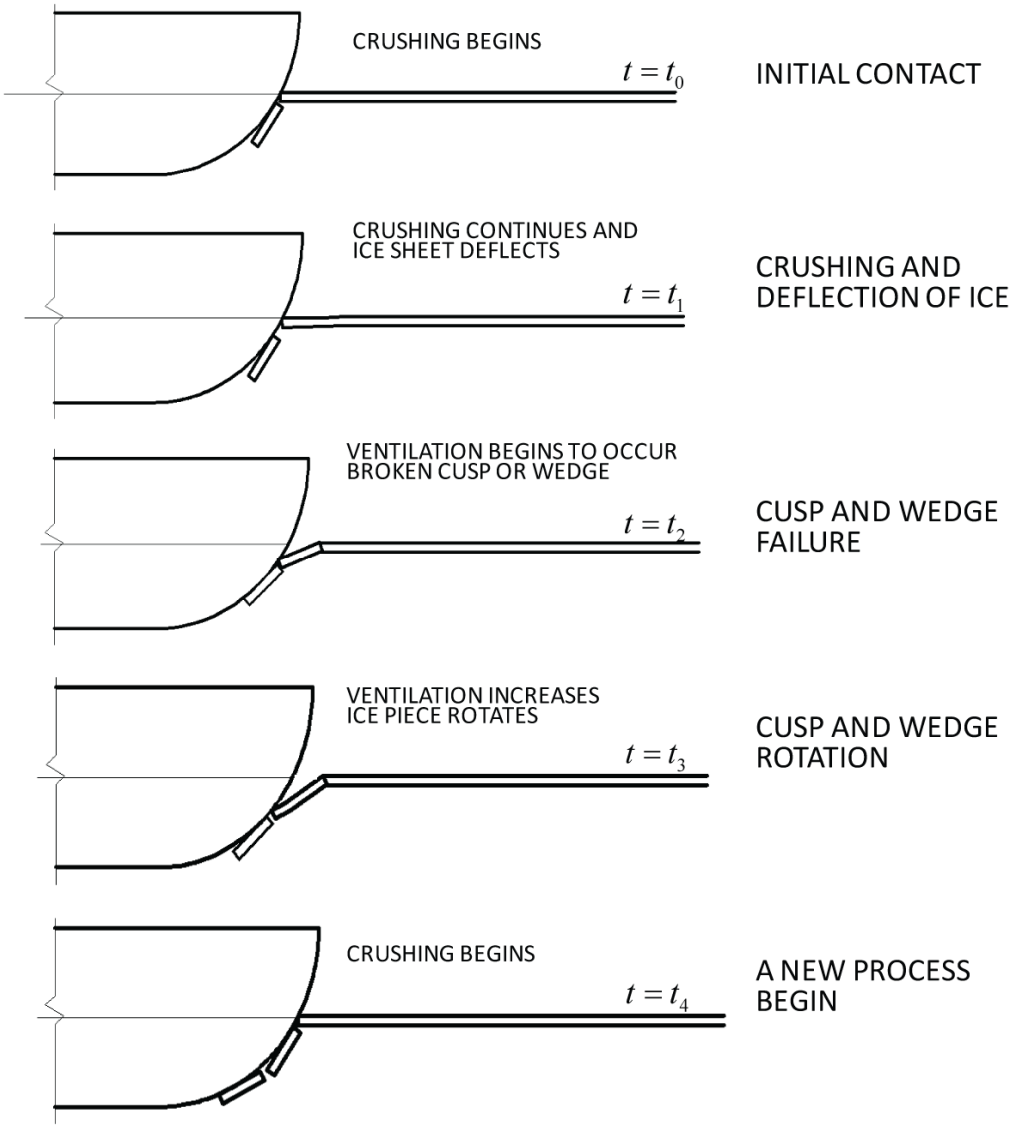

Figure 5.1 Depiction of icebreaking process (Kotras, 1983)

The numerical model constructed in Kotras's paper was mainly composed of the ice breaking model, floe turning model and floe submergence model. In each model, the participated load

components were written explicitly.

- Ice breaking model

In this model, it is mainly the ice breaking load involved. Two kinds of ice breaking shape, the cusps and wedges, were defined and treated separately. The ice breaking loads in normal and frictional direction were written as:

$$\begin{aligned} R_B &= 2\sum_{i=1}^{N_{cusp}} R_{B_{cuspi}} + 2\sum_{i=1}^{N_{wedge}} R_{B_{wedgei}} \\ R_{B_f} &= 2\sum_{i=1}^{N_{cusp}} R_{B_{fcuspi}} + 2\sum_{i=1}^{N_{wedge}} R_{B_{fwedgei}} \end{aligned} \tag{5.2}$$

In which

$R_{B_{cuspi}}$ is the *ith* cusp shape ice breaking load induced normal resistance;

$R_{B_{wedgei}}$ is the *ith* cusp shape ice breaking load induced normal resistance;

$R_{B_{fcuspi}}$ is the *ith* wedge shape ice breaking load induced frictional resistance;

$R_{B_{fwedgei}}$ is the *ith* wedge shape ice breaking load induced frictional resistance;

These ice breaking loads are relevant to the shape, size of the broken ice floes, and also the ice strength. Furthermore, it is also time dependent; the ice breaking loads are different at different time. The concept of 'PITCH[19]' was introduced in the detailed calculation formula to represent the time dependent of this ice breaking load.

- Turning resistance model

In this phase, the load components involved include:

- The buoyancy of the broken ice pieces;
- Combined effects from hull induced pressure field (e.g. bow wave) and ventilation;
- Viscous drag;
- Inertia force when turning the broken ice mass.

The total ice load calculated by this model is based on the following formula. Since some calculation methods was borrowed from here, this part will be introduced into more detail comparing with the ice breaking load.

[19] Definition of PITCH: *when the ship has advanced a distance equal to the pitch, a breaking cycle for each row of cusps and wedges begins anew.*

$$R_T = 2\sum_{i=1}^{N_{cusp}} R_{T_{cuspi}} + 2\sum_{i=1}^{N_{wedge}} R_{T_{wedgei}}$$
$$R_{Tf} = 2\sum_{i=1}^{N_{cusp}} R_{T_{fcuspi}} + 2\sum_{i=1}^{N_{wedge}} R_{T_{fwedgei}} \tag{5.3}$$

where

$$R_{T_{cuspi}} = \sum_{j=1}^{N_{increment}} \frac{1}{PITCH_i}(\vec{P}_{N_{ij}} \bullet \vec{i})\delta_j$$
$$R_{T_{fcuspi}} = \sum_{j=1}^{N_{increment}} \frac{1}{PITCH_i}((\mu P_{N_{ij}}) \bullet \vec{t} \bullet \vec{i})\delta_j$$
$$R_{T_{wedgei}} = \sum_{j=1}^{N_{increment}} \frac{1}{PITCH_i}(\vec{P}_{N_{ij}} \bullet \vec{i})\delta_j \tag{5.4}$$
$$R_{T_{fwedgei}} = \sum_{j=1}^{N_{increment}} \frac{1}{PITCH_i}((\mu P_{N_{ij}}) \bullet \vec{t} \bullet \vec{i})\delta_j$$

where a common term $P_{N_{ij}}$ was found[20]. It represents the normal force of the *ith* cusp at *jth* increment in direction normal to the hull; μ is hull-ice friction coefficient; $\vec{t}$ and $\vec{\imath}$ are unit vectors in the tangent of and in the direction of ice movement. *PITCH* is the same definition as before. From the above Equation(5.4) the load's time dependent could be found in the ratio between the pitch increment δ_j over *PITCH.*

The common term $P_{N_{ij}}$ is calculated based on:

$$P_{N_{ij}} = P_{1N_{ij}} + P_{2N_{ij}} + P_{3N_{ij}} + P_{4N_{ij}} \tag{5.5}$$

in which

the first term $P_{1N_{ij}}$ represents the buoyancy from the broken ice pieces;

the second term $P_{2N_{ij}}$ represents the force induced by the combined effects from both the hull induced pressure (e.g. bow wave) and ventilation;

the third term $P_{3N_{ij}}$ represents viscous drag force;

the forth term $P_{4N_{ij}}$ represents inertia force;

Since in the following, the method to calculate the viscous drag force on the conical structure is borrowed here, the original viscous drag force calculation method in Kotras's paper will be further written and discussed in the following:

$$P_{N_{3ij}} = 0.1575\rho_w C_d U_t^2 D_{Ci} W_{Ci} / \cos\delta_{ij} \tag{5.6}$$

[20] The calculation methods of this term are different for cusp-shape broken floes and for wedge-shape broken floes.

This formula is to calculate the viscous drag force of a *cusp shape* broken ice floe[21] based on classical method taking into consideration the shape of the broken ice pieces. In the formula:

ρ_w is the density of water [kg/m^3];

C_d is the drag coefficient assuming to be 1;

U_t is the velocity of the broken ice floe [m/s];

D_{ci}, W_{ci} are the cusp depth and cusp width respectively with unit [m]. They are used to describe the shape of the broken ice floes.

δ_{ij} is the angle between the hull and ice sheet at pitch increment *j* for *i*th cusp.

Other load components as shown in Equation(5.5) could be calculated based on their physical meaning according to classic theories in the *level ice-conical structure interaction* numerical model to be introduced soon.

- Submergence resistance model

When the broken ice floes were rotated paralleling to the ship hull, due to the long body of the ship, the submerged broken ice pieces will keep sliding along the hull of the ship. The load in this model was calculated in a simple way in Kotras's model. Only the buoyancy of the broken ice pieces was considered.

Kämäräinen's (2007) research concerning the ice load during this ice sliding processes as will be introduced at a later stage.

5.2.1.3 The weight of different ice load components within the total ice load during level ice-ship interactions

Similar as introduced in the previous section, Puntigliano (2000) discerned four different phases during the level ice-ship interaction processes. These are the ice breaking phase; the rotative phase; the sliding phase and the final phase. The first three phases are shown in the following. These terms used to describe the interaction processes will be adopted in the future description of the *level ice-conical structure interaction* numerical model.

[21] The viscous drag force for wedge-shape broken ice floes are not written here since in the ice-conical structure interactions, only cusp shape failure was assumed.

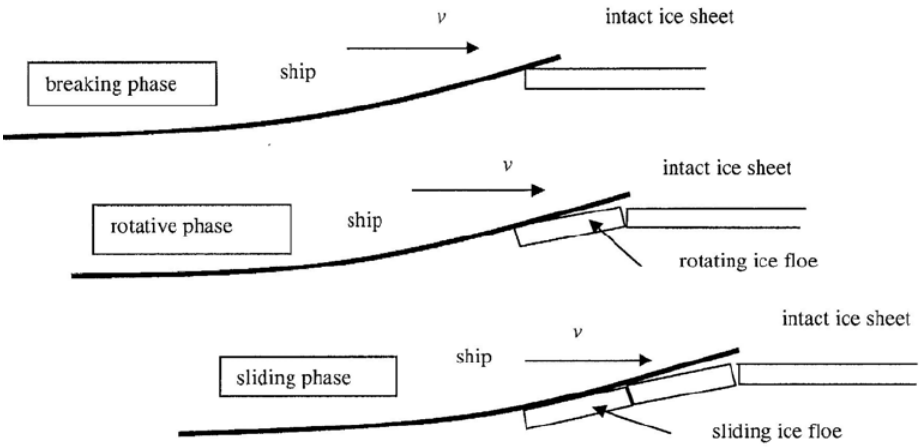

Figure 5.2 First three phases of the icebreaking processes (Puntigliano, 2000)

Valanto (2001) calculated different load components' contribution to the total ice load based on his numerical model and other already existed models. The calculation results together with the measured data were plotted in Figure 5.3.

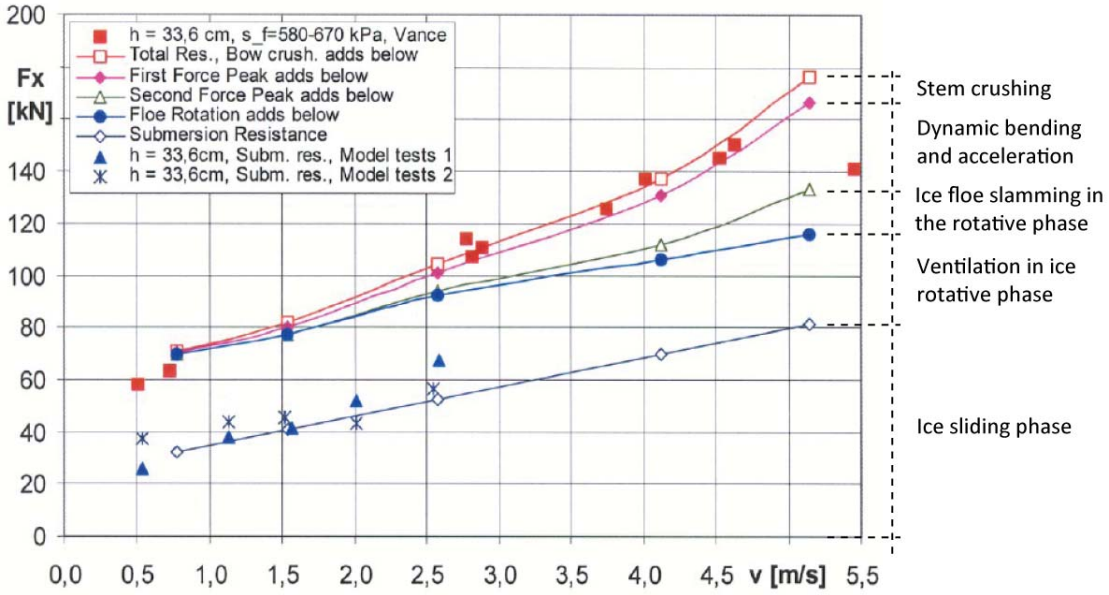

Figure 5.3 Measured and computed ice load values and computed ice load components in level ice for Bay-class ice breakers (Valanto (2001), Figure 24).

From Figure 5.3 it can be seen that the ventilation contribution and ice sliding contribution are two major parts to the total ice load for a ship in level ice. Moreover, it can be seen from the above figure that ventilation induced ice load is not sensitive to the ice speed. This has been explained by that higher ship velocity induces more void space but smaller broken ice pieces; lower ship velocity induces less/no void space but longer broken ice pieces. The ice

speed relevant contributors include loads induced by ice sliding, ice slamming against the ship hull at the end of the rotating phase, ice floe being accelerated to the ship velocity and ice crushing. Among all these speed dependent loads, the ice sliding induced load may even cover nearly 65% of the total resistance for a ship advancing in level ice.

According to Kämäräinen (2007), the following loads may be involved in the *ice sliding phase:*

- Broken ice buoyancy (*mechanical contact force resulting from the static lift of the ice floes caused by the difference in densities of water and ice*);
- Forces induced by the pressure change in the gap between the ice floe and ship hull or below the ice floe;
- Forces induced by the viscous shear stress caused by the flow of water in the gap between the ice floe and ship hull.

He also explained the reason why the ice sliding load is increasing with the ice speed. This is mainly induced by the pressure change, and viscous shear stress in the gap between the ice floe and ship hull.

Based on the above introductions, lots of useful knowledge could be borrowed from this regime to the *level ice-conical structure interactions*. In the next section, the comparisons between these two different cases will be conducted in the ice breaking, ice rotating and ice sliding phases.

5.2.1.4 A general comparison of ships and conical structures interacting with level ice

Similar as the previous introduction, the level ice-conical structure interaction processes are also split into the ice breaking phase, ice rotating phase and ice sliding phase in the time domain. The comparisons are made as shown in Figure 5.4.

As we can see from Figure 5.4, due to the similarities between the ship stem and the sloping face of the conical structure, it is reasonable to assume that the level ice-structure interaction processes are the same with the ice-ship interactions from the ice breaking phase until the end of the ice rotating phase. The load components happened in these two phases could be borrowed from the previous research based on the level ice-ship interactions.

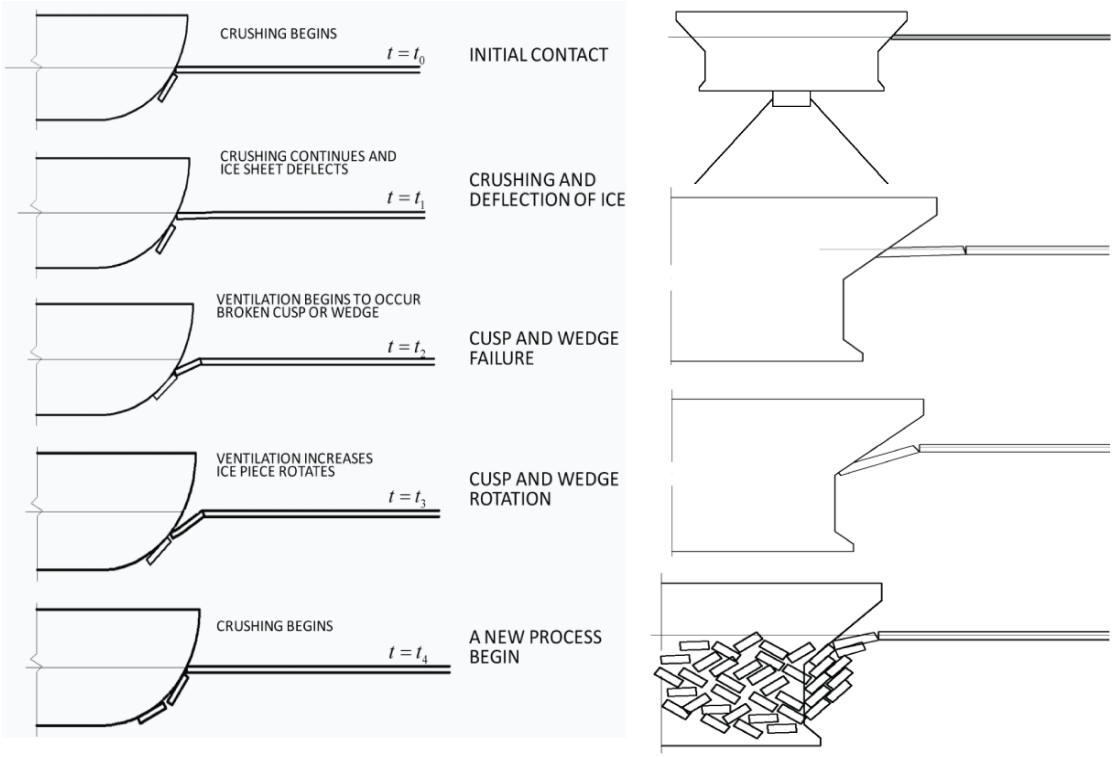

Figure 5.4 Comparisons of ships and conical structures interacting with level ice

However, in the ice sliding phase, different from ice-ship interaction processes, there will be a certain amount of broken ice pieces accumulated in the bow region of the conical structure. And these accumulated broken ice pieces slide through a much shorter length along the hull of the conical structure comparing with broken ice pieces sliding through almost the whole underwater body of the ship. Furthermore, the relative speed between structure and ice are much larger in the level ice-ship interaction case. For the conical structure, it is mainly the ice drift speed that attribute to the relative speed between the structure and ice. This ice drift speed is usually much smaller than the ship speed. Accordingly, among all three load components identified by Kämäräinen (2007) as shown previously for level ice-ship interactions, it is assumed that it is mainly the mechanic contact force (buoyancy) that are dominant in the low speed interaction of level ice and conical structures.

Based on the previous introductions about the level ice-ship interactions and also the comparisons conducted between the ship and conical structures interacting with level ice, the major borrowed knowledge could be listed in the following:

- The ship-ice interaction processes
- The identified ice load components and their physical meanings.

- Two major load components in the ice rotating phase and ice sliding phase (will be confirmed later by a numerical model)

The borrowed knowledge will be applied in the following numerical model and also the test data explanations in Part II of this thesis.

5.2.1.5 Level ice and conical structure interactions

In this section, the interaction processes of level ice and the conical structure will be described. Terms used throughout this thesis will also be defined accordingly. The ice load contributor will also be discussed.

In a similar way as ship-level ice interaction, for the conical structure (fixed or moored) interacting with level ice, the interaction processes are also discerned into *ice breaking phase*, *ice rotating phase* and *ice sliding phase* in the time domain. These processes are shown in the following figures:

- **Initial contact**

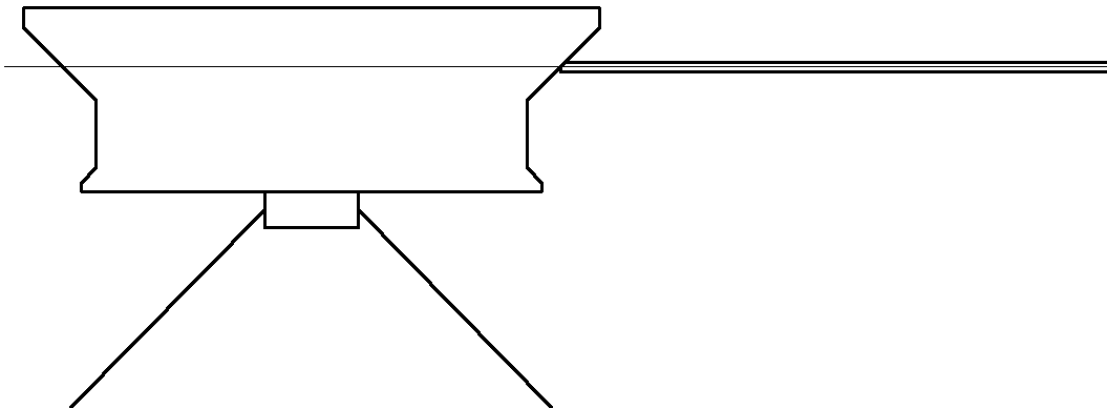

Figure 5.5. Conical structure first contact with the encountering intact level ice[22].

At first, the structure has a first contact with the incoming level ice. The intact level ice starts to be deflected downward by the conical hull. As the vertical deflection increases, the flexural stress also increases inside the intact level ice.

- **Ice breaking phase**

[22] Although a moored structure was shown in the figure, the following processes are also applicable to fixed conical structures.

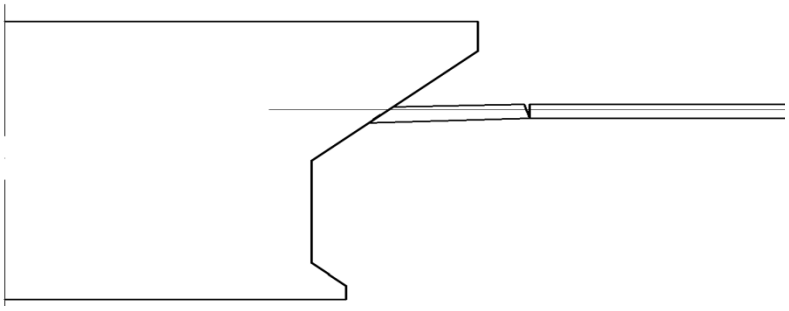

Figure 5.6. Cracks appeared and ice beams break in the bending failure mode (ice breaking phase).

Due to the sloping face effect, the inner flexural stress will first exceed the relatively lower flexural strength. The ice fails in bending. Cracks will appear and the level ice breaks. This process was categorized in the *ice breaking phase*. The ice load in this phase was termed as *ice breaking load* in this thesis.

- **Ice rotating phase**

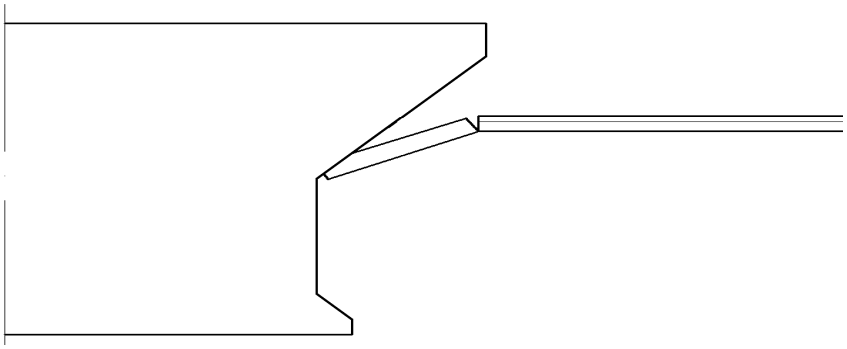

Figure 5.7. The broken ice pieces being rotated by the conical structure and ventilation increases (ice rotation phase).

The broken ice pieces will continue to be "pushed" downwards by the conical structure. During this process, ventilation effects may appear as shown in Figure 5.7. It has been illustrated that the extent of ventilation increases with increasing ice speed. During the rotating process, the water also attempt to flush into the void area above the broken ice pieces. At certain moments, the water starts to gradually fill the void space as shown in Figure 5.8. These two processes are categorized in the *ice rotating phase*. The ice load in this phase will be termed as *ice rotating load* which includes:

- Load results from accelerating the broken ice pieces;
- Rotating the broken ice mass (with or without the ventilation effect);
- Ice floe slamming against the structure at the end of the rotating;
- A small portion of possible ice crushing load.

Due to the large contributor of the ice load induced by the ventilation effect, the term ***ventilation load*** was used to describe the static rotation load required to rotate the broken ice piece. The calculation method of which is shown in Figure 5.10.

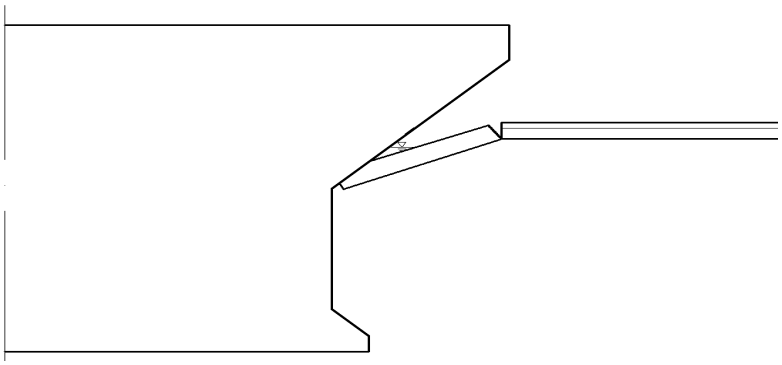

Figure 5.8. Water flushes into the void space as the broken ice piece's rotation angle increases (ice rotation phase).

- **Ice sliding phase**

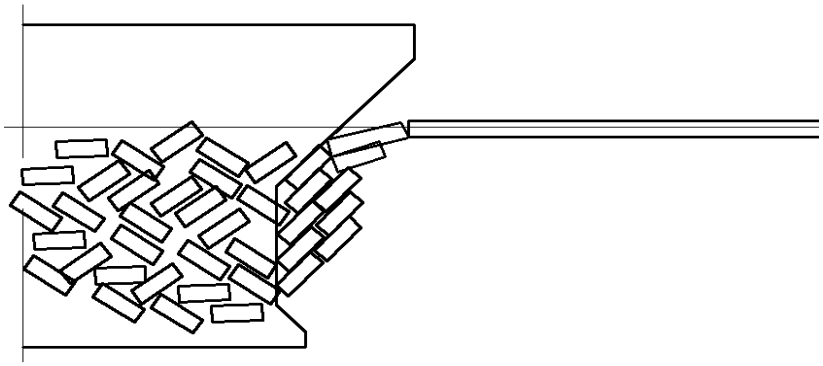

Figure 5.9. The broken ice pieces accumulating around the structure (ice sliding phase).

After the broken ice pieces were rotated paralleling the conical hull of the structure, the ice pieces will continue sliding along the structure. Different from the ship-level ice interaction situation, lots of broken ice pieces tend to accumulate in the bow region of the conical structure. The term *ice accumulation load* will be used here representing the static buoyancy of the broken ice pieces induced resistance. Based on the test videos, it has been found that as the ice speed increases, less broken ice pieces are accumulated in the bow region of the models. This means that a faster ice speed leads to a good ice clearing ability of the conical structures and hence a smaller *ice accumulation load*. The total ice load during the ice sliding phase is termed as *ice sliding load* which includes the *ice accumulation load*, *gap pressure change* induced load and gap fluid induced *viscous drag force*.

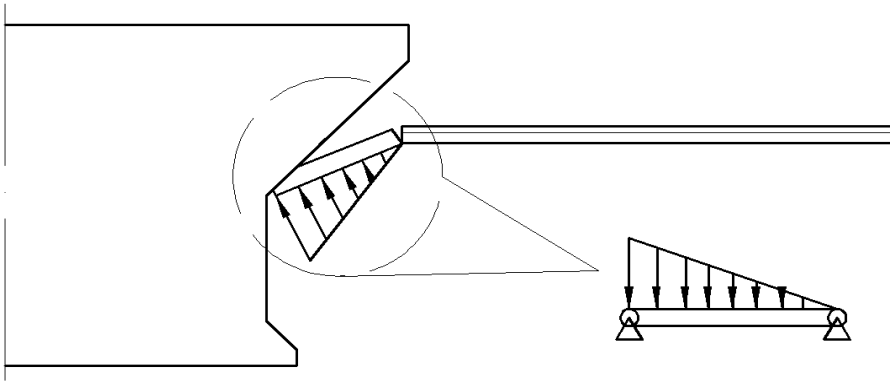

Figure 5.10. Simple *ventilation load* calculation model to illustrate the definition of *ventilation load.*

- **Conclusions of level ice and conical structure interaction**

Based on the above descriptions, the interaction phases and loads contributions for a conical structure interacting with level ice could be listed in the following:

- Ice breaking phase

Ice breaking load

- Ice rotating phase

Ice rotating load = *Ventilation load* + Load (decelerating the broken ice piece) + Other loads

Other loads include the ice slamming force at the end of the rotation phase, and certain portion of ice crushing during the ice rotating process.

- Ice sliding phase

Ice sliding load = *Ice accumulation load* + Load (gap pressure change)+ Load (gap fluid viscous drag force

Two major contributors to the ice load are thought to be the *ice rotating load* and *ice sliding load*. Since the *ice accumulation load* decreases with increasing ice speed, the *ventilation load* is not sensitive to the ice speed, and other load components increase with ice speed, it is reasonable to expect the total ice load varies little with the ice speed.

Based on the previous discussions, a numerical model used to describe *most* of the above mentioned physical processes will be introduced in the following section.

5.3 Description of the numerical model

This numerical model was developed to predict the responses of the moored structure in

level ice. As mentioned before, the responses of the moored structure will further make the ice load situation more complicated. Accordingly, a coupled ice load and structure responses model will be developed taking into consideration the surge, heave and pitch responses' influence on the external ice load.

A flow chart describing the logic route behind this numerical model is shown in Figure 5.11.

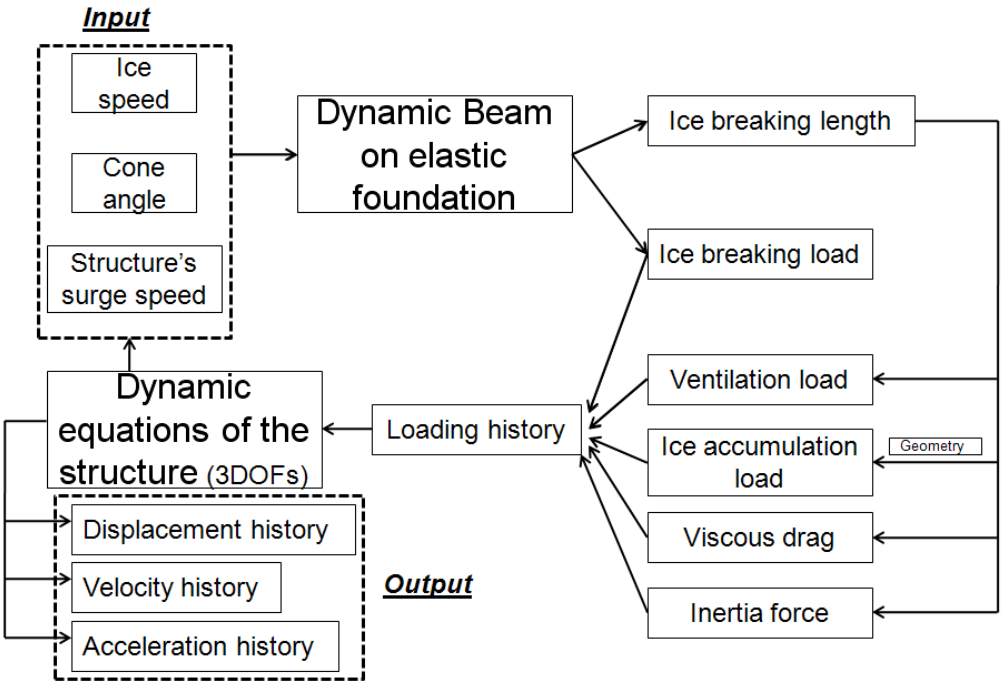

Figure 5.11 The logical route of the numerical model

This numerical model is mainly composed of two parts: the ***level ice model*** (dynamic beam on elastic foundation) and the ***moored conical structure model*** (dynamic model with 3 DOFs). Based on this flow chart, each item inside the logical route will be introduced in detail in the following sections.

5.3.1 The intact level ice model (dynamic beam on elastic foundation)

Due to the buoyancy of the sea water, the level ice was first model in a 2D scenario as a beam resting on an elastic foundation (see Figure 5.12) and later it will be generalized in a 3D scenario to calculate the relevant loadings.

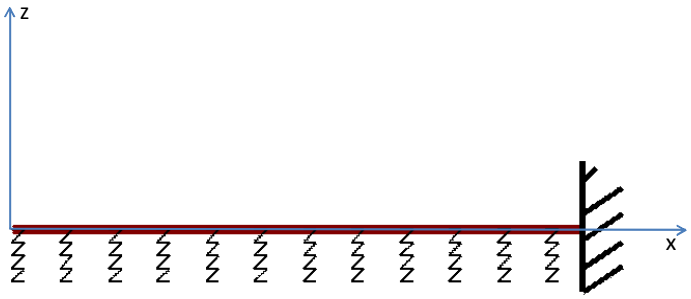

Figure 5.12. The 2D level ice model, a one-end-fixed beam resting on an elastic foundation

The ice beam is assumed to be long enough that the other end will have minimal influence during the ice-moored structure interaction and hence is fixed. The control equation for a beam resting on an elastic foundation could be written as:

$$EI\frac{\partial^4 z}{\partial x^4} - N_A\frac{\partial^2 z}{\partial x^2} + \rho_w g z = -\rho_i g\frac{\partial^2 z}{\partial t^2} \tag{5.7}$$

where

E is Young's modulus of the ice beam;

I is moment of inertia of the ice beam's cross section. It can be calculated by $I = \frac{1}{12}Wh^3$;

W is the width of the beam [m];

h is the thickness of the ice beam [m];

ρ_i is the density of the ice [kg/m^3];

ρ_w is the density of the water [kg/m^3];

g is the gravitational acceleration [m/s^2];

N_A is the axial force of the ice beam [N];

t is time [s];

z and x are displacements according to the coordinate system as shown in Figure 5.12

It will be shown later, the ice breaks instantly under the vertical loading, and the vertical displacement will be very small. By knowing this, we can further assume the axial force induced stress to be zero and hence the sheer force term $N_A\frac{\partial^2 z}{\partial x^2}$ could be assumed to be zero so as to simplify the Equation (5.7) into Equation (5.8) as:

$$EI\frac{\partial^4 z}{\partial x^4} + \rho_w g z = -\rho_i g\frac{\partial^2 z}{\partial t^2} \tag{5.8}$$

In order to solve this high order partial differential equation, the Finite Element Method is adopted. The detailed procedures are shown in the following:

- Using Galerkin's method to change Equation(5.8) into a weak form

$$\int_0^L (EI\frac{\partial^4 \mathbf{z}}{\partial x^4} + \rho_w g z + \rho_i g \frac{\partial^2 \mathbf{z}}{\partial t^2})\boldsymbol{\omega} dx = 0 \tag{5.9}$$

The above Equation(5.9) can further be written as:

$$\int_0^L (EI\frac{\partial^4 \mathbf{z}}{\partial x^4})\boldsymbol{\omega} dx + \int_0^L (\boldsymbol{\omega}\rho_w g z) dx + \int_0^L (\rho_i g \frac{\partial^2 \mathbf{z}}{\partial t^2})\boldsymbol{\omega} dx = 0 \tag{5.10}$$

For the first term of Equation(5.10), using step integration twice as shown below:

$$\int_0^L (EI\frac{\partial^4 \mathbf{z}}{\partial x^4})\boldsymbol{\omega} dx = \int_0^L (\frac{\partial^2 \omega}{\partial x^2} EI \frac{\partial^2 \mathbf{z}}{\partial x^2}) dx + [EI\frac{\partial^3 \mathbf{z}}{\partial x^3}\boldsymbol{\omega}]_0^L - [EI\frac{\partial^2 \mathbf{z}}{\partial x^2}\frac{\partial \boldsymbol{\omega}}{\partial x}]_0^L \tag{5.11}$$

The last two terms are boundary conditions for an element (boundary sheer force and moment respectively), which will be eliminated at the joints of two elements after writing all the elements together into a system equation. In the system equation, only the first and last element's boundary conditions will be left which are the boundary conditions of the whole 'structure'.

Similarly, the other two terms in Equation(5.10) could be written as

$$\int_0^L (\boldsymbol{\omega}\rho_w g z) dx \tag{5.12}$$

and

$$\int_0^L (\rho_i g \frac{\partial^2 \mathbf{z}}{\partial t^2})\boldsymbol{\omega} dx \tag{5.13}$$

According to Galerkin's method, $\boldsymbol{\omega} = \mathbf{N_s}^T$ where $\mathbf{N_s}$ is the shape function for a beam.

- FEM, Element matrix

For a beam considering only vertical displacement and joint rotation, the vertical displacement z can be written as

$$z = \mathbf{N_s} \cdot \mathbf{v} = N_{s1} \times v_1 + N_{s2} \times \theta_1 + N_{s3} \times v_2 + N_{s4} \times \theta_2 \tag{5.14}$$

where the shape function could be obtained by using Hermite interpolation as:

$$\begin{aligned} N_{s1} &= 1-\frac{3x^2}{\Delta l^2}+\frac{2x^3}{\Delta l^3} \\ N_{s2} &= x-\frac{2x^2}{\Delta l}+\frac{x^3}{\Delta l^2} \\ N_{s3} &= \frac{3x^2}{\Delta l^2}-\frac{2x^3}{\Delta l^3} \\ N_{s4} &= -\frac{x^2}{\Delta l}+\frac{x^3}{\Delta l^2} \end{aligned} \tag{5.15}$$

in which, Δl is the length of the beam element while x represents the position on the beam.

Then Equation(5.10) could be written as[23]:

$$\int_0^L(\boldsymbol{\omega}\rho_i g\frac{\partial^2 z}{\partial t^2})dx+\int_0^L(\frac{\partial^2\boldsymbol{\omega}}{\partial x^2}EI\frac{\partial^2 z}{\partial x^2})dx+\int_0^L\boldsymbol{\omega}\rho_w gzdx+[EI\frac{\partial^3 z}{\partial x^3}\boldsymbol{\omega}]_0^L-[EI\frac{\partial^2 z}{\partial x^2}\frac{\partial\boldsymbol{\omega}}{\partial x}]_0^L=0 \tag{5.16}$$

$$\int_0^L(\mathbf{N_s}^{\mathbf{T}}\rho_i g\mathbf{N_s})\ddot{\mathbf{v}}dx+\int_0^L(\mathbf{N_s}^{\mathbf{T}})''EI(\mathbf{N_s})''\mathbf{v}dx+\int_0^L(\mathbf{N_s}^{\mathbf{T}}\rho_w g\mathbf{N_s})\mathbf{v}dx+[EI\frac{\partial^3 z}{\partial x^3}\boldsymbol{\omega}]_0^L-[EI\frac{\partial^2 z}{\partial x^2}\frac{\partial\boldsymbol{\omega}}{\partial x}]_0^L=0$$

(5.17)

This can be further written as:

$$[\int_0^L(\mathbf{N_s}^{\mathbf{T}}\rho_i g\mathbf{N_s})dx]\ddot{v}+[\int_0^L(\mathbf{N_s}^{\mathbf{T}})''EI(\mathbf{N_s})''dx+\int_0^L(\mathbf{N_s}^{\mathbf{T}}\rho_w g\mathbf{N_s})dx]v+[EI\frac{\partial^3 z}{\partial x^3}\boldsymbol{\omega}]_0^L-[EI\frac{\partial^2 z}{\partial x^2}\frac{\partial\boldsymbol{\omega}}{\partial x}]_0^L=0$$

(5.18)

From the above equation, the mass matrix **M**, and stiffness matrix **K** could be identified as following:

$$\mathbf{M}=\int_0^L(\mathbf{N_s}^{\mathbf{T}}\rho_i g\mathbf{N_s})dx \tag{5.19}$$

$$\mathbf{K}=\int_0^L(\mathbf{N_s}^{\mathbf{T}})''EI(\mathbf{N_s})''dx+\int_0^L(\mathbf{N_s}^{\mathbf{T}}\rho_w g\mathbf{N_s})dx \tag{5.20}$$

The above equation for an element could eventually be written as:

[23] In the following formulas, the convention of deviation in space using (') and in time using (˙) will be applied in the whole thesis.

$$\mathbf{M}\ddot{v} + \mathbf{K}v + [EI\frac{\partial^3 z}{\partial x^3}\boldsymbol{\omega}]_0^L - [EI\frac{\partial^2 z}{\partial x^2}\frac{\partial \boldsymbol{\omega}}{\partial x}]_0^L = 0 \tag{5.21}$$

- FEM, System matrix

After knowing the element matrix, the system matrix could be constructed according to the elements' geometric position. For a beam, this will be easily programmed in MATLAB. With the known element mass matrix and stiffness matrix, the system mass matrix and stiffness matrix could be written as **M** and **K** following standard FEM procedures. And eventually the dynamic equation for the beam could be written as following:

$$\mathbf{M}\ddot{\mathbf{Y}} + \mathbf{K}\mathbf{Y} = \mathbf{F} \tag{5.22}$$

The boundary condition is included in **F**. More details about how to obtain **F** and how to solve Equation(5.22) will be discussed in the later section.

Based on this model and the previous discussions, different load components will be calculated in the following.

5.3.1.1 Ice breaking load

In the previous section, the finite element method was applied to form the final system dynamic Equation(5.22). Solving this dynamic equation will give the ice breaking length and also the ice breaking load.

- **Boundary conditions**

In this dynamic equation, the boundary condition of the beam is known. It is assumed that the contact point of the beam's displacement, velocity and acceleration are as following:

$$\mathbf{Y}(x = 0) = \mathbf{V}t\sin(\alpha)$$

$$\dot{\mathbf{Y}}(x = 0) = \mathbf{V}\sin(\alpha)$$

$$\ddot{\mathbf{Y}}(x = 0) = 0$$

The beam is assumed to be fixed in the far end from the structure. Accordingly, in the beam's far end from the structure, the boundary conditions are as following:

$$\mathbf{Y}(x = \infty) = 0$$

$$\dot{\mathbf{Y}}(x = \infty) = 0$$

$$\ddot{\mathbf{Y}}(x=\infty)=0$$

The external forces are assumed to be 0 except the contact point and far end of the beam.

So, Equation(5.22), after applying the boundary conditions, becomes Equation(5.23)

$$\begin{pmatrix} M_{11} & \cdots & M_{1n} \\ \vdots & \ddots & \vdots \\ M_{n1} & \cdots & M_{nn} \end{pmatrix}\begin{pmatrix} 0 \\ unknown \\ 0 \end{pmatrix}+\begin{pmatrix} K_{11} & \cdots & K_{1n} \\ \vdots & \ddots & \vdots \\ K_{n1} & \cdots & K_{nn} \end{pmatrix}\begin{pmatrix} vt\sin(\alpha) \\ unknown \\ 0 \end{pmatrix}=\begin{pmatrix} unknown \\ 0 \\ unknown \end{pmatrix} \quad (5.23)$$

There are *N* equations above, (*N*-2) acceleration unknowns, (*N*-2) displacement unknowns, and 2 external force unknowns. Since there is a relationship between the acceleration and displacement (Appendix E), the (*N*-2) acceleration unknowns could be replaced by the (*N*-2) displacements. Accordingly in total, there are (*N*-2)+2 unknowns and *N* independent equations. The above equation is theoretically solvable.

In order to solve the above ordinary differential equation system with boundary conditions, the *direct integration method* is adopted, but different from an initial condition problem, during each time step, the newly calculated displacement vector is changed to fulfill the boundary condition before the next iteration loop. The output of the above calculation is the time history of the beam displacement and angle in each node.

- **Stress calculation and ice breaking criteria**

After knowing the displacement of the ice beam along its length, the stress within the beam could be calculated by first calculate the internal moment of the beam using the following formula:

$$M = EI\frac{d^2y}{dx^2} \quad (5.24)$$

In which

M is the moment of within the beam;

y is the vertical displacement of the beam.

The above equation could be approximated with $\frac{d^2y}{dx^2}=\frac{y(i+1)-2y(i)+y(i-1)}{\Delta l^2}$

So the internal moment could be calculated by

$$M = EI\frac{y(i+1)-2y(i)+y(i-1)}{\Delta l^2} \quad (5.25)$$

In which E is Young's modules of ice, I is the moment of inertia of the ice beam, $y(i+1)$, $y(i)$ and $y(i-1)$ are displacements in node i, $(i+1)$ and $(i-1)$; Δl is the length between two nodes, and it is also the element length. The internal moment in node i could be calculated from Equation(5.25). Then the stress in node i could be calculated:

$$Stress(i) = \frac{M(i)}{I} \times \frac{h}{2} \tag{5.26}$$

In which, h is the thickness of the ice beam. The stress on the upper or lower surface of the ice beam on node i could be calculated by this equation. Here it is assumed that *the ice is broken when the above calculated stress exceed the flexural strength of the ice.* Based on this, the breaking length and breaking force of the ice beam can be calculated by programming the above criteria in the numerical model.

- **From 2D to 3D**

The above calculation results are based on a 2D ice model. In order to get the total ice impact load on to the structure, the calculated results need to be expanded to a 3D situation. Since the moored structure has a circular shape, the *relative velocity* between the structure and the ice is varying at different place.

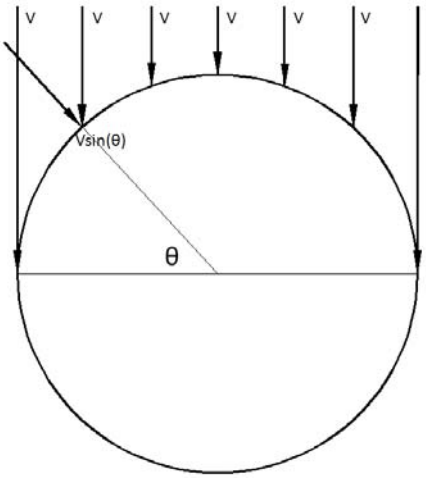

Figure 5.13. The *relative velocity* between the structure and ice in a 3D scenario

With different *relative velocity*, by applying the same calculation methods given before, it is possible to calculate the ice breaking length, breaking duration and breaking force distribution around the structure. However, two obstacles were observed:

- The lower *relative velocity* on the sideways of the structure will lead to longer ice breaking length, hence the assumption of a wedge shape failure is not applicable;
- Different point of around the circular structure may have different ice breaking duration. The earlier-broken ice will change the boundary conditions of those intact ice beams. Although in the model, all the intact ice was assumed to be one-end-fixed beam resting on elastic foundation, with the presence of early broken ice beams, the boundary conditions of the remaining intact ice beams will be more or less influenced.

In order to solve the afore-mentioned two obstacles, the following assumptions are made.

- The ice breaks in a cusps shape. If there is any neighbouring ice beam breaks in advance, the calculation results of those ice beams which break later will be neglected. Because due to the influence of the cracks induced by the early-broken ice beams, the boundary conditions of the later-broken ice beams has already changed, and cannot be modeled in a similar way. This assumption actually ensures a simultaneous ice breaking. All the ice beams around the structure fails at the same time. Furthermore, the shape of all the broken ice beams appears to be a cusp shape.
- The breaking lengths at two lee sides of the structure ($\theta = 0^{o}$ and $\theta = 180^{o}$) are assumed to be 0. And the breaking forces at these two points are also assumed to be 0;
- Based on the previous two assumptions, after the calculation, some points around the structure will have *effective* ice breaking length and ice breaking load while some other points, due to their late breakings, the calculated breaking length and breaking load are thought to be unreliable and neglected. These *value-blank* points will be artificially given *effective* values based on other reliable points' values (ice breaking length and ice breaking load) according to *SPLINE* interpolation.

The above three assumptions will ensure a *simultaneous ice breaking* and a *cusp shape* ice breaking pattern. With the known ice breaking length around the conical structure, some other load components in the *ice rotating phase* could be further calculated.

5.3.1.2 Ventilation load

In the ice rotating phase, the ventilation load is a major contributor to the total ice load. In this section, the method of calculating the ventilation load will be introduced.

- Ventilation load

As can be seen from Figure 5.7 and Figure 5.8, the broken ice is rotated and a void space in

front of the structure is formed. Due to the large difference between the air density and water density, huge pressure force will be formed beneath the broken ice beam as shown in Figure 5.14:

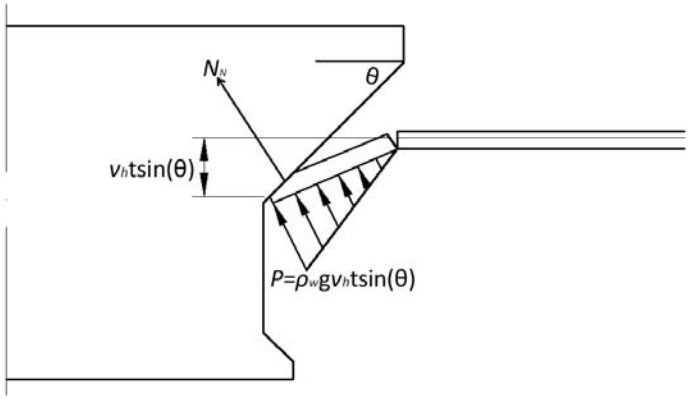

Figure 5.14. Ventilation load of the broken ice

Before the water flushes into the void space, as the ice being rotated downward, the water pressure increases significantly. The distribution of the water pressure could be seen in Figure 5.14. It is assumed that the broken ice is rotated at a speed equaling to $v_h tsin(\theta)$, in which v_h is the *relative speed* between the ice and the structure, and θ is angle between the conical face with the water level. The normal force transferred to the moored structure can be calculated by:

$$N_N = \frac{2}{3}[\frac{1}{2}\rho_w g v_h \sin(\theta) L w_b] \tag{5.27}$$

In which, L is the breaking length of the ice, w_b is the width of the broken ice beam. It is calculated by $w_b = degree\_step \times radius$ in the numerical program.

- Sub-break of the broken ice

A beam with two hinged ends is adopted to model the rotating broken ice as shown in Figure 5.15:

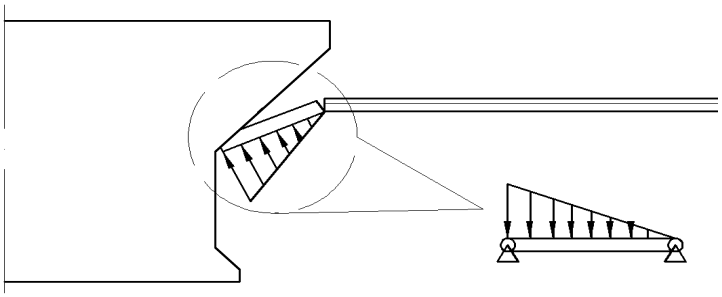

Figure 5.15. Illustration of the broken ice model

It is logical to check if the internal stress of the broken ice will exceed the strength of the ice material and hence *sub-break* of the already broken ice occurs.

According to *structural mechanics*, the moment distribution along a two-end hinged beam can be calculated as following:

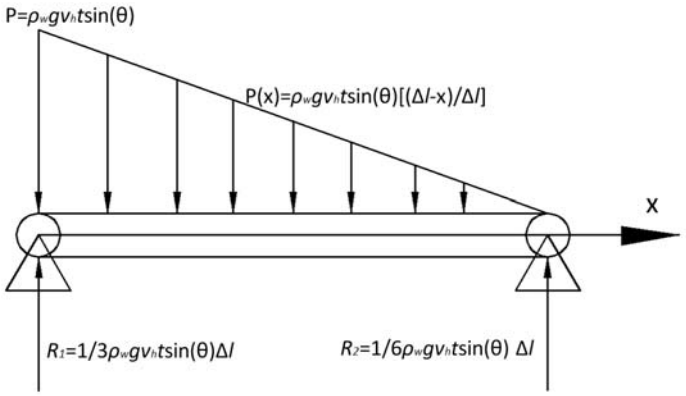

Figure 5.16. Two hinged ends model for broken ice

$$M(x) = [\frac{1}{2}P(x)(\Delta l - x)] \times \frac{1}{3} \times (\Delta l - x) - R_2 \times (\Delta l - x) \tag{5.28}$$

$$M(x) = \rho_w g v_h t \sin(\theta)[\frac{(\Delta l - x)^3}{6\Delta l} - \frac{\Delta l(\Delta l - x)}{6}] \tag{5.29}$$

By applying the first order differentiation equals to 0, the place where suffering from the largest moment could be identified:

$$\frac{dM(x)}{dx} = \rho_w g v_h t \sin(\theta)(-\frac{(\Delta l - x)^2}{2\Delta l} + \frac{\Delta l}{6}) = 0 \tag{5.30}$$

$$x = (1 - \frac{\sqrt{3}}{3})\Delta l = 0.42\Delta l \tag{5.31}$$

and the corresponding largest moment is

$$M_{\max} = \rho_w g v_h t \sin(\theta)[\frac{(0.58\Delta l)^3}{6\Delta l} - \frac{0.42 \times 0.58\Delta l^2}{6}] = -0.00808\rho_w g v_h t \sin(\theta)\Delta l^2 \tag{5.32}$$

hence the largest internal stress of the broken ice beam under such sub-break condition could be calculated by:

$$Stress_{\max} = \frac{M_{\max}}{EI} \times \frac{h}{2} \tag{5.33}$$

If $Stress_{max}$ (absolute value) is larger than the ice beam flexural strength, sub-break of the broken ice will occur. However, theoretically such sub-break case is very rare. It is coded in the program mainly for logical completeness.

- Water entry in the void space

It is observed that due to the high water pressure beneath the rotated ice, water may enter the void space before the broken ice being rotated paralleling to the conical face. An angle reduction parameter has been introduced to describe such phenomenon.

$$\alpha_{water\_in} = \varepsilon_{water\_in} \times \alpha \tag{5.34}$$

In which, α_{water_in} is the angle when water starting to flush into the void space; α is the angle between the conical face and water level. It is also the maximum ice rotating angle under full ventilation cases. ε_{water_in} is a reduction number between *(0,1]*.

Moreover, it is assumed that the water flush speed is constant. This means that once the water starts to flush in the void space above the broken ice, the original accumulated ventilation load (calculated by Equation(5.27)) reduces linearly until the void space being inundated by water. In order to describe the relative time required to inundate the void space, another reduction parameter $\varepsilon_{water\ flush\ speed}$ was introduced. This will be further illustrated in Figure 5.21

5.3.1.3 Viscous drag force and ice inertia force

According to Kotras (1983), based on the assumption of ice wedge breaking patterns and classic theory about viscous drag force, the viscous drag force was calculated according to Equation(5.6). Based on this equation, since the ice breaking patter was also assumed to be cusp failure shape, the viscous drag force on the conical structure can be calculated by the following equation:

$$F_{drag,Normal} = 0.1575 \times \rho_w C_d v^2 Dw \tag{5.35}$$

In which,

F_{drag_Normal}	is the viscous drag force normal to the contact surface of the structure [N];
ρ_w	is the density of water [kg/m^3];
C_d	is the drag coefficient assuming to be 1;
v_h	is the *relative velocity* between ice and structure [m/s]
$D,\ w$	are the cusp depth and cusp width respectively with unit [m].

According to Figure 5.20, in the current calculation, it is assumed D equals to the ice breaking length right at the bow region of the moored conical structure and $W = 2 \times r_w$, where r_w represents the radius of the waterline area.

According to Liu (2006), the ice inertia force could be calculated by dividing the broken ice's Kinetic energy by its travelling distance. Accordingly, in the numerical model, the horizontal inertia ice load is calculated by the following method:

$$F_{inertia,horizontal} = \frac{\frac{1}{2}\rho_{ice} A_{cusp} h v_h^{\,2}}{L_{break}} \tag{5.36}$$

In which,

$F_{inertia,hrizontal}$ is the horizontal inertia load induced by the broken ice pieces [N];

ρ_{ice} is the density of ice [kg/m^3];

A_{cusp} is the area of the broken ice cusp as shown in Figure 5.20 circled by the black crack line and the structure's water plane circle [m^2];

h is the thickness of the level ice [m];

v_h is the horizontal *relative velocity* between the moored conical structure and level ice [m/s];

L_{break} is the breaking length of the ice in the bow region of the moored conical structure [m].

5.3.1.4 Ice sliding load

As can be seen from Figure 5.9, the broken ice, after being accelerated to approximate the same speed as the moored structure, tends to accumulated around the moored structure. The volume of the ice accumulation is determined by the geometry of the moored conical structure, the *relative speed* between the moored conical structure and level ice, and also the displacement of the moored conical structure.

It may be natural to think that a higher *relative velocity* between the broken ice and the moored conical structure will lead to less ice accumulation (this has been confirmed in Part II of this thesis); and larger displacements (positive direction displacement of surge, heave and pitch, see Figure 2.2 for the coordinate system) tend to induce larger ice accumulation volume.

When calculating the ice accumulation load, the following assumptions have been made:

- Assume wet contact between the broken ice pieces and the moored structure.

According to Jorma Kämäräinen (2007), the pressure in the gap between the ice and hull may vary with the ship speed. For the current case, ice and moored conical structure

interaction, the *relative speed* is very low. So, it is reasonable to assume the *ice accumulation load* is the major contributor to the total *ice sliding load*. And the *ice accumulation load* is actually from the mechanical contact force induced by the buoyancy of the submerged broken ice pieces.

At first a "constant" maximum accumulation volume is assumed. Simple geometry estimation method is adopted to identify the reasonable maximum accumulation volume. Then the effect of *relative velocity* change is added to this constant maximum accumulation volume so as to better describe the ice accumulation load. Based on the calculations, it is recommended the ice accumulation volume can be calculated by the following equation:

$$V_{ice\_volume} = \frac{1}{2} \times (4A_{slope} + A_{vertical}) \times (1 - \Delta v \times \beta) \tag{5.37}$$

in which,

V_{ice_volume}	is the ice accumulation volume of the specific analyzed structure [m^3];
A_{slope}	is the area of the conical hull [m^2];
$A_{vertical}$	is the area of the vertical part (neck) of the hull [m^2];
Δv	is the *relative velocity* change between the moored conical structure and level ice [m/s];
$\frac{1}{2}$	assumes only half of the slope area and vertical area will be covered with submerged ice;
4	assumes there are 4 layers of submerged ice below the slope area as shown in Figure 5.20;
$\frac{1}{2} \times (A_{slope} \times 4 + A_{vertical})$	represents the constant ice accumulation volume part;
$-\Delta v \times \beta$	represents the effect of *relative velocity* to the submerged ice volume, when the *relative velocity* between the moored conical structure and level ice increases, Δv will be positive, and hence the ice volume will decrease; if the *relative velocity* between the moored conical structure and level ice decrease, Δv will be negative, so the ice accumulation volume will increase; it is found that this formula gives good approximation when $\beta = 7.5$.

- When calculating the pitch moment induced by the ice accumulation, the pitch moment arm is assumed to be constant.

5.3.1.5 Some general approaches during the calculation

In the previous sections, different loads have been identified and their calculation methods have been discussed. Usually, the first step is always to calculate the normal contact force with the structure. After knowing the normal force, the general approach to obtain the vertical ice load and horizontal ice load are to be introduced herein:

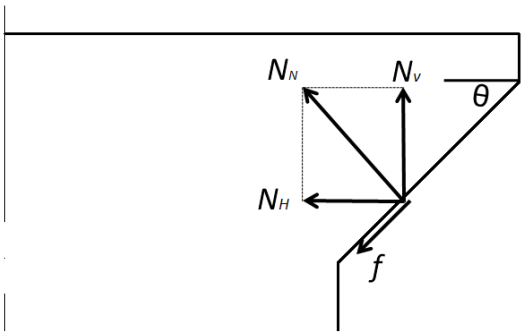

Figure 5.17. Normal contact force and friction

$$N_v = N_N \cos(\theta) \tag{5.38}$$

$$N_H = N_N \sin(\theta) \tag{5.39}$$

$$f = \mu N_N \tag{5.40}$$

Accordingly, the vertical force F_V and horizontal force F_h could be calculated by the following formulas:

$$F_v = N_N \cos(\theta) - \mu N_N \sin(\theta) \tag{5.41}$$

$$F_h = N_N \sin(\theta) + \mu N_N \cos(\theta) \tag{5.42}$$

in which

N_N	is a general normal force acting on the conical hull of the structure [N];
N_v and N_H	are vertical and horizontal component of the normal force respectively [N];
f	is the friction force [N];
μ	is the friction coefficient [-];
θ	is the angle of the conical hull [^{o}];

Based on the above calculation method, the ice load history could be constructed and will be acting on the structure. The dynamic model for the structure taking into consideration 3 DOFs (surge, heave, and pitch) will be introduced in the next section.

5.3.2 The moored conical structure model

Only surge, heave and pitch response are considered in this moored conical structure model. And the coordinate system is shown in Figure 5.18.

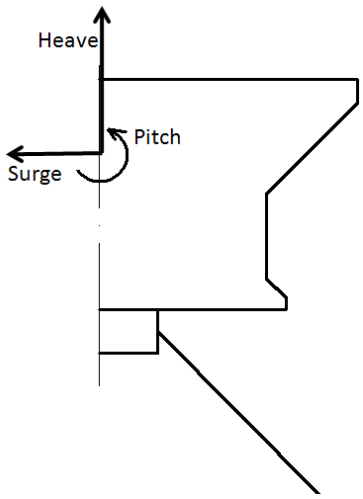

Figure 5.18 The coordinate system of moored conical structure

First the dynamic equation needs to be constructed as following:

$$[\mathbf{M}+\mathbf{A}]\ddot{\mathbf{Y}}+\mathbf{B}\dot{\mathbf{Y}}+(\mathbf{C}+\mathbf{K})\mathbf{Y}=\mathbf{F} \tag{5.43}$$

in which

Y is a 3×1 vector representing the surge, heave and pitch displacement;

M and **A** are 3×3 mass matrix and added mass matrix in surge, heave and pitch direction;

B is the added damping in surge, heave and pitch direction;

C is the hydrostatic stiffness matrix in surge, heave and pitch direction;

K is the mooring stiffness in surge, heave and pitch direction;

F is the excitation load (ice load).

It is assumed the hydrodynamic coefficients are remaining the same for the moored structure in both open water and icy water. Although this is not true, due to the lack of hydrodynamic coefficient experiment data in icy water and limited time for the author to construct a fully ice-water-structure interaction model, it is accepted as an expedient assumption.

It has been introduced in Section 4.1 that the hydrodynamic coefficients (Added mass and

added damping) were calculated using HYDRO-D under different frequencies. These hydrodynamic coefficients were stored in a source file. During the calculation, based on the external load frequency, the relevant hydrodynamic coefficients will be selected from the source file automatically for further calculation.

In order to solve the above ordinary differential equation (ODE) system, the *direct integration method* was used (refer to Appendix E for detail). The structure's responses in time history were obtained.

5.4 Numerical model calculation results analysis

In the previous Section 5.3, the numerical was introduced. Two major parts compose this numerical model. These are the *intact level ice model* (dynamic beam on elastic foundation), which was used to obtain the ice breaking length and ice breaking load. Then the ice load history will be constructed by different calculation methods given in the previous section. Afterwards, the load history will be applied to the *dynamic moored structure model* to calculate the structural response histories.

In this section, the intact level ice model will be first tested by an example. Afterwards, the numerical model will be run for one loop to show the characteristics of the constructed ice load history. In the end, this numerical model was run for 200 loops to generate the structural response histories which will be compared with the test results.

5.4.1 Intact level ice model calculation results

The theory behind this model has been introduced in Section 5.3.1. Now the calculation results will be illustrated. The following example is tested:

Input data:

$v_h = 0.5$ m/s	the *relative velocity* between level ice and moored structure;
$L = 200$ m	the length of 'ice beam' in the calculation;
$\rho_w = 1025$ kg/m^3	the density of sea water;
$\rho_{ice} = 900$ kg/m^3	the density of ice;

$h = 2$ m	thickness of the level ice;
$E = 5 \times 10^9$ Pa	Young's module of ice;
$\sigma_f = 0.54 \times 10^6$ Pa	Flexural strength of ice;
$\Delta l = 1$ m	Length step (element length) during the calculation using FEM;
$\Delta t = 0.1$ s	Time step during the calculation of the ordinary differential equation

After running this model the ice beam deflection at different time will be calculated as shown in Figure 5.19.

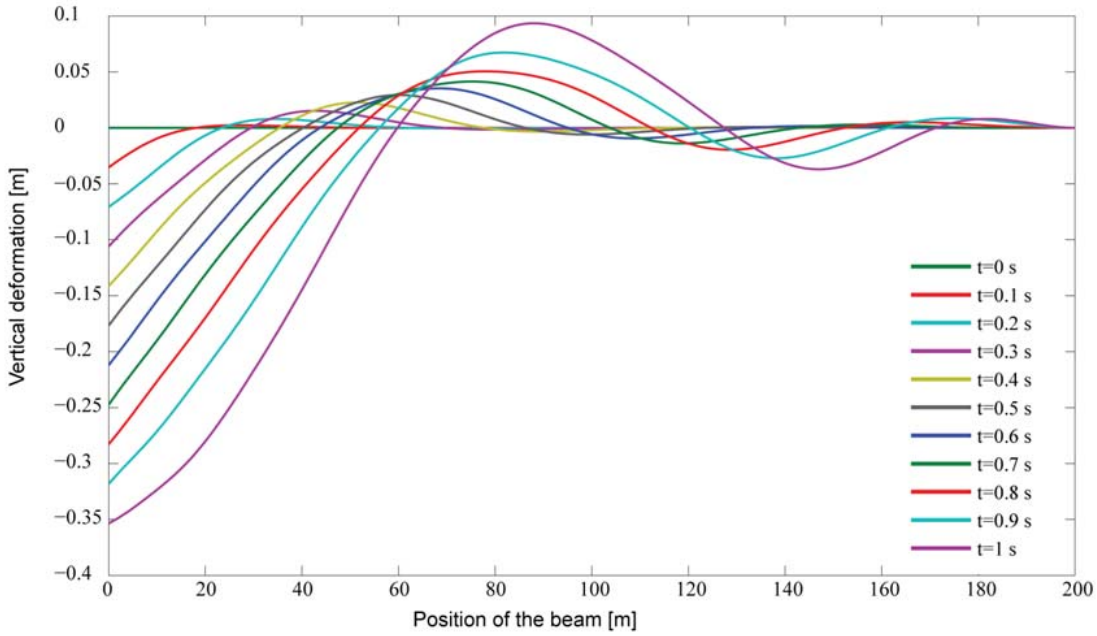

Figure 5.19. The displacement of ice beam along its length at different time

The ice will break before it can deform as shown in the above Figure 5.19. Usually the ice breaks at 0.2 second. The deformation is as shown by the first green line in the above Figure 5.19. Generally, after applying the ice break criteria, the ice breaking length, ice breaking time and also the ice breaking load (impact load) can be calculated.

Using simple geometric relationship, the ice breaking length around the structure could also be calculated. The results are shown in Figure 5.20.

Under the above conditions, the ice breaking length in the bow region is 9 m, break time is at 0.2 s.

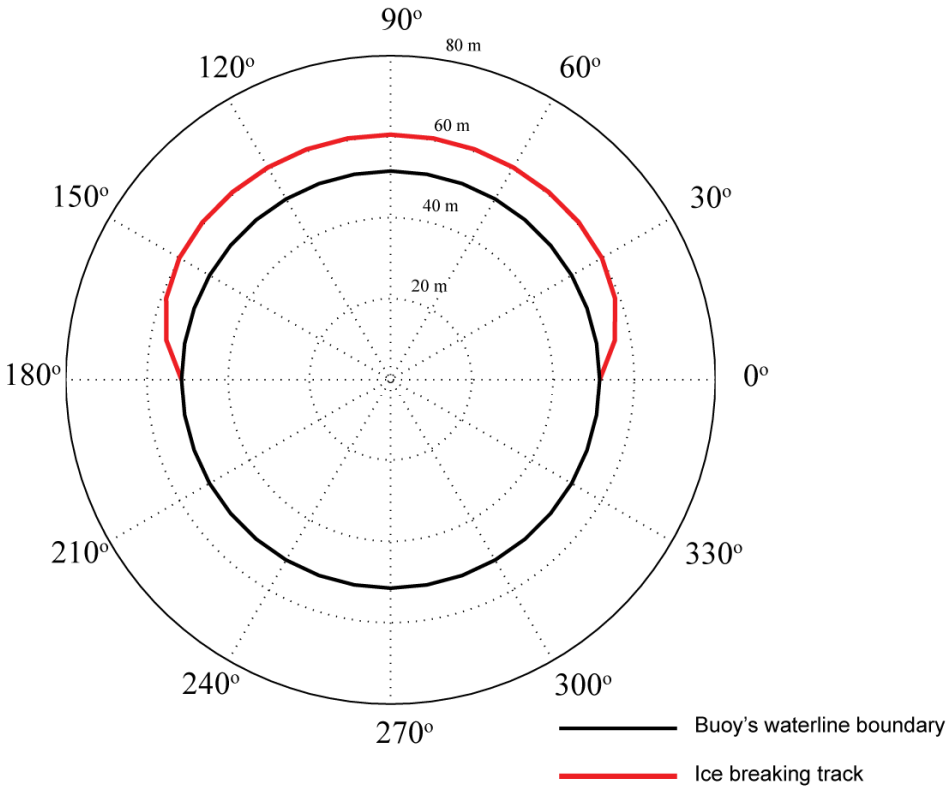

Figure 5.20. The bird view of the ice breaking around the moored structure

(Polar coordinate; Unit [m] and unit [degree])

With the known ice breaking length and breaking area, the ice load history could be calculated based on the previous introduced calculation methods.

5.4.2 Level ice load history

As introduced in Section 5.3.1, *ice breaking load, ventilation load, inertia load, viscous drag force* and *ice accumulation load* will be considered in the numerical model so as to construct a loading history applying to the moored conical structure. The time history of horizontal load applying on the structure has been shown in Figure 5.21 in one loop.

As can be seen from the following figure, four sections have been identified. The *first* section is the *ice breaking load*; the *second* section is the *ventilation load* increasing with the angle of the rotating ice pieces; the *third* section is the *ventilation load* decreasing after water entering; the *forth* section is induced by the already submerged broken ice pieces. And *ice accumulation load* exists in all the sections. Each loading section will be described in detail in the following.

Section I:

At first, the ice breaking load has been calculated in the previous section, under the same example, the impact load is integrated along the contact area between the moored structure and level ice. The duration of the ice breaking load is 0.2 s as shown in the above example.

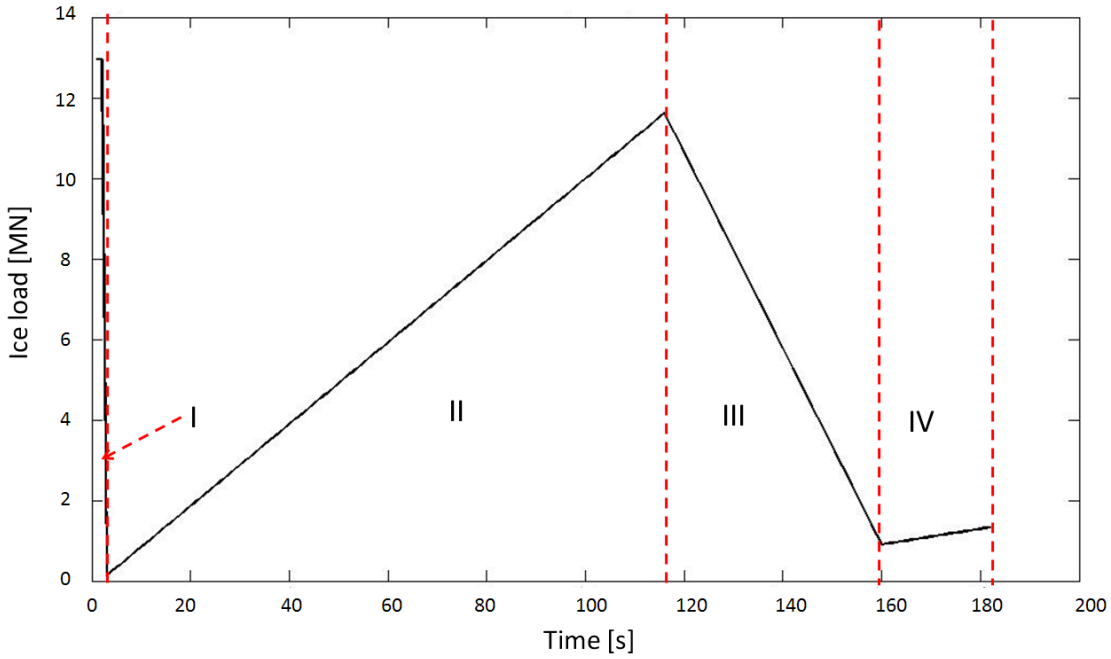

Figure 5.21. The horizontal ice load history in one loop simulation

Section II:

Later, based on the known ice breaking length around the moored circular structure, the broken ice area to be rotated can be calculated, and the ventilation load can be calculated. As discussed before, a ventilation parameter ε_{water_in} has been introduced in the calculation so as to describe the extent of ventilation. In the current example ε_{water_in} is assumed to be 2/3. It can be seen from Figure 5.21, in Section II the *ventilation load* keeps increasing before the water entering into the void space.

Section III

When the void space above the broken ice was gradually inundated by the flushed in water, the previous accumulated ice rotating force starts to decrease. As discussed before, a parameter used to describe the speed of flushing-in water $\varepsilon_{water\ flush\ speed}$ was introduced. In the current example $\varepsilon_{water\ flush\ speed}$ is also assumed to be 2/3.

The time length from the beginning of Section II until the end of Section IV describes the whole ice rotating phase, and Section II is before water entering; Section III describes situation after water entering; and Section IV describes the load history after the void space

being totally inundated. In this example $\varepsilon_{water\_in} = 2/3$ and $\varepsilon_{water\ flush\ speed} = 2/3$. This means that the time duration of Section II is 2/3 of the whole ice rotation duration (if we assume $\varepsilon_{water\_in} = 1$, the *ventilation load* will keep increasing until the end of Section IV, which means that the calculation is under a fully ventilated situation). During the duration of Section III, the water is flushing in the void space, the previous accumulated *ventilation load* is gradually decreasing in Section III according to $\varepsilon_{water\ flush\ speed} = 2/3$. This means Section III is 2/3 of the whole duration of Section III and Section IV. (if we assume $\varepsilon_{water\ flush\ speed} = 1/2$, the *ventilation load* will decrease to 0 in only 1/2 duration of Section III and Section IV)

Section IV

This section describes the increasing horizontal ice load with the increasing submerged ice volume. The calculation method has been introduced before. The submerged ice induced loading will keep increasing until it reaches a maximum ice accumulation volume as discussed with Equation(5.37).

Meanwhile, during the whole process, the *inertia load* and *viscous drag force* are also recorded in the ice load history. The above Figure 5.21 shows only the ice load history in one loop of ice-structure interaction. In Figure 5.22, a 10 loops ice-structure interaction processes induced ice load history will illustrate how the submerged ice induced loads (*ice accumulation load*) influence the whole ice load history.

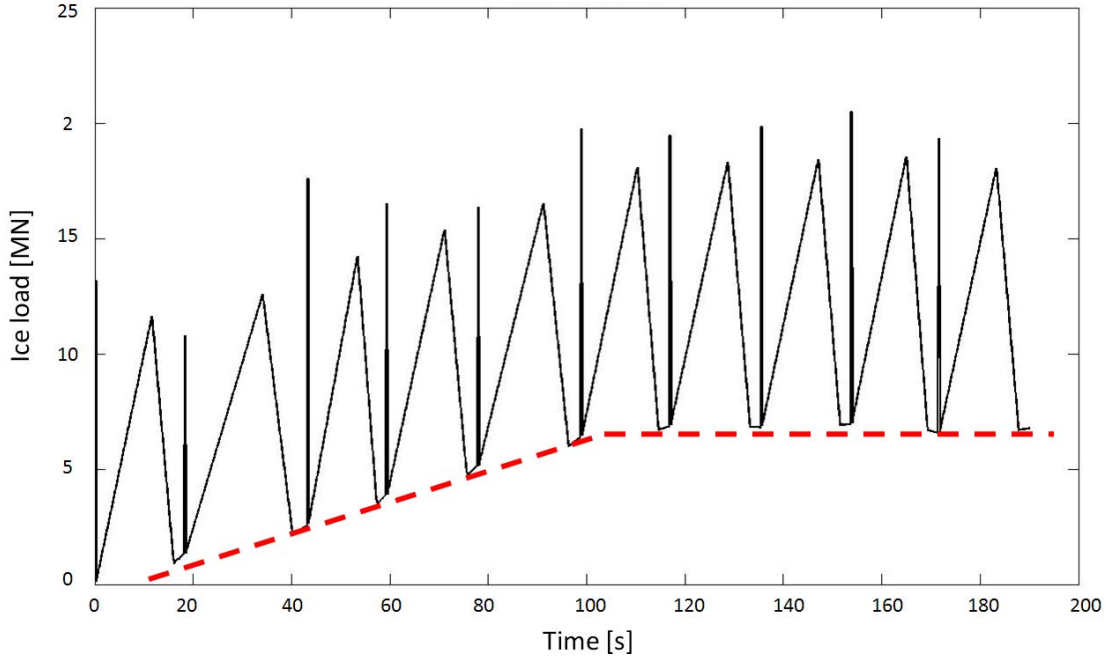

Figure 5.22. The horizontal ice load history in 10 loops simulation of the numerical model

As can be seen from the above Figure 5.22, in each loop, the ice load history is composed of

the above mentioned 4 sections. More important to notice is the *ice accumulation load*. As can be seen from the dashed line which gives a better illustration of how the *ice accumulation load* increases with the increasing submerged broken ice volume. When the submerged ice volume reaches a 'maximum', the ice accumulation induced load will remain around that constant, although there will be certain variations due to the change of the *relative velocity* between the moored conical structure and level ice (see Equation(5.37)).

In Figure 5.23 and Figure 5.24, the ice load history in heave direction and pitch direction are also constructed. All of these load histories will be applied on the moored structure in the next stage of calculation.

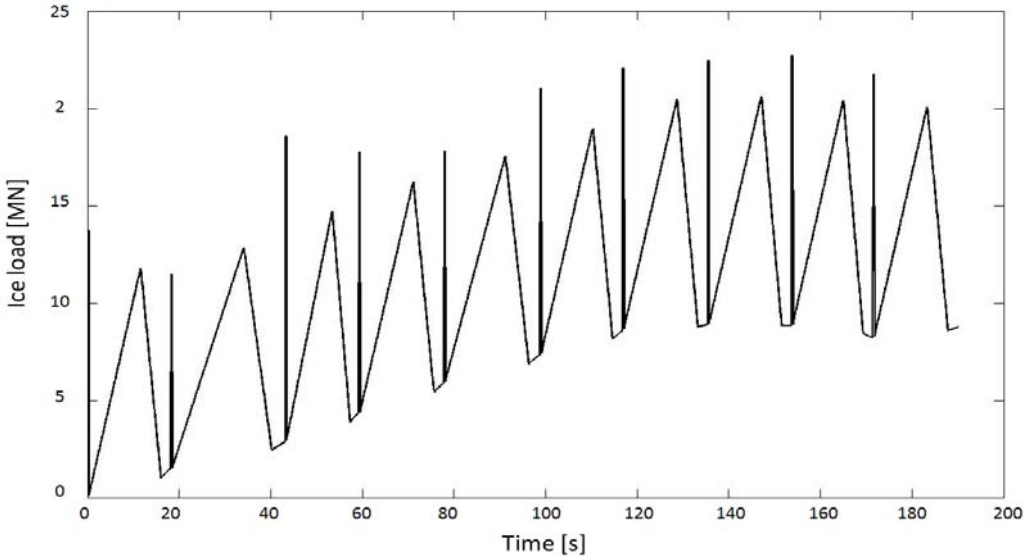

Figure 5.23. The vertical ice load history in 10 loops simulation of the numerical model

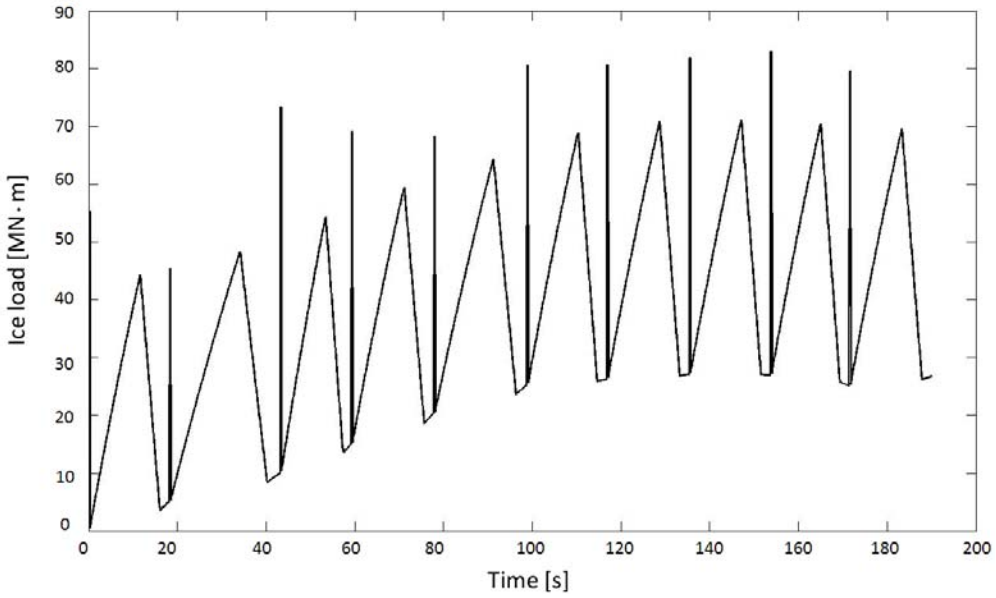

Figure 5.24. The ice load induced pitch moment history in 10 loops simulation

5.4.3 Moored conical structure's responses under the prescribed loading histories

It should be noted that this numerical model is not a real time interaction model. The ice loads and the structure interact with each other in about every 20 s. The interaction is:

- Based on the ice breaking characteristic, about 20 s ice load history is constructed;
- This 20 s time history is applied on the moored structure and the structure's responses are calculated.
- Based on the new moored structure's response, a new ice breaking characteristic is calculated and again new ice load histories are formed.
- New ice load histories will be applied on the moored conical structure.

The moored structure's responses influence the ice load at each time. Such as the moored structure's surge velocity will influence the *ice rotation speed*, *inertia force*, *viscous drag force*, and *ice accumulation volume* etc. A precise numerical model should be a real time interaction model, which means that the interaction is conducted in a very small time step rather than 20 s.

However, after calculation tests, it is found that the structure's velocity change is very small in a 20 s time period as will be shown later. The *relative velocity* between the moored conical structure and level ice remains more or less around 0.5 m/s in the current example. So the *relative velocity* used to calculate the *ventilation load*, *inertia force*, and *viscous drag force* is assumed to be constant during the 20 s loading history.

In Figure 5.22, Figure 5.23, and Figure 5.24, the ice load history has been constructed. In this section, this prescribed ice load history will be applied to the moored conical structure. Some of the inputs for the moored conical structure are listed below:

$r_w = 53.5$ m; the radius of the waterline area

Hydrostatic stiffness is calculated in Appendix E. In the current calculation, only surge, heave and pitch are considered. Hence the hydrostatic stiffness is:

Table 5.1 the hydrostatic stiffness input in the current simulation of the numerical model

	Surge	Heave	Pitch
Surge	0 N/m	0 N/m	0 N^2/rad
Heave	0 N/m	85415826 N/m	1462.625521 N^2/rad
Pitch	0 N^2/rad	1462.62552 N^2/rad	43654116429 N·m/rad

Mooring stiffness:

With the already known experiment data, using the average value to back calculate the mooring stiffness in surge and heave direction which is:

$K_{surge} = 3200000$ N/m;
$K_{heave} = 1578958$ N/m;

Based on the mooring line geometry, the pitch direction stiffness supplied by the mooring lines can be calculated as

$$K_{pitch} = K_{surge} \times (27.5\text{m})^2 + K_{heave} \times (12.5\text{m})^2 = 2666712188 \text{ N·m/rad}$$

Added mass and added damping have been calculated in Section 4.1, they will be stored in a matrix in the numerical program. Once the ice load history has been constructed, it will be easy to calculate the ice load frequency. Assuming the structure's response will be at *steady state.* Then the response frequency will be same as the loading frequency. Based on this, the right added mass and added damping will be selected from the 'added mass and added damp source' for future calculation. Similarly, only the surge, heave and pitch direction are taken into consideration.

With all the above inputs, after calculation, the structure's responses are shown in Figure 5.25:

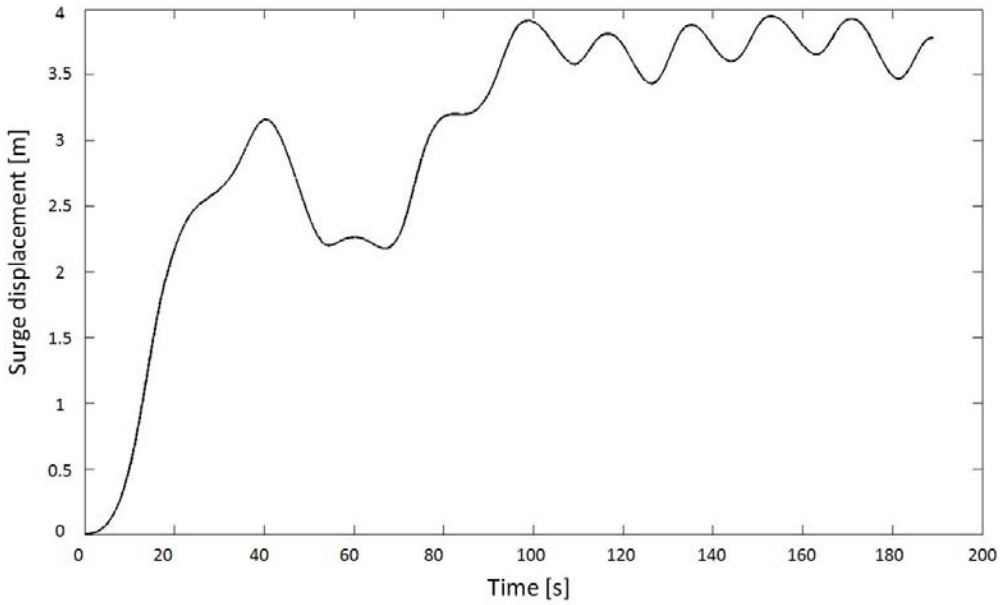

Figure 5.25. The moored conical structure's surge history in 10 loops simulation

As can be seen from the above Figure 5.25, the moored structure's surge displacement increases to around 4 m and then varies around 4 m as time goes by. This is in agreement with the experiment data as will be shown in the next section. Similarly, the heave response and pitch response can also be calculated as shown in Figure 5.26 and Figure 5.27 respectively.

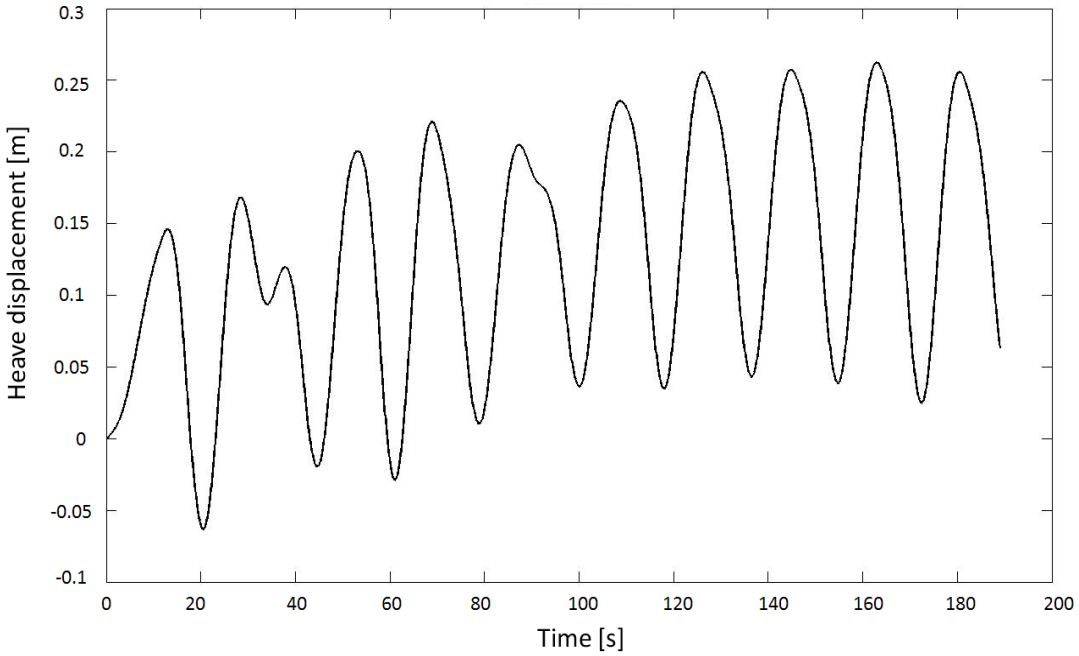

Figure 5.26. The moored conical structure's heave history in 10 loops simulation

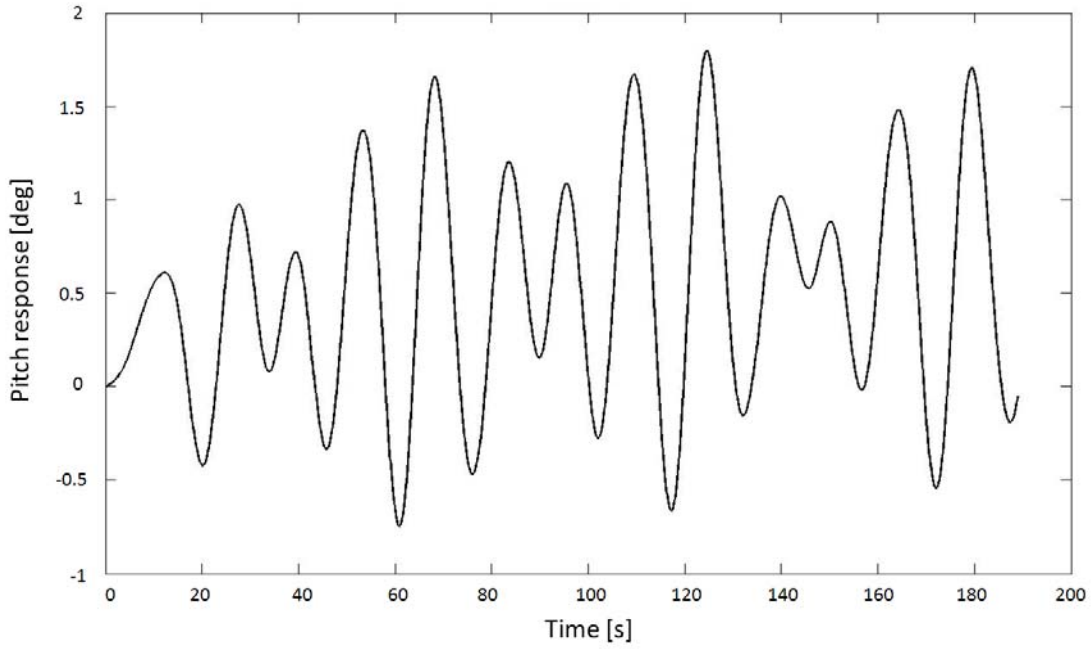

Figure 5.27. The moored conical structure's pitch history in 10 loops simulation

Some other useful outputs:

Besides the structure's surge, heave and pitch response histories, some other structural responses such as velocity and acceleration in surge, heave and pitch direction can also be calculated by the numerical model.

Here the most important surge direction *relative velocity* between the structure and the incoming level ice will be shown at the end of each interaction loop in Figure 5.28. The *relative velocity* is the boundary condition of the calculation in each loop of the numerical model.

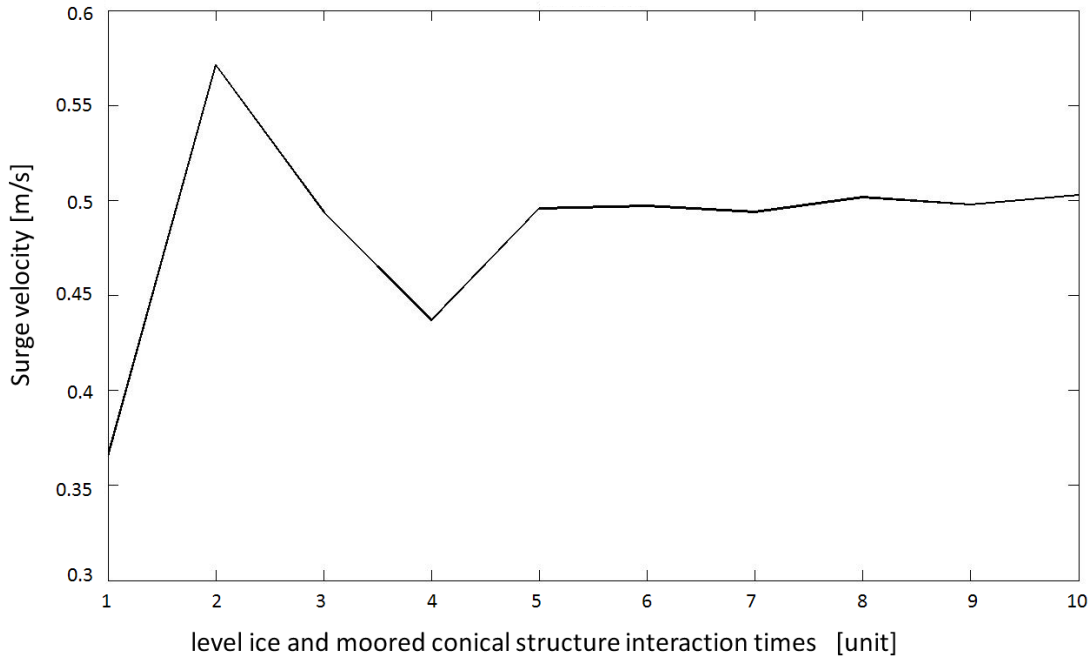

Figure 5.28. The moored conical structure's surge velocity history in 10 loops simulation

As can be seen from the above Figure 5.28 that the initial *relative velocity* between the level ice and moored structure varies with relatively larger amplitudes, but later the velocity appears to converge to the initial velocity, 0.5 m/s in this example. Accordingly, as mentioned before, when calculating the *ventilation load*, *ice inertia force*, and *viscous drag force*, assuming the *relative velocity* to be constant in a 20 s duration is reasonable.

However, it should be noted that this numerical model can calculate the structural velocity at each time step (0.1 s in this example). For simplicity, only the velocity at the end of each loop was shown in the above Figure 5.28. The actual capability of this model is beyond the results in the above Figure 5.28.

With the known hydrodynamic added damping and the velocity of the moored structure in different directions, it is possible to calculate the damped energy during the whole time history. Most of such damped energy is transferred in the fluid field and hence changes the pressure field (e.g. bow wave). This will open a more detailed ice, structure and water interaction research, which will not be covered in the current master thesis. This ice, moored structure and water interaction will be treated in future work.

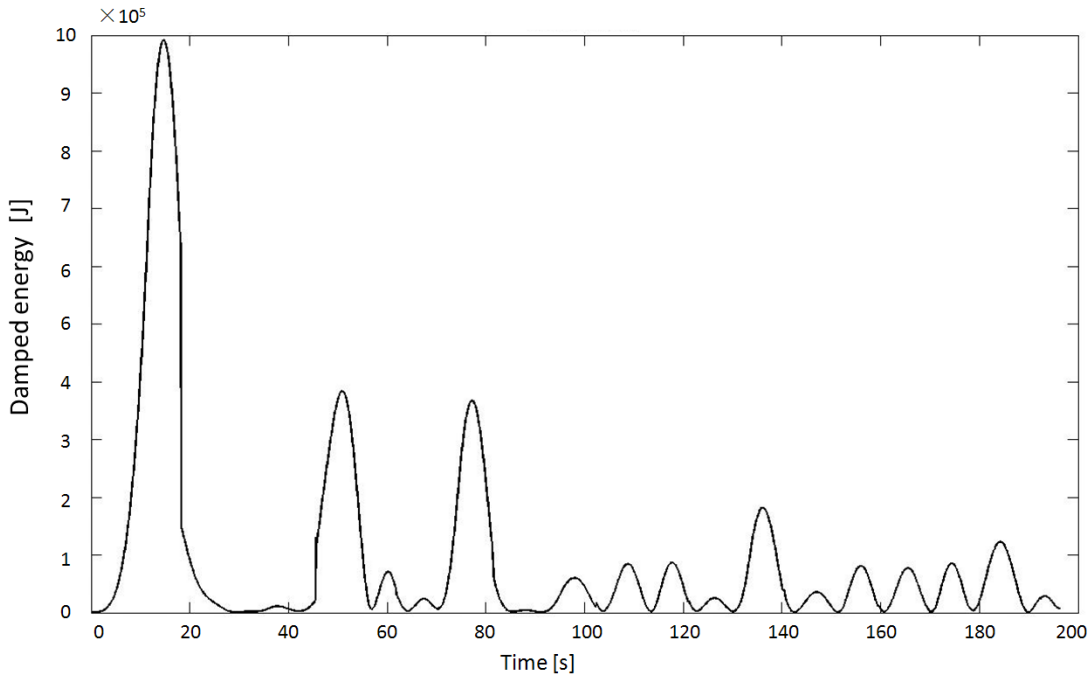

Figure 5.29. The damped energy of the structure in level ice

5.4.4 The numerical simulation results comparing with the experiment data

In the previous section, a simple example with up to 10 loops (about 200 s duration) of the interaction has been introduced so as to illustrate the basic characteristics of the moored conical structure and level ice interactions. In the next stage, this numerical model will run for a sufficient long time so as to obtain the ice load histories and the moored conical structure's response histories which will be compared with the experiment data.

The experiment is conducted in the Hamburg Ship Model Basin (HSVA), the moored model in the current calculation is based on the full-scale of SEVAN FPU-Ice Buoy with draft 26 m operating in ice conditions. The main geometry of the SEVAN FPU-Ice has been entered in the numerical model as input data. The ice condition has been chosen as the same as the level ice in Test #1000. The main inputs are listed in the following:

$v_h = 0.5$ m/s	the *relative velocity* between level ice and moored structure;
$L = 200$ m	the length of 'ice beam' in the calculation;
$\rho_w = 1025$ kg/m^3	the density of sea water;

$\rho_{ice} = 900$ kg/m^3	the density of ice;
$h = 2$ m	thickness of the level ice;
$E = 5 \times 10^9$ Pa	Young's module of ice;
$\sigma_f = 0.54 \times 10^6$ Pa	Flexural strength of ice;
$\Delta l = 1$ m	Length step (element length) during the calculation using FEM;
$\Delta t = 0.1$ s	Time step during the calculation of the ordinary differential equation

Based on the above inputs, the numerical model runs for 100 loops. The structural response histories and the ice load history are given as output.

- Comparisons of the numerical results of structure's surge, heave and pitch responses with the experiment data

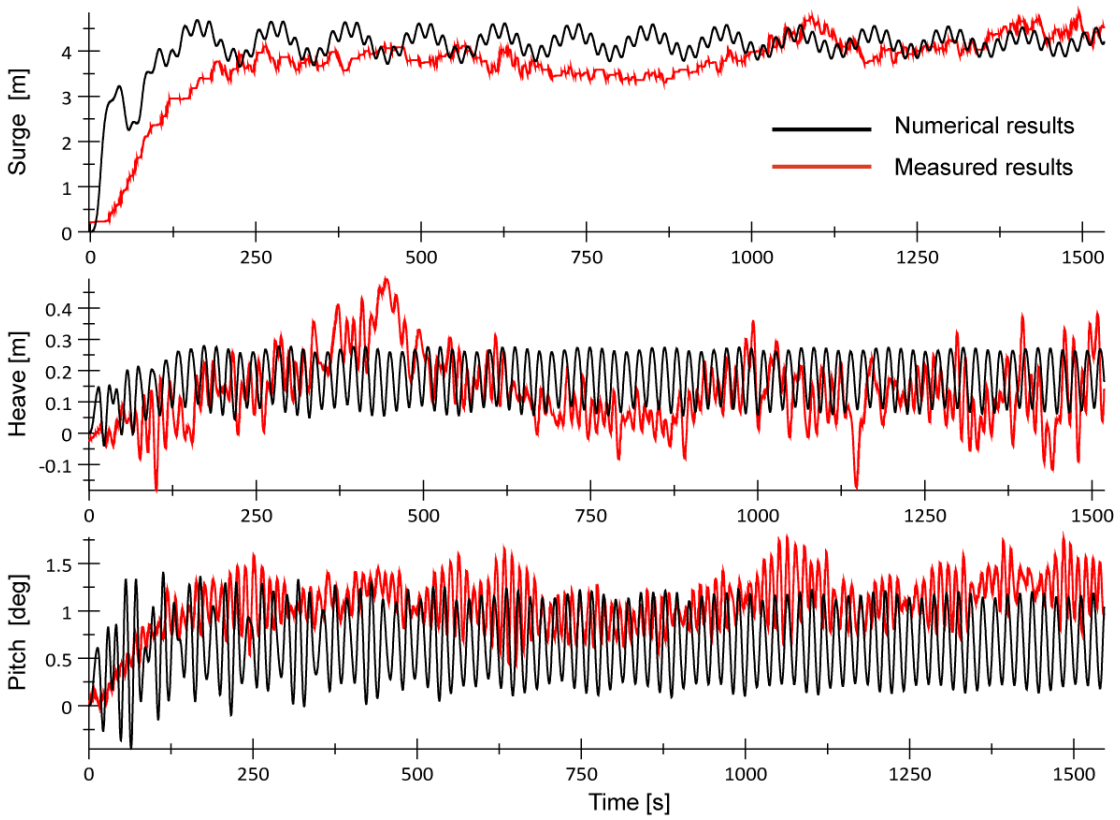

Figure 5.30. The comparison of numerical results with experiment data

(*Upper*: Surge displacement comparison; *Middle*: Heave displacement comparison; *Lower*: Pitch displacement comparison)

As can be seen from the above Figure 5.30, the calculated results of surge, heave and pitch responses are compared with the experiment data respectively. Comments will be given

below:

- Surge displacement:

Advantages of the numerical results:

- A mean surge displacement of 4 m has been predicted well with the experiment data;
- The predicted average surge displacement vibration amplitude is about 0.5 m which is also in agreement with the experiment results;
- The predicted surge response period (high frequency part) also agrees well with the experiment data;

Limitations of the numerical model:

- In the beginning, the predicted surge displacement is much larger than the experiment data. It takes only 200 s for the numerical model to arrive the mean surge displacement 4 m while it takes up to 250 s in experiment.

  The reason for this difference is that in the test, the ice in the transition area of open water to level ice is not as strong as expected. And the structure was not totally enveloped by the ice in the beginning. The overestimated ice loads around the structure leads to the above mentioned difference.

- A longer period of vibration has not been predicted comparing with the test data. This may due to the effect of ice accumulation. It is expected that the ice accumulation volume is relevant with both the structure's geometries and responses. However, in the current model, the ice accumulation volume was only assumed to be relevant with structure's geometry and the surge velocity. Further research regarding the ice accumulation volume with surge displacement is required.

- Heave displacement:

Advantages of the numerical results:

- A mean heave displacement about 0.15 m has been successfully predicted;
- The predicted heave response's frequency and amplitude agree well with the experiment data;

Limitations of the numerical model:

- The difference in the beginning can also be explained by the same reason as in surge situation;
- A larger period heave response has not been predicted in the numerical simulation, this may also due to the incomplete consideration of ice accumulation;

- Several heave spikes have not been predicted in the numerical model, especially in the region from 1250 s to 1500 s. These sudden decreases may due to the random event of water flushing in the void space which has lowered the ice load. However, in the simulation, the *water-flush-in angle*[24] has been assumed to be a constant, 2/3 of the conical face lope angle. The author tried to use random *water-flush-in angle* to calculate the structure response, it is found that the random *water-flush-in angle* allows the presence of such sudden changes in the structural response.

- Pitch response:

Generally speaking, the pitch response prediction is not as good as for surge and heave.

Advantage of the numerical results:

- The pitch vibration frequency has been well predicted.

Limitations of the numerical model:

- The positive pitch response is larger than the numerical simulation result;

  This difference may due to the incorrect calculation method of pitch moment induced by the ice accumulation. Specifically speaking is the incorrect assumption of the pitch moment arm. According to the experiment video, it is hard to determine the submerged ice pieces' action arm on the structure. In the calculation, it has been assumed a constant vertical force action arm around the origin of the coordinate.

- The absolute value of the negative pitch response is much less than the numerical simulation;

  This difference may due to the underestimation of the pitch direction damping effect in ice condition. As pointed out before, because the lack of experiment data, the hydrodynamic coefficients in ice conditions are all assumed to be the same as in open water conditions. This assumption underestimates the damping effect in ice conditions especially with a large amount of broken ice pieces accumulating in the bow region of the structure. The actual pitch direction damping effect should be much larger than in the numerical model.

- The predicted pitch vibration amplitude is much larger (nearly 2 times) than the experiment response.

  This difference is because the dominant ice load period is about 18 s which is quite

[24] The water-flush-in angle is the angle of the rotating broken ice piece with the horizontal water level, at the time when the water start to flush in the void space above the broken ice pieces.

close to the pitch natural vibration period 11.3 s. As explained before, the underestimated damping effect will also lead to a relatively larger pitch response. All these reasons acting together leads to the amplification of the simulation result of pitch response. (see Figure 3.11 for the relationship between response amplification with the frequency ratio)

In order to better predict the pitch response, it is very important to find a reliable calculation method to model the ice accumulation in the bow region of the moored conical structure. This includes the hydrodynamic effects due to the presence of the ice accumulation; the real action arm of the ice accumulation loads; the effect of ice accumulation on ice breaking characteristics (ice breaking length, ice breaking period, etc).

- Some other important outputs of the numerical simulation

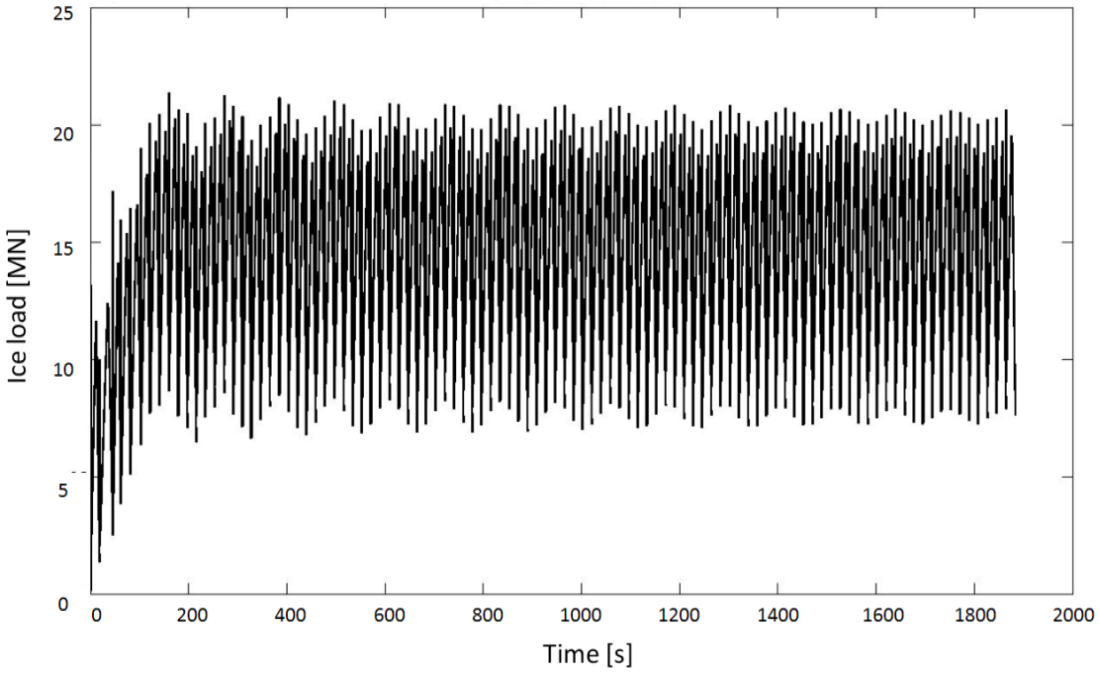

Figure 5.31. Horizontal ice load history

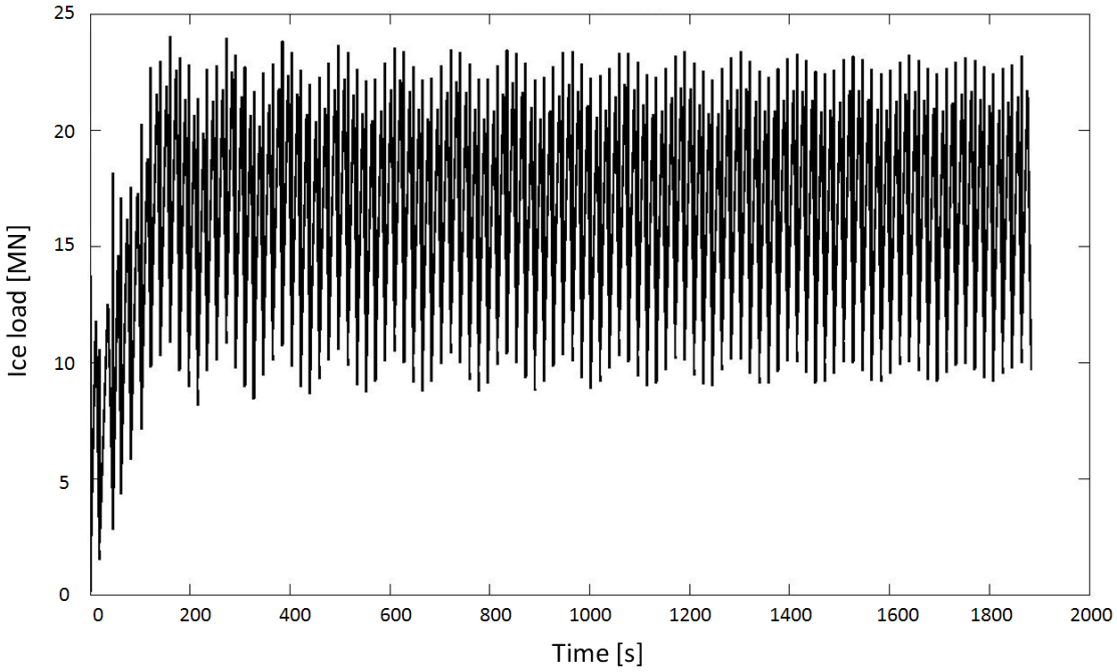

Figure 5.32. Vertical ice load history

From the above two

Figure 5.31 and Figure 5.32 it can be seen that the vertical ice load is generally larger than that of horizontal ice load. This is because the normal ice load was decomposed in the vertical and horizontal direction in a different way. See Section 5.3.1.5 for detailed calculation method.Similarly, the pitch moment history can also be calculated. However, it should be noted the inaccurate assumptions made on the pitch moment arm.

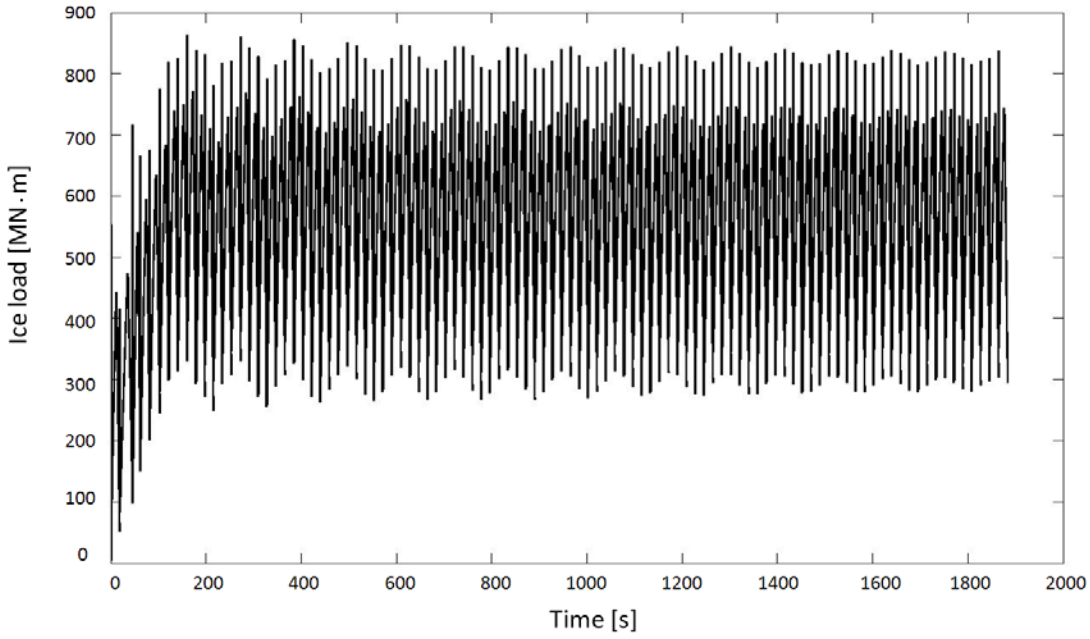

Figure 5.33. Pitch moment history

Furthermore, the surge velocity at the end of each interaction loop can also be recorded and will be shown in Figure 5.34:

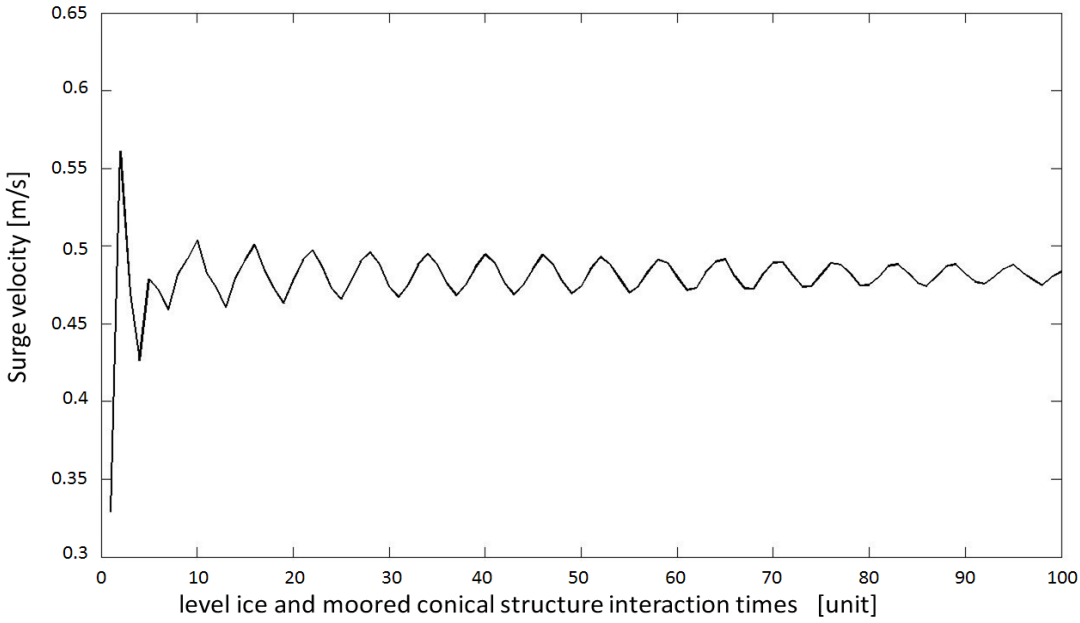

Figure 5.34. Surge velocity history in 100 loops simulation of the numerical model

It can be seen from Figure 5.34 that the moored structure's response (relative horizontal velocity) remains around an almost constant value. The breaking pattern of the ice tends to remain steady as time increases. However, it should bear in mind this happens only in the current situation with the assumption of constant ventilation extent and constant water flush-in speed. In reality, the random situation such ventilation extent, water flush in speed will significantly alter the relative speed and hence change the ice breaking pattern in the next interaction round and accordingly change the ice load histories.

5.5 Discussions about the limitations and suggestions about the current numerical model

The construction and testing of a numerical model to predict the level ice and moored conical structure were conducted in Chapter 5. After introducing the selected simulation models and calculation methods of different ice load components, the simulated response of the structure are compared with the experiment results as shown in Figure 5.30.

It is found that:

- The current model gives good prediction of the surge and heave responses' mean value and vibration frequency.
- The pitch response's frequency is also well predicted by the current numerical model.

However, due to the limitations of this model such as:

- Cannot predict the extent of ventilation which appears as a random phenomena;
- Cannot predict the speed of water flushing in the void space;
- The pitch moment arm is very difficult to determine.
- The hydrodynamic effect in icy water is unclear.

This numerical model cannot predict sudden changes in the response history.

In order to solve the above limitations, the fluid domain should be considered, a comprehensive *ice, structure and fluid interaction* model should be built. Under such comprehensive model, the hydrodynamic properties in icy water condition may be calculated; the pitch moment can be more reliably calculated.

Furthermore the ice properties can be more comprehensively included by changing the 'ice beam' model into a 2D plane model; the ice's strength distribution can also be included; and a more reliable breaking criteria should be chosen.

All of the above suggestions need further research. Concerning the current *level ice and moored conical structure interaction model*, a sentence to conclude this chapter would be:

"*This numerical model predicts well the response of surge and heave, further improvements and adjustments are still needed*"

6 Conclusions

In Part I of this thesis, with the available data regarding the SEVAN FPU-Ice Buoy's model test conducted in HSVA, the level ice and moored conical structure interactions were analyzed based on the structure's responses and the recorded load histories.

Through the frequency domain analysis, and correlation coefficient calculations of different structural responses, relationships between different ice load components and different structural responses were constructed. It is found that:

- The surge displacement was mainly governed by the *ice sliding load* (mainly *ice accumulation load*);
- The pitch displacement is a sensitive indicator of the ice breaking length.
- The *ice rotating load* frequency and pitch response frequency interacts with each other. Based on the analysis, it is found that in most of the cases, the dominant pitch frequency tends to "converge" to its natural frequency. Only with *right-size* of the broken ice could control the pitch response according to the external loading frequency which is required to be away of the natural frequency of pitch.
- Heave responses were influenced by both the *ice accumulation load* and *ice rotating load*. The PSD of heave response was not as concentrated as surge and pitch response.

In the above analysis, a discussion in terms of the ice load transferring processes was made taking into consideration the interface between the ice and structure. The major ice load's transferring paths have been depicted. This load transferring process further confirmed the above conclusions.

Through the discussions about cracks' influence on ice breaking size, a point of view based on *Energy conservation* was introduced in the ice-structure interaction processes. With almost constant energy input from the kinetic energy of the drift ice sheet (almost constant speed and mass), and also almost same ice clearing energy (almost constant volume of broken ice pieces to be cleared), the presence of cracks may induced less ventilation effect and hence reduce the ice rotating energy, with the increased ice breaking energy, relatively larger broken ice floes may be expected. Based on this discussion, it is found in the tests that:

- The presence of cracks may lead to relatively larger broken ice floes;
- Larger broken ice pieces are relatively easier for the structure to clear since structures with larger broken ice pieces around may suffer larger influences from the fluid;
- With increased ice clearing efficiency, the surge response frequency is also expected to increase.

Based on the research in each term of the governing dynamic equation describing the ice and conical structure interactions in surge direction, the ice load was back calculated and compared with the mooring load. It is found that:

- Generally, the inertia load has a double-edged function in breaking ices due to its continuous direction changes. When it is acting in an opposite direction as the ice drift, it is helping the structure to break the ice, hence a relatively lower mooring force than the ice load was encountered; when it is acting in a same direction as the ice drift, the mooring force is expected to be larger than ice load. From the time history, some time the mooring load is larger than the ice load, while some other time the ice load is larger than the mooring load;
- Based on the frequency domain analysis, it is found the *ice sliding load* is mainly counterbalanced by the mooring force while the *ice breaking load* and *ice rotating load* are mainly counterbalanced by both the mooring force and inertia force.

Regarding the influence of different ridges, based on the surge responses under different ridge conditions. It is found that:

- Under the same boundary condition, ridges with less cross sectional area tend to induce less surge responses;
- With similar cross sectional area, the unconfined ridges induce less surge displacement comparing with the confined ridges;
- With similar cross sectional area and similar boundary conditions, the ice management behind the ridge could reduce the surge response.
- After exiting the ridge, the ice accumulation still influences the structure's responses. The PSD of the structural responses appear not as concentrated as before entering the ridge, and in most cases, a low frequency response becomes more dominant comparing with before entering the ridge.

In the end, the level ice and ship interactions were briefly introduced. Based on the knowledge borrowed from this area, the level ice and conical structure interaction processes and involved load components were identified. In developing the numerical model, different

load components' calculation methods were given. After running the numerical model, the outputs (response histories) were compared with the test results. It was found that this numerical model gives good predictions concerning the surge and heave responses. The pitch response was not well predicted due to the inappropriate constant *pitch arm* that has been chosen in the calculation model.

Appendix A. Signal selections

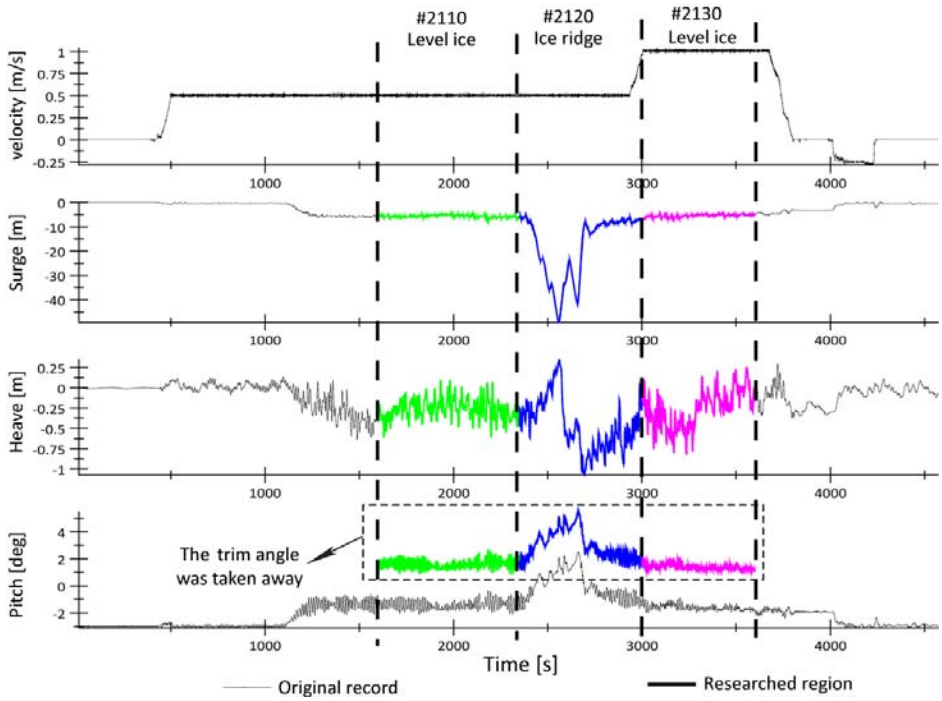

Figure A 1 Signal selection for Test #2000

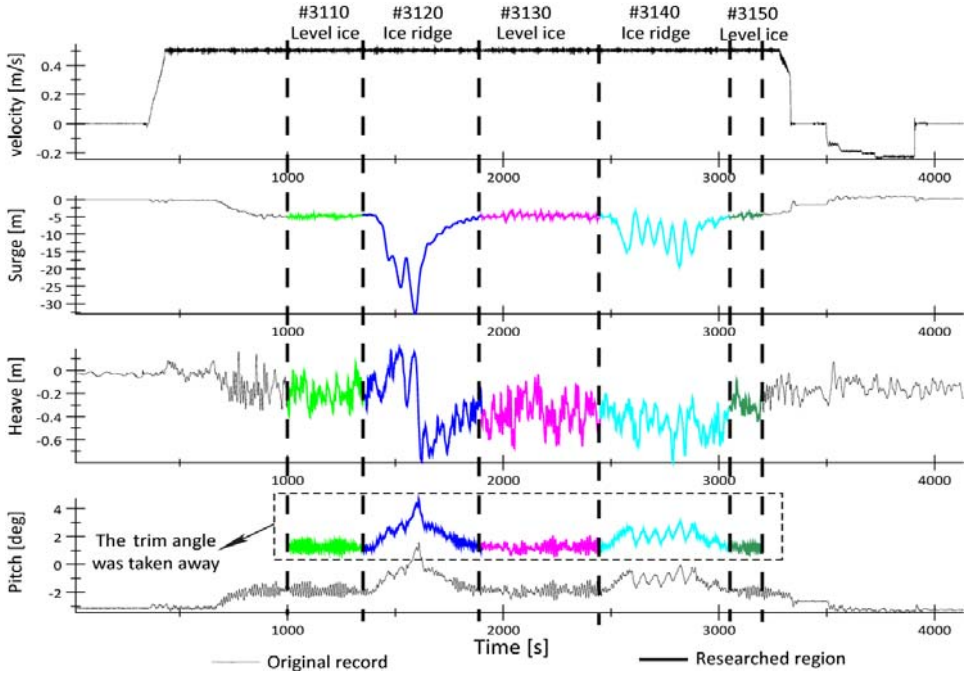

Figure A 2 Signal selection for Test #3000

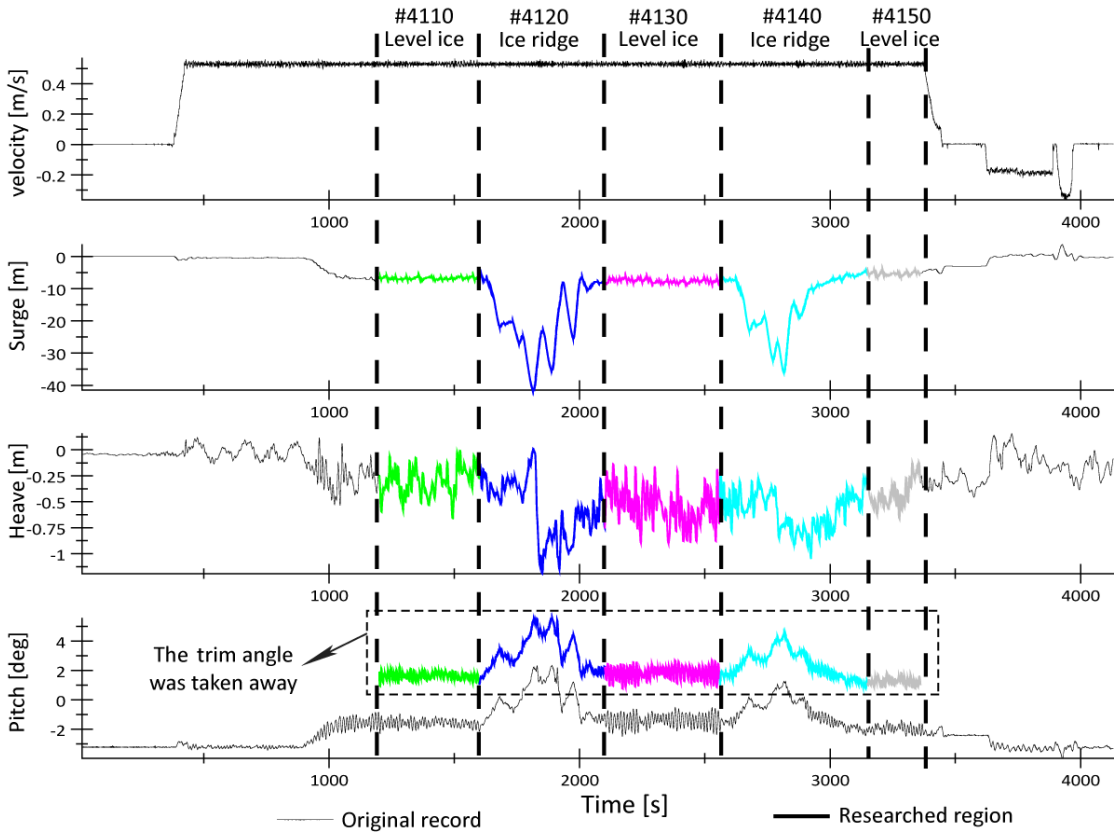

Figure A 3 Signal selection for Test #4000

Appendix B. Fast Fourier Transform and Welch's algorithm

- **Fast Fourier Transform**

At first the basic Fourier transform method for discrete series are introduced:

A Fourier transform allows the transformation of a time domain signal history into the frequency domain. For a continuous time history signal, the transformation can be implemented using the following Fourier Transform Pair:

$$X(\omega) = \frac{1}{2\pi}\int_{-\infty}^{\infty} X(t)e^{-i\omega t}dt$$

$$X(t) = \int_{-\infty}^{\infty} X(\omega)e^{i\omega t}d\omega$$

For discrete time series as in our case, the discrete Fourier transform method is adopted. Formula used when transferring from time domain to the frequency domain can be written as:

$$X(t) = a_0 + a_1\cos\frac{2\pi t}{T} + a_2\cos\frac{4\pi t}{T} + \cdots + b_1\sin\frac{2\pi t}{T} + b_2\sin\frac{4\pi t}{T}$$

$$X(t) = a_0 + \sum_{k=1}^{x}(a_k\cos\frac{2\pi kt}{T} + b_k\sin\frac{2\pi kt}{T})$$

In which the coefficients are calculated by the following formulas:

$$a_0 = \frac{1}{T}\int_{-T/2}^{T/2} X(t)dt = \frac{1}{N}\sum_{t=0}^{T} X(t)$$

$$a_k = \frac{2}{T}\int_{-T/2}^{T/2} X(t)\cos\frac{2\pi kt}{T}dt = \frac{2}{N}\sum_{t=0}^{T} X(t)\times\cos\frac{2\pi kt}{T} \quad (k \geq 1)$$

$$b_k = \frac{2}{T}\int_{-T/2}^{T/2} X(t)\sin\frac{2\pi kt}{T}dt = \frac{2}{N}\sum_{t=0}^{T} X(t)\times\sin\frac{2\pi kt}{T} \quad (k \geq 1)$$

In the above two equations, N is the number of the signal series' value; the $\sum_{t=0}^{T}$ is conducted by every time step Δt; the relationship among Δt, T and N is $N = \frac{T}{\Delta t}$

Since $\frac{2\pi k}{T} = \omega_k$, the above equations can be written as:

$$A(\omega_k) = \frac{2}{N}\sum_{t=0}^{T} X(t) \times \cos(\omega_k t) \quad (\omega_k = \frac{2\pi k}{T}, k \geq 1)$$

$$B(\omega_k) = \frac{2}{N}\sum_{t=0}^{T} X(t) \times \sin(\omega_k t) \quad (\omega_k = \frac{2\pi k}{T}, k \geq 1)$$

Define $X(\omega) = A(\omega) - iB(\omega)$, which is the Fourier Transform of *X(t)*. When introducing the complex number, for $a_0 = 0$, the above calculation for discrete number can be further written as:

$$X(\omega) = \frac{2}{N}\sum_{t=0}^{T} X(t)\, e^{-i\omega t} = 2 \times \sum_{t=0}^{T} X(t)\, e^{-i\omega t} \qquad \text{(B.1)}$$

Then the theory of Fast Fourier Transform will be introduced in the following:
The above deviated Discrete Fourier Transform (DFT) will be re-written here as

$$X_k = \frac{1}{N}\sum_{r=0}^{N-1} X_r\, e^{-i(2\pi kr/N)} \qquad (K = 0,1,2,\dots,(N-1))$$

which has the same meaning as in Equation B.1 except that the parameter '2' in the above equation is omitted for better illustration of the Fast Fourier Transform method.

The FFT is an algorithm for calculating the Discrete Fourier Transform (DFT). The direct calculation approach requires N^2 times of multiplications while FFT reduce the calculation to the order of $N\log_2 N$. The basic algorithm will be introduced below:

Suppose X_r $(r = 0,1,2,\dots,(N-1))$ is a series of signal values. This series can be sub-divided into the following two series Y_r and Z_r by the following relationship:

$Y_r = X_{2r}$ and $Z_r = X_{2r+1}$ $r = 0,1,2,\dots,(\frac{N}{2}-1)$

Applying DFT to Y_r and Z_r separately, we can obtain:

$$Y_k = \frac{1}{N/2}\sum_{r=0}^{N/2-1} Y_r\, e^{-i(2\pi kr/(\frac{N}{2}))} \qquad \text{(B.2)}$$

$$Z_k = \frac{1}{N/2}\sum_{r=0}^{N/2-1} Z_r\, e^{-i(2\pi kr/(\frac{N}{2}))} \qquad \text{(B.3)}$$

$$(K = 0,1,2,\dots,(N-1))$$

Since,

$$X_k = \frac{1}{N}\sum_{r=0}^{N-1} X_r\, e^{-i(2\pi kr/N)}$$

$$= \frac{1}{N}\left\{ \sum_{r=0}^{N/2-1} X_{2r}\, e^{-i(2\pi k(2r)/(\frac{N}{2}))} + \sum_{r=0}^{N/2-1} X_{2r+1}\, e^{-i(2\pi k(2r+1)/(\frac{N}{2}))} \right\}$$

After substitute the above equation with Equation B.2 and B.3, the following relationship could be obtained:

$$X_k = \frac{1}{2}\left\{Y_k + e^{-i(2\pi k/N)} Z_k\right\} \quad k = 0,1,2,\dots,(\frac{N}{2}-1)$$

Since Y_k and Z_k are periodic in k and repeat themselves with period $N/2$, the full version of the calculation can be written as

$$X_k = \frac{1}{2}\left\{Y_k + e^{-i(2\pi k/N)} Z_k\right\} \quad k = 0,1,2,\dots,(\frac{N}{2}-1) \tag{B.4}$$

$$X_k = \frac{1}{2}\left\{Y_{k-N/2} + e^{-i(2\pi k/N)} Z_{k-N/2}\right\} \quad k = \frac{N}{2},\left(\frac{N}{2}+1\right),\dots,(N-1) \tag{B.5}$$

By following this basic method, the signal series could be further sub-divided into smaller series. Applying DFT to these smaller series will return the frequency values of these smaller series. And then these results will be added up together according to the above Equation (B.4) and (B.5). This can increase the calculation speed.

- **Welch's Algorithm (based on the "help file" from MATLAB)**

Welch's method will be practically introduced here by following the command "pwelch". The algorithm behind "pwelch" is

1) The input signal vector *x* is divided into *k* overlapping segments according to window and noverlap (or their default values).
2) The specified (or default) window is applied to each segment of *x*.
3) An *nfft*-point FFT is applied to the windowed data.
4) The (modified) periodogram of each windowed segment is computed.
5) The set of modified periodograms is averaged to form the spectrum estimate $S(e^j\omega)$.
6) The resulting spectrum estimate is scaled to compute the power spectral density as $S(e^j\omega)/S$, where S is the sampling frequency.

This method reduces the calculation times and saves the core storage. It is convenient to apply in nonstationarity tests (Welch, 1967).

Appendix C. Normalized correlation coefficient for sway, roll and yaw

Table C. 1 Normalized cross correlation of sway and roll

Test	Test # 1000	Test # 2000	Test # 3000	Test # 4000
Level ice_1	-0.72	-0.748	-0.785	-0.743
Ice ridge_2	-0.901	-0.811	-0.642	0.534
Level ice_3		0.454	-0.596	
Ice ridge_4		-0.779	0.302	
Level ice_5				

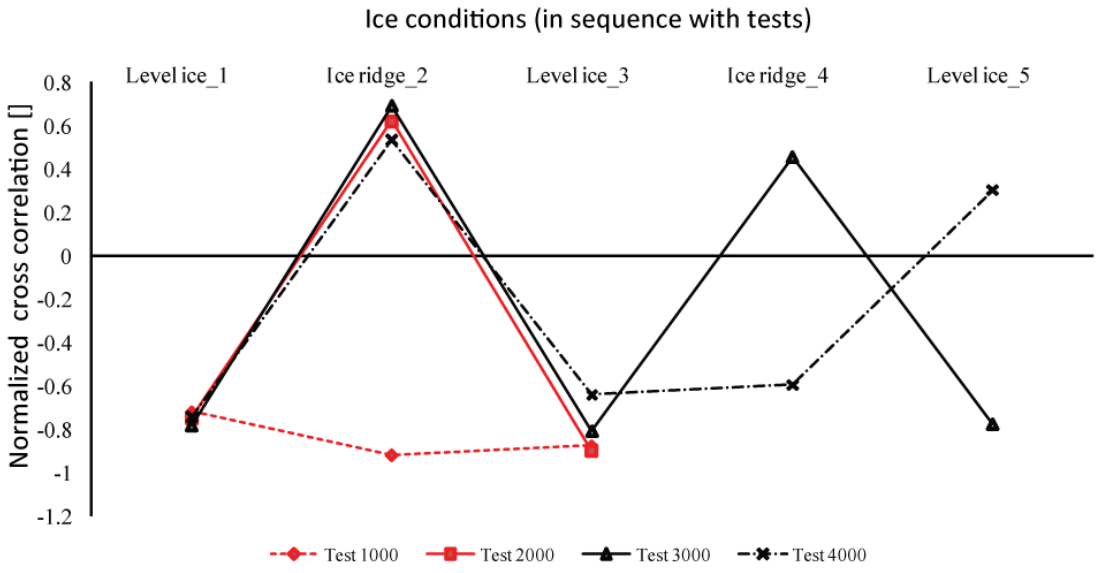

Figure C. 1 Normalized cross correlation of sway and roll in various ice conditions

Different from the correlation for< *Surge*, *Pitch*>, the correlation of <*Sway, Roll*> behaves in an opposite way. Generally speaking, the correlation coefficient for <*Sway, Roll*> is higher in level ice situation than in the ice ridge situation. But the correlation differences between level ice and ice ridge are not consistent in all the tests.

Table C. 2 Normalized cross correlation of sway and yaw

Test	Test # 1000	Test # 2000	Test # 3000	Test # 4000
Level ice_1	0.278	0.266	0.361	0.519
Ice ridge_2	-0.326	0.517	0.715	0.492
Level ice_3	-0.592	0.719	0.605	0.499
Ice ridge_4			0.637	0.627
Level ice_5			0.53	0.552

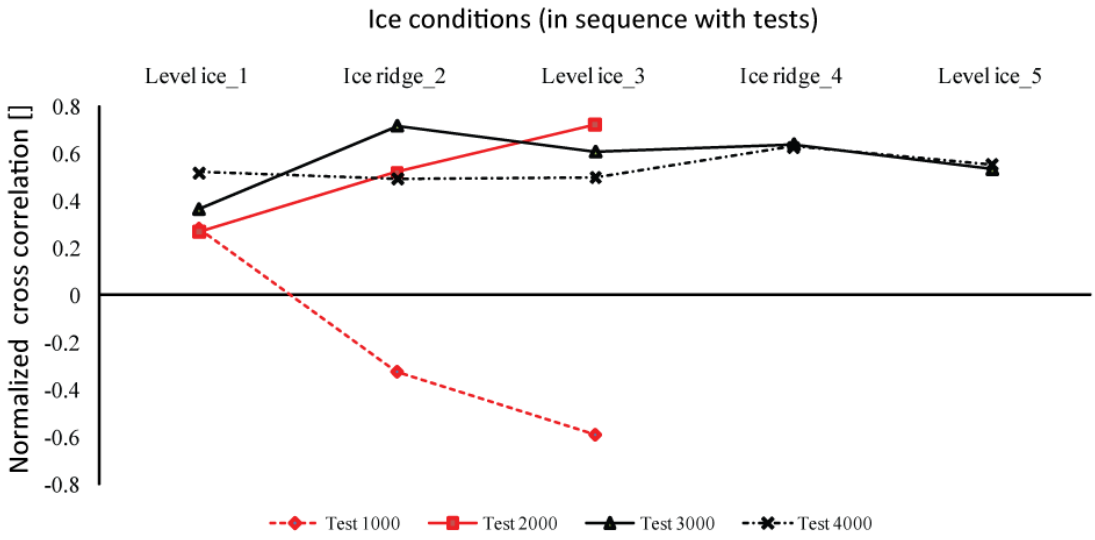

Figure C. 2 Normalized cross correlation of sway and yaw in various ice conditions

The correlations of <*Sway, Yaw*> are relatively smaller than those of <*Sway, Roll*>. All the correlation coefficients in different ice conditions are less than -0.63 and most of them are around 0.5. No consistent difference between level ice and ice ridge is observed.

Table C. 3 Normalized cross correlation of roll and yaw

Test	Test # 1000	Test # 2000	Test # 3000	Test # 4000
Level ice_1	0.22	-0.318	-0.265	-0.246
Ice ridge_2	0.385	0.466	0.649	-0.184
Level ice_3	0.499	0.578	-0.368	-0.322
Ice ridge_4			0.364	-0.38
Level ice_5			0.421	-0.474

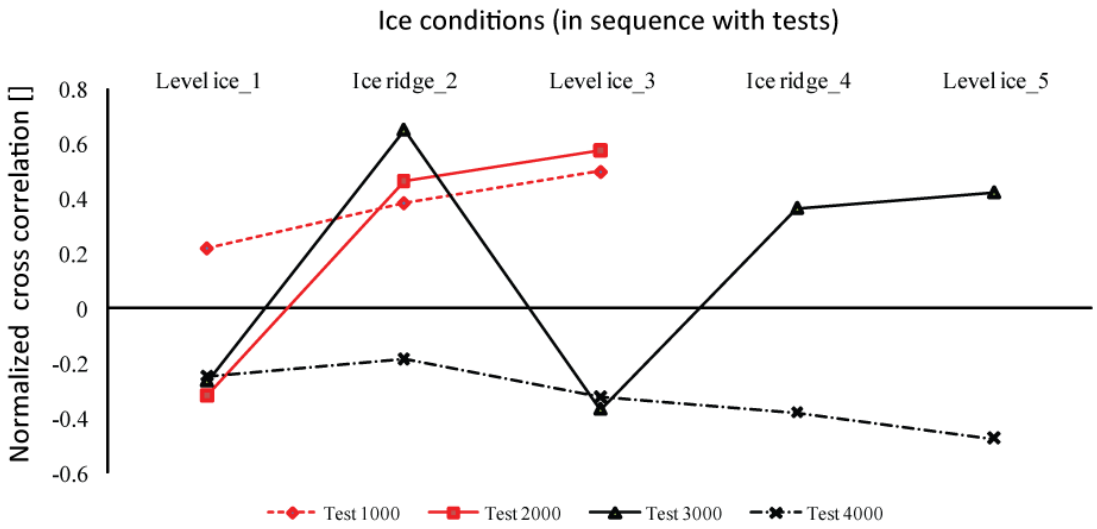

Figure C. 3 Normalized cross correlation of roll and yaw in various ice conditions

The relationship of the correlation of <*Roll, Yaw*> between different ice situations is not obvious.

Based on the above calculation results, the most important observation is that in ice ridge, the correlation between *surge*, *heave* and *pitch* are larger than in level ice.

Appendix D. Hydro-dynamic/static properties of the SEVAN FPU-Ice Buoy

- Hydrostatic properties

	Surge	Sway	Heave	Roll	Pitch	Yaw
Surge	0	0	0	0	0	0
Sway	0	0	0	0	0	0
Heave	0	0	85415825	-2.76	1462.62	0
Roll	0	0	-2.76	4361345	-13284	156.5
Pitch	0	0	1462.6	-13284	4.37E+10	2.6
Yaw	0	0	0	0	0	0

- Hydrodynamic properties

	Surge	Sway	Heave	Roll	Pitch	Yaw
Surge	17270 0000	0	0	0	-7784452 50	69
Sway	0	1727000 00	0	778445 2	0	15952 8
Heave	0	0	1727000 00	-0.69	-159528	0
Roll	0	7784452	-0.69	141988 75	-808	16944
Pitch	-7.78E +08	0	-159528	-808	1.4198E+ 11	-127
Yaw	69.6	159528.1 7	0	16944	-127	2.3E+ 11

Appendix E. Direct integration method to solve the ordinary differential equation system

In this thesis, two ordinary differential equation systems are written in the same form (E-0) and solved by using the direct integration method.

$$[M]\ddot{Y} + [B]\dot{Y} + [K]Y = F \tag{E-0}$$

Due to the unconditionally stability of the implicit methods, and no restriction on the time step size other than as required for accuracy, all the ordinary differential equation system in this thesis are attacked by this effective and stable method, the theory of which will be introduced herein.

The trapezoidal rule relates displacement, velocities and accelerations by:

$$[Y]_{n+1} = [Y]_n + \frac{\Delta t}{2}([\dot{Y}]_n + [\dot{Y}]_{n+1}) \tag{E-1}$$

$$[\dot{Y}]_{n+1} = [\dot{Y}]_n + \frac{\Delta t}{2}([\ddot{Y}]_n + [\ddot{Y}]_{n+1}) \tag{E-2}$$

By applying Taylor's series, the (n+1) term in the right-hand side of the above equations could further be written as:

$$[\dot{Y}]_{n+1} = \frac{2}{\Delta t}([Y]_{n+1} - [Y]_n) - [\dot{Y}]_n \tag{E-3}$$

$$[\ddot{Y}]_{n+1} = \frac{4}{\Delta t^2}([Y]_{n+1} - [Y]_n) - \frac{4}{\Delta t}[\dot{Y}]_n - [\ddot{Y}]_n \tag{E-4}$$

Putting (E-1) to (E-4) back to (E-0), and writing all the (n+1) terms on the left-hand side, and (n) terms on the right-hand side of the equation will allow the results to flow from a previous time (n) to the next time (n+1) during the numerical calculation. The procedures are shown as following:

1. Write the ordinary differential equation at (n+1) time

$$[M][\ddot{Y}]_{n+1} + [B][\dot{Y}]_{n+1} + [K][Y]_{n+1} = F_{n+1}$$

2. Replace the acceleration and velocity terms in (n+1) time with (E-3) and (E-4)

$[M]\left\{\frac{4}{\Delta t^2}([Y]_{n+1}-[Y]_n)-\frac{4}{\Delta t}[\dot{Y}]_n-[\ddot{Y}]_n\right\}+[B]\left\{\frac{2}{\Delta t}([Y]_{n+1}-[Y]_n)-[\dot{Y}]_n\right\}+$

$[K][Y]_{n+1}=F_{n+1}$

3. The next step is to write the (n+1) term on the left-hand side of the equation.

$$([M]\frac{4}{\Delta t^2}+[B]\frac{2}{\Delta t}+[K])[Y]_{n+1}$$
$$=F_{n+1}+[M](\frac{4}{\Delta t^2}[Y]_n+\frac{4}{\Delta t}[\dot{Y}]_n+[\ddot{Y}]_{n)}+[B](\frac{2}{\Delta t}[Y]_n+[\dot{Y}]_n)$$

4. Rewrite the above equation and introduce the effective stiffness and external force term

$$[K^{eff}][Y]_{n+1}=F_{n+1}^{eff} \quad \text{(E-5)}$$

$$\left[K^{eff}\right]=([M]\frac{4}{\Delta t^2}+[B]\frac{2}{\Delta t}+[K]) \quad \text{(E-6)}$$

$$F_{n+1}^{eff}=F_{n+1}+[M](\frac{4}{\Delta t^2}[Y]_n+\frac{4}{\Delta t}[\dot{Y}]_n+[\ddot{Y}]_{n)}+[B](\frac{2}{\Delta t}[Y]_n+[\dot{Y}]_n) \quad \text{(E-7)}$$

With the known initial condition, combining (E-5), (E-6), and (E-7) the time history of the system response could be easily solved by programming in Matlab.

The following programming procedures are adopted (Robert D. Cook, David S. Malkus, Michaele. Plesha, 1989)

1. Form $[M]$, $[B]$, and $[K]$
2. Setting initial conditions: $[Y]_0$, $[\dot{Y}]_0$ and $[\ddot{Y}]_{n+1}=[M]^{-1}(F_0^{eff}-[B][\dot{Y}]_0-[K][Y]_0)$
3. Form the effective stiffness matrix (E-6)
4. Form the effective force matrix (E-7)
5. Solve $[K^{eff}][Y]_{n+1}=F_{n+1}^{eff}$ for $[Y]_{n+1}$
6. Update the velocity $[\dot{Y}]_{n+1}$ and acceleration $[\ddot{Y}]_{n+1}$ using (E-3) and (E-4)
7. Output if desired; or $n\leftarrow n+1$, go to step 4.

Reference of Part I

Anil K. Chopra (2005), *Dynamics of structure*, 2nd edition, P.R.China: Tsinghua University Press (English reprint edition), pp.73

D.E. Newland, (1993), *An introduction to random vibration, spectral and wavelet analysis*, 3rd edition, John Wiley & Sons, pp.61.

Jiancheng Liu, Michael Lau, F. Mary Williams, 2006, *Mathematical modeling of ice-hull interaction for ship maneuvering in ice simulations*, ICETECH06-126-RF

Jorma Kämäräinen, (2007), *Theoretical investigation on the effect of fluid flow between the hull of a ship and ice floes on ice load in level ice*, doctoral thesis

Puntigliano F.M. (2000). Ice Performance of the MPV Neuwerk. *On the Low Pressure Phenomenon between Ice and Hull, Full-Scale Trials, Physical and Mathematical Modelling*. HSVA Report No. 1640 Part B.

R.Federking and J.Schwarz, (1982), M*odel test of ice forces on fixed and oscillating cones*, cold regions science and technology, Vol. 6, pp.61-72

Robert D. Cook, David S. Malkus, Michaele. Plesha, 1989, *Concepts and application of finite element analysis*, 3rd edition, John Wiley & Sons, p406.

Sveinung Løset, (1995), *Science and technology for exploitation of oil and gas-an environmental challenge*, European Networking Conference on Research in the North, Svalbard, 12-16 Sep.

Sveinung Løset, Jan Vidar Aarsnes, (2009), *ICEBREAKING BUOY IN ARCTIC WATERS*

Thomas V. Kotras, Andrew V. Baird, John N. Naegle, 1983, *Predicting ship performance in level ice*, SNAME Transactions, Vol.91, pp329-349.

Wilfrid A. Nixon and Robert Ettema, 1987, *Ice-sheet interaction with a cable moored platform*, IIHR limited distribution report NO. Iowa Institute of Hydraulic Research

Welch, P.D, 1967, "*The Use of Fast Fourier Transform for the Estimation of Power Spectra: A Method Based on Time Averaging Over Short, Modified Periodograms*," IEEE Trans. Audio Electroacoustics, Vol. AU-15 (June 1967), pp. 70-73

Part II

ICE AND CONICAL STRUCTURE INTERACTION BASED ON AKERSOLUTIONS DESIGNED CONICAL STRUCTURES

Table of content for PART II

List of figures for Part II

List of tables for Part II

1 Introduction

Part II of the thesis focuses on the test results of a group of conical structures designed by AkerSolutions. As part of a Joint Industry Project (JIP) “Ice Model Testing of Structures In Ice”, a second ice model test campaign (Phase II) with different models and configurations operating in different ice conditions has been performed in the Large Ice Tank at the Hamburg Ship Model Basin (HSVA), Hamburg, Germany from December 2009 till February 2010. The test campaign is a part of the feasibility study for optimization of structures with downward facing cone at the waterline. The tests were performed by HSVA with support from NTNU. The Ice Model Test Specification was made by AkerSolutions.

This part provides analysis of the results provided by HSVA. The objectives are:

- to interpret the various model test results;
- to discuss and clarify difference in load and behaviour of different tested geometries;
- to discuss and clarify difference in load and structural behaviour in different tested ice conditions (level ice, managed ice, ice ridge, and ice speed).

Chapter 3 in Part II of the thesis provides a general introduction to the test specified in the report “Ice Model Test Specification” prepared by AkerSolutions.

The results for both fixed and moored structures are investigated and analyzed in Chapter 4. Chapter 5 provides comparisons between the measured loads and calculated loads by using the ISO/FDIS 19906 (2009) standard. The results are further discussed in Chapter 6.

Appendix A gives qualitative descriptions of the processes for the maximum loads for different fixed models at a ice speed of 0.1 m/s (full-scale).

Appendix B presents the input data used in the calculations of the ridge load on conical structures following ISO/FDIS 19906 (2009).

2 Summary

Part II of the thesis contains analysis of the results from the tests campaign performed in the Large Ice Tank at the Hamburg Ship Model Basin (HSVA), Hamburg, Germany from December 2009 till February 2010. The analysis is based on the data supplied by HSVA, a technical note "Ice Model Test Specification Rev 02" prepared by AkerSolutions, and the test results reported in the "HSVA Report IO442/10".

Three fixed models and two moored models were tested in different ice conditions with different ice speeds. In the tests, the fixed models were towed through the ice; while for the moored models, the ice was pushed against them.

Among these tests, two fixed models (B&D) were tested with 3 different speeds (0.1 m/s, 0.5 m/s and 1 m/s in full-scale) in intact multi-year level ice and two managed ice floe conditions (with different ice floe size). Except being tested in a larger ice floe condition, the same tests have been conducted for another fixed model (F) and it was also further tested in a multi-year ice ridge with an ice speed of 0.5 m/s. The two moored models were tested in level ice and two different first-year ice ridges with an ice drift velocity of 0.1 m/s. Note that all reported values in Part II of the thesis are full-scale values. Note also that fixed models are labelled "_F" and moored "_M".

The ice conditions in the tests were good and the results are reliable. Although relatively large deviations were observed between the target flexural ice strength and actual flexural strength[25], based on the analysis of the test results, the influence of discrepancy in the flexural ice strengths is not significant enough to blur the comparison and to impair the conclusions.

The influence of ice speed on the dominant ice load frequency was identified. A higher ice speed always induces a higher load frequency. However, the influence of ice speed on the ice load[26] amplitude was not obvious for Model B_F and Model D_F. This was explained as the improvement of ice clearing ability with the increase of ice speed for Models B_F and D_F. The improved ice clearing ability will reduce the *ice accumulation load* so as to offset other

[25] For example, Test #01Li12 with a flexural ice strength of 1000 kPa while the target ice flexural strength was 750 kPa; Test #06Li10 with a flexural strength of 324 kPa while the target ice flexural strength was 500 kPa.

[26] "Ice load" will be frequently used in this part of the thesis. Unless specially pointed out, it means the average ice load the structure encountered.

load components that increase with ice speed. However, for Model F_F, the ice load increases with increasing ice speed. This has been explained by the excellent ice clearing ability of Model F_F regardless of the ice speed difference. Without the improvement of ice clearing ability to offset the load components which increase with increasing ice speed, the total ice load can be expected to increase with the ice speed for Model F_F.

Based on the test results from managed ice (intact level ice broken into distinct floes), it was found that managed ice can largely reduce the ice load, about half of that in level ice. However, the difference in ice floe sizes does not bring too much difference to the amplitude of the average ice load, although slightly larger average ice load was found for the larger ice floe conditions. Similarly, different ice floe sizes only influence the dominant ice load frequency. It was found that the dominant ice load frequency is largely determined by the size of the floes.

It was also found that a larger waterline diameter leads to a longer ice breaking length. If the ice clearing efficiency of two structures are similar (e.g. same shape), the ice load ratio between these two structures is about the ratio of the waterline diameters of these two structures.

The total ice load also depends on the ice clearing ability of the structure. It has been found that the ice clearing ability is related to the diameter and the "neck" width[27] of the structure. Model F_F and Model E_M as updated versions of Model D_F and Model D_M in the Phase I tests were proved to be more effective in clearing ice rubbles.

Comparing with the fixed models, as stated in the conclusions of the Phase I Report, the moored models are believed to have much lower ice load amplitudes and frequency. However, the ridge load for moored models is found to be larger than similar fixed models under similar ridge conditions.

Concerning the first-year ice ridge, certain linear relationships between the ridge cross-sectional area and the ridge load were further confirmed. For moored models, it was also found that the ridge load increases with decreased ice speed.

Concerning the multi-year ice ridge, the major contributor to the ridge load was identified as

[27] The "neck" of the models is used in this report representing the relatively narrow vertical part of the models.

the *ice breaking load* and *ice rotating load*[28]. And the multi-year ridge loading processes are identified.

Furthermore, an ice accumulation induced load with low frequency and high amplitude is believed to exist in the total ice load.

The recommended methods in ISO/FDIS 19906 (2009) were adopted to calculate the ice load and compared with the measured values. It was found that the code tends to underestimate the actual ice loads.

The maximum values in each test (regardless of speed difference) were illustrated in the following figure:

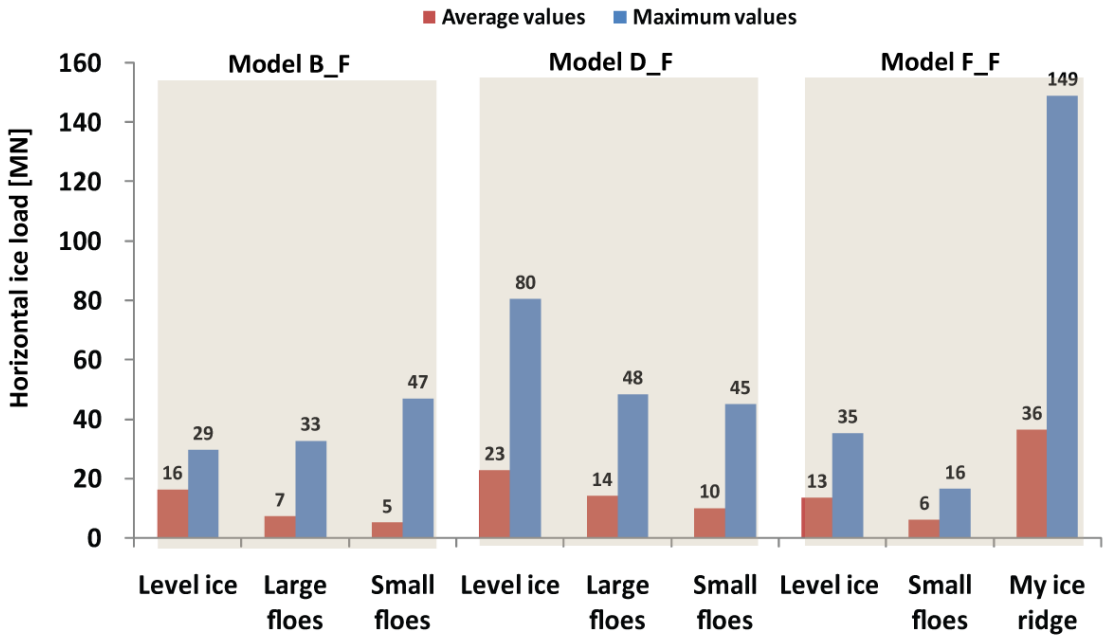

Figure 2.1. Recorded maximum and average horizontal ice loads in different ice conditions for fixed models[29].

Although the above figure is based on tests for an ice speed equaling 0.1 m/s, the dependence of the ice load amplitude on ice speed is not obvious. Figure 2.1 can represent the overall trend of tests for different ice speeds. Moreover, based on the test videos, the maximum load cases for an ice speed of 0.1 m/s were identified and illustrated in Appendix A.

[28] *Ice breaking load* is defined in this report as the total load happened during the *ice breaking phase; Ice rotating load* was defined as the total load happened during the *ice rotating phase.* For detailed ice and conical structure interaction processes and specific definitions to different loads components, please refer to Part I (Chapter 5) of the thesis.

[29] Since the ice load dependence on ice speed is not obvious, only the results from tests with an ice speed of 0.1 m/s are chosen to be illustrated in Figure 2.1.

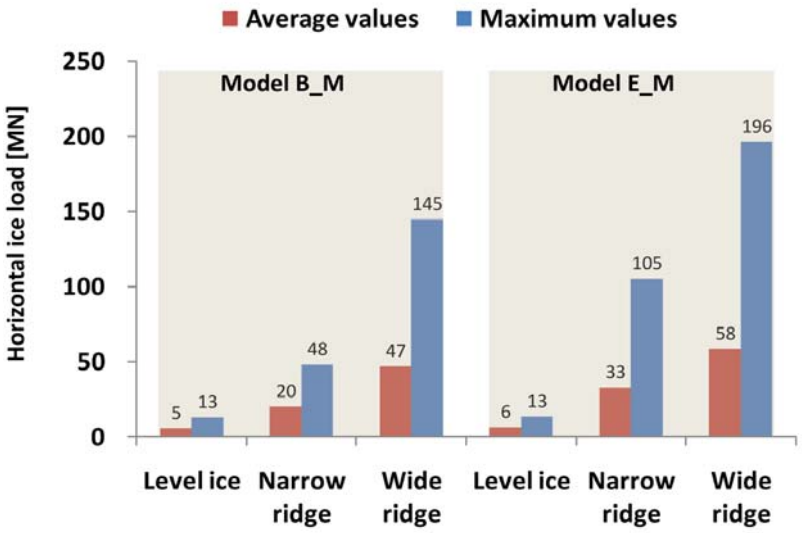

Figure 2.2. Recorded maximum and average horizontal ice loads in different ice conditions for moored structures.

3 Test description

The models were scaled undistorted in scale 1:36 ($\lambda = 36$), and Froude scaling was used as scaling method in order to reflect the inertia and gravity forces, which are dominant in ice-structure interaction problems. Both model quantities and ice properties are scaled according to this scale, meaning that the ice thickness and the flexural strength of the ice sheet is also Froude scaled (Table 3.1). All reported values in Part II of the thesis are full-scale values.

Table 3.1 Scaling factors of different parameters.

Parameters	Scaling factor
Length	λ
Time	$\lambda^{0.5}$
Speed	$\lambda^{0.5}$
Acceleration	1
Force	λ^{3}
Moment	λ^{4}
Mass	λ^{3}
Angle	1
Angular velocity	$\lambda^{-0.5}$
Flexural strength	λ
Crushing strength	λ
Modules of Elasticity	λ
Coefficient of friction	1

Note also that fixed models are labelled “_F” and moored “_M”.

3.1 Fixed models

Three fixed models were tested, all of which are conical hulls with a 45° slope angle at the waterline. Among these three fixed models, Model B and Model D have been tested in Phase I. In Phase II, Model B_F, Model D_F and Model F_F were tested in level ice, ice ridges and in managed ice with typical floe sizes of $150\ \text{m} \times 200\ \text{m}$ and $30\ \text{m} \times 50\ \text{m}$. The ice drift speeds were 0.1 m/s, 0.5 m/s and 1 m/s, respectively.

The geometries of the models are shown in the following figures in full-scale:

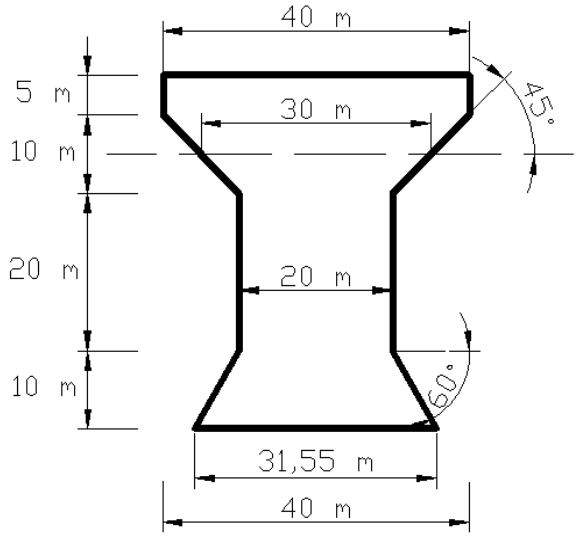

Figure 3.1 Geometry of Model B_F.

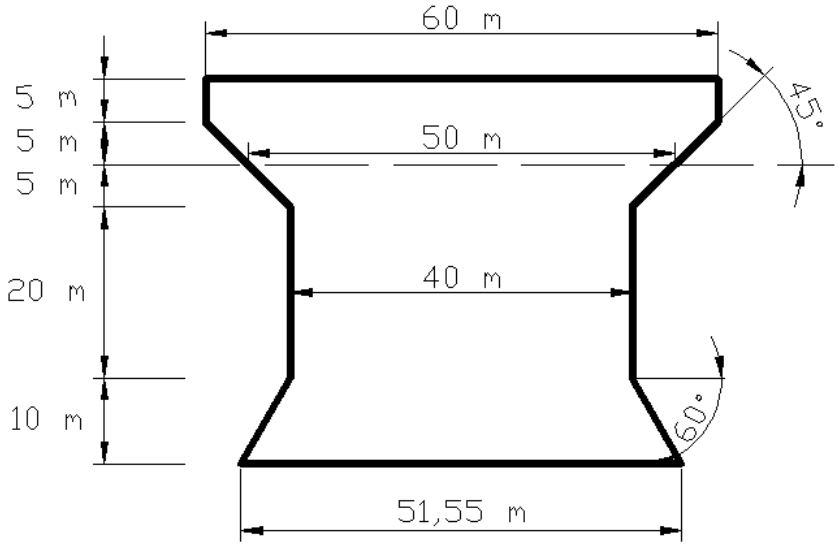

Figure 3.2 Geometry of Model D_F.

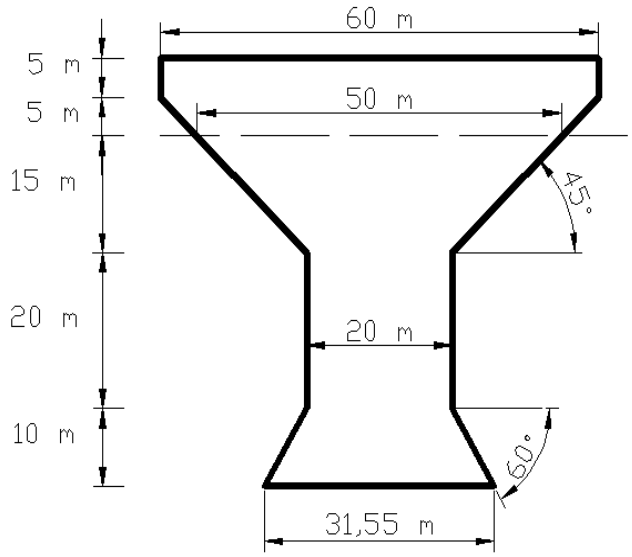

Figure 3.3 Geometry of Model F_F.

3.2 Moored models

Two moored models (Model B_M and Model E_M) were tested in first-year level ice and ice ridges with an ice speed of 0.1 m/s.

Model B_M is a spar-type floater and it was also tested in Phase I of this JIP.

Model E_M is a buoy-type floater and it is an updated version of Model D_M to improve the ice clearing ability by narrowing the vertical part of the structure.

The main characteristics of these two moored structures are shown in Table 3.2.

Table 3.3. Main characteristics of Model B_M and Model E_M.

Items	Model B_M	Model E_M
Hull height [m]	160	85
Maximum/minimum diameter [m]	41.7/ 20	100/37.2
Waterline diameter [m]	30	50
Draft [m]	150	70
Displaced volume [m^3]	169372	233539
Centre of Gravity above Elevation 0.0 [m]	58.4	17.1
Metacentric height, GM [m]	4.9	4.2
Radius of gyration about centre of Gravity [m]	49.5	25
Cone angle [^{o}]	45	30

The main geometries of these two models are shown in the following figures.

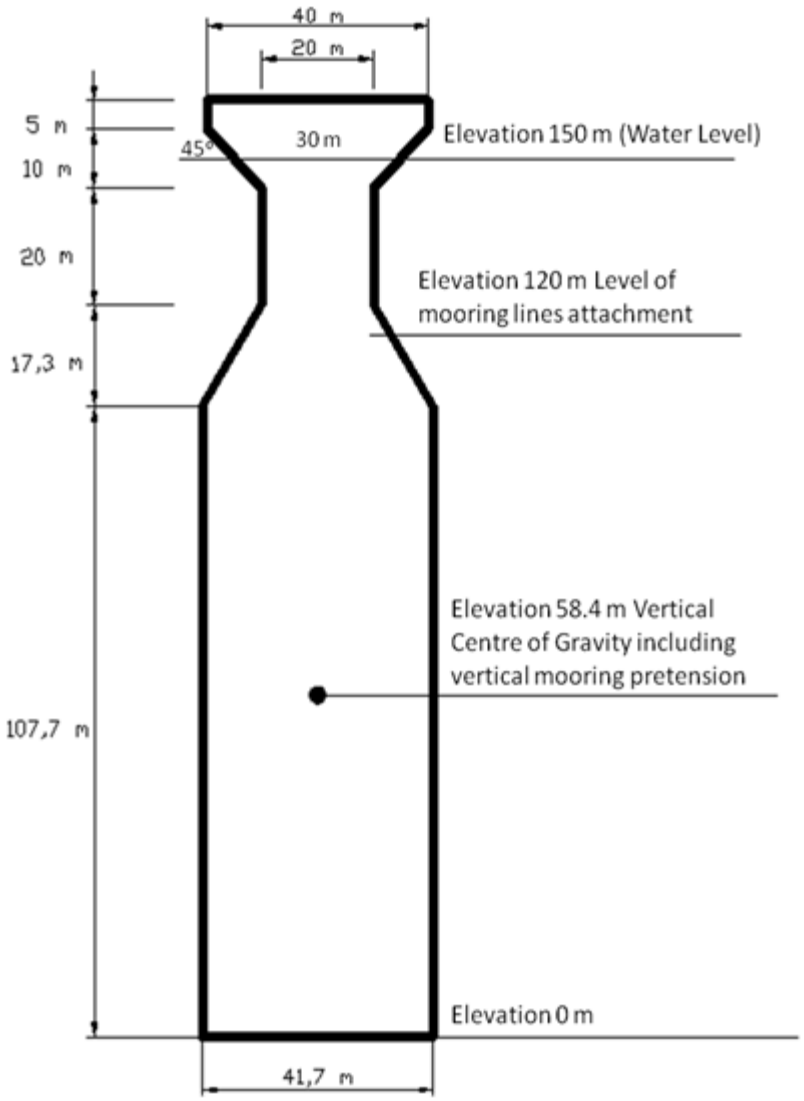

Figure 3.4 Geometry of Model B_M.

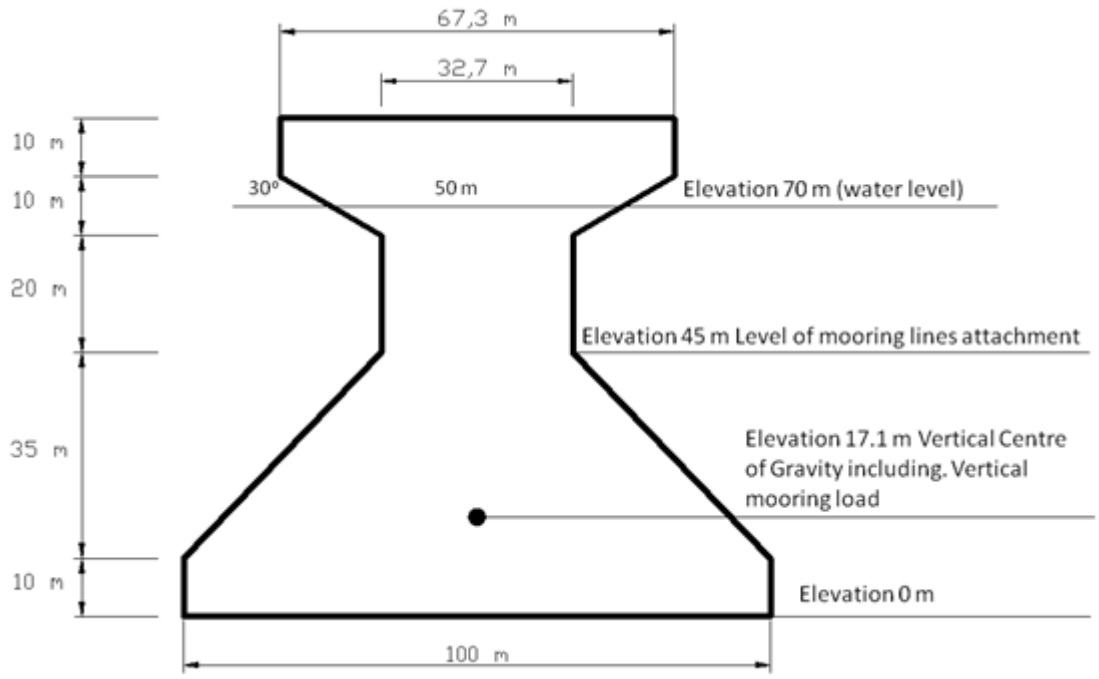

Figure 3.5. Geometry of Model E_M.

3.3 Test description

The test series and main characteristics are described in the following tables. Models B_F and D_F were tested in level ice and two different managed ice conditions for three different ice speeds.

Table 3.4. Test series for Model B_F.

Test series	Ice feature	Speed [m/s]	Thickness [m]	Concentration [%]	Floe size [m]
01Li10	Level ice	0.1	3	Intact ice	-
01Li11	Level ice	0.5	3	Intact ice	-
01Li12	Level ice	1	3	Intact ice	-
01Li30	Managed ice	0.1	3	9/10	150-200
01Li31	Managed ice	0.5	3	9/10	150-200
01Li32	Managed ice	1	3	9/10	150-200
01Li40	Managed ice	0.1	3	9/10	30-50
01Li41	Managed ice	0.5	3	9/10	30-50
01Li42	Managed ice	1	3	9/10	30-50

Table 3.5. Test series for Model D_F.

Test series	Ice feature	Speed [m/s]	Thickness [m]	Concentration [%]	Floe size [m]
02Li10	Level ice	0.1	3	Intact ice	-
02Li11	Level ice	0.5	3	Intact ice	-
02Li12	Level ice	1	3	Intact ice	-
02Li30	Managed ice	0.1	3	9/10	150-200
02Li31	Managed ice	0.5	3	9/10	150-200
02Li32	Managed ice	1	3	9/10	150-200
02Li40	Managed ice	0.1	3	9/10	30-50
02Li41	Managed ice	0.5	3	9/10	30-50
02Li42	Managed ice	1	3	9/10	30-50

Table 3.6. Test series for Model F_F.

Test series	Ice feature	Speed [m/s]	Thickness [m]	Floe size [m]
03LI10	Level ice	0.1	3	-
03LI11	Level ice	0.5	3	-
03RI12	Multi-year ice ridge	0.5	-	-
03LI13	Level ice	1	3	-
03Li40	Managed ice	0.1	3	30-50
03Li41	Managed ice	0.5	3	30-50
03Li42	Managed ice	1	3	30-50

The two moored models were tested in level ice and two different ice ridges with the same speed of 0.1 m/s. The main characteristics are shown in the following tables.

Table 3.7. Test series for Model B_M.

Test series	Ice feature	Speed [m/s]	Thickness [m]	Consolidated layer [m]	Keel width [m]	Keel depth [m]
04Li10	Level ice	0.1	2	-	-	-
04Ri50	Ice ridge	0.1	2	3	80	20
05Li10	Level ice	0.1	2	-	-	-
05Ri50	Ice ridge	0.1	2	3	120-160	20

Table 3.8. Test series for Model E_M.

Test series	Ice feature	Speed [m/s]	Thickness [m]	Consolidated layer [m]	Keel width [m]	Keel depth [m]
06Li10	Level ice	0.1	2	-	-	-
06Ri50	Ice ridge	0.1	2	3	80	20
07Li10	Level ice	0.1	2	-	-	-
07Ri50	Ice ridge	0.1	2	3	120-160	20

4 Analysis of the test results

4.1 Fixed structures

4.1.1 Intact level ice

In Tests #10Li10_11_12 and Tests #02Li10_11_12, Model B_F and Model D_F were tested in 3 m thick level ice with ice speeds of 0.1 m/s, 0.5 m/s and 1 m/s, respectively. The ice load histories were recorded. In the current analysis, only the horizontal ice loads were examined in the frequency domain and their statistics were identified. The results are reported in tables and figures in the following.

4.1.1.1 Model B_F

As can be seen from Figure 4.1, three samples of the horizontal ice load histories were exemplified (left) together with the Power Spectral Density (PSD) of the whole ice load histories for different ice speeds.

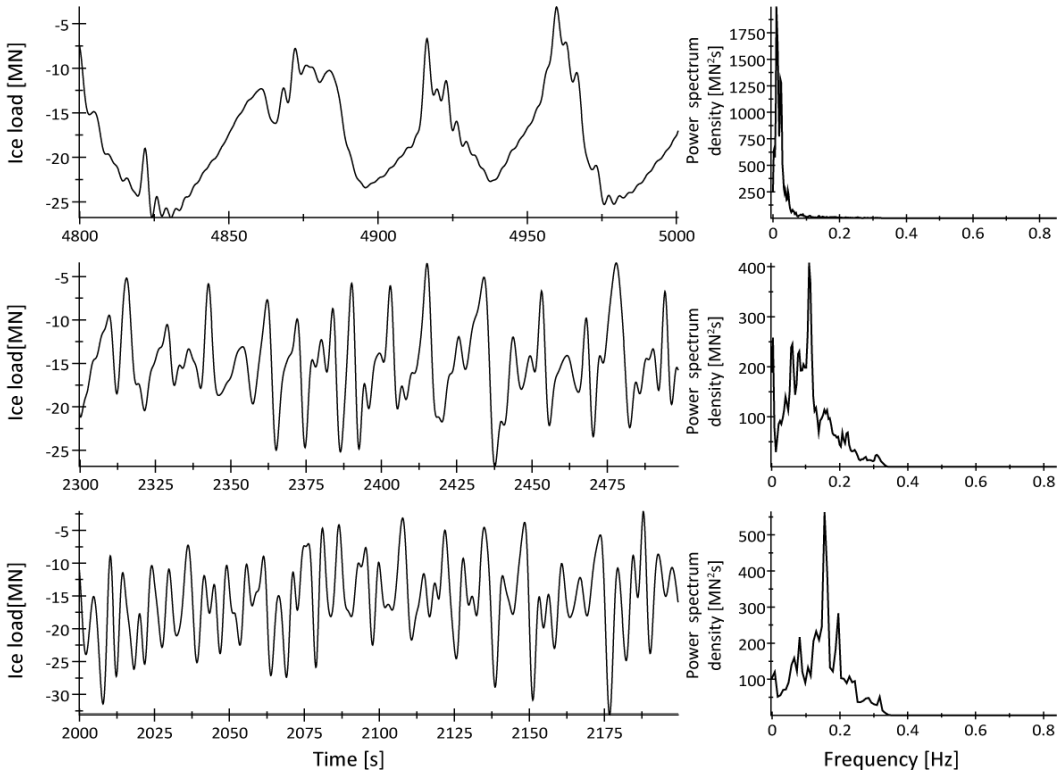

Figure 4.1. Model B_F in level ice for different ice speeds (v).

(*top:* 0.1m/s; *middle*: 0.5m/s; *bottom:* 1m/s).

It is found from Figure 4.1 that:

1) As the ice speed increases, the dominant ice load frequency also increases. This is in agreement with natural sense.
2) Generally speaking, the dominant ice load frequency resides in low frequency.

Assuming that the ice load period is coinciding with the ice breaking period, by multiplying the ice speed, the ice breaking length can be related to the ice load period as shown in Table 4.1.

Table 4.1. Frequency domain analysis and statistics of horizontal ice load for Model B_F in level ice.

Model B_F	Level ice	Natural frequency [Hz] = 1.052 Hz	
Speed [m/s]	Peak frequency [Hz]	Dominant Period [s]	Breaking length [m]
0.1	0.010	98.04	9.80
0.5	0.11	9.09	4.55
1	0.155	6.45	6.45
Speed [m/s]	Maximum Load [MN]	Average Load [MN]	Std. deviation [MN]
0.1	-29.48	-16.17	5.57
0.5	-32.87	-16.97	5.21
1	-34.89	-16.05	5.99

From Table 4.1, it can be concluded that as the ice speed increases, the average breaking length decreases. The dominant breaking length for an ice speed equaling 1 m/s is 6.45 m which is larger than 4.55 m for an ice speed of 0.5 m/s. However, due to the fact that for an ice speed of 1 m/s, a relatively larger portion of the ice load frequency resides in the high frequency band as shown in Figure 4.1. This will induce relatively shorter breaking lengths. It is reasonable to expect that the average ice breaking length is shorter when the ice speed is 1 m/s.

The statistics of the ice load history has been calculated and listed in Table 4.1. The average horizontal load doesn't change too much. Since the *ventilation load*[30] and *ice sliding load*[31] contribute to a large portion of the total ice load (Kämäräinen, 2007), it is useful to explain

[30] *Ventilation load* is defined here as the force required to rotate the broken ice pieces with the presence of the (partial/full) ventilation phenomena. It is calculated by considering only the pressure difference above and below the broken ice pieces. It is a part of the *ice rotating load* during the *ice rotative phase.* For detailed process and definition, see Part I (Chapter 5).

[31] *Ice sliding load* is the load arising during the *ice sliding phase*, induced by the already submerged broken ice pieces sliding around the conical structure. It is further sub-divided into the *ice accumulation load*, and two other forms of loads. For detailed process and definitions, see Part I (Chapter 5).

the average ice load for different ice speeds by first explaining the *ventilation load* and *ice sliding load* for different ice speeds.

It has been point out by Kämäräinen (2007) that the *ventilation load* is not sensitive to the ship velocity during the ship-level ice interaction process. In our ice and conical structure interaction situation, the same conclusion can be drawn as will be discussed in the following.

It is recognised that higher ice speeds lead to shorter ice breaking lengths. Shorter ice breaking lengths mean smaller broken ice masses for the conical hull to rotate. However, as can be seen from the video of the tests, as the ice speed increases, the void space above the broken ice pieces becomes more obvious (see Figure 4.2, Figure 4.3 and Figure 4.4). For relatively low speeds, although longer ice breaking lengths are present, the broken ice was soon submerged into the water and only a partial (or no) ventilation phenomena were induced. While at high ice speeds (1 m/s), a void space above the shorter broken ice is obviously observed. It can be generalized as at low ice speeds, we have longer broken ice pieces together with less void space above it; at high ice speeds, we have shorter broken ice pieces but a larger void space above it. In both cases, the *ventilation load* may remain almost the same. Accordingly it is reasonable to conclude that the *ventilation load*'s contribution to the total average ice load is not sensitive to the ice speed.

Figure 4.2. The water flush-in area above the broken ice for an ice speed of 0.1 m/s.
(The photo was visually cut from the video just before the next breaking and water flush (stitched area) was processed visually as well; the area above the broken ice is totally submerged).

Figure 4.3. The water flush-in with indication of direction and area above the broken ice for an ice speed of 0.5 m/s. (The photo was visually cut from the video just the before the next breaking and the water flush-in area was processed visually as well; the area above the broken ice is partially ventilated).

Figure 4.4. The nearly fully ventilation phenomenon for an ice speed of 1 m/s. (The photo was visually cut from the video just before the next breaking and no water flush-in phenomenon was visually observable; it can be assumed to be a fully-ventilated situation).

Another major contribution to the total ice loads comes from the *ice sliding load* arising during the ice sliding phase. This phenomenon relates to friction between ice and hull. Valanto (2001) claimed that the *ice sliding load* increases with increasing ship speed for ships advancing in ice. Kämäräinen (2007) discriminated at least three different load components in the ice sliding phase. One of them is the static buoyancy of the broken ice pieces which will

be termed as *ice accumulation load*[32] in Part II of the thesis. Another two load components increase with increased ship speed.

Different from the ship-ice interaction, for the test models, significant ice accumulations in the bow region of the tested models are observed. The volume of the accumulated broken ice pieces decrease with increased ice speed. As can be seen from the test videos (see Figure 4.5), for higher ice speeds, the ice clearing ability of the models has been improved. This means that higher ice speeds result in less ice accumulation induced loads. The *ice accumulation load* decreases with increasing ice speed.

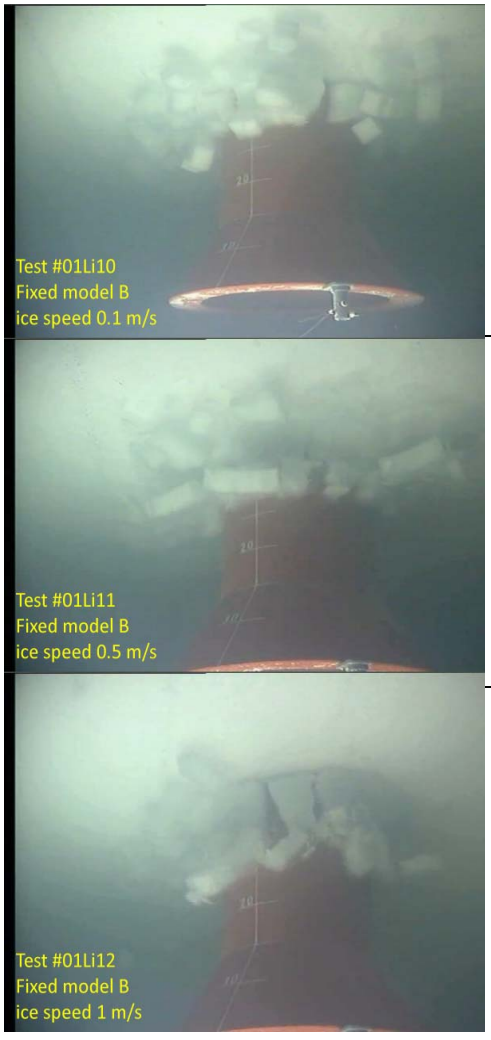

For an ice speed of 0.1 m/s the broken ice pieces after being pushed downward tend to be pitched back and accumulate in the bow region of the model.

As can be seen from the left figure, a large volume of broken ice pieces accumulated in the bow region of the model.

For an ice speed of 0.5 m/s, the same process happened for the broken ice pieces. However, due to the relatively larger ice speed, the broken ice pieces slide around the model with a relatively faster speed, and less volume of broken ice pieces accumulated in the bow region of the model.

For an ice speed of 1 m/s, instead of pitching back again, the broken ice pieces tend to slide around the structure directly. Very few broken pieces accumulated in the bow region of the model. For higher speeds we may also expect more flexing (heave) of the ice cover dynamics causing instabilities in the possible accumulations upstream.

Figure 4.5. Photo of ice accumulation volumes for different ice speeds for Model B_F.

Although the other two components of the *ice sliding load* increase with increasing ice speeds,

[32] For detailed ice and conical structure interaction process and definition please refer to Part I (Chapter 5) of the thesis..

due to the effect of a decreasing ice accumulation load with increasing ice speed, it is reasonable to assume that the total *ice sliding load* is not sensitive to ice speeds.

In conclusions, both the two major contributors (*Ventilation load* & *Ice sliding load*) are not sensitive to ice speeds. Moreover, the *ice accumulation load* decreases with increasing ice speed. It is reasonable not to expect an obvious ice speed dependency of the total ice load.

4.1.1.2 Model D_F

In Tests #02LI10_11_12, Model D_F was tested in level ice. Three ice load samples (left) and corresponding overall PSD (right) are displayed in Figure 4.6.

Similarities to Model B_F:

Similar conclusions as for Model B_F can be obtained herein:

1) As the ice speed increases, the ice load's frequency also increases.

2) The ice loads amplitude's dependence on ice speed is also not obvious.

The ice breaking length estimation based on the ice load frequency was also conducted and listed in Table 4.2. Similar conclusions that higher ice speeds lead to shorter ice breaking length were identified. The average ice loads under different ice speeds also remain more or less the same (around 23 MN). Same explanations apply as stated in Section 4.1.1.1, and similar *ventilation load* and *ice accumulation load*'s ice speed dependences have been observed in the relevant test videos which will not be illustrated again herein.

Difference to Model B_F:

1) Model D_F causes relatively larger ice breaking lengths;

2) Model D_F has larger horizontal ice loads.

The differences will be further discussed in Section 4.1.2.5.

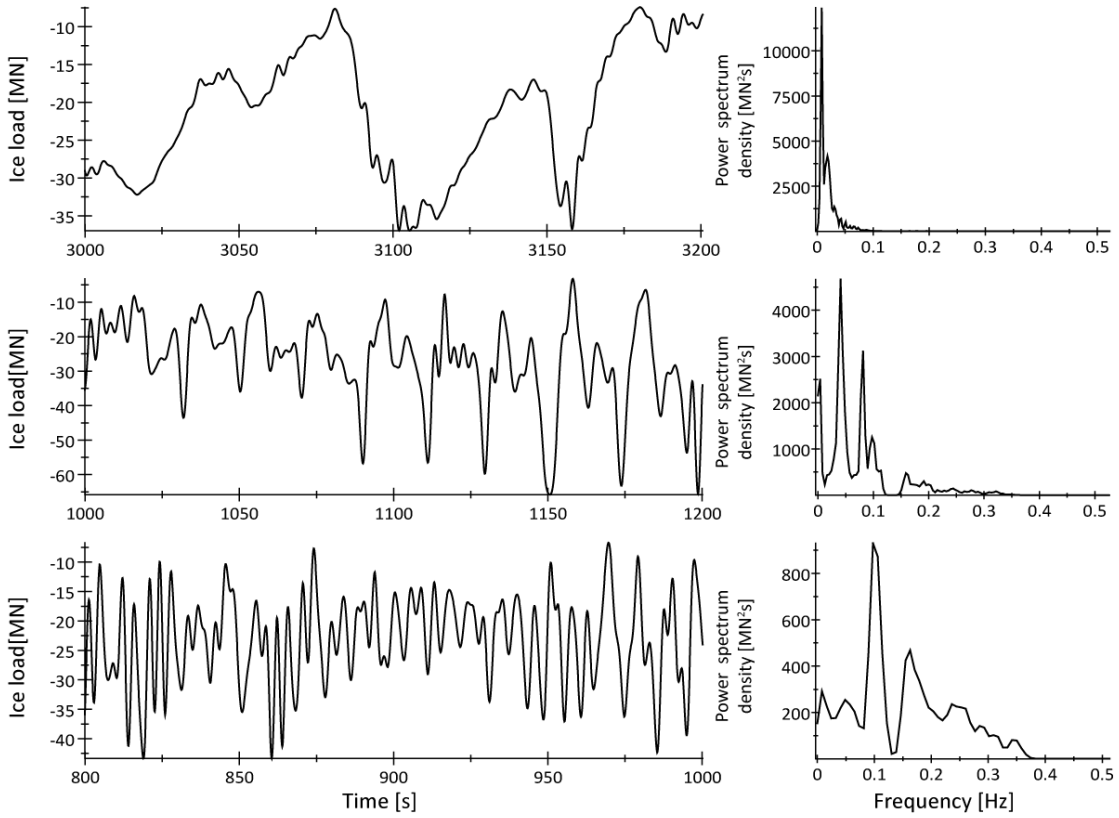

Figure 4.6. Model D_F in level ice for different ice speeds.

(*top:* 0.1m/s; *middle*: 0.5m/s; *bottom:* 1m/s)

Table 4.2. Frequency domain analysis and statistics for Model D_F in level ice.

Model D_F	Level ice	Natural frequency [Hz] = 1.167 Hz	
Speed [m/s]	Peak frequency [Hz]	Dominant Period [s]	Breaking length [m]
0.1	0.00814	122.85	12.29
0.5	0.0407	24.57	12.29
1	0.0977	10.24	10.24
Speed [m/s]	Maximum Load [MN]	Average Load [MN]	Std. deviation [MN]
0.1	-80.36	-22.66	9.54
0.5	-79.92	-25.22	11.42
1	-51.23	-23.93	7.83

4.1.1.3 Model F_F

Model F_F was tested in the ice tank for three different ice speeds in Tests # 03Li_10_11_13 and #03Ri_12. In these tests, the model was also tested in a multi-year ice ridge with a speed of 0.5 m/s as shown in Figure 4.7.

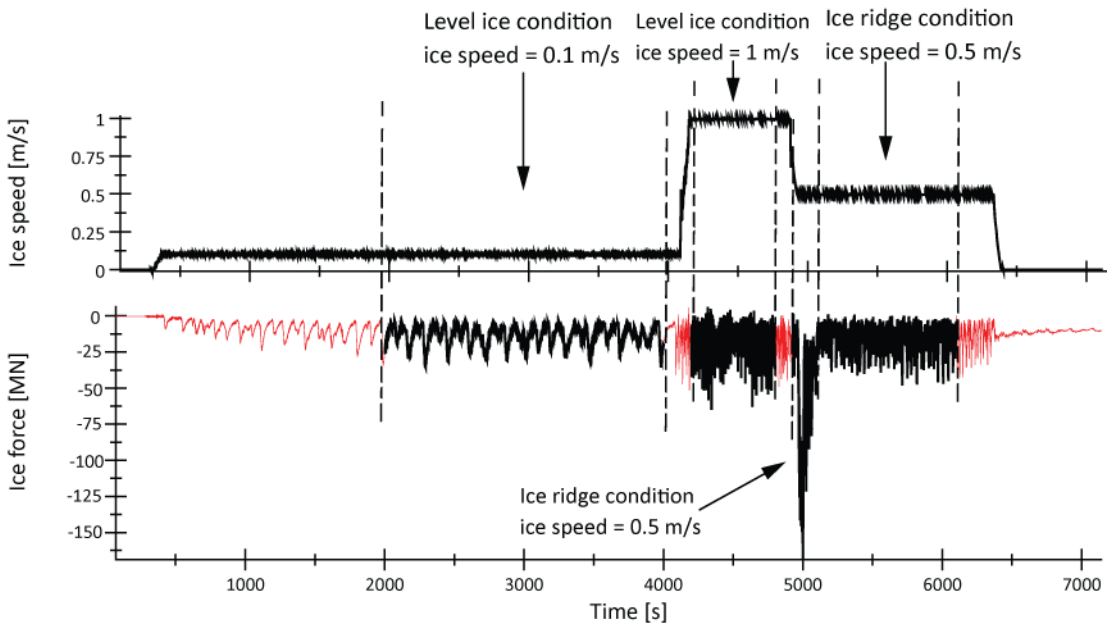

Figure 4.7. Time history of horizontal ice load for Tests #03Li_10_11_13 & Ri_12.

(Different sections of ice load histories for different ice conditions

were cut out (dark colour) for future analysis).

The test results in level ice will first be considered here. The time series of the horizontal level ice load for different ice speeds were identified from the record and displayed in the following figure. Three ice load time series' samples (left) and the relevant whole time history's PSD (right) are shown in Figure 4.8.

The dominant ice load's frequency is depending on the ice speed in a similar way as for Models B_F and D_F. However, since a different testing method was adopted for Model F_F, all the analysis and conclusions will further be repeated herein.

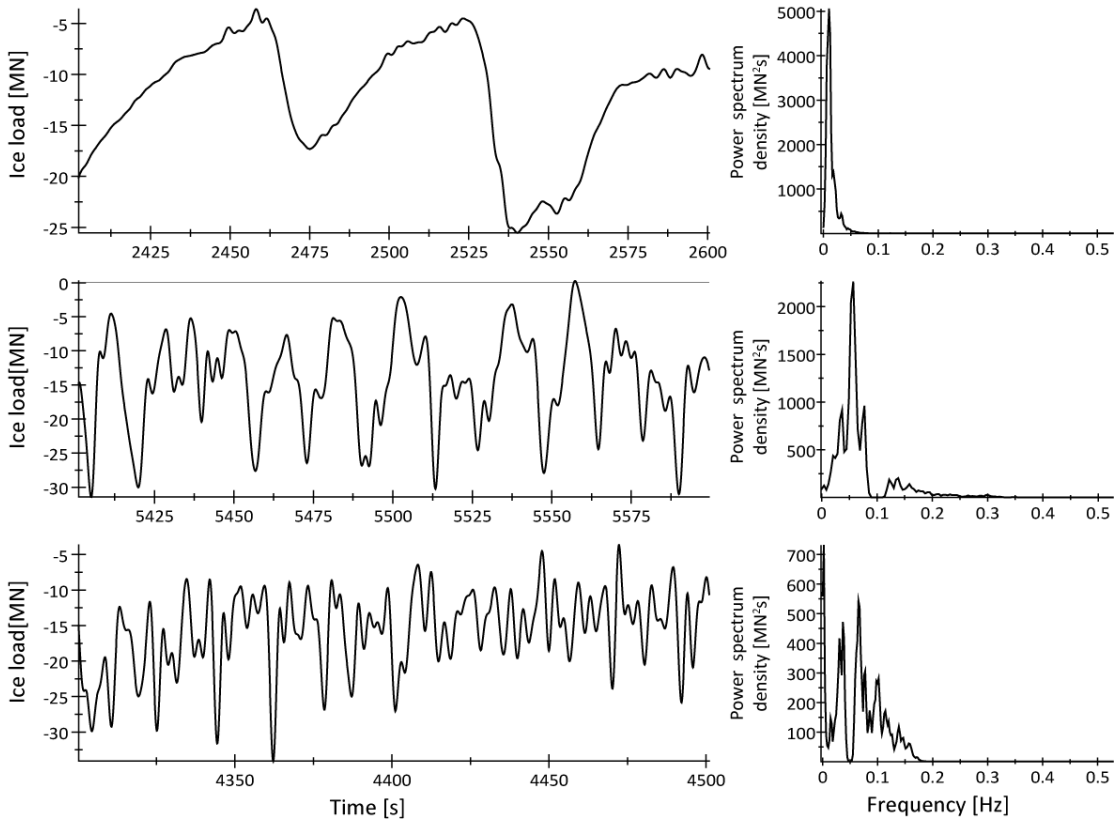

Figure 4.8. Model F_F in level ice for different ice speeds.

(*top*: 0.1 m/s; *middle*: 0.5 m/s; *bottom*: 1 m/s).

From Figure 4.8 we see that in a similar way as for Model B_F and Model D_F, the dominant ice load frequency increases as the ice speed increases.

The specific dominant frequencies for different ice speeds were identified and listed in Table 4.3 together with the estimated ice breaking length. From Table 4.3 we have the similar conclusions that higher ice speeds induce shorter ice breaking lengths. Statistical information of the horizontal ice load is calculated and listed in Table 4.3.

From Table 4.3 it is found that the ice load increases with increasing ice speed. However, it should be noted that different from the above two tests for Models B_F and D_F in Tests #03Li_10_11_13, Model F_F proved to be very effective in clearing the broken ice pieces. This means that very few broken ice pieces are accumulated in the bow region of Model F_F even at very low ice speeds (see Figure 4.10). Under such circumstances, the *ice accumulation load*'s contribution to the total *ice sliding load* is not as significant as for Models B_F&D_F. So, it is reasonable to expect that the *ice sliding load* increases with increasing ice speed. Similarly, the *ventilation load* is still insensitive to the ice speed. In total, the ice load will increase with increasing ice speed.

Table 4.3. Frequency domain analysis and statistics of Model F_F in level ice.

Model F_F	Level ice	Natural frequency [Hz] = 0.66 Hz	
Speed [m/s]	Peak frequency [Hz]	Dominant Period [s]	Breaking length [m]
0.1	0.010	98.04	9.80
0.5	0.057	17.54	8.77
1	0.065	15.36	15.36[33]
Speed [m/s]	Maximum Load [MN]	Average Load [MN]	Std. deviation [MN]
0.1	-35.16	-13.39	6.94
0.5	-39.89	-14.35	7.60
1	-44.13	-17.56	6.74

4.1.1.4 Comparisons of Models B_F, D_F and F_F in intact level ice

Ice breaking lengths

In the above analysis, the ice breaking lengths were estimated by multiplying the dominant ice load period with the ice speed. And the comparison of ice breaking length is listed in Table 4.4.

[33] Similar as the results listed in Table 4.1 for fixed Model B, the estimated ice breaking length at 1 m/s is 15.36 m which is larger than 8.77 m at an ice speed of 0.5 m/s. However, as can be seen from Figure 4.8, at an ice speed of 1 m/s, a large portion of the ice load resides in the high frequency band, which means in average the ice breaking length can still be less than at an ice speed of 0.5 m/s. The conclusion that ice breaking length decreases with increasing ice speed still holds true.

Table 4.4. Ice breaking length comparisons for the different fixed models.

Model D_F/Model B_F		
Ice speed [m/s]	Break length ratio []	Waterline diameter ratio []
0.1	1.25	1.66
0.5	2.70	
1	1.59	
Model F_F/Model D_F		
Ice speed [m/s]	Break length ratio []	Waterline diameter ratio []
0.1	0.80	1
0.5	0.71	
1	1.50	
Model F/Model B		
Ice speed [m/s]	Break length ratio []	Waterline diameter ratio []
0.1	1	1.66
0.5	1.93	
1	2.38	

Although Models D_F and F_F have the same waterline diameter, same sloping angle, and for the same ice speeds and similar flexural ice strength, the ice breaking lengths are not exactly the same. Model D_F tends to have a relatively larger ice breaking length. This may be due to the influence of broken ice pieces as will be shown in the following figures.

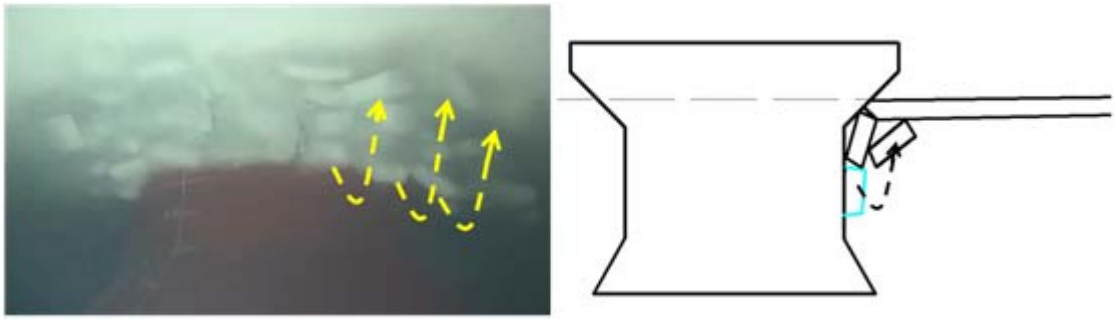

Figure 4.9. The broken ice pieces' track for Model D_F in Test #02Li12.

(*left*: actual broken ice track "dashed arrow line" *right*: a simplified schematization).

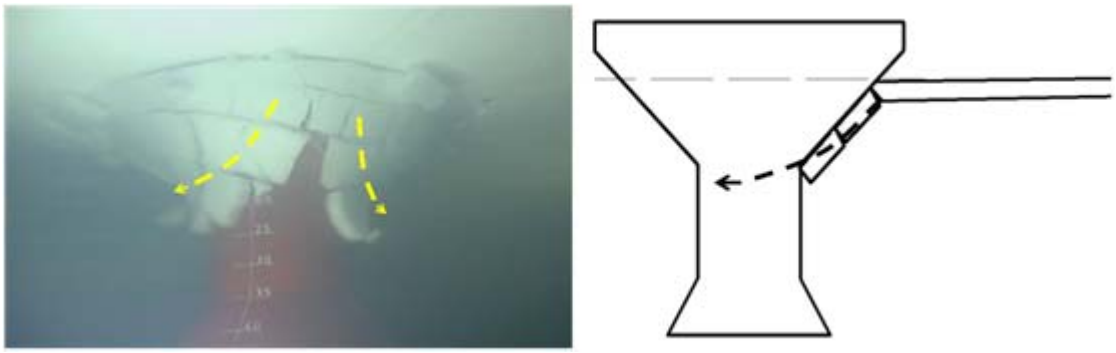

Figure 4.10. The broken ice pieces' track for Model F_F in Test #03Ri_12_13.

(*left*: actual broken ice track "dashed arrow line" *right*: a simplified schematization).

From the above two figures, it can be seen that for Model D_F, the broken ice tends to accumulate under the intact ice which will, to a larger degree, resist the intact level ice from being pushed downward along the conical face. However, for Model F_F, most of the broken ice rubble were cleared sideways immediately, thus the intact ice will be easier to push downward along the conical face. Based on this fact, two possible explanations can be given in the following:

Vertical velocity difference of the incoming ice

If we model the intact level ice as a beam resting on an elastic foundation, for Model F_F, the vertical velocity at the end point of the ice beam could be *assumed* as $v \times \sin(45^o)$ with v being the ice horizontal velocity and 45^o the angle of the conical face with the horizontal. However, for Model B_F, due to the presence of a relatively larger resistance, in the similar dynamic ice beam model, the vertical velocity of the end point of the ice beam will be less than $v \times \sin(45^o)$ in real life. For such a dynamic ice beam resting on an elastic foundation, a numerical model has been constructed (see Chapter 5 of Part I), based on which it has been found that a less vertical end point velocity leads to a longer ice breaking length.

The influence of axial force on the ice breaking length

Larger accumulated broken ice pieces will induce larger axial force in the incoming level ice. The incoming ice beam is in compression. This will reduce the tension flexural stress in the upper part of the ice beam. Due to this, the ice breaking length may become slightly longer with the presence of a larger ice accumulation volume.

However, in general, the ice breaking length's differences for Models D_F and F_F are not very huge as shown in Table 4.4.

From Table 4.4, it can also be observed that the ice breaking length ratios of Model F_F over Model B_F, and Model D_F over Model B_F are quite close to the ratio between the relative waterline's diameter ration (50/30). This proved that the diameter of the waterline is of importance in determining the ice breaking length. In other words, the size effect of the waterline is significant. Here a tentative and qualitative explanation of the size effect will be given as following:

Size effect on the ice accumulation

Figure 4.11. Displays of the waterline's size effect on ice accumulation.
(*Left*: Model B_F with 30 m diameter*; Middle*: Model D_F with 50 m diameter; *Right*: Model F_F with 50 m diameter; the ice speeds are 1 m/s in all cases).

As can be seen from the above figures, there is a shorter track for Model B_F to clear the ice rubble, while longer tracks are expected for Models D_F and F_F which are of larger waterline diameters. Hence we can conclude that the ice rubble's resistance to the intact level ice being pushed downward is stronger for Models D_F and F_F, and accordingly, a longer ice breaking length is expected for Models D_F and F_F with larger diameters. And the ice breaking length ratios between different models are quite close to the ratio of the waterline's diameter ratios.

Horizontal ice load

The comparison of horizontal ice loads have been listed in Table 4.5:

Table 4.5. The horizontal ice load ratio.

Model D_F/Model B_F			
Speed [m/s]	Maximum Load ratio []	Average Load ratio []	Std.deviation ratio []
0.1	2.73	1.40	1.71
0.5	2.43	1.49	2.19
1	1.47	1.49	1.31
Model D_F/Model F_F			
Speed [m/s]	Maximum Load ratio []	Average Load ratio []	Std.deviation ratio []
0.1	2.29	1.69	1.37
0.5	2.00	1.76	1.50
1	1.16	1.36	1.16
Model F_F/Model B_F			
Speed [m/s]	Maximum Load ratio []	Average Load ratio []	Std.deviation ratio []
0.1	1.19	0.83	1.25
0.5	1.21	0.85	1.46
1	1.27	1.09	1.13

Considering the *average ice load* ratio, from the above table it is found that Model F_F has the smallest horizontal ice load for nearly all three ice speeds. The horizontal ice load on Model F_F is even smaller than that on Model B_F which has a smaller waterline diameter.

This is due to Model F_F's effectiveness in ice clearing as can be seen from Figure 4.11. Here it is necessary to clarify the role of ice rubble in the *ice accumulation load* on the structure. In the previous explanation, in order to explain why a waterline with larger diameter leads to longer ice breaking lengths, we got the conclusion that: ice rubble for Model D_F and Model F_F have a larger resistance to the intact level ice due to their long track to clear the rubble. Now we will go one step further to clarify the resist force behind the ice rubble:

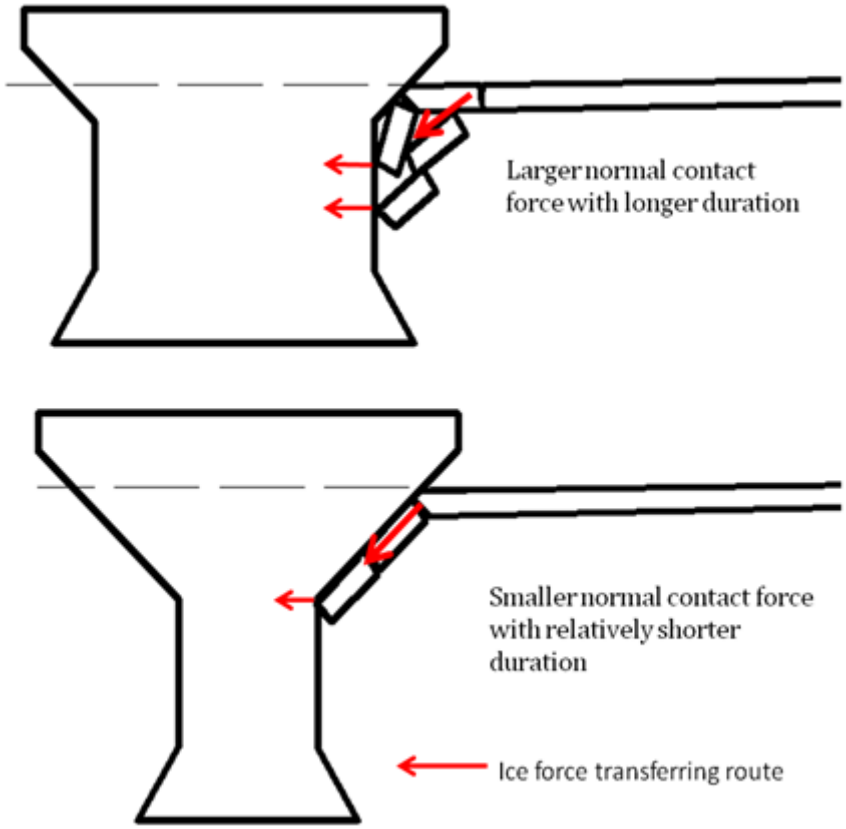

Figure 4.12 Illustration of ice rubble interacting with Models B_F/D_F and Model. F_F

(*Upper*: Models B_F/D_F; *Lower*: Model F_F)

As can be seen from the above figures, for structures with shorter conical face (e.g. Models B_F and D_F), the ice rubble tends to accumulate in the bow region of the structure and the ice load will be transferred to the structure directly by the normal contact with the vertical face of the structure and the duration of such loads tend to be long depending on the diameter of such a structure. However, for a structure with a sufficient long conical face (Model F_F), the approaching ice is mainly pushing the ice rubble downward and the rubble will be cleared sideways immediately. Accordingly, it is reasonable that a less *average ice load* was detected for Model F_F.

Considering the *maximum ice load*, it is found that a larger waterline diameter and wider "neck" width (Model D_F) lead to the largest *maximum ice load*, and thus Model F_F with the same large waterline diameter has a better ice clearing ability (narrow neck size). Model B_F with the smallest waterline diameter has the smallest *maximum ice load.*

Non-simultaneous ice breaking

As can be observed in the videos, wider structures tend to have more frequent

non-simultaneous ice breaking around their half perimeter.

4.1.2 Managed ice

After testing in intact level ice, each fixed model was also tested in managed ice; i.e. the level ice was broken into floes with two different ice floe sizes approximately $150\ \text{m} \times 200\ \text{m}$ and $30\ \text{m} \times 50\ \text{m}$ (see Figure 4.13). The procedure was the following: The level was manually broken into the larger floe size. The actual model was then tested. Thereafter the floes were broken further down into the smaller ice category and the model was run again.

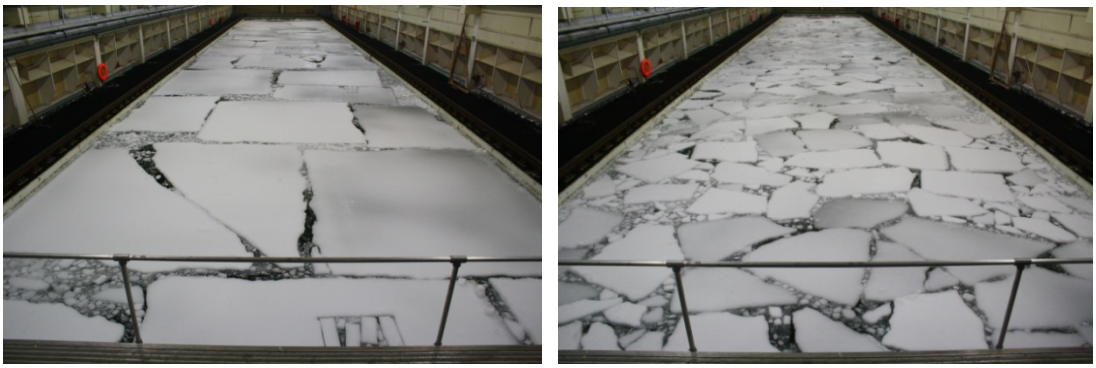

Figure 4.13 Photo of managed ice.

(*left*: 150 m × 200 m condition*; right*: 30 m × 50 m condition).

In a similar way as for the previous analysis, the *horizontal ice load* of each model test was analyzed in the frequency domain and statistical information of the ice loads was also calculated. The results are shown in the following tables and figures for the different models and ice conditions.

4.1.2.1 Model B_F in managed ice

Model B_F was first tested in the larger ice floe size condition in Tests #01Li30 to #01Li32 for different ice speeds.

The horizontal ice load's time domain samples and frequency domain PSD are shown in Figure 4.14.

The major differences between the managed ice and level ice tests are the dominant ice load frequency, which is much lower for the managed ice, and the ice load which are comparatively smaller than in level ice (about 40 % of the level ice case). There are several reasons in the explanation of this:

Smaller Ventilation load

This huge difference is mainly due to the more frequently absence of ventilation effects which results in very low *ventilation load*. As pointed out before, the *ventilation load* contributes to a large portion of the total ice load. The decrease in *ventilation load* is one of the reasons for a decreased *average ice load* in managed ice. The second reason is the fact that for managed ice, floes can be displaced without being broken. In this way the *ice breaking load* is hardly present causing a reduced total load.

Smaller ice sliding load

In managed ice, due to the relatively larger broken ice pieces, it is very difficult for the broken ice pieces to accumulate in the bow region of the models. Usually these broken ice pieces are cleared sideways more easily (see Figure 4.24, Figure 4.25, and Figure 4.26). So the *ice accumulation load* also becomes relatively smaller. And hence the *ice sliding load* can be expected to be smaller as well.

Boundary condition

Another major reason is mainly due to the boundary conditions of managed ice. In contrast to the level ice conditions where the broken ice pieces are further pushed downwards, the broken ice pieces in managed ice can be more easily pushed sideways. Comparing the force difference between pushing the broken ice pieces downwards with pushing the broken ice pieces sideways, it is obvious that the *average ice load* is smaller in managed ice.

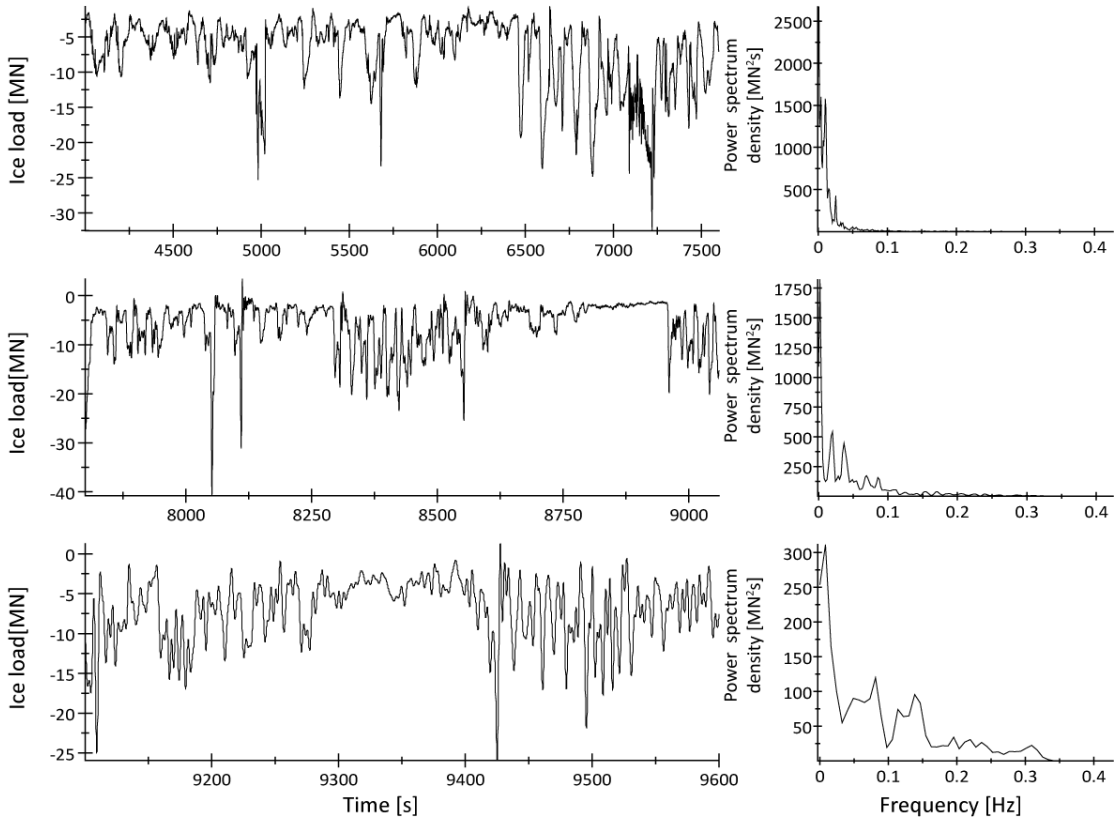

Figure 4.14. Model B_F in 150 m × 200 m managed ice for different ice speeds.

(*top*: 0.1 m/s; *middle*: 0.5 m/s; *bottom*: 1 m/s).

Table 4.6. Frequency domain analysis and statistics for Model B_F in managed ice with floe sizes 150 m × 200 m.

Model B_F	Large floes	Natural frequency [Hz] = 1.052 Hz	
Speed [m/s]	Peak frequency [Hz]	Dominant Period [s]	Breaking length [m]
0.1	0.00102	980.39	98.04
0.5	0.00204	490.20	245.10
1	0.00814	122.85	122.85
Speed [m/s]	Maximum Load [MN]	Average Load [MN]	Std. deviation [MN]
0.1	-32.56	-7.09	4.82
0.5	-40.79	-5.91	4.81
1	-25.93	-6.99	3.93

From Table 4.6 it is also found that the dominant ice load frequency (if multiplying the dominant ice load period with the ice speed) is coinciding with the ice floe size. This implies that the ice floe size has a strong influence on the ice load period.

Here, some more discussion about such a low frequency load will be conducted. Going back to the video, it was found that the interaction in managed ice is not as consistent as in level ice.

In level ice, the structure was experiencing similar ice loading processes. However, in managed ice, due to the “discrete” arrangement of the ice floes, the structure tends to have different contact with the managed ice floes at different time. The figure below shows generally how the structure interacting with the ice floes at different time together with the time series. Three possible contact scenarios were identified:

- Partial contact with large ice floes
- No contact with large ice floes
- Full contact with large ice floes

From the following figure, the ice load amplitude becomes largest when the structure has a full contact with the big ice floes; and the ice load amplitude becomes smallest when there is no contact with big floes. Different scenarios have been shown in the following figures with sequence.

Based on this discussion, a more detailed frequency domain calculation could be conducted in different managed ice-structure interaction scenarios. Based on the above mentioned three scenarios, the time series from the original test data will be further separated into at least two cases: the partial contact case and the full contact case. The criteria to choose the signal are a little bit “arbitrary” since there are no obvious line between a partial contact and full contact. A *visually observed stable* criterion was set here to select new signal for further analysis. As shown in the shaded area in Figure 4.15.

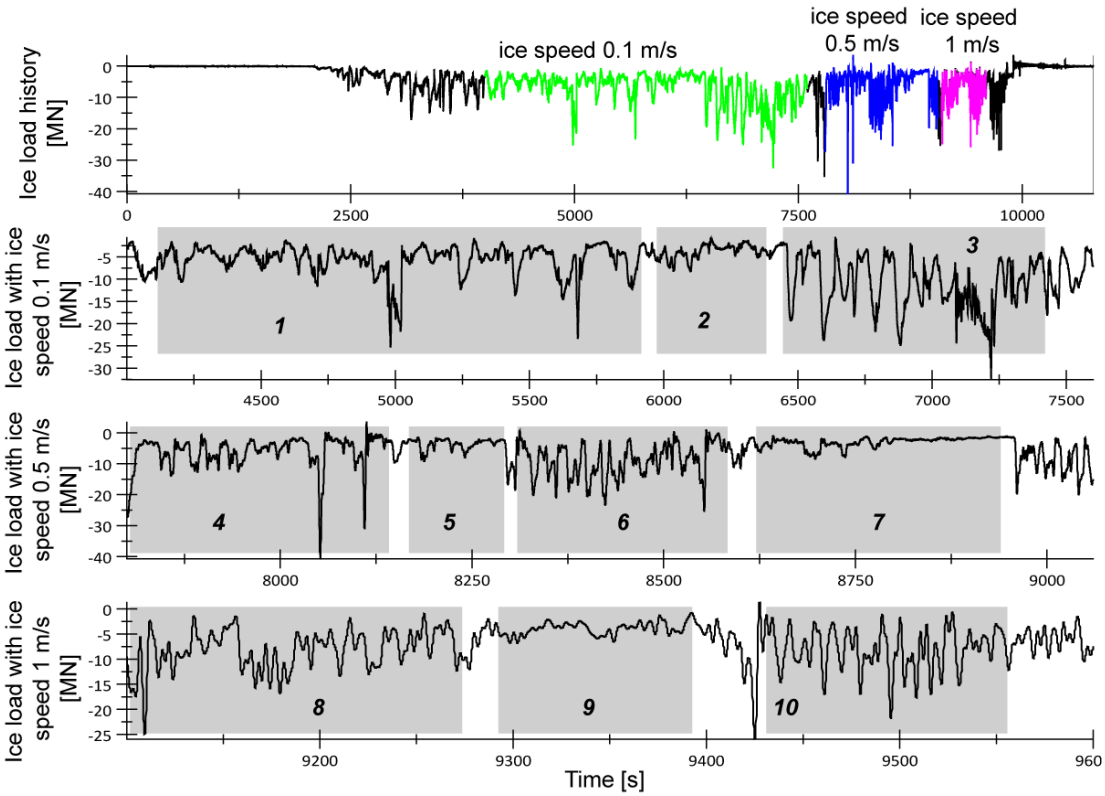

Figure 4.15 Further separation of the ice load time histories of Model B_F in managed ice with large floes

Figure 4.16 Managed ice-structure interaction scenarios for test #01Li30

(*Left:* partial contact; *Middle*: no contact; *Right*: full contact with large floes)

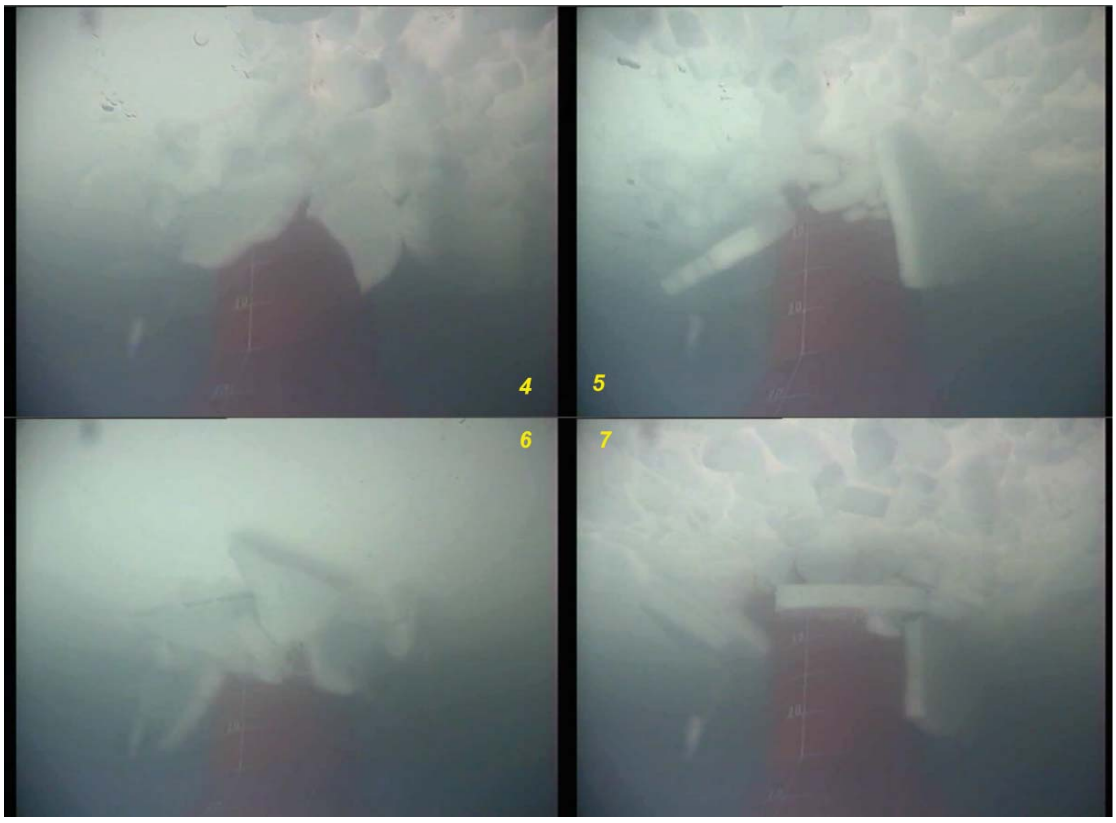

Figure 4.17 Managed ice-structure interaction scenarios for test #01Li31

(*Upper-Left:* partial contact; *Upper-right*: no contact; *Lower-left*: full contact; *Lower-right:* no contact with large floes)

Figure 4.18 Managed ice-structure interaction scenarios for test #01Li32

(*Left:* partial contact; *Middle*: no contact; *Right*: full contact with large floes)

As stated previously, the average horizontal ice load in managed ice is much smaller than in level ice.

Model B_F was also tested in managed ice (with ice floe size 30 m × 50 m) for different ice speeds. Horizontal ice load's time history samples and corresponding PSD in the frequency domain are shown in Figure 4.19, and the dominant frequency and statistical information of the horizontal ice load are listed in Table 4.7.

Similar to the tests in large floes, the dominant ice load frequency increases with increasing ice speed. If the dominant ice load period is multiplied by the ice speed, the outcomes are also in accordance with the ice floe size.

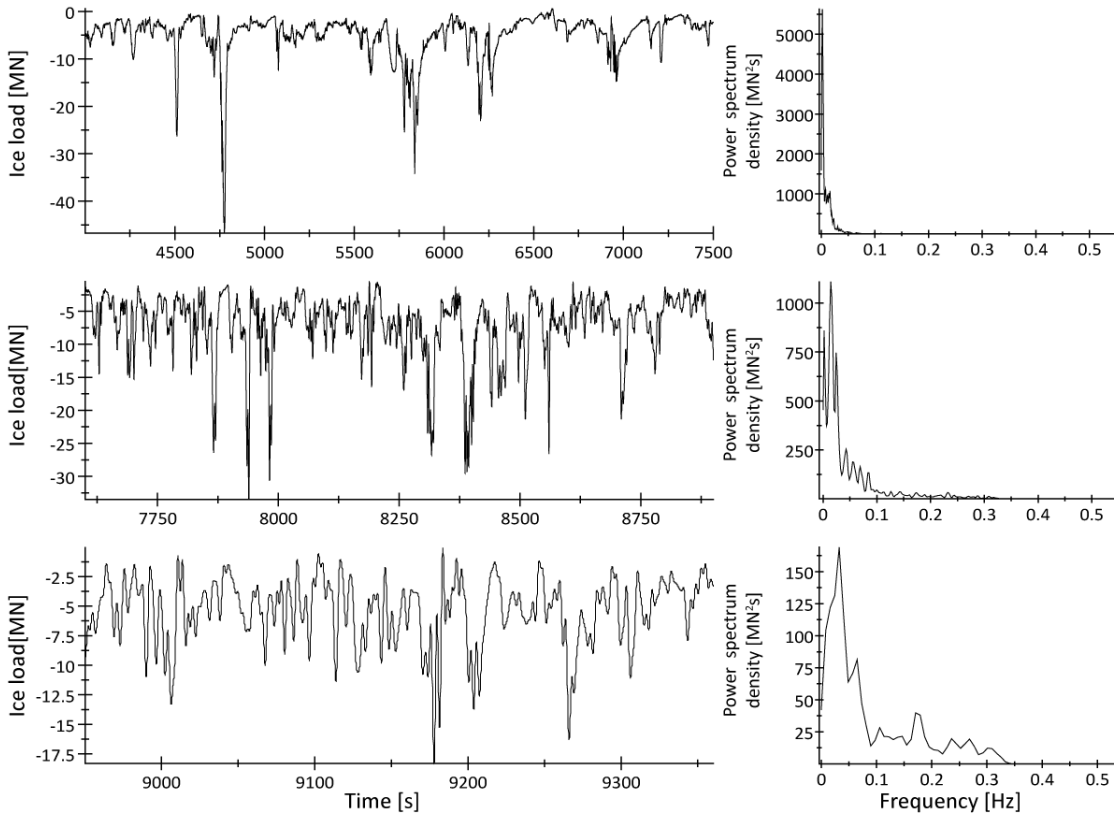

Figure 4.19. Model B_F in 30 m × 50 m managed ice for different ice speeds.

(*top*: 0.1 m/s; *middle*: 0.5 m/s; *bottom*:1 m/s).

Table 4.7. Frequency domain analysis and statistics for Model B_F in managed ice for floe sizes of 30-50 m.

Model B_F	Small floes	Natural frequency [Hz] = 1.052 Hz	
Speed [m/s]	Peak frequency [Hz]	Dominant Period [s]	Breaking length [m]
0.1	0.00204	490.19	49.02
0.5	0.0142	70.42	35.21
1	0.0326	30.67	30.68
Speed [m/s]	Maximum Load [MN]	Average Load [MN]	Std. deviation [MN]
0.1	-46.77	-4.92	4.71
0.5	-33.49	-7.03	4.85
1	-18.31	-5.39	2.79

From the above figure and table, a low frequency load was also found in test#01Li40 with ice

speed 0.1 m/s. The loading period is about 490 s as shown in the above table. Going back to the video and the time series as shown in the following Figure 4.20, it is found that, different from large-floe managed ice where three scenarios could be identified, in small ice floe conditions, the structure has continuously contact with the small ice floes.

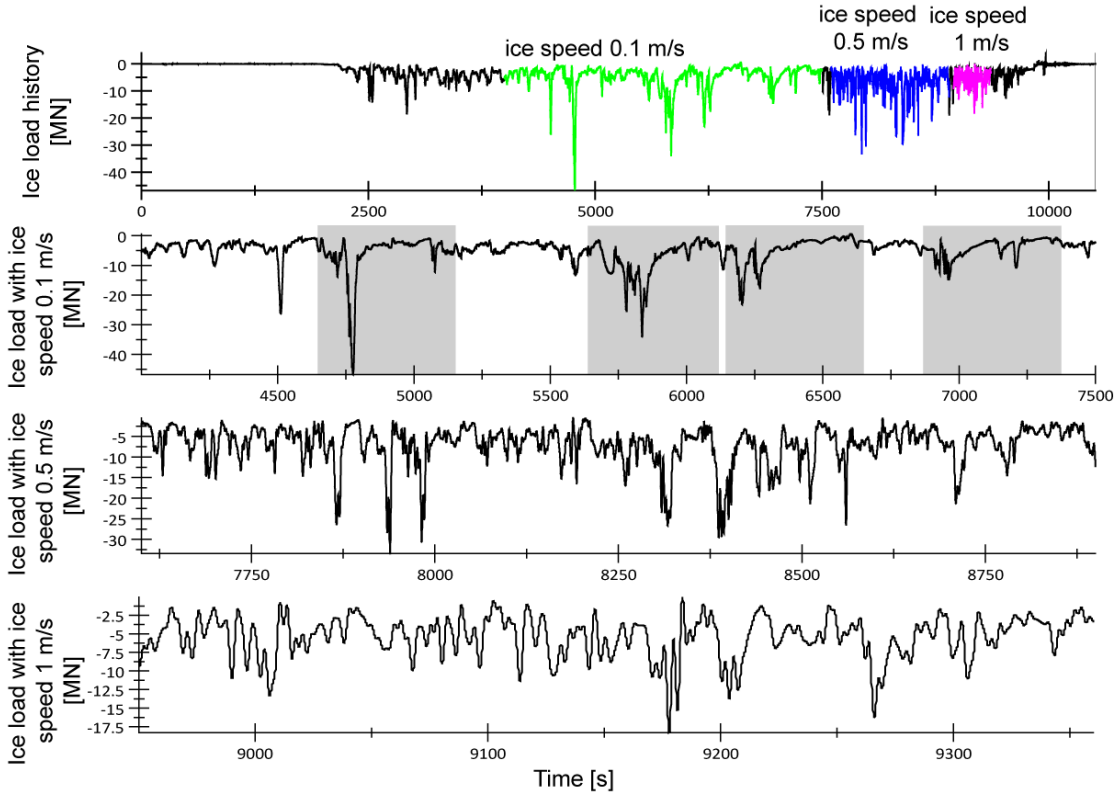

Figure 4.20 Ice load time histories of Model B_F in managed ice with small floes

Hence the ice load histories appear more ‘stable’ than in managed ice conditions with small ice floes, especially with ice speed 0.5 m/s and 1 m/s. In most cases, the peak ice loads as shown in the above Figure 4.20 are relating to rotating a relatively larger broken ice pieces. The duration of these peaks can to a certain degree tell the size of the broken ice pieces.

In test #01Li40, where the ice speed is 0.1 m/s, the dominant loading period is calculated to be 490 s. In Figure 4.20, several shaded areas with duration 500 s were depicted overlapping with the possible duration of the peak loads. This shows relatively good agreements.

Based on the above discussion, the calculation to obtain the frequency domain PSD so as to further identify the dominant ice load based on the *overall* ice load time history is reliable, no further signal selection based on different scenarios need to be conducted as in Test#01Li3X. The results in Table 4.7 are reliable.

Comparing with the test in the larger ice floe conditions, the amplitude of the horizontal ice load does not change too much (it is only slightly lower). The comparison of the horizontal ice load for large ice floes and small ice floes is shown in Table 4.8.

Table 4.8. Comparison of Model B_F in different ice floe conditions (150 m×200 m & 30 m×50 m).
(The ratio is between the larger ice floe conditions over the smaller ice floe conditions).

Speed [m/s]	Maximum Load ratio []	Average Load ratio []	Std. deviation ratio []
0.1	0.70	1.44	1.02
0.5	1.22	0.84	0.99
1	1.42	1.30	1.41

The reasons for the difference in horizontal ice loads are not obvious in these two different managed ice conditions and are in the following:

- Very small *ventilation load* in both cases;
- Very small *ice accumulation load* in both cases;

It is possible that the absence of the above two major contributors to the total ice load makes the *ice breaking load* the major contributor. However, the *ice breaking load*'s duration is too short to have significant influence on the total average ice load. This may explain why the average load difference between two different managed ice floe conditions is relatively small.

Although the average ice load difference is relatively small (not in a same scale as the floe size difference) in these two different managed ice conditions, *theoretically* speaking the average ice load for the managed ice floes of the larger size should be slightly larger than for the managed ice floes of the smaller size. This is because in the larger case more "ice breakings" tend to happen. Secondly larger forces are required to push the larger (broken) ice floes away. This has been confirmed by the average load ratio for an ice speed of 0.1 m/s and 1 m/s as shown in the third column in Table 4.8. In the same table, however, when the ice speed is 0.5 m/s, the average ice load for managed small ice floes is larger than in the managed large ice floe case. Such situations may happen if the models are advancing in the channels between the managed ice floes for *a sufficiently long period*. When advancing in the channel, the ice load could be reduced since less "ice breakings" happened[34].

[34] This gives one possible reason for why the average load in the smaller ice floe case may be larger than that in the larger ice floe case. However, it is difficult to define *a sufficient long period* in the channels, so no pictures showing the models advancing in the channel was supplied here.

4.1.2.2 Model D_F in managed ice

Model D_F was also tested in managed ice for both large and small floe sizes. Similar analysis as for Model B_F has been conducted and the results are shown in the following figures and tables.

First we present the results for the fixed model in large ice floes:

Similar conclusions as stated for Model B_F regarding the dependence of the ice load on the ice speed can be obtained. The average ice load in large ice floes is about 60 % of the level ice load. Generally speaking, the frequency of the ice load is very low and if multiplying the dominant ice load period with the ice speed, the results are in accordance with the ice floe size as expected. This again proves the influence of floe size on frequency of the ice load.

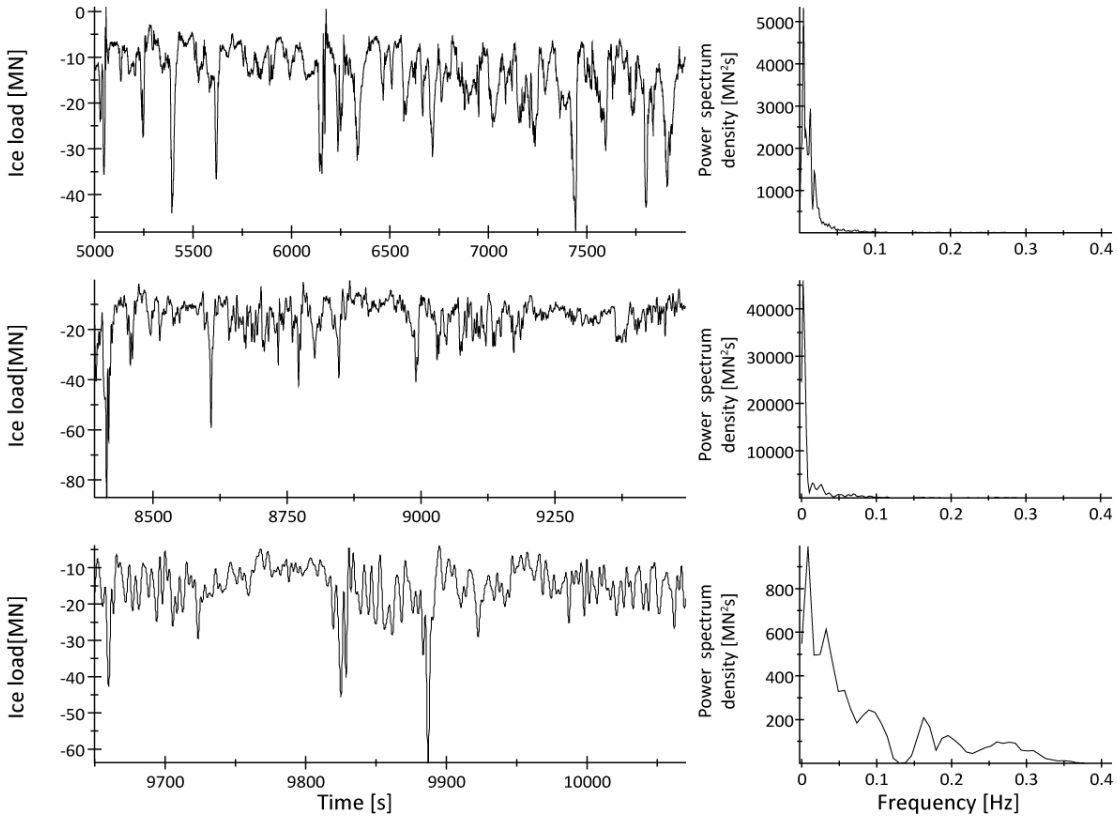

Figure 4.21. Model D_F in 150 m×200 m managed ice for different ice speed.

(*top*: 0.1 m/s; *middle*: 0.5 m/s; bottom: 1 m/s).

Table 4.9. Frequency domain analysis and statistics of Model D_F in managed ice (150-200 m).

Model D_F	Large floes	Natural frequency [Hz] = 1.167 Hz	
Speed [m/s]	Peak frequency [Hz]	Dominant Period [s]	Breaking length [m]
0.1	0.00509	196.46	19.65
0.5	0.00204	490.20	245.10
1	0.00814	122.85	122.85
Speed [m/s]	Maximum Load [MN]	Average Load [MN]	Std. deviation [MN]
0.1	-48.21	-13.96	6.96
0.5	-59.25	-21.31	20.87
1	-63.78	-15.30	6.66

Model D_F was also tested in small ice floes in Tests #02Li40_41_42. The results are shown in Figure 4.22 and Table 4.10:

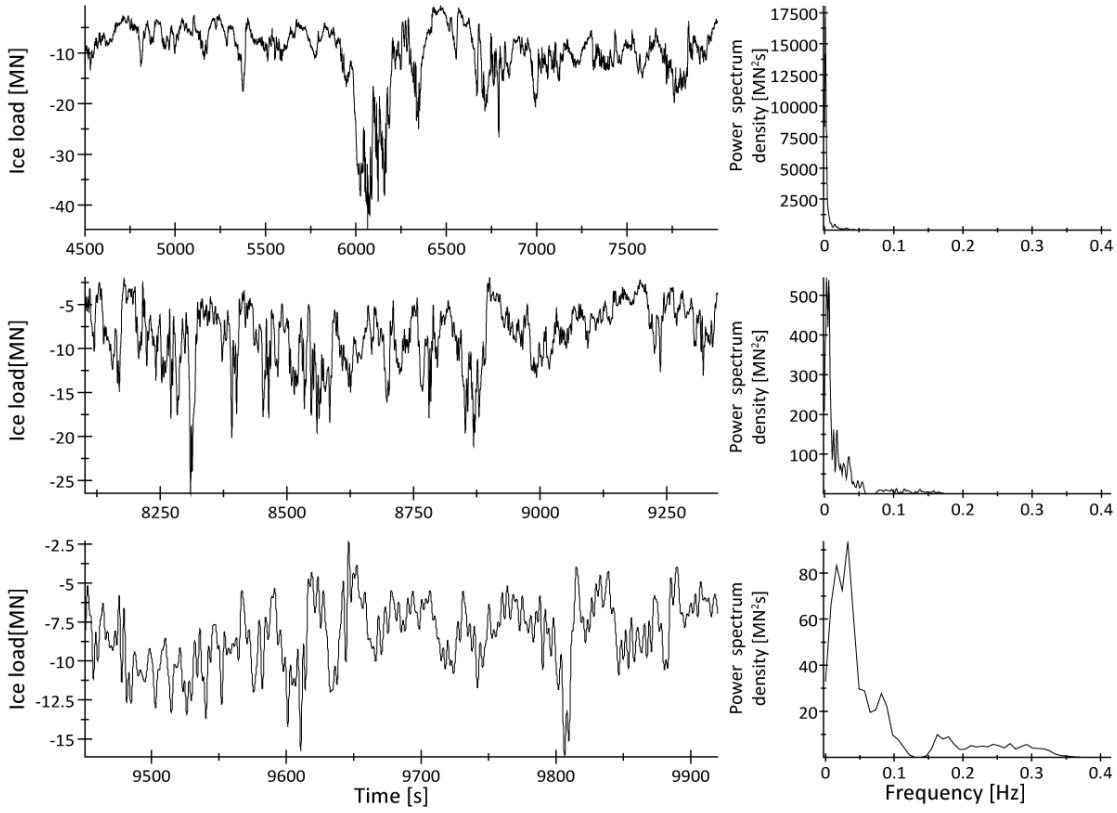

Figure 4.22. Model D_F in 30 m×50 m managed ice for different ice speeds.

(*top*: 0.1 m/s; *middle*: 0.5 m/s; *bottom*:1 m/s).

Table 4.10. Frequency domain analysis and statistics for Model D _F in 30-50 m managed ice.

Model D_F	Small floes	Natural frequency [Hz] = 1.167 Hz	
Speed [m/s]	Peak frequency [Hz]	Dominant Period [s]	Breaking length [m]
0.1	0.00102	980.39	98.04
0.5	0.0061	163.93	81.97
1	0.0326	30.67	30.67
Speed [m/s]	Maximum Load [MN]	Average Load [MN]	Std. deviation [MN]
0.1	-44.86	-9.97	6.33
0.5	-26.46	-8.52	3.58
1	-16.17	-8.34	2.19

The statistics of the ice load is listed in Table 4.10, and the comparison of the ice load for Model D_F in large ice floes and small ice floes is shown in Table 4.11.

Table 4.11. Comparison of Model D_F in different managed ice (150 m× 200 m; 30 m× 50 m).
(The ratio is between the larger ice floe conditions over smaller ice floe conditions).

Speed [m/s]	Maximum Load ratio []	Average Load ratio []	Std.deviation ratio []
0.1	1.07	1.40	1.10
0.5	2.24	2.50	5.83
1	3.95	1.83	3.04

From the above table, it is found that Model D_F in the larger ice floe case tends to have a slightly[35] larger horizontal ice load. The same explanation given for Model B_F tested in managed ice is also applicable here.

4.1.2.3 Model F_F in managed ice

Model F_F was tested only in managed ice of small ice floes (30 m×50 m). The results are shown in the following tables and figures.

[35] "Slightly" means the average load difference is not in a same scale as the ice floe sizes' difference.

Table 4.12. Frequency domain analysis and statistics for Model F in managed ice (30-50 m).

Model F_F	Small floes	Natural frequency [Hz] = 0.66 Hz	
Speed [m/s]	Peak frequency [Hz]	Dominant Period [s]	Breaking length [m]
0.1	0.00254	393.70	39.37
0.5	0.0061	163.93	81.97
1	0.0326	30.67	30.67
Speed [m/s]	Maximum Load [MN]	Average Load [MN]	Std. deviation [MN]
0.1	-16.28	-5.97	2.86
0.5	-18.36	-6.48	2.68
1	-19.86	-7.49	2.80

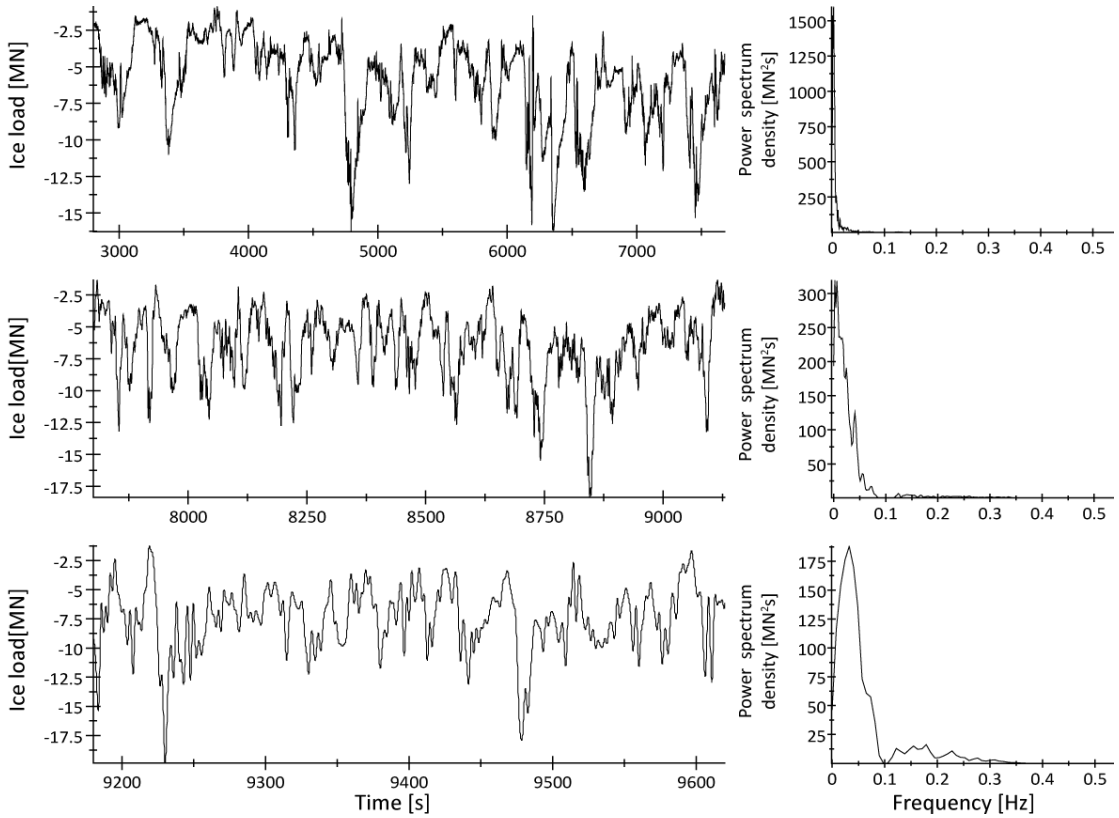

Figure 4.23. Model F_F in 30 m×50 m managed ice for different ice speeds.

(*top:* 0.1m/s; *middle*: 0.5m/s; *bottom:*1m/s).

Comparing with the Model F_F in level ice, the horizontal ice load is about 45 % of the level ice load in managed ice of small floes.

4.1.2.4 Conclusions of the similarities of different models in managed ice

In the previous three sections, all three models (B_F, D_F, and F_F) in managed ice (150 m×200 m and 30 m×50 m) are analyzed and compared with the corresponding behaviours in level ice. Many similarities have been observed and described in each section. Now all the similarities will again be concluded here:

1) All three models in managed ice have much smaller average horizontal ice loads compared with the average horizontal load in level ice. Specifically, the average horizontal load in managed ice in per cent of the level ice load is for Model B_F 40 %, for Model D_F 60% and for Model F_F 45%.
2) The dominant ice load frequencies for different speeds are much lower in managed ice than in level ice. Moreover, the dominant ice load frequency is strongly influenced by the ice floe size.
3) The horizontal ice load difference for the large ice floes and small ice floes is relatively small (not in scale with the ice floe size difference) mainly due to the unbounded boundary conditions. However, for larger ice floes, more ice are needed to be broken and relatively larger forces are required to push the (broken) ice floes away for the structure to 'run through'. The horizontal ice load measured in the larger ice floe test appears slightly higher than in the small ice floe test.

4.1.2.5 Comparisons of different models in managed ice

In the following the differences in the measured results in managed ice for the different models will be compared.

Comparison of the horizontal ice loads

Table 4.13. Horizontal load ratios for different managed ice conditions.

Average Load	Model B_F/Model D_F		Model B_F/Model F_F	Model D_F/Model F_F
ratio	150 m×200 m	30 m×50 m	30 m×50 m	30 m×50 m
Speed [m/s]	ratio []	ratio []	ratio []	ratio []
0.1	0.51	0.49	0.83	1.67
0.5	0.28	0.82	1.09	1.32
1	0.46	0.65	0.72	1.11

As can be seen from the first two columns, the horizontal ice load of Model B_F is almost half of that of Model D_F. The ratio is quite close to the ratio of waterline diameter of the

models; 30/50=0.6. The effectiveness of a smaller diameter in clearing ice rubble can be seen when comparing Figure 4.24, Figure 4.25 and Figure 4.26.

Model F_F was proved to be effective in reducing the ice load in managed ice when compared to Model D_F (the last column in Table 4.13). The effectiveness of Model F_F in clearing ice floe rubble is shown in Figure 4.26.

However, different from level ice where the average horizontal ice load for Model F_F is less than that of Model B_F, the opposite results are obtained in managed ice as shown in the third column of Table 4.13. There are many reasons for this result, one of which would be that in managed ice, the ice clearing contribution from a smaller diameter tends to be more obvious than for a longer conical slope. As can be seen from Figure 4.24, the broken ice floes have dimensions which are comparable with the waterline diameter of Model B_F, and the broken ice were easily cleared away rather than accumulated in the bow region which was the case in level ice.

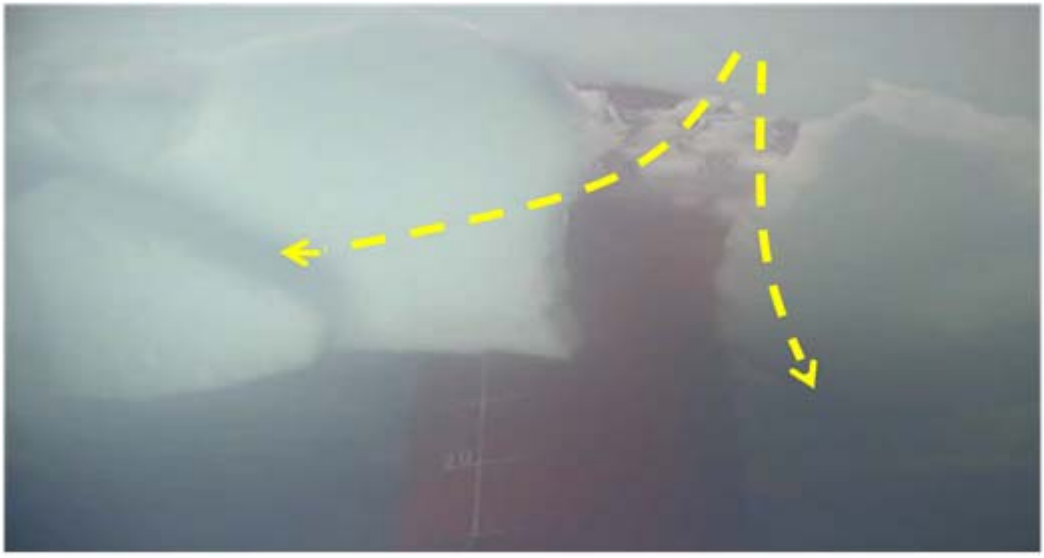

Figure 4.24 Photo of Model B_F's ice clearing ability in managed ice.

(30 m×50 m managed ice; in Test #10Li42; ice speed 1 m/s).

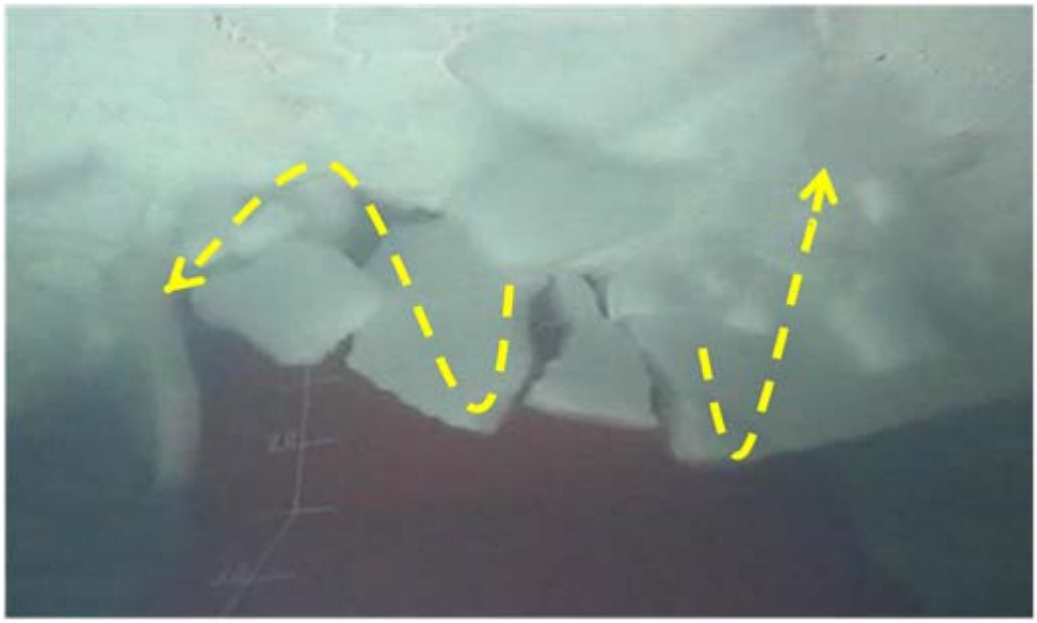

Figure 4.25. Photo of Model D_F's ice clearing ability in managed ice.

(30 m×50 m managed ice; in Test #02Li42; ice speed 1 m/s).

Due to the large diameter at the waterline, the broken ice pieces in managed ice tends to pitch back and accumulate in the bow region of Model D_F (similar as in the level ice case, but the accumulation volume is not as large as in level ice). Then the rubble was 'cleared' sideways along the structure as shown by the dashed arrow track in Figure 4.25.

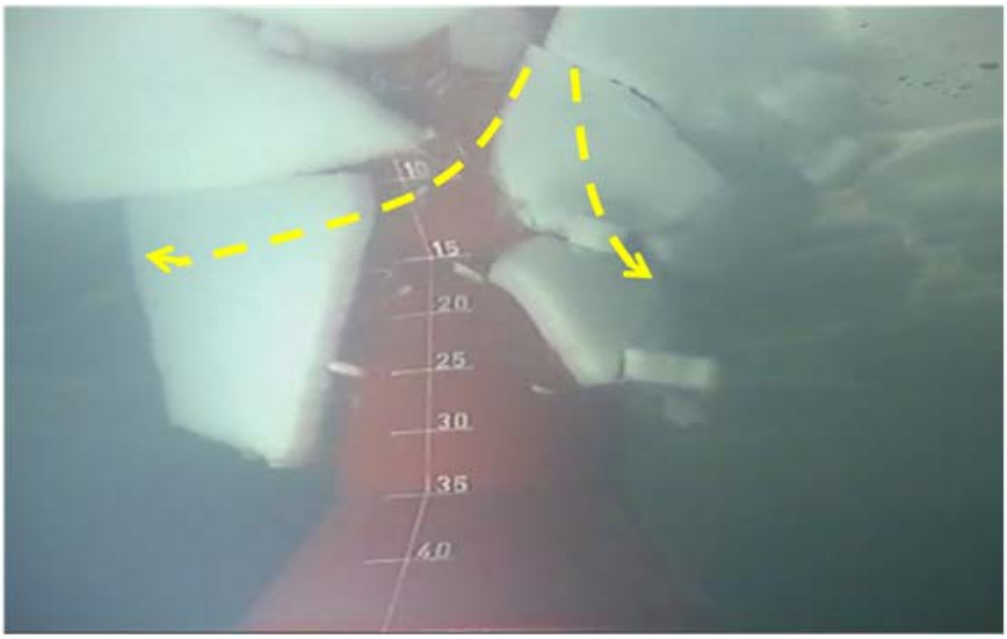

Figure 4.26. Photo of Model F_F's ice clearing ability in managed ice.

(30 m×50 m managed ice; in Test #03Li42; ice speed 1 m/s).

Similar as in level ice, the ice rubbles were immediately cleared away along the sideway of Model F_F.

4.1.2.6 Information regarding ice breakings in managed ice

In the previous analysis and discussion, the comparisons, especially in the frequency domain, are based on the overall time record. However, as pointed out before, the ice and structure interactions in managed ice are not consistent as in level ice. The structure experiences different contact scenarios with the managed ice with large floes. At least three possible scenarios have been identified based on the discussion about Model B_F's load history record and test videos. In most of the previous analysis, a dominant low frequency load was identified for the structure in managed ice. This dominant low frequency is corresponding to a long loading period. This period, if multiplying with the relevant ice speed, is in a scale of the floe size.

Accordingly, most of the dominant ice load frequencies identified before are relevant to the whole processes of breaking the managed ice floes, rotating the broken ice floes and clearing the broken ice floes. This explained that the size of the managed ice floe has a large influence on the ice load frequency. However, focusing on that long period loading process distract us from the ice breaking and rotating frequencies.

After all, in that long loading period, a relatively large portion of the time was used for the structure advancing in the "channel" of the managed ice floes, where no large floes were encountered as shown in "2" of Figure 4.16, "5,7" of Figure 4.17 and "9" of Figure 4.18. However, the ice breaking processes in managed ice are of more interests as shown in "1,3" of Figure 4.16, "4, 6" of Figure 4.17, and "8, 10" of Figure 4.18. In these processes, the ice breaking and ice rotating information are available.

Accordingly, in this section, the "*stable*" part (partial contact or full contact) of the ice load histories will be taken out for further frequency domain analysis so as to get some insights about the ice breaking and rotating characteristics in managed ice. It should be noted here that not all the test series were conducted again here. Only those with extremely long dominant ice load period or with exotic load peaks will be reanalyzed here.

- Model B_F in large floe conditions (Test 01Li30_31_32)

As mentioned before, the partial contact scenarios and full contact scenarios were identified based on the video record. In this section, the load histories in each scenario were taken out

for further analysis to see the ice breaking characteristics. The calculation results are shown in Figure 4.27, Figure 4.28 and Figure 4.29; and detailed ice load frequencies are listed in Table 4.14 in comparison with the dominant frequency calculated based on the overall time histories.

Table 4.14 Ice breaking& rotating induced dominant ice load frequency in managed ice for Model B_F

Model B_F Test	Partial contact		Full contact		Overall time series	
	Frequency [Hz]	Period [s]	Frequency [Hz]	Period [s]	Frequency [Hz]	Period [s]
#01Li30	0.00407	246	0.0122	82	0.00102	980
#01Li31	0.0326	31	0.0326	31	0.00204	490
#01Li32	0.0326	31	0.0977	10	0.00814	123

As can be seen from the above table, in full contact scenarios, the ice breaking frequency is higher than in partial contact scenarios. As the ice speed increases, the dominant ice breaking frequencies are also increasing. Based on the above dominant ice breaking frequency, the *real* ice breaking length can be further estimated by multiplying the dominant ice load period with the ice drift speed. The ice breaking length is about 24.6 m, 15 m and 31 m in partial contact scenarios under ice speed 0.1 m/s, 0.5 m/s and 1 m/s; the ice breaking length is about 8.2 m, 15 m and 10 m in full contact scenarios under ice speed 0.1 m/s, 0.5 m/s and 1 m/s. The later groups are very close to the estimated ice breaking length in intact level ice, but appear slightly larger. This is in agreement with the previous statement.

The detailed signal selections in time domain and relevant frequency domain PSD are shown in the following figures with different ice speed cases.

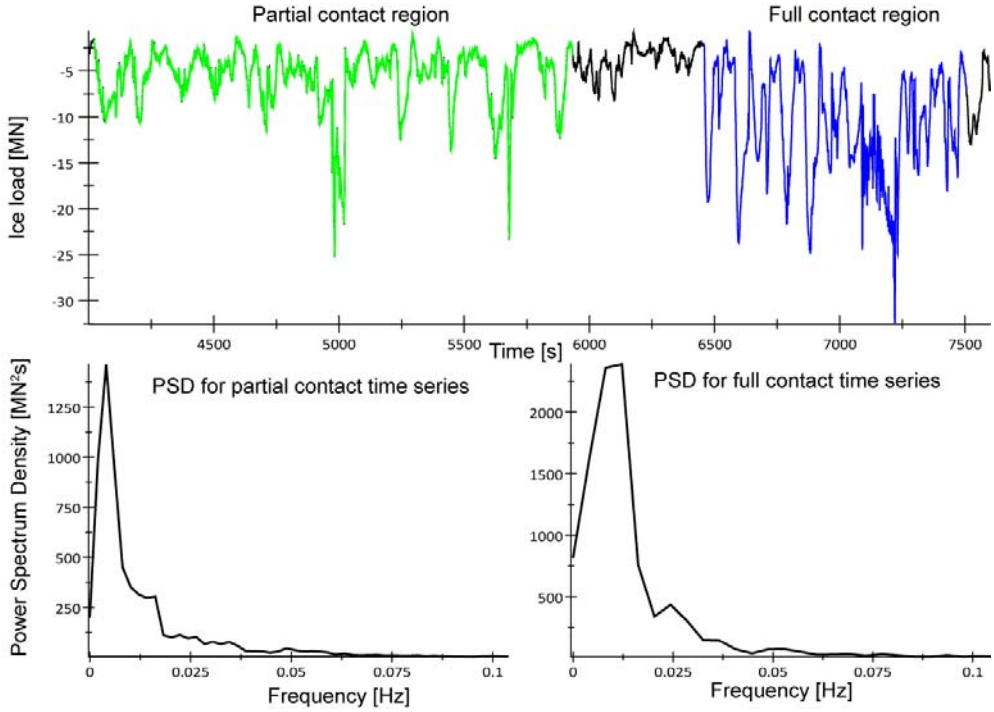

Figure 4.27 Ice breaking& rotating induced dominant ice load frequency in managed ice in test #01Li30 with ice speed 0.1 m/s

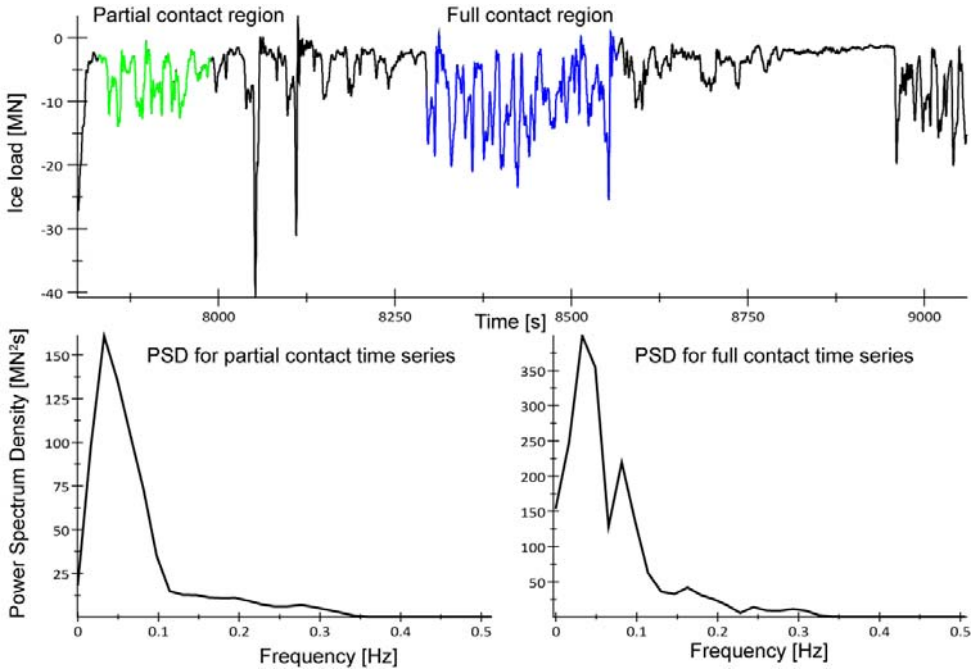

Figure 4.28 Ice breaking& rotating induced dominant ice load frequency in managed ice in test #01Li31 with ice speed 0.5 m/s

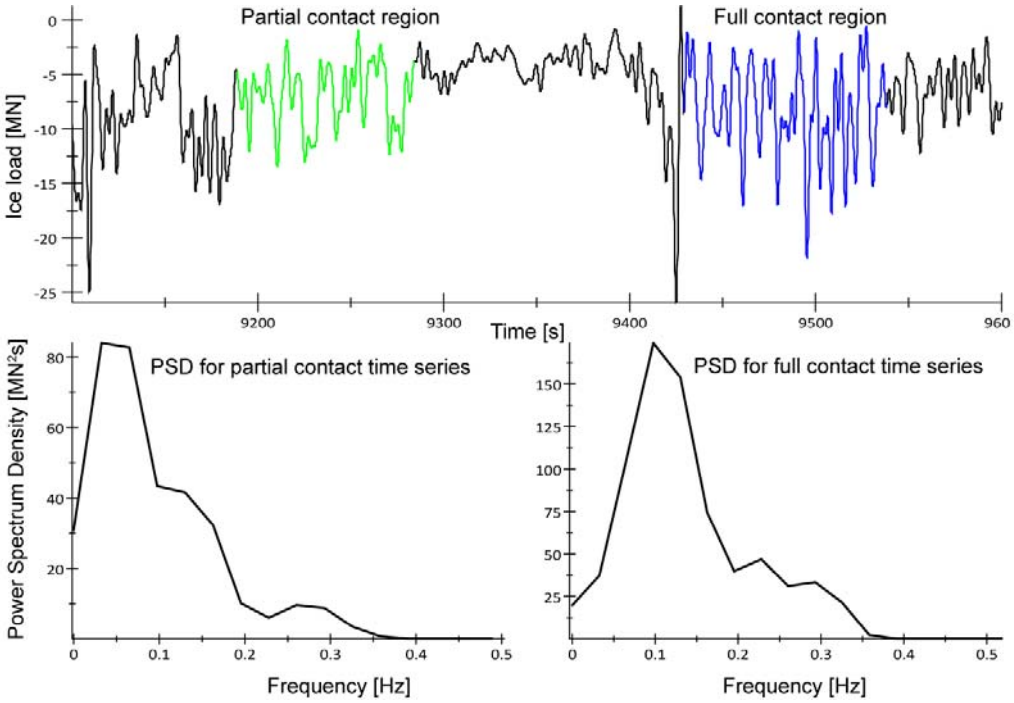

Figure 4.29 Ice breaking& rotating induced dominant ice load frequency in managed ice in test #01Li32 with ice speed 1 m/s

- Model D_F in large floe conditions (Test 02Li30_31_32)

  From the ice load history, the "stable" parts were identified and further analyzed in the frequency domain. The results are listed in the following table.

Table 4.15 Ice breaking& rotating induced dominant ice load frequency in managed ice (large floes) for Model D_F

Model D_F Test	Stable part 1		Stable part 2		Stable part 3		Overall time series	
	Frequency [Hz]	Period [s]	Frequency [Hz]	Period [s]	Frequency [Hz]	Period [s]	Frequency [Hz]	Period [s]
#02Li30	0.00814	123	-	-	-	-	0.00509	196
#02Li31	0.0326	31	0.0651	15	-	-	0.00204	490
#02Li32	0.0326	31	0.163	6	0.0977	10	0.00814	123

The signal selection concerning the "stable" part and the calculated PSD in each test are shown in the following figures.

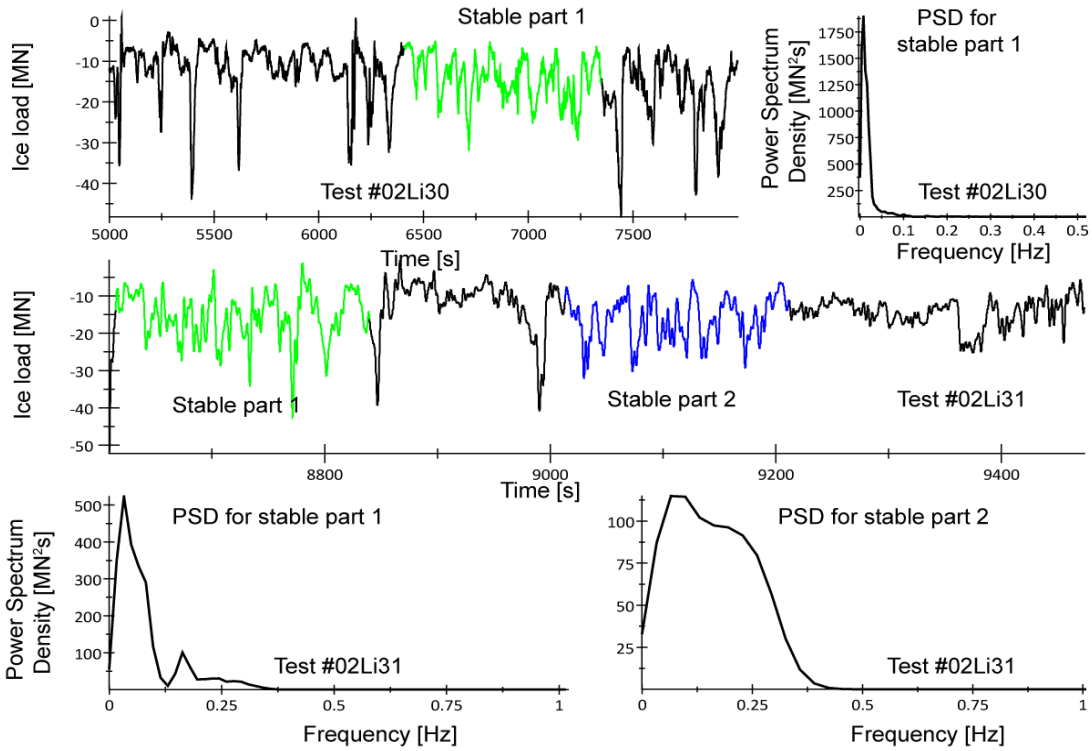

Figure 4.30 Ice breaking& rotating induced dominant ice load frequency in managed ice in test #02Li30 (upper) and #02Li31 (middle and lower) with ice speed 0.1 m/s and 0.5 m/s respectively

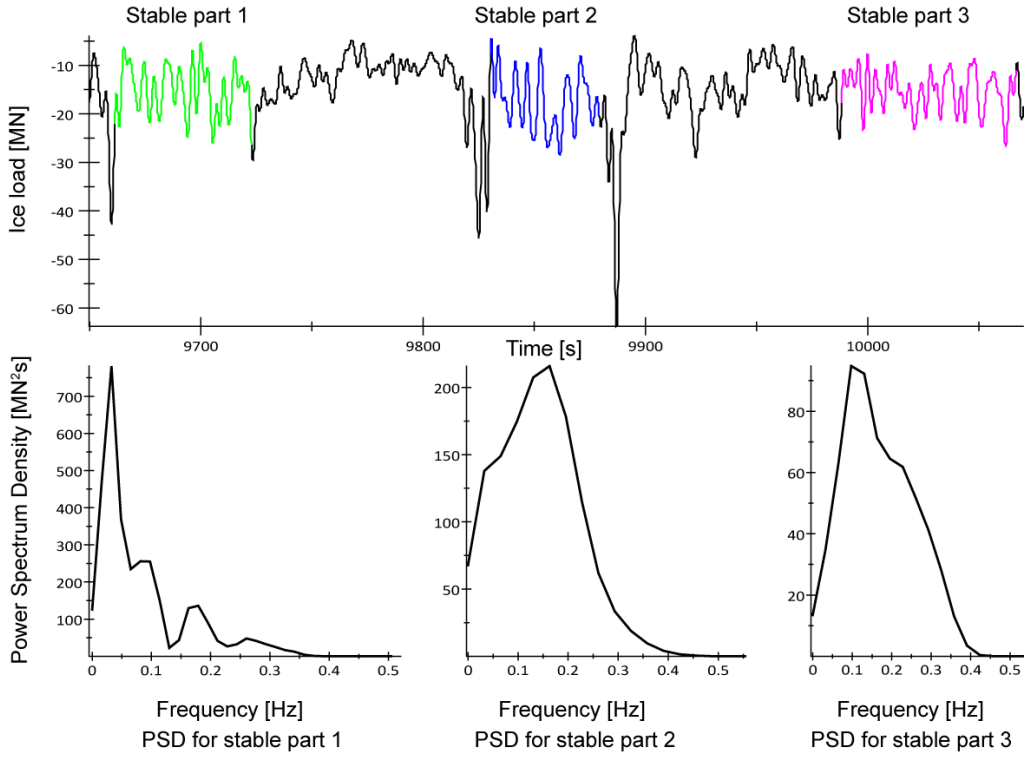

Figure 4.31 Ice breaking& rotating induced dominant ice load frequency in managed ice in test #02Li32 with ice speed 1 m/s

As can be seen from the above two figures and calculation results in Table 4.15 that the

dominant ice load frequency has been increased. This means during the whole ice load period induced by a managed floe, a relatively small portion of the time was used to break and rotate the ice. Another long period was used to clear the already broken ice pieces sideways for the structure to keep advancing in the ice field.

Here, one question would be asked is that “how to choose the so called stable ice load history”. As can be seen from Figure 4.30 and Figure 4.31, the stable load histories were chosen to be of the following traits:

1) A series of loading variations with almost the similar amplitude;
2) Behind this “stable” ice breaking and ice rotating load history, a relatively “calm” ice load history was found. It is believed this relatively “calm” load history is when the structure is clearing the already broken ice pieces sideways. So it is not included in the analysis.
3) Exotic load peaks were excluded from the “stable” ice breaking and rotating histories. Although such large load peaks may also be induced by breaking or rotating a relatively large ice piece. In order to exclude the error induced by this large signal record in the frequency domain analysis, it was excluded. The overall ice breaking characteristics will not be influenced too much by this exclusion.

- Model D_F in small floe conditions (Test 02Li40_41_42)

  It has been pointed out in the discussion of Model B_F in small floe conditions, the interaction between the structure and the small ice floes are relatively more continuous than in large ice floe conditions. In large ice floe conditions, at least three interaction scenarios could be identified. (partial contact, full contact or no contact with a large ice floe). In small ice floe conditions, the structure and small floes has full contact and seems only one obvious scenario could be identified. This is why the PSD calculation could be directly applied to Model B_F and Model F_F without further separating the ice load history for detailed frequency domain analysis as for large floe conditions.

  However, for Model D_F, it is a different story. As pointed before, Model D_F has a relatively poorer ice clearing ability. So the influence of the ice clearing process, even in small ice floe conditions becomes very dominant. For example, one of its maximum loads as identified in test #02Li40 as shown in Figure A. 9 is thought to be induced by ice accumulation (see discussion is Appendix A). This extremely large *ice accumulation load* has to certain degree altered the whole ice load characteristics. Accordingly a relatively long ice load period containing the ice clearing process was calculated. Here, in order to dig out the information in terms of ice breaking and ice rotating processes only. The recorded time signal for Model D_F

in small floe conditions will also be re-analyzed based on the “stable” ice load signal. The results are shown in the following table and figures:

Table 4.16 Ice breaking& rotating induced dominant ice load frequency in managed ice (small floes) for Model D_F

Model D_F Test	Stable part 1		Stable part 2		Overall time series	
	Frequency [Hz]	Period [s]	Frequency [Hz]	Period [s]	Frequency [Hz]	Period [s]
#02Li40	0.00407	246	0.00407	246	0.00102	980
#02Li41	0.0163	61	-	-	0.0061	164
#02Li42	0.0651	15	-	-	0.0326	31

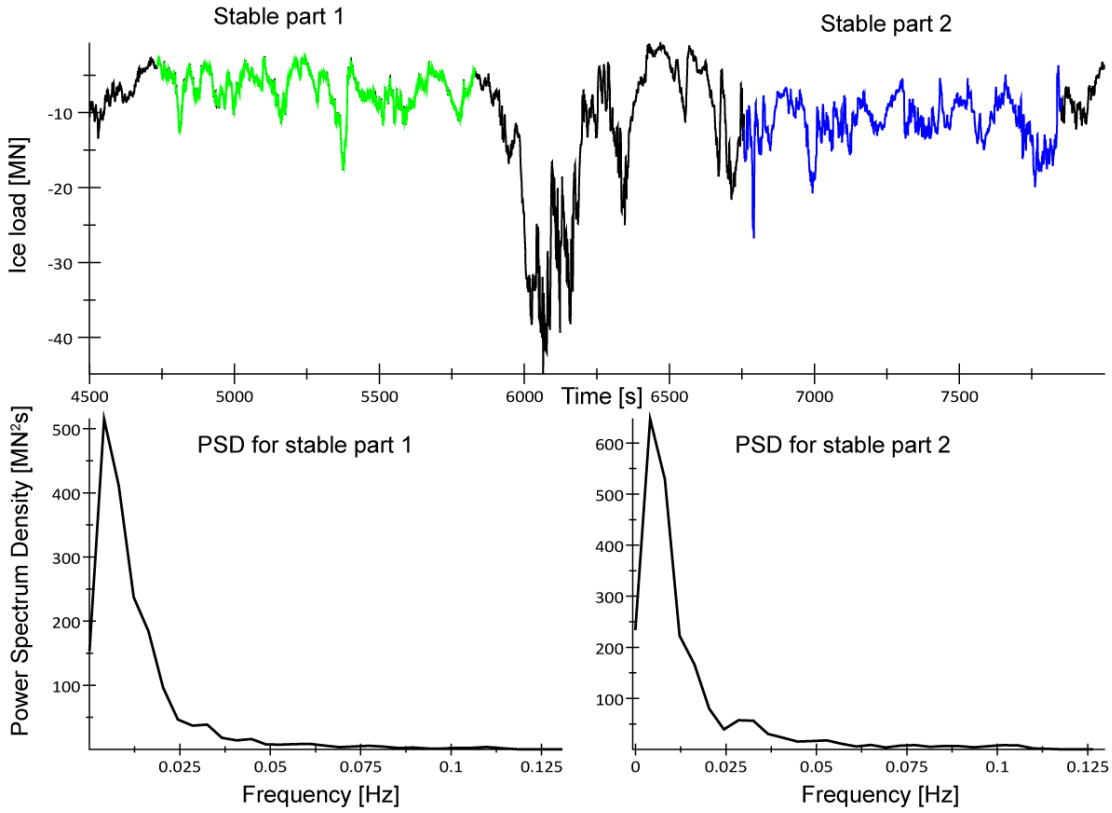

Figure 4.32 Ice breaking& rotating induced dominant ice load frequency in managed ice in test #02Li40 with ice speed 0.1 m/s

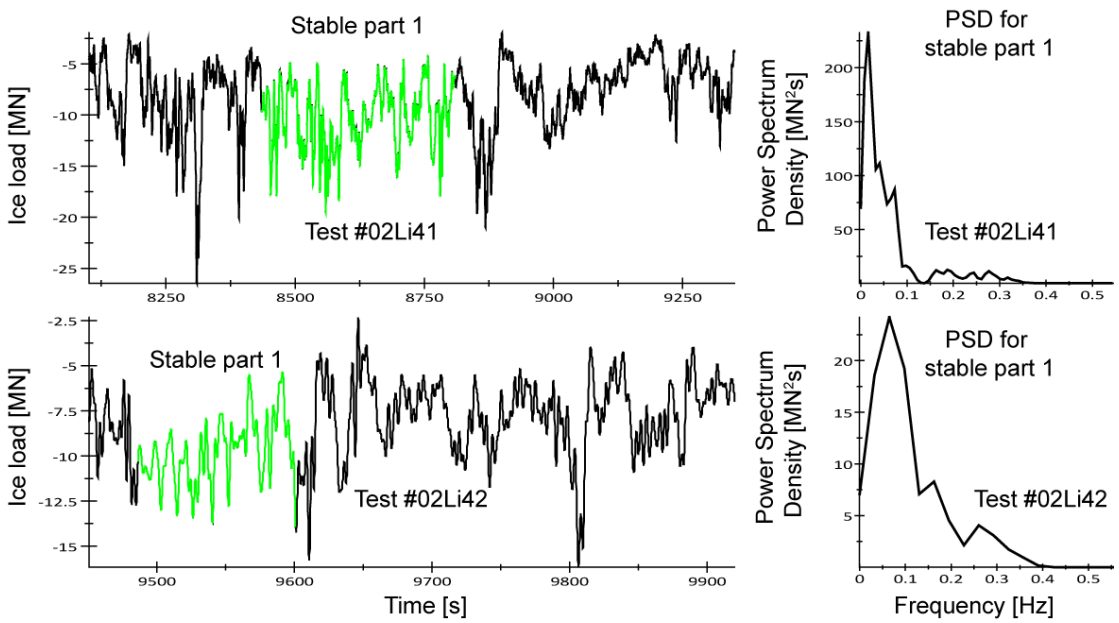

Figure 4.33 Ice breaking& rotating induced dominant ice load frequency in managed ice in test #02Li41 (upper) and #02Li42 (lower) with ice speed 0.5 m/s and 1 m/s respectively

From the above two figures and the calculation results in the above table, it demonstrates again the total ice load period includes a significant ice clearing process. But different from in large floe conditions, in small ice floe conditions, the above calculated load frequency will not include mainly the ice breaking and rotating frequencies as in large floe conditions. In small ice floe conditions, the ice floes generally become easier (faster) to be cleared. So the above calculated dominant ice load frequency may still be a combination of ice breaking, rotating and clearing process. But the longer ice accumulation process has been excluded by sampling a relatively "stable" loading process. However, since the ice accumulation load is relevant to many factors (geometry, velocity, displacement, etc), further investigations regarding this part are still needed.

4.1.3 Ice ridge testing

Model F_F was the only fixed structure being tested in the multi-year ice ridge. A layering technique (3 layers) was used to construct the multi-year ice ridge (see Figure 4.34). Each layer was 2.27 m in full-scale.

The statistical information of the results are listed in Table 4.17.

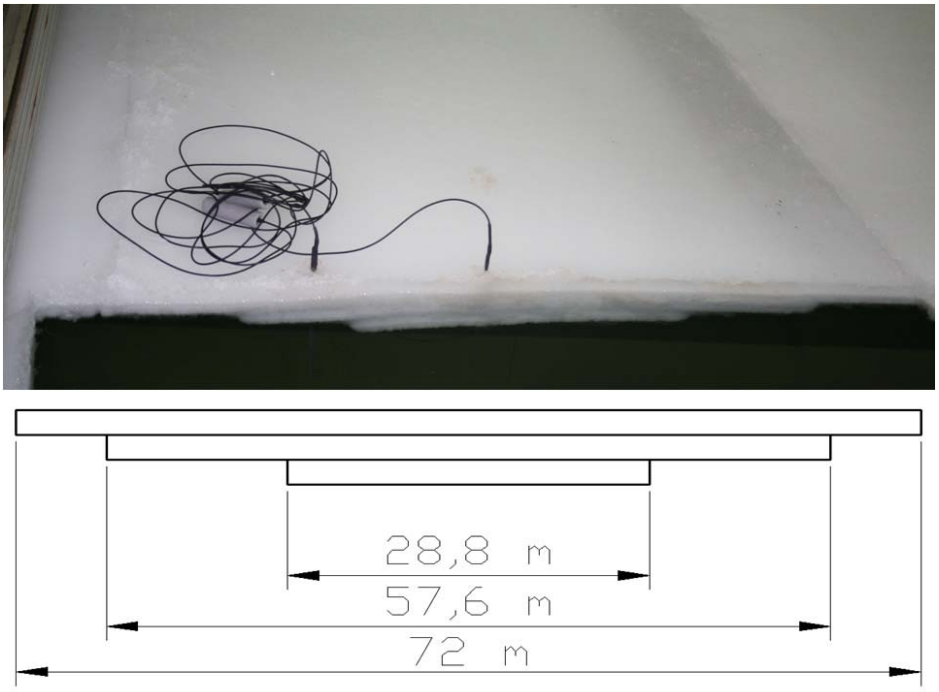

Figure 4.34 Photo of the multi-year ice ridge in Test #03Ri12 for Model F_F.

(*Upper*: Preparation in the test; *lower*: geometries of the multi-year ice ridge).

The multi-year ridge loading history is shown together with the multi-year ridge profile in Figure 4.35. From the figure it is found that the ice ridge load increases substantially when the structure enters the ridge. It arrives at the maximum ridge load when the structure just entered the thickest region of the multi-year ice ridge (6.84 m). Then the ice ridge load starts to decrease gently to a load level of first-year level ice. The whole process is intersected by 6 dashed lines where the videos are shown in Figure 4.36.

- In the first picture of Figure 4.36, Model F_F starts to enter the multi-year ice ridge, and more and more ice pieces start to accumulate in the bow region of Model F_F. And the ice breaking length is still relatively small.
- In the second picture of Figure 4.36, Model F_F entered the thickest layer (6.84 m) of the multi-year ice ridge. The ice accumulation volume also reaches maximum. And the ice breaking length becomes relatively large. The large *ice accumulation load*[36] and *ice rotating load* may be the reason of the occurrence of the maximum load shown in Figure 4.35.
- In the third picture of Figure 4.36, Model F_F is about to exit the thickest layer of the multi-year ice ridge. It was able to see that the accumulated ice volume is not as

[36] Although we are discussing the interaction between the conical structure and a multi-year ice ridge, since the multi-year ice ridge could roughly be viewed as a "thicker level ice", all the terms used here have the same meaning as used for level ice and conical structure interaction processes. For detailed definitions of these terms (in italic) we refer to Part I (Chapter 5).

much as in the second picture.

- In the forth picture of Figure 4.36, the fixed model is about to leave the second layer of the multi-year ice ridge. The accumulated volume of ice pieces has further decreased.
- In the fifth picture of Figure 4.36, Model F_F is about to enter the first-year level ice. The afore-accumulated ice pieces have largely disappeared. Only a little portion of ice rubble is still accumulated in the bow region.
- In the sixth picture of Figure 4.36, Model F_F is in some random place in the first-year level ice. Basically no ice accumulation happened in the bow region of Model F_F. Most of the broken ice pieces are immediately cleared sideways.

From the analysis of the above interaction processes, it can be concluded that:

- The maximum ridge load happened immediately after the model entered the thickest layer (6.84 m) of the multi-year ridge.
- The maximum load is considered to mainly arise from the *ice breaking load* and *ice rotating load* (see Figure 4.35 and the second picture in Figure 4.36). Several evidences supporting this conclusion will be listed in the following:
  1) From Figure 4.35, three ice load peaks are identified. These three peaks are more or less on the same level. Based on the video, three major ice breakings happened at the thickest part of the multi-year ridge. Accordingly the *ice breaking load* in the *ice breaking phase* and *ice rotating load* in the *ice rotating phase* may be the cause of these three ice load peaks. This evidence builds the relationship between the ice load peaks with the ice breakings.
  2) When Model F_F was advancing through the thickest part of the multi-year ridge, the lowest ice loads (absolute value) recorded is around -25 MN which is on the same level as the ice load before Model F_F entered the multi-year ridge (in first-year level ice). If there exists a huge *ice accumulation load,* the lowest ice load should be much larger than the absolute value of -25 MN. Moreover, the *ice accumulation load* tends to have a longer period than the *ice breaking load* and *ice rotating load*. So the possibility for the *ice accumulation load* to have the maximum and minimum values at the same time with the *ice breaking load* and *ice rotating load* is very low. This evidence excludes the contribution of the ice accumulation load to the ice load peaks.

  Based on the first evidence which built *certain* connection between the ice breakings and ice load peaks; and the second evidence which excluded the *ice accumulation load* contribution to the load peaks, together with the fact that usually

the *ice rotating load* and *ice sliding load* are the two major contributors to the total ice load for conical structures interacting with level ice, it is reasonable to conclude that for the conical structure interacting with a multi-year ridge, it is mainly the *ice breaking load* and *ice rotating load* that contributes to the maximum ice load.

- The ice breaking length is relatively small when the ice thickness is 6.84 m. Based on the three times ice breakings observed in the video at the thickest part of the multi-year ridge, the estimated ice breaking length in the test would be:

$$28.8 \text{ m} / 3 = 9.6 \text{ m}$$

Li (2003) recommended a ratio value of ice breaking length over ice thickness equaling 3.5 for the plate mode of bending failure. Based on this recommendation, the ice breaking length would be 23.94 m. Comparing with this recommended value, 9.6 m ice breaking length in the test is very small for an ice thickness of 6.84 m. From this comparison, it can be seen that, strictly speaking, the multi-year ridge cannot be simply treated as “thicker” level ice without caution.

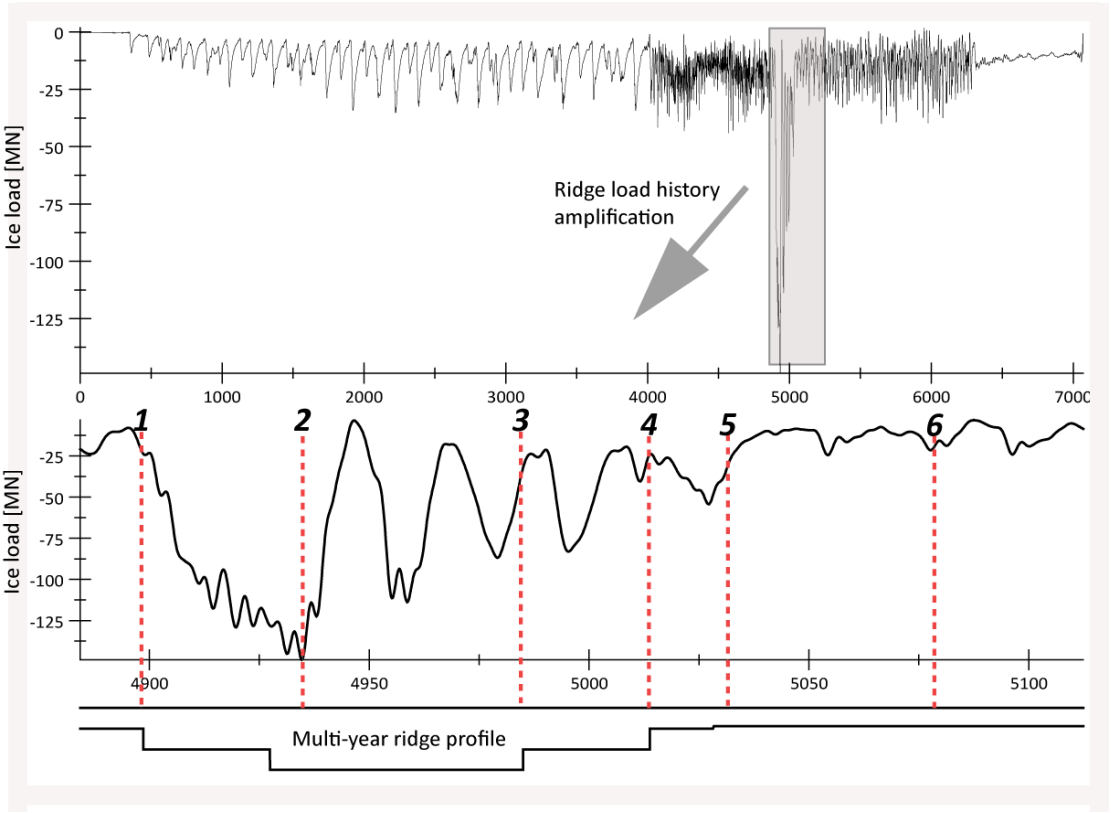

Figure 4.35. Trace of the loading history accompanied with the multi-year ridge profile.

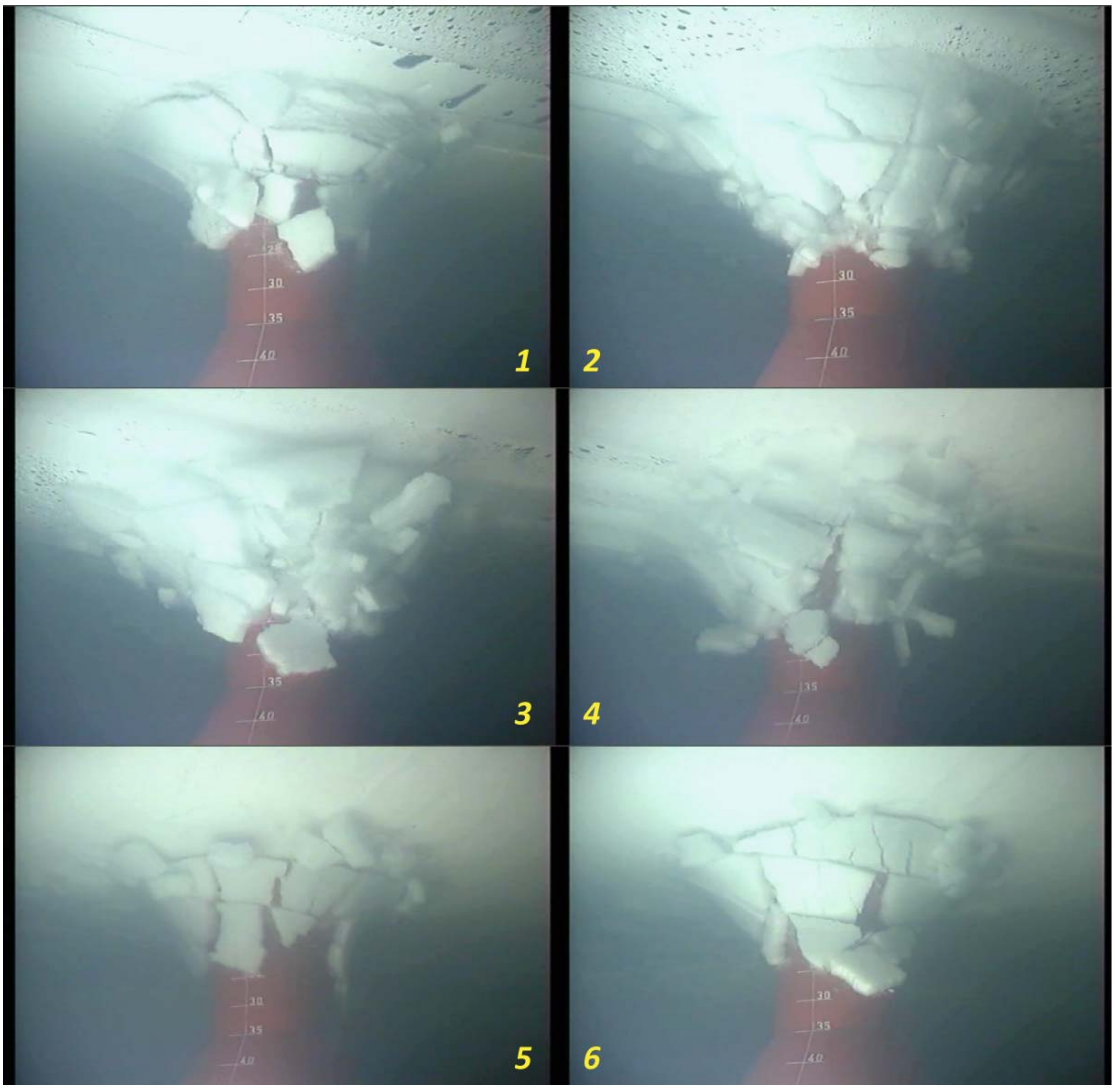

Figure 4.36. Model F_F interacting with the multi-year ridge in six different points.

The statistics of the horizontal multi-year ridge load is also calculated and presented in Table 4.17.

Table 4.17. Statistics of the horizontal ice load for the multi-year ridge for Model F_F.

Speed [m/s]	Average Load [MN]	Maximum Load [MN]	Std. deviation [MN]
0.5	-37.92	-168.90	37.6

As shown before, the average load and maximum load for Model F_F in 3 m level ice were -14.35 MN and -39.89 MN (see Table 4.3). If multiplying these two values with 3, we have:

$$-14.35 \times 3 = -43.05 \text{ MN}$$

$$-39.89 \times 3 = -119.67 \text{ MN}$$

These two values are close to the values measured for the multi-year ridge. As will be stated in Chapter 5, if calculating the multi-year ridge load by using the "level ice load on narrow conical structure formula" recommended by the ISO/FDIS 19906 (2009), the results

underestimate the actual ice ridge load.

4.2 Moored structures

Two moored models (Model B_M and Model E_M, see
Figure 3.4 and Figure 3.5) were tested in both level ice and ice ridges. Two different keel widths (80 m and 120-160 m) at the waterline were considered. The ice sheets (level ice and ice ridge) were pushed towards the structure at a constant speed of 0.1 m/s in all the tests. Different from the tests for fixed structures; the ice thickness was chosen to be 2 m (first-year level ice).

The only 'variables' of the ice for each moored model in the tests are the keel width at the waterline. Here the 80 m keel width and 120-160 m keel width will be termed as *narrow ridge* and *wide ridge*, respectively. Before entering the ice ridge section, the structures first entered the level ice section. Due to the different length of the keel width (narrow and wide), longer and shorter level ice track conditions are discerned due to a relatively small ice mass put into the *narrow ridge* and opposite to the *wide ridge*. In the following analysis, the terms '*long level ice track*' means the level ice in front of a ridge with narrow keel width (Tests #04 and #06) and '*short level ice track*' means the level ice in front of a ridge with wide keel width (Tests #05 and #07).

To analyze the behaviour of the moored structures in level ice and ridges, the recorded horizontal ice load, horizontal mooring force, surge, and pitch history were cut out in *(short/long) level ice* and *(wide/narrow) ice ridges*, respectively

.

Similar as analysis for fixed models, the time history will be analyzed in the frequency domain calculating the PSD so as to identify the dominant frequency. Afterwards, the statistics of the interested structural behaviours and forces will be calculated and compared with each other.

4.2.1 First-year level ice tests

4.2.1.1 Model B_M in first-year level ice

For Model B_M in *long level ice track conditions* (Test #04Li10), the peak frequency of each interested items are calculated and listed in Table 4.18. From Table 4.18 it is found that for the

moored structure with an ice speed of 0.1 m/s, the dominant ice load frequency is much lower than for a fixed structure. This is in agreement with common sense that a moored structure tends to have larger responses lasting for a longer duration. The response of the structure will in turn change the ice load/mooring force. It is reasonable to conclude that the response frequency of the moored structures has a large influence on the ice/mooring[37] force history. This can also be seen from Table 4.18, the ice load, mooring force and surge displacements have the same dominant frequency.

The load in level ice was significantly reduced when comparing with the fixed models. This is partly due to a thinner ice thickness (2 m) and partly because a moored structure tends to have less ice load compared with the fixed structures in level ice (see the conclusions in the Phase I Report, (2009)).

Table 4.18. Frequency domain analysis of Model B_M in *long level ice track.*

#04Li10	Long level ice track			
Model B_M	Level ice		Speed=0.1m/s	
Items	1st Dominant frequency	2nd Dominant frequency	1st Dominant Period	2nd Dominant Period
Ice load	0.000509 Hz	0.00916 Hz	1964.64 s	109.17 s
Mooring force	0.000509 Hz	0.0132 Hz	1964.64 s	75.76 s
Surge	0.000509 Hz	0.00356 Hz	1964.64 s	280.90 s
Pitch	0.00916 Hz	0.00917 Hz	109.17 s	109.18 s

The natural frequencies and periods for Model B_M are shown in Table 4.19:

Table 4.19. Natural periods and frequencies of Model B_M.

Model	Items	Natural Frequency [Hz]	Natural Period [s]
Model B_M	Surge	0.00877193	114
	Pitch	0.030864198	32.4

Two dominant frequencies have been recorded in the above Table 4.18. It is thought the first dominant low frequency is induced by ice accumulation. See from the following Figure 4.37, an about 2000 s period variation could be identified from the time history. This variation is

[37] Ice/mooring force represents ‘ice force and mooring force’. This expression will be repeatedly used in the following sections.

thought to be induced by the *ice accumulation load* variation as will be discussed in the following. The second dominant frequency will be the ice breaking and rotating processes. Both of them should be paid attention to since the lower frequency is the dominant frequency expressing the whole ice breaking, ice rotating and ice clearing process and the second dominant frequency is relating to the interested ice breaking and rotating processes. The second dominant period of the ice load, if multiplying by the ice drift speed, could be used to approximate the ice breaking length. The second dominant frequencies of interested items in long level ice track conditions are quite close to those in short level ice track conditions, meaning the ice breaking and ice rotating processes in both cases are more or less the same. The only difference is the ice accumulation load induced low frequency load.

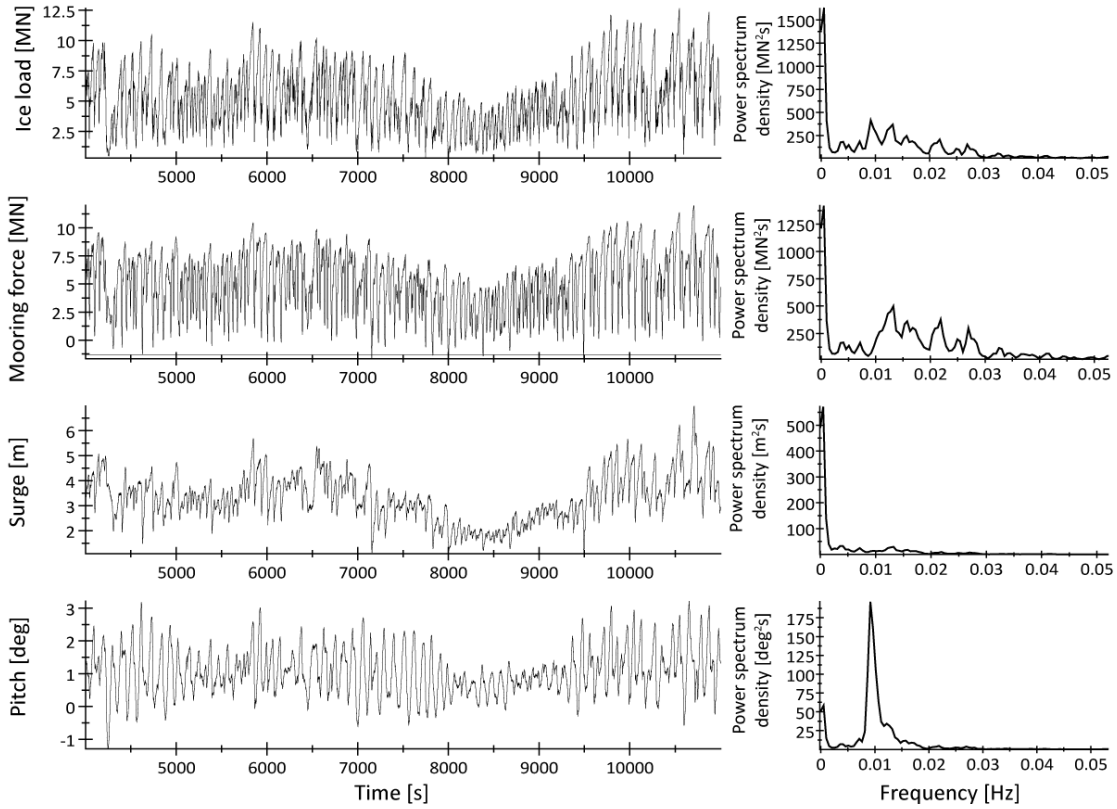

Figure 4.37. Model B_M in long level ice track.

The following results are for Model B_M in the *short level ice track* conditions (see Table 4.20, Figure 4.38).

Table 4.20. Frequency domain analysis of Model B_M in the *short level ice track.*

#05Li10	Short level ice track	
Model B_M	Level ice	Speed=0.1m/s
Items	Dominant frequency [Hz]	Dominant Period [s]
Ice load	0.0224	44.64
Mooring force	0.0224	44.64
Surge	0.0163	61.35
Pitch	0.0102	98.04

When comparing Table 4.20 with Table 4.18, it was found that the ice/mooring force and structural response have a much higher frequency in *short level ice track* conditions. It will be explained later, this is due to the absence of the low frequency *ice accumulation load.*

Similarly, the statistics for Model B_M in both the *long level ice track* and *short level ice track* situation is listed in Table 4.21.

Table 4.21. Statistics of Model B_M in level ice.

Model B_M	Maximum		Average		Std. deviation	
Level ice[38]	LLi-#04Li	SLi-#05Li	LLi-#04Li	SLi-#05Li	LLi-#04Li	SLi-#05Li
Surge [m]	6.98	3.47	3.30	2.11	0.95	0.30
Pitch [deg]	3.21	2.03	1.05	0.70	0.71	0.33
Ice load [MN]	12.67	8.77	5.37	4.14	2.42	1.46
Mooring force [MN]	12.00	8.76	5.09	3.76	2.63	1.97

[38] In this and the following tables, LLi represents Long Level ice track conditions; SLi represents Short Level ice track conditions.

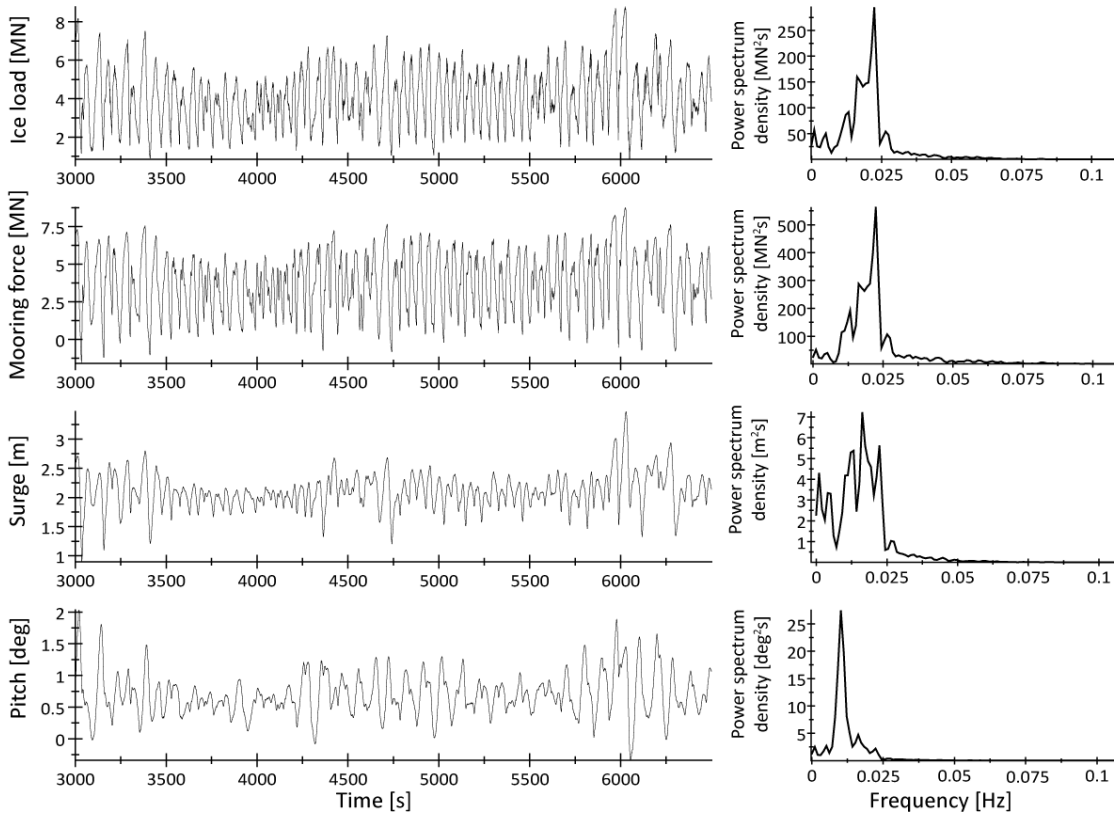

Figure 4.38. Model B_M in *short level ice track* conditions.

Different from the calculation results given by the *long level ice track* condition, the average ice load, mooring force and structural responses are lower. This is not the consequence of different ice flexural strength in the tests[39]. As will be illustrated in the next section for Model E_M in Tests #06Li10 and #07Li10, the same trend happened in the tests, although the flexural strength of the level ice in the *short level ice track* Test #07Li10 (648 kPa) is larger than that in the *long level ice track* Test #06Li10 (324 kPa).

The main reason behind such a discrepancy may be due to the *ice accumulation load* which is believed to have a low frequency component. It is highly possible that the ice accumulation volume is not only relevant to the geometry of the structure, but also highly relevant to the speed and displacement of the structure, which will in turn induce a low frequency component for the *ice accumulation load*.

As in the *long level ice track* test, the *ice accumulation load* has sufficient time to increase and decrease within its own long loading period. Therefore there is a higher chance for a large *ice accumulation load* to exist. However, for the *short level ice track* test, there is no

[39] For moored Model B_M, the ice flexural strength in the long level ice track situation (675 kPa) is larger than that in the short level ice situation (468 kPa). However, as will be shown later, this is not the major reason leading to a larger ice/mooring force and structural responses in the long level ice track test.

sufficient time for the *ice accumulation load* to increase high enough. Accordingly, for the *short level ice track* test, the average ice load, mooring force and structural responses are smaller than in the *long level ice track* test.

Similarly, for the interested items' dominant frequencies, due to the presence of such low frequency *ice accumulation load* in the tests, the overall ice load, mooring force and structural response's dominant frequencies are lower than those in the *short level ice track* tests.

4.2.1.2 Model E_M in first-year level ice

Similar analyses were also conducted for Model E_M. The results are shown in the following tables and figures. As reported by HSVA (2010), the average flexural strength of the level ice in the *long level ice track* (Test #06Li10) is smaller than the average flexural strength in the *short level ice track* situation (Test #07Li10). However, the same trend that the average ice/mooring force, and structural responses in the *long level ice track* situation are larger than those in the *short level ice track* situation was observed (see Table 4.25). This confirms again the above explanation that a low frequency *ice accumulation load* exists in the tests, which induce a larger ice/mooring force and structural responses in the *long level ice track* situation than in the *short level ice track* situation.

Based on the above discussion and the following tables and figures, similar conclusions are given below:

1) For Model E_M, the amplitude of the ice load is much smaller compared with the fixed structure (see Table 4.25); Thicker ice thickness for fixed model test may be one of the reasons. Moored models' load reduction comparing with fixed models in level ice may be another reason.Table 4.25
2) The frequency of the ice load is much smaller compared with the fixed structure (see Figure 4.39 and Figure 4.40);[40]
3) There exists a low frequency *ice accumulation load* for the moored structure (interesting items[41]' frequency is higher and the average amplitudes are lower in the *short level ice track* test than in the *long level ice track* test, see the comparison between Table 4.22 and Table 4.24).

The same explanations can be found in the previous section.

[40] Note the above two comparisons between the moored models and fixed models are under different ice thickness. The different ice thickness may be one of the reasons that lead to the differences.

[41] Interesting items in this chapter means the ice load, mooring force, surge, and pitch response.

Table 4.22. Frequency domain analysis of Model E_M in *the long level ice track* situation.

#06Li10	Long level ice track			
Model E_M	Level ice		Speed=0.1m/s	
Items	1st Dominant frequency	2nd Dominant frequency	1st Dominant Period	2nd Dominant Period
Ice load	0.000509 Hz	0.0158 Hz	1964.64 s	63.29 s
Mooring force	0.000509 Hz	0.0178 Hz	1964.64 s	56.18 s
Surge	0.000509 Hz	0.0158 Hz	1964.64 s	63.29 s
Pitch	0.0158 Hz	0.0158 Hz	63.29 s	63.29 s

The natural frequencies and periods for Model E_M are shown in the following table:

Similar as for Model B_M in long level ice track conditions, two dominant frequencies have been identified in the above table. It is also though the first one is relating to the ice accumulation while the second one is relating to the general ice breaking and ice rotating frequencies. Multiplying the second dominant period of ice load with the ice drift speed could estimate the ice breaking length. In the current case, the ice breaking length could be estimated to be 6.3 m. The second dominant frequencies of interested items in long level ice track conditions are quite close to those in short level ice track conditions, meaning the ice breaking and ice rotating process in both cases are more or less the same. The only difference is the ice accumulation load induced low frequency load.

Table 4.23. Natural periods and frequencies of Model E_M.

Model	Items	Natural Frequency [Hz]	Natural Period [s]
Model E_M	Surge	0.00877193	114
	Pitch	0.01618123	61.8

From Table 4.22 and Table 4.23 it is found that the dominant frequency of the ice load and surge in the *long level ice track* situation are very low compared with the natural frequency of the structure. As pointed out before, this low frequency force and response may be induced by the ice accumulation.

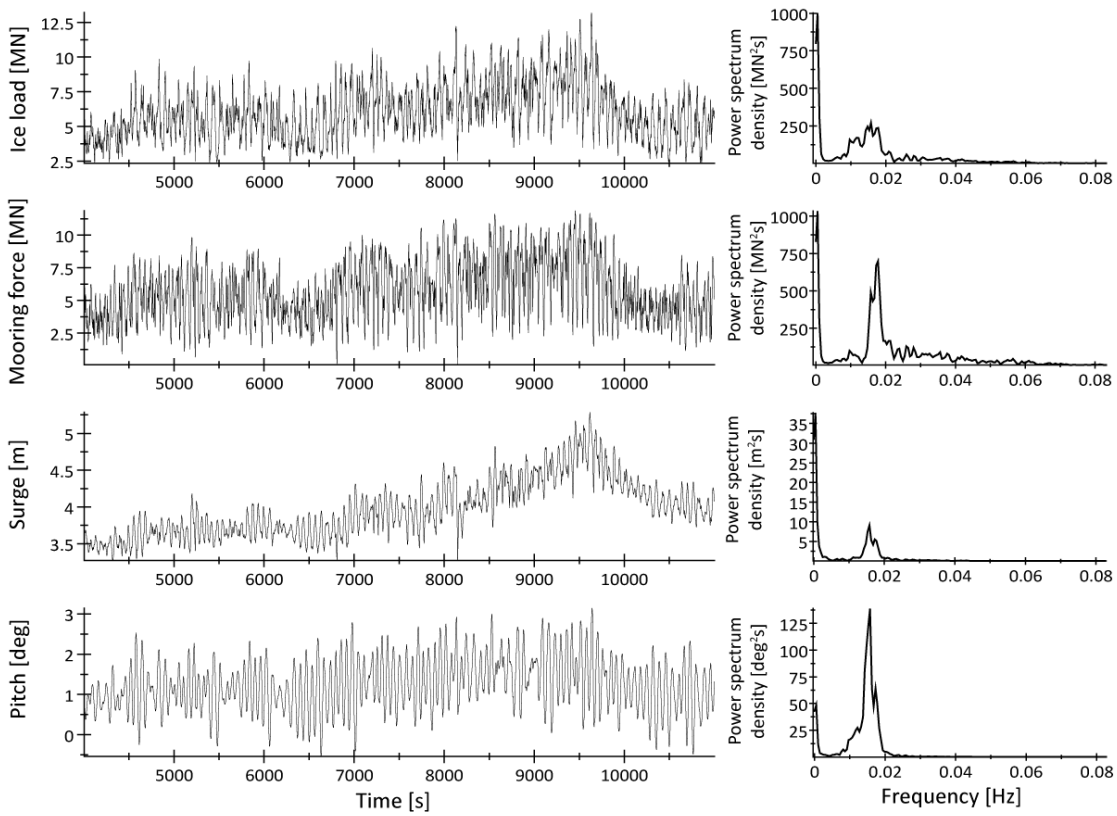

Figure 4.39. Model E_M in the *long level ice track* situation.

The PSD and dominant frequencies for interested items in Test #07Li10 in the *short level ice track* situations for Model E_M are shown in Table 4.24 and Figure 4.40.

Table 4.24. Frequency domain analysis of Model E_M in the *short level ice track* situation.

#07Li10	Short level ice track	
Model E_M	Level ice	Speed = 0.1m/s
Items	Dominant frequency [Hz]	Dominant Period [s]
Ice load	0.0132	75.76
Mooring force	0.0173	57.80
Surge	0.0163	61.35
Pitch	0.0163	61.35

Similar as for Model B_M, in the *short level ice track* condition, the dominant frequencies of the ice load and structural responses become larger due to the incomplete development of the low frequency component of the *ice accumulation load*.

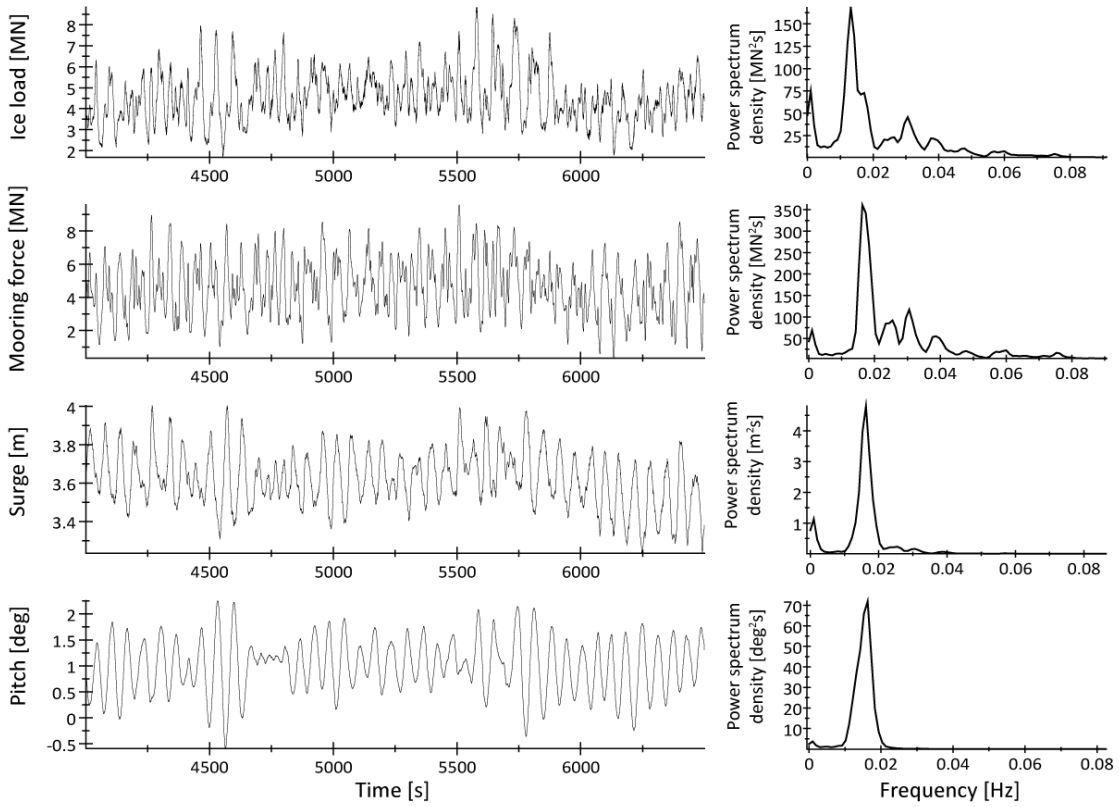

Figure 4.40. Model E_M in the *short level ice track* conditions.

Table 4.25. Statistics of Model E_M in level ice.

Model E_M	Maximum		Average		Std. deviation	
Level ice	LLi-#06Li	SLi-#07Li	LLi-#06Li	SLi-#07Li	LLi-#06Li	SLi-#07Li
Surge [m]	5.29	4.00	3.97	3.62	0.39	0.15
Pitch [deg]	3.14	2.25	1.24	1.00	0.67	0.52
Ice load [MN]	13.19	8.83	6.05	4.54	1.89	1.17
Mooring force [MN]	11.87	9.59	5.68	4.62	2.23	1.70

4.2.1.3 Comparison of Models B_M and E_M in first-year level ice

The comparisons are mainly conducted for the horizontal ice load, mooring force and the structure's surge and pitch responses. Based on the above calculated results, the comparisons are shown in the following tables.

Ice load, mooring force and structural responses comparison

Table 4.26. The comparison of Model B_M with Model E-M in the *long level ice track.*

Models B_M/E_M	Level ice	Speed = 0.1m/s	Long level ice track
LLi-#04&#06	Maximum value	Average value	Std. deviation
Surge ratio []	1.32	0.83	2.46
Pitch ratio []	1.02	0.85	1.06
Ice load ratio []	0.96	0.89	1.28
Mooring force ratio []	1.01	0.90	1.18

Table 4.27. The comparison of Model B_M with Model E_M in *the short level ice track.*

Model B_M/E_M	Level ice	Speed = 0.1m/s	Short level ice track
SLi-#04&#06	Maximum value	Average value	Std. deviation
Surge ratio []	0.87	0.58	2.03
Pitch ratio []	0.90	0.70	0.64
Ice load ratio []	0.99	0.91	1.25
Mooring force ratio []	0.91	0.82	1.15

From the above two tables, it is found that the ice load on both Model B_M and Model E_M are very close to each other. The ice load and structural responses of Model B_M are slightly lower. Although the average ice flexural strengths are different during different moored model tests as shown in Table 4.28.

Table 4.28. The average ice flexural strength in the moored model tests.

Mode	Description	Test series	Ice flexural strength
Model B_M	Long level ice track	04LI10	675 kPa
	Short level ice track	05LI10	468 kPa
Model E_M	Long level ice track	06LI10	324 kPa
	Short level ice track	07LI10	648 kPa

The average flexural strength difference cannot explain why the ice/mooring force and structural response for Model E_M are slightly larger than those of Model B_M. After excluding the ice flexural influence, the main reason becomes that Model E_M has a lager waterline diameter (50 m) than Model B_M (30 m).

4.2.2 Ice ridge tests

Models B_M and E_M were tested in two ridges with different keel widths at the waterline. Similar as before, the horizontal ice load, mooring force, and the surge and pitch responses of the structures are examined and discussed in the following:

4.2.2.1 Horizontal ice ridge load analysis

As described in the Phase I Report, the ice load was found to be related to the mean cross-section of the ridge area. Based on the test results, the normalized horizontal ice load versus the mean cross-section area of the ridge is depicted in Figure 4.41.

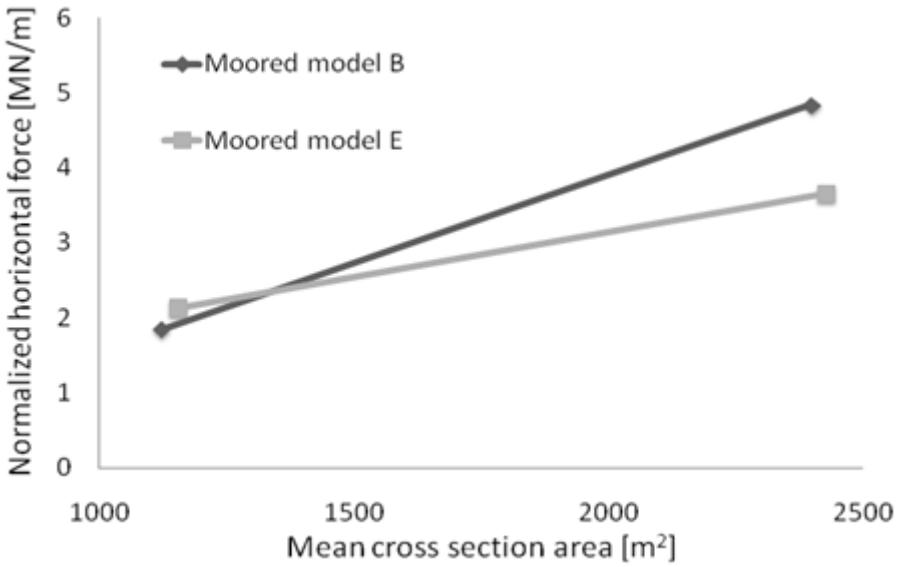

Figure 4.41. Normalized peak ice ridge load versus the mean cross-section of ice ridge.

(Only the normalized ice load where compared with the ridge mean cross-section).

From Figure 4.41 it is found that the slopes of these two lines (representing the ice ridge load over the ridge's mean cross-section area) are very close. Certain linear relationships between the mean ice ridge cross-section area and the ice ridge load may be obtained. This is in accordance with the similar results shown in Figure 4.20 of the Phase I Report (2009).

The ice load, mooring force and structural responses' statistics for Model B_M is listed in Table 4.29.

Table 4.29. Statistics of Model B_M in ice ridge.

Model B_M	Maximum Load [MN]		Average Load [MN]		Std. deviation [MN]	
Ice ridge	Narrow ridge #04Li	Wide ridge #05Li	Narrow ridge #04Li	Wide ridge #05Li	Narrow ridge #04Li	Wide ridge #05Li
Surge [m]	34.66	50.77	15.28	26.46	10.38	15.61
Pitch [deg]	10.09	13.28	2.87	5.15	2.87	3.36
Ice load [MN]	47.83	144.56	19.86	46.60	13.19	36.38
Mooring force [MN]	48.05	143.01	19.22	45.42	12.67	36.05

In average, for Model B_M the ice load and surge displacement in wide ice ridge are about *2 times* of that in narrow ice ridge.

The test results for Model E_M are listed in Table 4.30.

Table 4.30. Statistics of Model E_M in ice ridge.

Model E_M	Maximum Load [MN]		Average Load [MN]		Std. deviation [MN]	
Ice ridge	Narrow ridge #06Li	Wide ridge #07Li	Narrow ridge #06Li	Wide ridge #07Li	Narrow ridge #06Li	Wide ridge #07Li
Surge [m]	38.54	50.22	19.15	24.72	11.36	16.22
Pitch [deg]	7.19	8.80	3.03	3.97	1.54	2.32
Ice load [MN]	104.95	195.91	32.65	58.15	24.49	53.91
Mooring force [MN]	111.60	223.47	33.21	62.61	26.38	60.64

Similarly, in average, the ice load and surge displacements in wide ice ridge are about *2 times* of that in narrow ice ridge.

The comparison of ice ridge loads and structural responses of Model B_M and Model E_M will be given in Table 4.31 and Table 4.32.

Table 4.31. Comparison of Models B_M and D_M in *narrow ice ridge*.

Model B_M/E_M	Narrow ice ridge	Speed = 0.1m/s	Long level ice track
#04&#06	Maximum Load ratio []	Average Load ratio []	Std.deviation ratio []
Surge ratio []	0.90	0.80	0.91
Pitch ratio []	1.40	0.95	1.86
Ice load ratio []	0.46	0.61	0.54
Mooring force ratio []	0.43	0.58	0.48

Table 4.32. Comparison of Models B_M and D_M in *wide ice ridge*.

Models B_M/E_M	Wide ice ridge	Speed = 0.1m/s	Long level ice track
#05&#07	Maximum Load ratio []	Average Load ratio []	Std.deviation ratio []
Surge ratio []	1.01	1.07	0.96
Pitch ratio []	1.51	1.30	1.45
Ice load ratio []	0.74	0.80	0.67
Mooring force ratio []	0.64	0.73	0.59

Similar comparison results can be obtained as in level ice. The surge displacement and pitch angle are very close for Models B_M/E_M in either ice ridges. The average ice load and surge displacement are slightly lower for Model B_M. Explanations concerning the waterline diameter have been given for the level ice conditions. The waterline diameter ratio for Model B_M over Model E_M is 30/50=0.6 which is quite close to the ice/mooring force ratios presented in the above two tables.

Different from in level ice conditions, the surge response and pitch angle for Model B_M seemed to have increased comparatively. The ratio results extracted from Table 4.26, Table 4.27, Table 4.31 and Table 4.32 concerning the surge and pitch response ratio are shown in the following:

Table 4.33. Moored structure responses comparisons between level ice and ice ridges.

Model B_M/E_M	Long level ice track	Short level ice track	Narrow ice ridge	Wide ice ridge
Average surge ratio []	0.83	0.58	0.80	1.07
Average pitch ratio []	0.85	0.70	0.95	1.30

Model B_M's responses increase becomes more obvious in wide ice ridge.

This is mainly due to the larger restoring force/momentum supplied by the mooring lines. As can be seen from *Figure 8* and *Figure 10* in HSVA (2009), the target horizontal restoring force

and target pitch restoring moment of Model E_M is larger than for Model B_M.

Moreover, Model E_M also has a larger hydrostatic stiffness in the pitch direction as shown by the following calculations:

Model E_M has a much larger mass (233530 t) than Model B_M (169372 t). With known metacentric height (GM) for Model B_M (5 m) and Model E_M (4.2 m), the hydrostatic stiffness in the pitch direction could be calculated as:

$$C_{55,B} = \rho g V_B \times 5 = 8307.6 \text{ MN} \cdot \text{m/rad}$$

$$C_{55,E} = \rho g V_E \times 4.2 = 9621.9 \text{ MN} \cdot \text{m/rad}$$

From the above calculation, it can be seen that Model E_M has a larger hydrostatic stiffness in the pitch direction.

Different from in level ice, less inertia loads (fewer dynamic effects) participate in the structure and ridge interaction process. So the static restoring effect (including both static mooring stiffness and hydrostatic stiffness) becomes predominant in determining the structural responses. This explained why the surge and pitch responses of Model B_M become comparatively larger than Model E_M in ice ridge conditions, especially in wide ice ridge.

4.2.2.2 Ridge load history

Similar as in the Phase I Report (2009), the ice ridge's horizontal load and mooring force are depicted along the penetration of the structure as shown in the following figures. From Figure 4.42 and Figure 4.43 it can be seen that the ice/mooring load first increases gradually. After reaching the peak, they decrease immediately. The peak ice/mooring force appears almost right at the ice ridge position for both models in *narrow ice ridge* (see the left sides of Figure 4.42 and Figure 4.43). This means that both Model B_M and Model E_M have good ice clearing ability in *narrow ice ridge*.

Comparing with Figure 4-22, p. 22 of the Phase I Report (2009), Model E_M can be proved to be more effective in clearing the ice rubbles than Model D_M.

However, in *wide ice ridge*, for both models, the peak load appeared slightly after the ice ridge, meaning for *wide ice ridge*, the ice rubble accumulation is unavoidable.

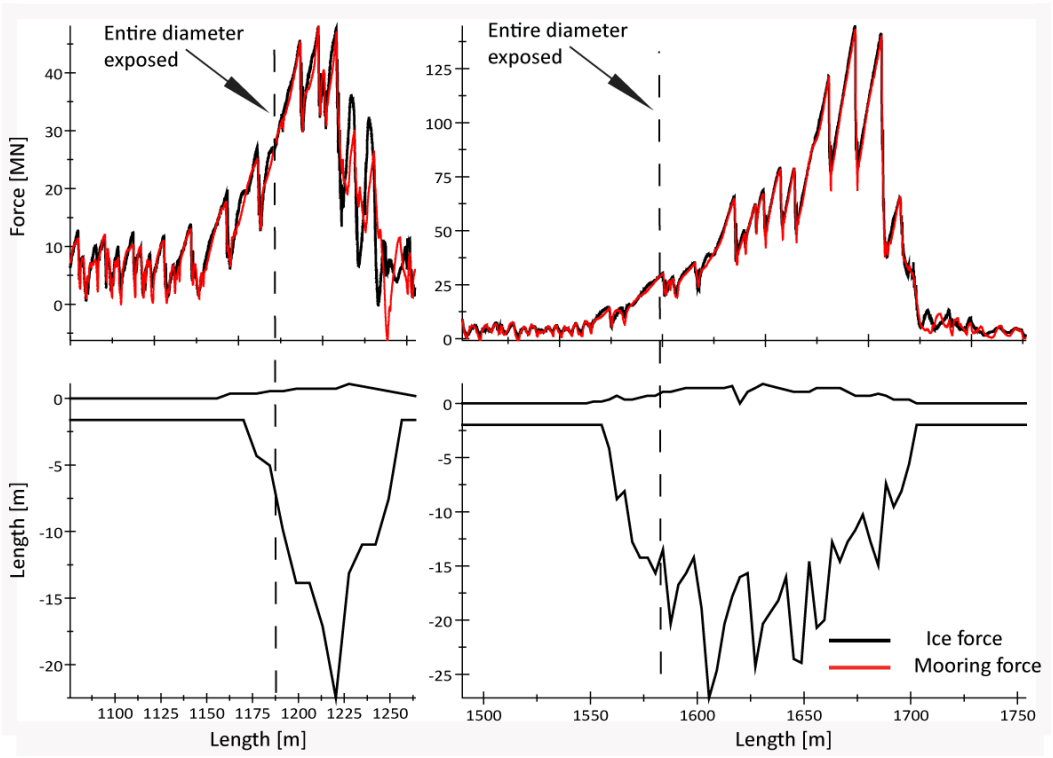

Figure 4.42. Model B_M in ice ridge.

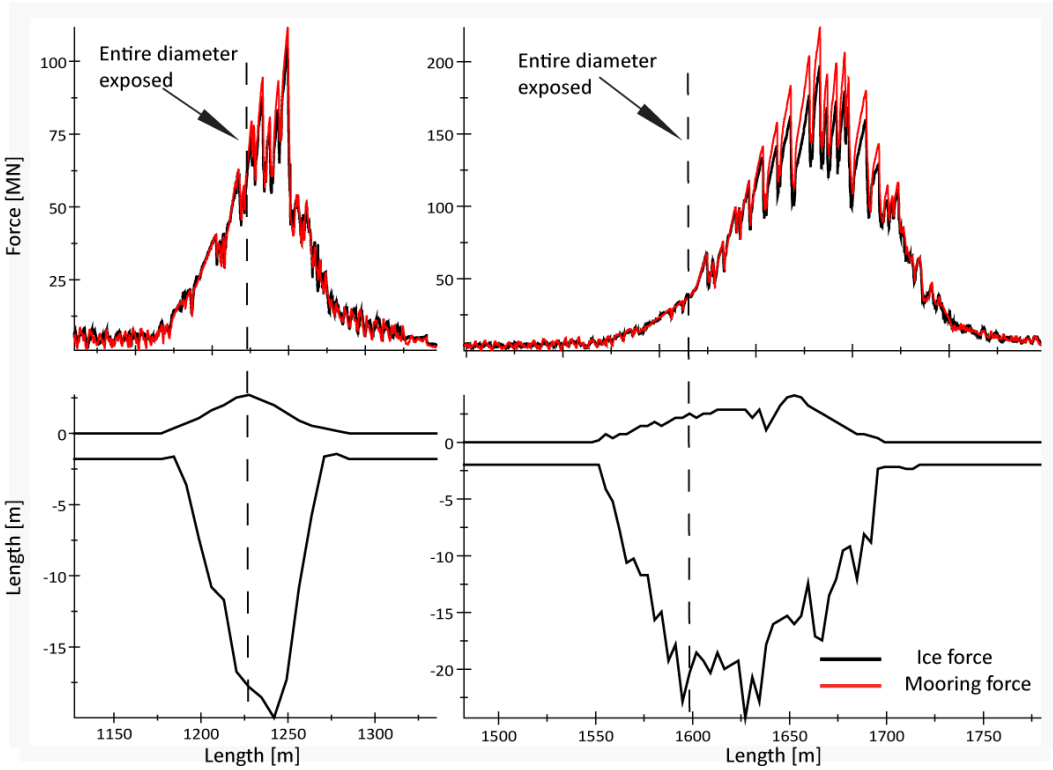

Figure 4.43. Model E_M in ice ridge.

4.2.2.3 Comparison with Phase I ridge load

In order to get a more comprehensive understanding concerning the ice ridge load's characteristics, the recorded ridge load for Model B_M and Model E_M are depicted together with the previous Phase I ice ridge load for Model B_F, Model D_F, Model D_M[42]. The results are shown in the following:

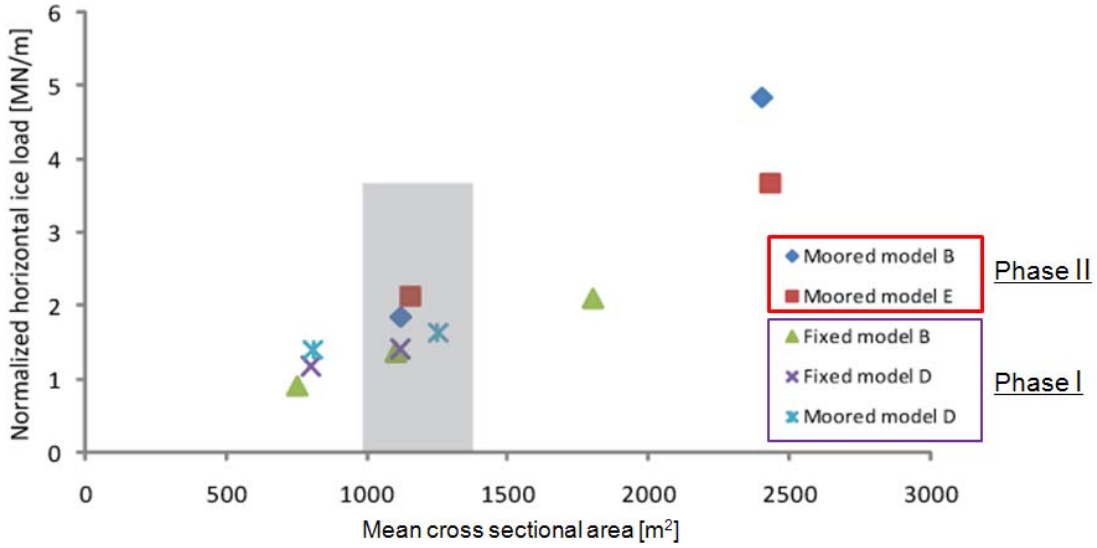

Figure 4.44. Measured horizontal peak forces versus the mean cross sectional area of the ice ridge for both Phase I and Phase II tests.

From Figure 4.44, the following conclusions can be made:

- A certain linear relationship may be established between the mean cross-sectional area of the ice ridge and the peak horizontal ice ridge load;
- From the *shaded area*, comparing the results of Model D_M in Phase I with Model B_M and Model E_M in Phase II, it can be concluded that lower ice speed leads to larger ice ridge loads[43].
- Similar conclusions as in Phase I that moored structures tend to have larger ridge loads compared with fixed structures can still be claimed.

[42] The ice ridge load for moored Model B in the Phase I test was not included since there exist some questionable ice loads during the test.

[43] The ice speed in the Phase I test was 0.5 m/s whilst in the Phase II test, it was 0.1 m/s.

5 Comparison with ISO/FDIS 19906

5.1 Comparison with ISO/FDIS in level ice

Models B_F, D_F, and F_F were tested in level ice. In this section, the ice loads on these conical structures will be calculated according to the plastic method in ISO/FDIS 19906 (2009) and compared with the measured peak ice loads.

Similar as in the Phase I Report, the plastic method will be adopted here and the ice ride-up thickness was set as two times the ice thickness. The results are displayed in Table 5.2 and Table 5.3. The inputs of the calculations were based on Table 25 of (HSVA, 2010) and will be summarized here in Table 5.1.

Table 5.1. The input value of the level ice load calculations.

Model	Test Series	ice flexural strength	ice thickness [m]	water density	ice density	waterline diameter	Top diameter of the cone	Cone angle
Model B	01Li10	720 kPa	3.0852	1005 kg/m	845.6 kg/m	30 m	20 m	45 deg
	01Li11	936 kPa	3.0384					
	01Li12	1008 kPa	2.9772					
Model D	02Li10	756 kPa	2.9772	1005 kg/m	832.8 kg/m	50 m	40 m	
	02Li11	828 kPa	3.0132					
	02Li12	900 kPa	2.8044					
Model F	03Li10	792 kPa	2.9736	1005 kg/m	857.4 kg/m	50 m	20 m	
	03Li11	792 kPa	3.0960					
	03Li12	792 kPa	2.8692					

Other input values such as the Poisson ratio, friction coefficient are taken the recommended values 0.3 and 0.1, respectively.

Based on the above known input values, the calculated horizontal values and vertical values are compared with the measured ones in Table 5.2 and Table 5.3.

As can be seen from Table 5.2 and Table 5.3, the ISO/FDIS 19906 (2009) code underestimated the actual ice loads. From the last column, the ratio between the measured values and calculated values were given.

Table 5.2. Comparison of measured maximum horizontal ice load with calculated horizontal ice load.

Model	Test Series	Measured	Calculated maximum horizontal load		Measured/ calculated	
		Maximum Horizontal load [MN]	Johansen [MN]	Tresca [MN]	Johansen [-]	Tresca [-]
Model B_F	01Li10	-29.48	-20.09	-17.42	1.47	1.69
	01Li11	-32.87	-24.40	-20.99	1.35	1.57
	01Li12	-34.89	-25.05	-21.52	1.39	1.62
Model D_F	02Li10	-80.36	-23.60	-21.13	3.40	3.80
	02Li11	-79.92	-25.71	-22.92	3.11	3.49
	02Li12	-51.23	-24.13	-21.50	2.12	2.38
Model F_F	03Li10	-35.16	-28.01	-25.40	1.26	1.38
	03Li11	-39.89	-29.91	-27.07	1.33	1.47
	03Li13	-44.13	-26.43	-24.00	1.67	1.84

Table 5.3. Comparison of measured maximum vertical ice load with calculated vertical ice load.

Model	Test Series	Measured	Calculated maximum vertical load		Measured /calculated	
		Maximum vertical load [MN]	Johansen [MN]	Tresca [MN]	Johansen [ ]	Tresca [ ]
Model B_F	01Li10	26.655	20.73	18.00	1.29	1.48
	01Li11	27.74	25.12	21.64	1.10	1.28
	01Li12	29.501	25.78	22.17	1.14	1.33
Model D_F	02Li10	43.624	24.50	21.98	1.78	1.99
	02Li11	42.984	26.65	23.80	1.61	1.81
	02Li12	46.612	25.01	22.33	1.86	2.09
Model F_F	03Li10	36.174	29.39	26.73	1.23	1.35
	03Li11	42.567	31.37	28.47	1.36	1.50
	03Li13	46.084	29.81	27.76	1.55	1.66

As can be seen from the above two tables, the theoretical values are all less than the measured data. The Johansen results gave relatively larger theoretical results than the Tresca results. In the calculation, the input data were all chosen to be the measured data. However, due to the lack information regarding the ice ride-down thickness, it was chosen as two times of the level ice thickness.

In the following table, based on the ISO/FDIS formula, the estimated theoretical *ice ride-down thickness* was calculated to approximate the measured data.

Table 5.4 Ice ride-down estimation to approximate the measured value

Model	Test Series	Measured	Ice accumulation estimation based on Johansen method
		Maximum Horizontal load [MN]	Theoretical ice ride-down thickness requirement/structure's underwater height [m]
Model B_F	01Li10	-29.48	42/35
	01Li11	-32.87	30/35
	01Li12	-34.89	33/35
Model D_F	02Li10	-80.36	90/35
	02Li11	-79.92	84/35
	02Li12	-51.23	45/35
Model F_F	03Li10	-35.16	11/45
	03Li11	-39.89	13/45
	03Li13	-44.13	19/45

As we can see from the above Table 5.4, the approximate ice ride-down thicknesses requirement to approximate the calculation results were given together with the underwater –body's height of the structure. It is found that the "theoretical" ice ride-down thickness is very large. For Model B_F and Model D_F, they even became larger than the geometry of the structure which is not realistic. Generally model D_F has the largest discrepancy with the measured data. This can also be seen from Figure 5.1 which will be introduced later.

The previous comparisons were between the measured *maximum* values and the theoretical values. In order to get a general overall comparison, the measured data are compared with the

theoretical data visually in the following figure. It should be noted that in the following figure, the theoretical prediction is based on the target values which means the average flexural strength and ice thickness are chosen to be 750 kPa and 3 m respectively. For detailed calculation results based on measured values, please refer back to the previous two tables.

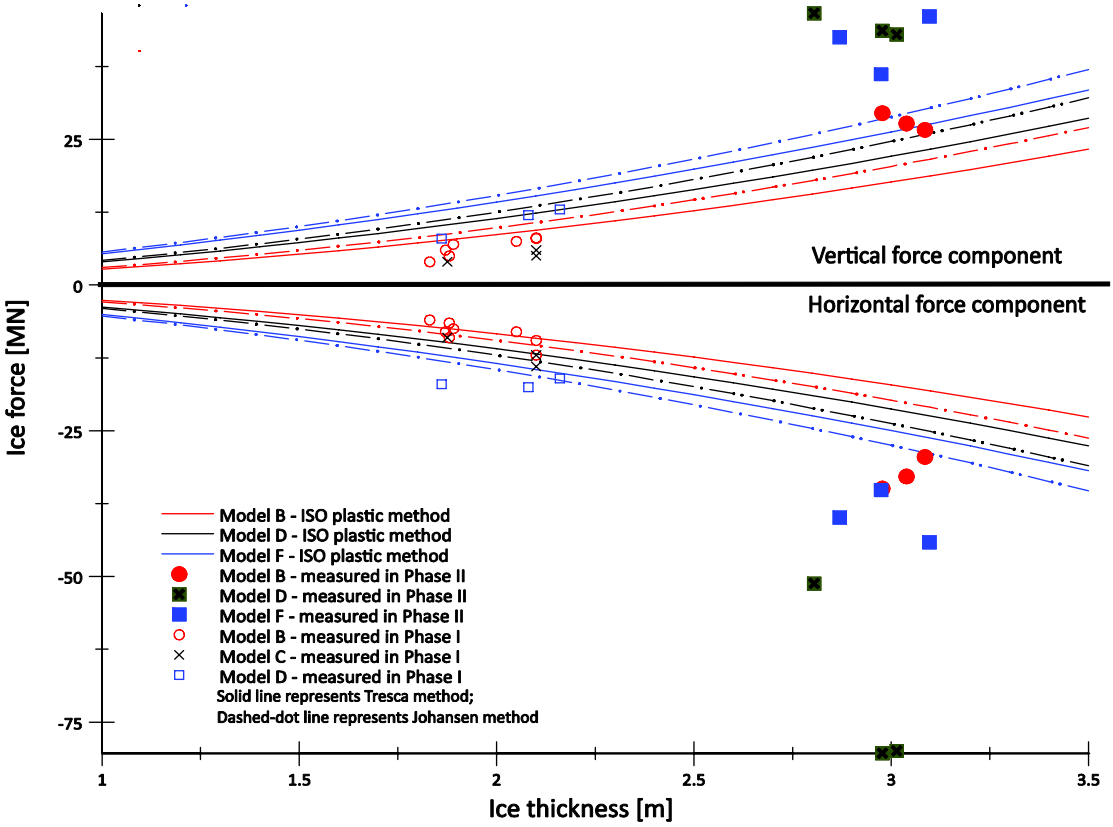

Figure 5.1. Comparisons between the plastic ice load method for cones (ISO/FDIS 19906, 2009) and measured *maximum* ice load in each of the level ice tests for fixed models.

(Note: the average flexural strength and ice thickness of the level ice in the calculation were chosen to be the target ice strength 750 kPa and target thickness 3 m; the ice thicknesses of the measured values were chosen as the average values of the ice thickness in each test).

From Figure 5.1, besides the conclusion that the ISO/FDIS code tends to give lower ice load values, larger discrepancy between the measured values and calculated values are found for Model D_F. This is mainly due to the poor ice clearing ability of Model D_F; and during the calculation based on the ISO/FDIS code, the *ice ride-down thickness* was chosen to be two times of the ice thickness (Ralston, 1977). This may underestimated the *ice accumulation load* for Model D_F and hence induce such a large discrepancy.

5.2 Comparison with ISO/FDIS in ice ridges

Similar as in Phase I report (2009), the (A.8-49) formula in the code was used to calculate the load from the unconsolidated part of the ridge $F_{k.}$. It should be noted that this formula is intended for calculation of the *keel load* on vertical structures. However, since there is no recommendation in the code for calculating *keel loads* for conical structures, this formula is used here instead.

And similar method as in the previous section was adopted to calculate the ice load on the conical structure under the consolidated part of the ridge. The same average flexural strength as in level ice was used for the consolidated layer. The real flexural strength of the consolidated layer is larger than the surrounding ice, but it is not easy to measure the real value. However, it is not likely that the keel load and the consolidated layer have the maximum value at the same time during the ridge failure, and the assumption of a slightly lower flexural strength is therefore appropriate.

The structural diameters of the conical structures used in the calculations were chosen to be the diameter at the waterline in the keel calculations. This is a conservative value. And the cohesion parameters and internal friction angle were chosen according to the code recommendation as 5 kPa and 30°, respectively.

The major input data are shown in Appendix B. (Based on Table 26, p. 76 of (HSVA, 2010)).

The comparison is shown in Table 5.5:

Table 5.5. Horizontal ridge loads calculated according to the recommendations given in the ISO/FDIS 19906 (2009) standard, and comparisons to measured loads. The measured ridge load is the horizontal average ice load.

Model (Test #)	Keel load [MN]	Consolidated layer load [MN]	Total ridge load [MN]	Maximum measured ridge load [MN]	Maximum measured/calculated [-]
Model F_M (03Ri)	-	101.99*	101.99	148.83	1.46
Model B_M (04Ri50)	17.58	16.35	33.92	47.83	1.41
Model B_M (05Ri50)	19.79	11.94	31.73	144.56	4.56
Model E_M (06Ri50)	35.41	6.97	42.38	104.95	2.48
Model E_M (07Ri50)	37.54	11.69	49.22	195.91	3.98

(*Note: This multi-year ridge load value was calculated using the "level ice and conical structure interaction formula" recommended in ISO/FDIS 19906 (2009) by assuming the thickness to be 6.8 m (3 layers together) as shown in Figure 4.34).

From the last column of Table 5.5, it can be seen that the calculated results underestimated the measured values. One major reason would be the underestimation of the flexural strength of the consolidated part of the ice ridge. As stated before, in the calculation, the flexural strength of the level ice was taken as the flexural strength of the consolidated part of the ice ridge. As labelled in colour of the chosen flexural strength in Appendix B's table, very low flexural strengths were used in the calculation for the consolidated ice ridge load.

In order to improve the calculations, more reliable flexural strength of the consolidated part of the ice ridge is required.

From the above table, it was further found that the discrepancy between the measured data and the calculated data become larger in wide ridge conditions than in narrow ridge

conditions. This may to certain degree point out the importance of the mean cross-sectional area to the ice ridge load which the code did not take into consideration.

6 Discussion

6.1 Measured loads compared to ISO/FDIS 19906

The ice loads on conical structures in level ice were calculated based on ISO/FDIS 19906 (2009) and compared with the measured values. It was found that the method presented in ISO/FDIS 19906 (2009) underestimates the actual ice loads. The calculated ice load was only in the same range as the *average* measured values.

Similarly, as calculated according to the ISO/FDIS 19906 (2009) code, the predicted ridge load is much lower than the actual ridge load. This may be due to the inappropriate choice of the level ice flexural strength to be the consolidated part's flexural strength and the low keel load. As can be seen in Appendix B, the flexural strengths of the level ice are relatively low.

6.2 The influence of ice speed

In both intact level ice and managed ice, as the ice speed increases, the dominant ice load frequency also increases. This is in agreement with natural sense that a higher ice speed leads to more frequent breakings of the encountered ice.

In level ice the estimated ice breaking length was decreasing with increasing ice speed. This conclusion was also verified by a numerical model based on the 'dynamic ice beam resting on an elastic foundation' theory.

In both intact level ice conditions, for Models B_F and D_F, the ice speed's influence on the ice load amplitude is not obvious.

For the level ice conditions, one major contributor to the total ice load is the *ventilation load*[44] which is not sensitive to the ice speed. Another major contributor is the *ice sliding load*, which has a major component, the *ice accumulation load* decreasing with ice speed. This means that the ice clearing ability of the models gets better as the ice speed increases. In total, all the other loads that may increase with the ice speed may be expected to be offset by the *ice*

[44] For detailed definitions of these load terms we refer to Part I (Chapter 5).

accumulation load which decreases with increasing ice speed.

On the other hand, for Model F_F in intact level ice, the horizontal ice load increases with increasing ice speed. This is because Model F_F has a much better ice clearing ability compared with Models B_F and D_F. So the *ice accumulation load* for Model F_F was expected to be relatively small and its ice speed dependence is not as significant as for Models B_F and D_F. Without the large *ice accumulation load*'s decrease to offset the other loads' increase with the ice speed, the total ice load is expected to increase with increasing ice speed.

6.3 The influence of ice conditions (intact level ice, managed ice)

In managed ice, the ice loads are significantly decreased to only about half of that in level ice. This has been explained as the consequence of a much lower *ventilation load* and *ice accumulation load* in managed ice; and another reason is the unbounded boundary conditions in managed ice where the broken ice pieces can be pushed sideways instead of downwards.

It was also found that the ice load in *larger ice floe conditions* is only *slightly* higher than that in *smaller ice floe conditions*. It has been pointed out that in managed ice, the *ventilation load* and *ice accumulation load* have been reduced significantly. This may accounts for the minimal differences of the ice load in these two managed ice floe conditions. Since in *large ice floe conditions*, the structure is required to break more ice and push larger broken ice pieces sideways, a *slightly* larger ice load is expected in *large ice floe conditions*.

However, the ice load's dominant frequency is *largely* determined by the size of the ice floes.

Moreover, in managed ice, the size of the broken ice pieces is much larger than those in level ice. This is mainly due to the boundary conditions in managed ice floe conditions.

6.4 Effect of waterline diameter

Based on the test results of Models B_F, D_F and F_F, it was found that as the waterline diameter increases, the estimated ice breaking lengths also increase slightly. This has been

explained by considering that a larger diameter at the waterline induces larger resistance to the incoming intact level ice which will result in a longer ice breaking length.

Comparing Model B_F with Model D_F, it was found that the ice load for Model D_F is almost 1.6 times the ice load of Model B_F, a similar ratio as for the waterline diameters. With almost the same ice clearing ability (e.g. the same shape), the larger waterline diameter causes a larger ice load.

6.5 Ice clearing ability

6.5.1 Fixed models

Model F_F with a very long conical face and narrow “neck” (20 m) was proved very effective in clearing ice rubble and reducing the ice load. Although the waterline diameter of Model F_F is about 1.6 times of Model B_F, the average ice load of Model F_F sometime is even less than that of Model B_F in intact level ice. As can be seen from the video, the broken ice rubble was immediately pushed sideways around Model F_F and very little rubble was accumulated in the bow region of Model F_F.

However, for Model B_F and Model D_F with the same shape, a smaller waterline diameter means a better ice clearing ability.

In managed ice, Model B_F was proved to be very effective in clearing the relatively larger broken ice pieces. As stated in the previous section, the broken ice pieces in managed ice are relatively larger than those in level ice. It can be seen from the video, larger broken ice pieces become easier to be cleared sideways by a smaller structure; and very little ice pieces were accumulated in the bow region of Model B_F. This may explain why the ice load on Model B_F is very small in managed ice.

6.5.2 Moored models

Model B_M and Model E_M were tested in level ice and ice ridge. As mentioned in Section 3.2, Model E_M is an updated version of Model D_M in Phase I. The “neck” of Model D_M was narrowed from 40 m to Model E_M with only 20 m. Based on the previous analysis (Figure 4.42 and Figure 4.43), it can be concluded that the ice clearing ability of Model E_M is almost as good as for Model B_M.

Based on the above discussion concerning the ice clearing ability for fixed models in intact level ice and managed ice, and moored models in level ice and ice ridge, it can be concluded that:

"Shorter waterline diameter and smaller "neck" diameter lead to better ice clearing ability. And Model F_F was proved to be very effective in clearing ice rubble."

6.6 Effects of multi-year ice ridge

In Test #03Ri_12, Model F_F was tested in multi-year ice ridge. A layering technique (3 layers) was adopted to prepare the multi-year ice ridge. It was found that 3 times of the original level ice load is very close to the measured loads in the multi-year ice ridge situation.

As pointed out in Section 6.1, if calculating the multi-year ice load following the ISO/FDIS 19906 (2009), the obtained values are much less than the measured ones.

The maximum ridge load appeared right at the beginning when the model entering the thickest layer of the multi-year ice ridge. Based on the loading history and the video analysis, it was further identified that it is mainly the *ice breaking load* and *ice rotating load* that contribute to the total maximum ice load. The contribution from the *ice accumulation load* is relatively smaller.

6.7 Ridge load dependence on the cross sectional area and ice speed

Based on the measured values from the tests for the two moored models in ice ridge and the test results in Phase I, it again confirmed that the cross-section area of the ridge largely influences the ridge load. As stated in the Phase I Report, a larger cross-sectional area means more ice rubbles for the structure to clear away during the ridge-structure interaction process, hence leading to a larger ice ridge load.

And it was also confirmed that moored structures tend to have larger ice load compared with fixed structures under similar ice ridge cross sectional areas.

Since the Phase II tests are based on a different ice speed (0.1 m/s), the ridge load's speed dependence for moored structures was also identified as smaller ice speed leads to larger ice ridge load.

6.8 Comparisons between fixed and moored models

For detailed and reliable comparisons, please refer to the Phase I Report where it has been concluded that the ice load is lower in level ice and larger in ice ridge for a moored structure compared with fixed structures.

In the Phase II test campaign, the comparison cannot be strictly done as in Phase I since the ice flexural strength and ice thickness are different for the fixed model tests and moored model tests[45].

From the measured data, it was found that the average ice load on the moored structures has been substantially decreased (not in a same scale as the values obtained for fixed models in level ice). And the frequency of the ice load is very low.

Based on the differences between the *long level ice track* and *short level ice track* tests, it was assumed that a low frequency ice accumulated load exists in the total ice load. This can explain why in the *long level ice track* condition, the measured ice loads have higher amplitude and a lower frequency.

6.9 The influence of ice conditions in the test

6.9.1 General discussion

All the previous analysis is based on the data supplied by HSVA. It was mentioned in the beginning that the test conditions are good and the data are reliable. Here a more detailed discussion about influence induced by the possible errors in the tests will be given.

[45] For fixed models, all the tests are based on an ice thickness of 3 m and an average ice flexural strength of about 750 kPa. Furthermore, the fixed models were not tested in the first-year ice ridge; for moored models, the tests are based on an ice thickness of about 2 m and an average ice flexural strength of 500 kPa.

We will mainly concentrate on the flexural strength of the tested ice in the following discussion since it shows the largest deviations from the target value. First is a comparison of the ice thickness and flexural strength between the test values and target values as shown in Table 6.1.

Table 6.1 The major level ice morphologies and their errors with the target value

Multi-year level ice	Ice thickness	errors [%]	Flexural strength	errors [%]
01Li10	3.0852	2.84	720 kPa	-4
01Li11	3.0384	1.28	936 kPa	24.8
01Li12	2.9772	-0.76	1008 kPa	34.4
02Li10	2.9772	-0.76	756 kPa	0.8
02Li11	3.0132	0.44	828 kPa	10.4
02Li12	2.8044	-6.52	900 kPa	20
03Li10	2.9736	-0.88	792 kPa	5.6
03Li11	3.0960	3.2	792 kPa	5.6
03Li13	2.8692	-4.36	792 kPa	5.6
Target value	3	-	750 kPa	-
04Li10	1.8828	-5.86	684 kPa	36.8
05Li10	1.9152	-4.24	468 kPa	-6.4
06Li10	1.9476	-2.62	324 kPa	-35.2
07Li10	1.9692	-1.54	648 kPa	29.6
Target value	2	-	500 kPa	-

As we can see from the above table that the ice thickness were all well guaranteed with all errors less than 10% and most of the errors less than 5%.

In the flexural strength section, some relatively larger discrepancies were observed. In the tests, the flexural strength mainly influences the ice breaking process which determines the ice actions on the conical structure. In order to quantify the possible errors it may bring to the total ice actions, the ISO/FDIS (2009) formula concerning the ice action on narrow cones was applied to calculate the target ice action based on the target flexural strength as inputs comparing with the actual ice action based on the measured values as inputs. (Except the flexural strength, all the other values were chosen to be the measured values)

Table 6.2 Ice action errors induced by the ice flexural strength error

	Measured		Ice action based on		Errors
Level ice	Flexural strength	errors [%]	target flexural strengh	measured flexural strength	of Ice action [%]
01Li10	720 kPa	-4	-20.7891	-20.09	-3.4
01Li11	936 kPa	24.8	-20.2136	-24.4	20.7
01Li12	1008 kPa	34.4	-19.4729	-25.05	28.6
02Li10	756 kPa	0.8	-23.4416	-23.6	0.7
02Li11	828 kPa	10.4	-23.9299	-25.71	7.4
02Li12	900 kPa	20	-21.164	-24.13	14.0
03Li10	792 kPa	5.6	-27.0797	-28.01	3.4
03Li11	792 kPa	5.6	-28.9045	-29.91	3.5
03Li13	792 kPa	5.6	-25.5666	-26.43	3.4
04Li10	684 kPa	36.8	5.55566	7.15233	28.7
05Li10	468 kPa	-6.4	6.03184	5.74194	-4.8
06Li10	324 kPa	-35.2	5.26222	4.22578	-19.7
07Li10	648 kPa	29.6	5.73758	6.63554	15.7

As we can see from the above table, although relatively large error was found in the ice flexural strength, the ice action error induced by such error is not that large. The calculation results were based on the ISO/FDIS formula which, as shown before, tends to underestimate the actual ice actions; however, the results here at least imply that the ice action's error induced by the flexural strength is not that big.

This is understandable, since the flexural strength mainly determines the *ice breaking load*, which is only a portion of the total ice resistance. As shown by the numerical model, the ice breaking load actually counts relatively small portion of the total ice resistance whose major two parts are the *ventilation load* and *ice accumulation load* both of which are not that much relevant to the ice flexural strength. The flexural strength influences the ice breaking length and will accordingly influences the ventilation load. However, the influence of ice flexural strength to the ice breaking length seems not that big. This will be discussed in the following concerning the flexural strength's influence to all the conclusions up to now.

6.9.2 Flexural strength's influence to all the relevant conclusions

During the previous analysis in each chapter, when making every conclusion, the possible flexural strength influences were taken into consideration. Here, the possible influence from ice flexural strength variation on our previous conclusion will be discussed one by one.

- Regarding the average ice load

  When discussing the speed influence on average load for Model B_F and Model D_F, no obvious speed dependence was found. However, the tested ice flexural strength was increasing in both cases. This means ice flexural strength's influence does not have sufficiently large influence to the average load comparing with other factors. This was confirmed again by the results in Model F_F where an increasing average ice load with increasing ice speed was observed, however, in this case, the tested ice flexural strength was constant. Both cases exclude the dominant influence from ice flexural strength on the average ice load.

- Regarding the ice breaking length

  When discussing the ice speed's influence on the ice breaking length and also the dominant ice load frequencies, the influence from ice flexural strength's variation was also excluded. For all three fixed models, the ice breaking length was found to be decreasing with increasing ice speed. However, in Model B_F and Model D_F, the ice flexural strengths were increasing, and in Model F_F, the ice flexural strength was constant. It may be natural to expect a longer ice breaking length with larger ice flexural strength. However, the opposite results (decreasing ice breaking length) were found. It seems the influence of ice drift speed has absolutely outweighed the influence from ice flexural strength.

  (The above two descriptions addressed conclusion 1, 2, 3 in the next chapter)

- Regarding the structure's geometric influences

  When discussing the geometry influence of the structure, it was found that the average ice load is proportional to waterline diameter and the neck size influences the ice clearing efficiencies. These conclusions are based on the average load and ice breaking length comparisons. In the above two discussion, the ice flexural strength's influences on these two items (average load and ice breaking length) have been excluded. So the conclusion regarding the geometry's influences are reliable.

  (The above descriptions addressed conclusion 7, 8, 9 in the next chapter)

- Regarding managed ice

  The ice flexural strength in managed ice is thought to be the same as in level ice.

  Similar conclusions concerning average ice load and dominant ice load frequency were made in managed ice as in level ice. This should also be reliable.

  Conclusions based on the comparisons between level ice and managed ice are also reliable since they have same flexural strength in a same series of test (e.g. test #01Li10 has same ice flexural strength with test #01Li30 and test #01Li40).

  (The above descriptions addressed conclusion 4, 5, 6 in the next chapter)

- Regarding the comparisons between short level ice track and long level ice track

  The conclusion from this comparison is the expectation of a low frequency and high amplitude ice accumulation load existing in the total ice resistance. In the discussion, the possible ice flexural strength influence has been excluded.

  (The above descriptions addressed conclusion 15 in the next chapter)

Other conclusions are mostly related to the ice ridges whose information about the consolidated part's ice flexural strength is unclear. However, the conclusion made has less relationship with flexural strength unless specially pointed out.

The conclusion about the maximum load is based on logic reasoning and recorded video. Further research concerning a maximum value with statistic information needs to be conducted so as to exclude/reduce extreme situations that may lead to the 'one value' maximum.

From the above discussions and calculations, it is found that the ice flexural strength variations did not blur our conclusions. Furthermore, based on the calculations, it is found that in most cases, the ice flexural strength leads to only around 20% errors in the total ice resistance. And from the analysis, it further confirmed that the ice flexural strength's influence on the average load and ice breaking length is not as strong as other factors such as ice drift speed. Accordingly, it can be concluded that the ice flexural strength of the tested ice is reliable. And again, after checking all the ice conditions in the test, such as ice thickness, water density, ice density, etc, very small discrepancies were found comparing with target values. It can further to say that the values from the tests are reliable.

7 Conclusions

The Phase II test campaign involves investigations of three different fixed models and two moored models in various ice conditions with three different ice speeds. These tests are extensions of the Phase I test campaign with updated models (Model F_F and Model E_M). Based on the test results and previous analysis and discussions, the major findings from the test campaign are:

1. The ice speed influences frequency of the ice load in both intact level ice and managed ice. Higher ice speed leads to higher ice load frequency. In level ice, as the ice speed increases, the ice breaking length tends to decrease. In managed ice, the size of the ice floes strongly influences the dominant ice load frequency.
2. The ice speed seems to have little influence on the average ice load's amplitude for Models B_F and D_F in level ice due to the fact that the ice clearing ability increases with speed for Models B_F and D_F. The decreased *ice accumulation load*[46] with increased ice speed will offset the other load components that increase with ice speed.
3. For Model F_F, the average ice load's amplitude appears to increase with the ice speed. This may due to the good ice clearing abilities of Model F_F regardless of the ice speed. Without the decreased *ice accumulation load* at high ice speed to offset other load components that increase with the ice speed, the overall ice resistance appeared to be increasing with increased ice speed.

4. The ice load has been largely reduced in managed ice (nearly half of the ice load in level ice).
5. In managed ice, the differences of the average ice load's amplitude under different ice floe size conditions are comparatively small.
6. The broken ice pieces are much larger in managed ice than in level ice.

7. A larger waterline diameter leads to longer ice breaking lengths; if the ice clearing efficiency for two structures is similar (e.g, same shape), the longer waterline diameter will lead to larger average ice loads. Moreover, the ratio between the average ice loads of these two structures is around the value of the ratio between the diameters of these two structures.

[46] Check Part I (Chapter 5) for detailed definition of each load component, and also the conclusion concerning the total ice resistance's dependence on ice speed.

8. The ice clearing ability is also strongly affected by the “neck” size of the structure. Narrower “necks” seems to have improved the ice clearing efficiency so as to reduce the average ice load.
9. Model F_F and Model E_M were proved to be effective in ice clearing ability compared with the original concepts of Model D_F and Model D_M in Phase I test.

10. The moored structure is believed to be able to reduce the ice load in level ice[47].
11. The ridge load for moored structure is larger than for a similar fixed structure (same cone angle and waterline diameter) under similar ice ridge conditions.
12. The ridge load is expected to increase with decreased ice speed for moored structures (Figure 4.44).

13. For a structure entering a multi-year ice ridge, the ridge load first increases substantially. After reaching the maximum, it starts to decrease gently. The peak load may be expected to appear at the beginning of the thickest layer.
14. The major contributor to the ice ridge load in a multi-year ridge is expected to be the *ice breaking load* and *ice rotating load,* although significant ice accumulation was observed during the interaction processes.

15. A low frequency, high amplitude, ice accumulation induced load is believed to exist in the total ice load.

16. The maximum loads appeared in the record were identified mainly related to the following three processes:
    1) The buckling failure of a relatively long ice breaking length. (see Figure A. 4)
    2) Rotating of a relatively large broken ice pieces (see Appendix. A)
    3) Ice accumulation induced load. (see Appendix. A)
17. One important case (as shown in Figure A. 8) worth noting is that in managed ice, relatively larger broken ice pieces tend to be rotated directly by the structures. For a moored structure with shallow draft, such huge submerged broken ice floe may interact with the mooring lines and risers.

[47] Although the ice conditions are totally different, but the measured ice load for a moored model is not in a same scale (largely smaller than) with the ice loads for a fixed structure. So it is reasonable to have such a belief.

Appendix A: Interpretation on processes of peak loads

In this section, the selected signal for the previous analysis will be illustrated here. Although only the fixed structures' signal series are shown, the same method also applies for moored structures.

Based on the signal series, the maximum values are also marked. Since it is relatively easy to synchronize the video with the signal series for the low speed (0.1 m/s), only the maximum value at low speed are further investigated together with the video as shown in the following figures.

However, since it is relatively difficult to get precise enough synchronization, the stories behind each peak load can only be roughly described together with logical reasoning. Usually, three major causes attribute to the advent of peak loads:

1) Buckling failure of a relatively long ice breaking length
2) Rotation of a relatively larger broken ice pieces
3) Ice accumulation

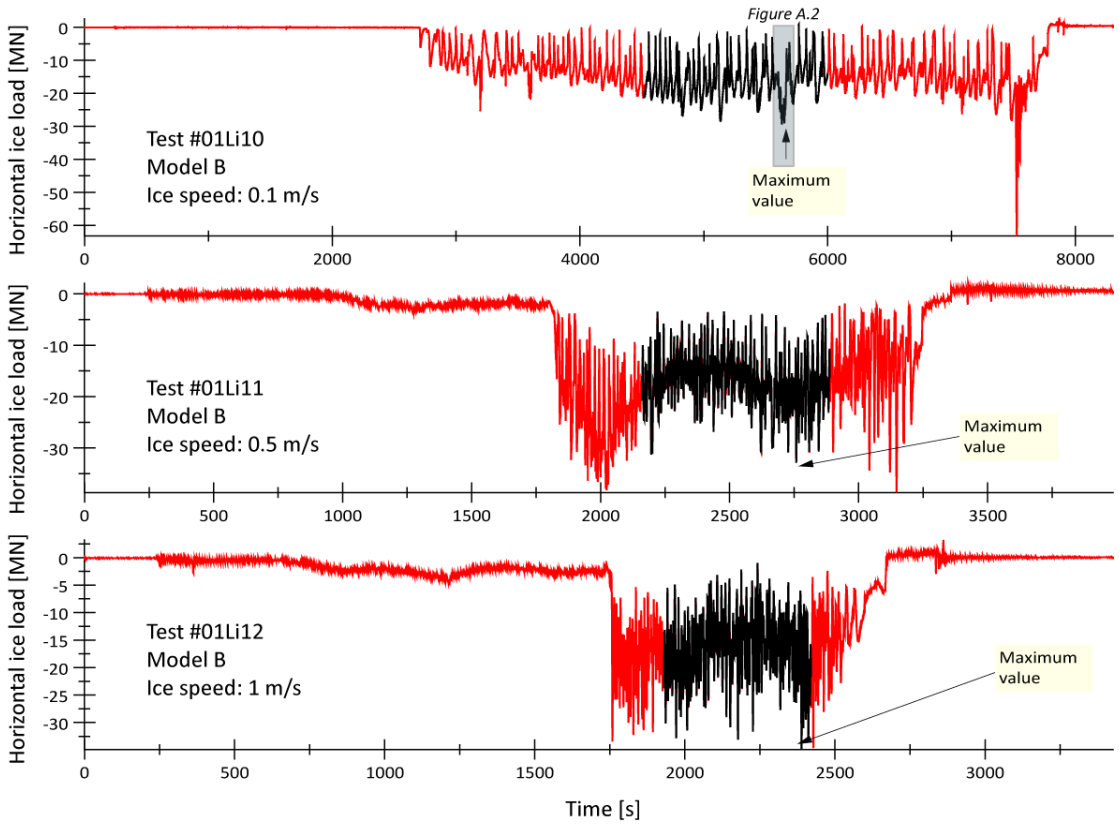

Figure A. 1 Signal selection and maximum value for Model B_F in level ice.

As can be seen from Figure A. 1, approximately 5 m (model scale) of the recorded values have been deleted from the beginning and end of the time history to skip the run in time and also a portion of the tank that has temperate ice, the remaining of which are left for analysis (in dark colour). The same signal selection criteria were made for all the recorded data. The story behind the maximum value in the above selected time history is shown in the following figure:

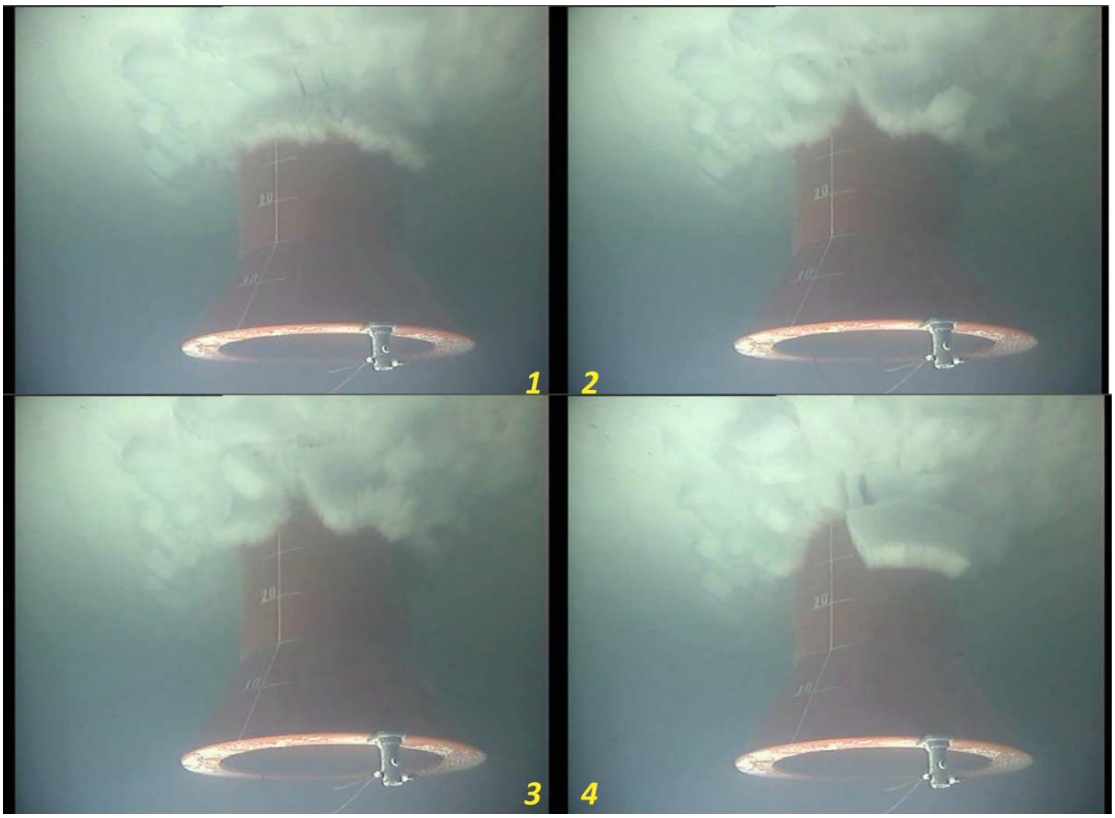

Figure A. 2 Demonstration of maximum loading process for Model B_F in level ice.

As can be seen from Figure A. 2, in the beginning the broken ice breaks into very small pieces, then a relatively large submerged block appeared. This *ice rotating load* required to rotate the relatively large broken ice mass may be the cause of the maximum load.

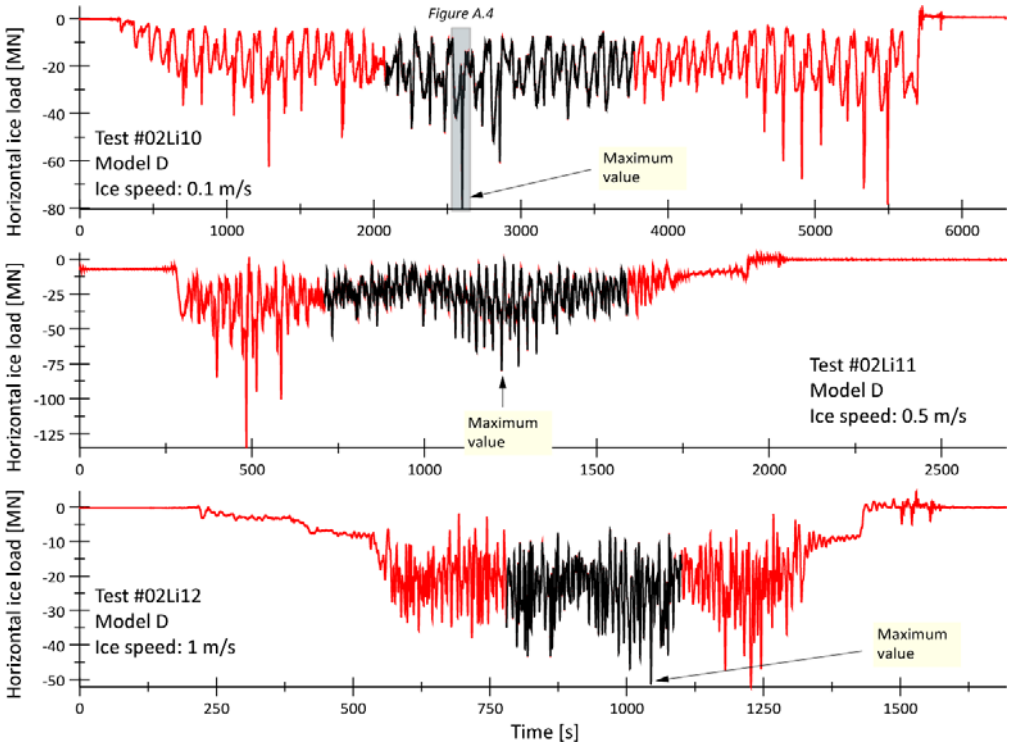

Figure A. 3 Signal selection and maximum load of Model D in level ice.

A similar signal selection method has also conducted for Model D_F. The maximum load's causes are shown in the following figure.

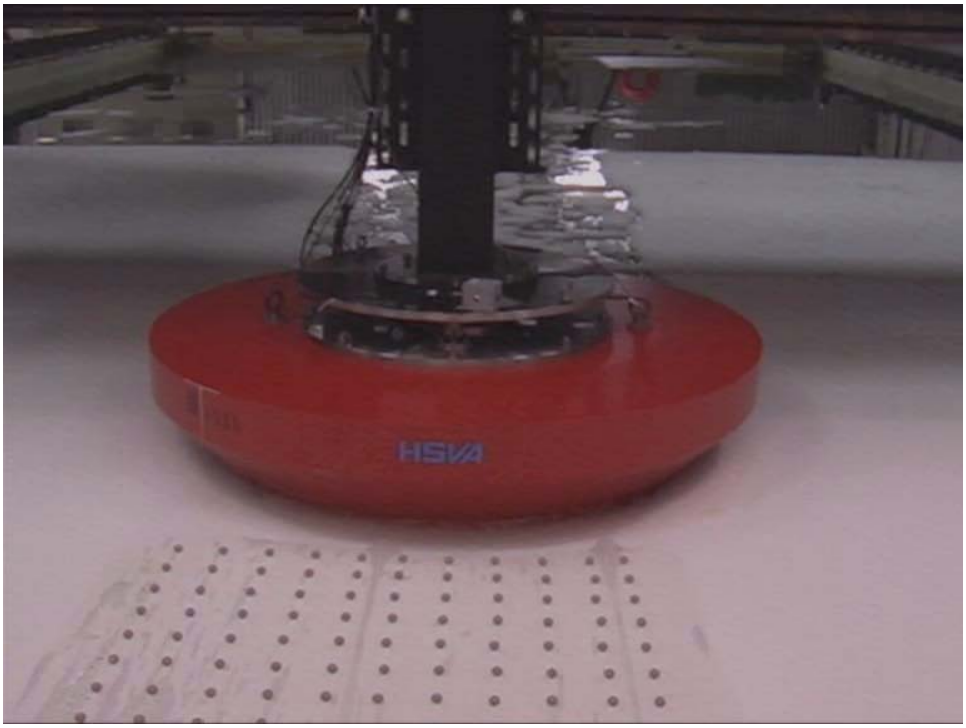

Figure A. 4 Maximum loading process for Model D_F in level ice

As can be seen from Figure A. 4, when the maximum load appeared, a relatively large ice

breaking length was identified. The advent of the peak load may due to the buckling failure of the relatively large ice breaking length.

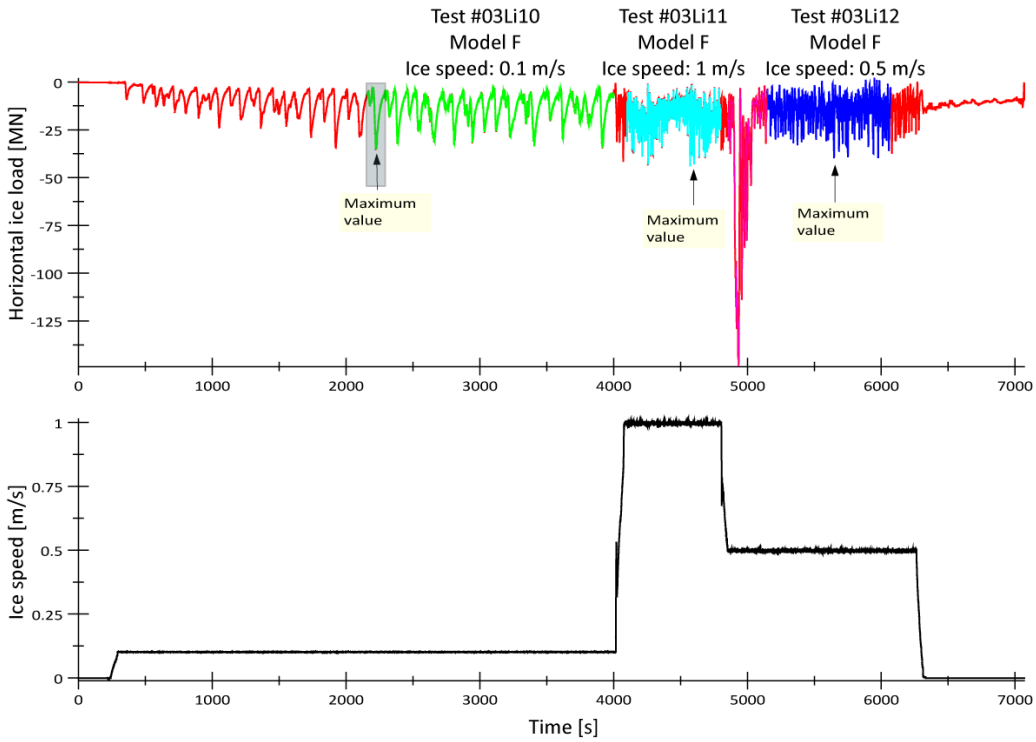

Figure A. 5 Signal selection and maximum value for Model F_F in level ice.

As can be seen from the loading history of Model F_F, the loading is very “well organized”. Since no extreme peak load appeared in the 0.1 m/s ice speed test, no more video photos will be displayed here for the “common” maximum load in the above figure.

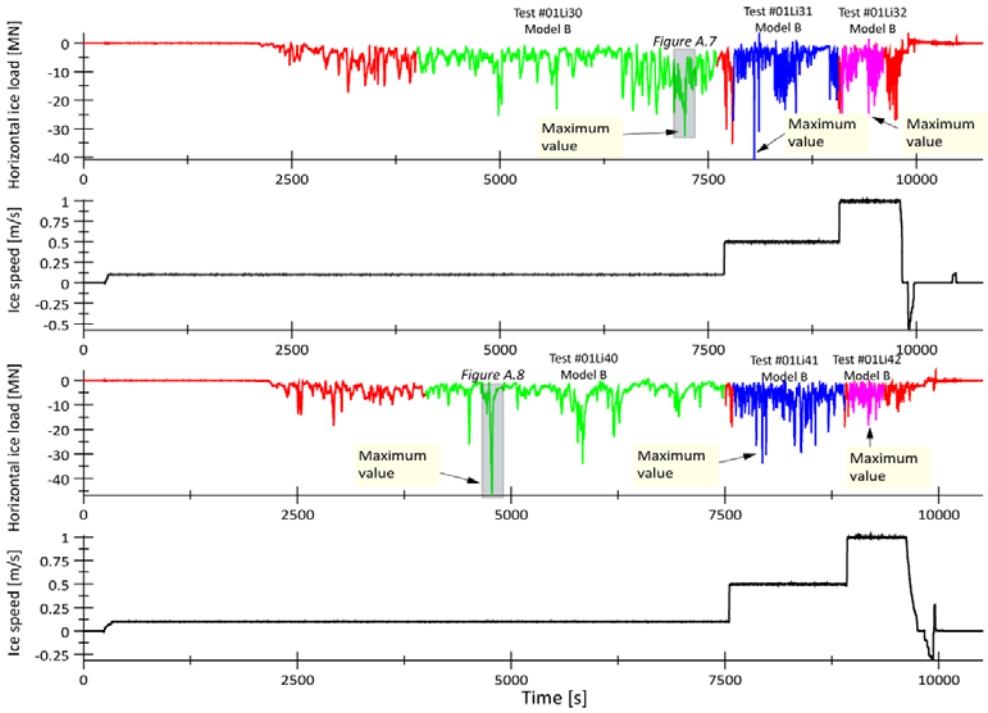

Figure A. 6 Signal selection and maximum value for Model B_F in managed ice

Figure A. 7 Loading process of Model B_F in managed ice (large floes)

Ice accumulation and subsequent ice breaking were identified from the video when the maximum load appears in Test #01Li30 (large floes, 0.1 m/s).

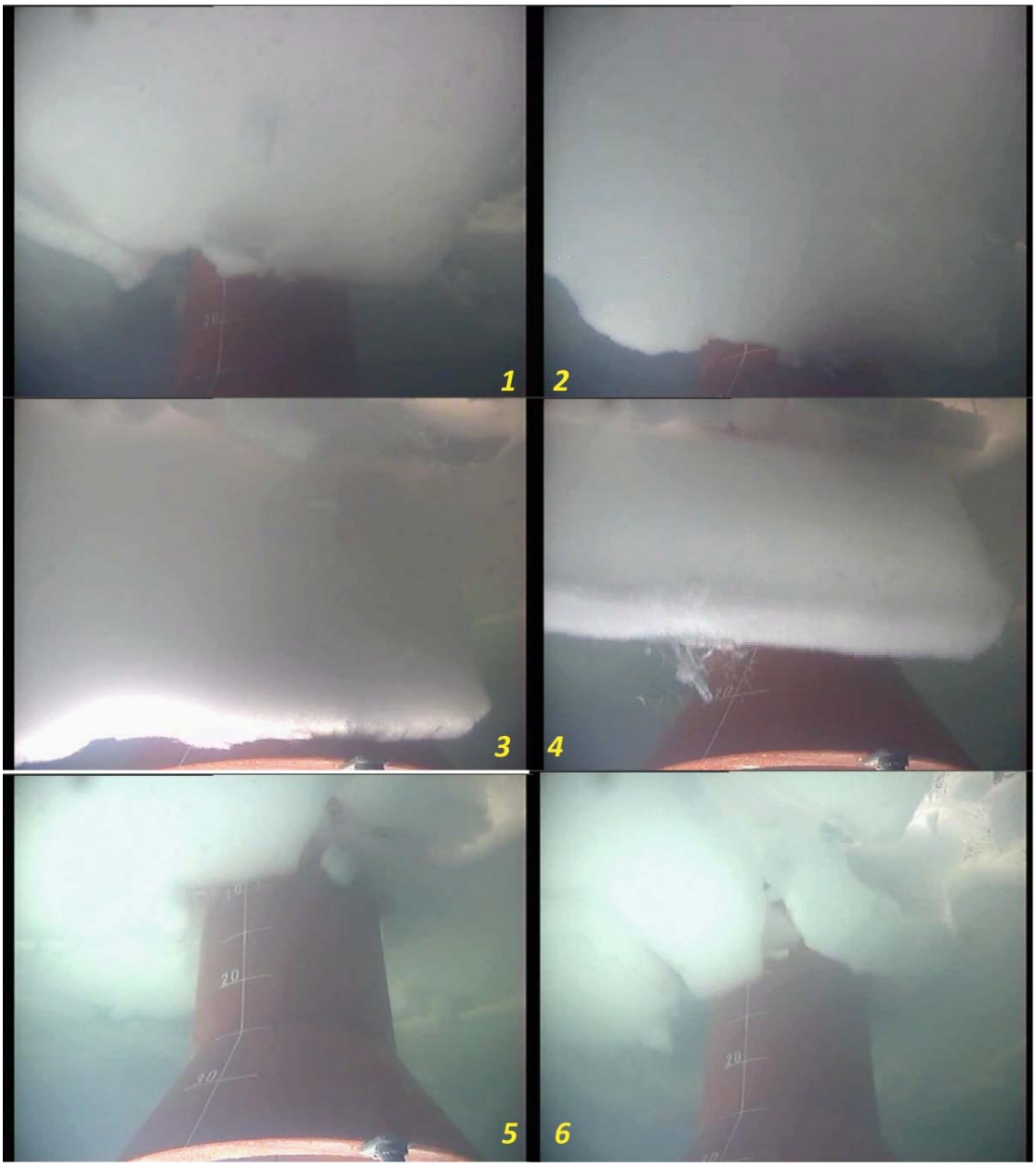

Figure A. 8 Loading process analysis of Model B_F in managed ice (small floes)

As can be seen from Figure A. 8, in Test #01Li40, an extremely large ice floe was encountered and rotated by the structure. The extremely large floe was first rotated, and then it pitched back and broke at the sideways of the structure. The maximum load appeared during this process.

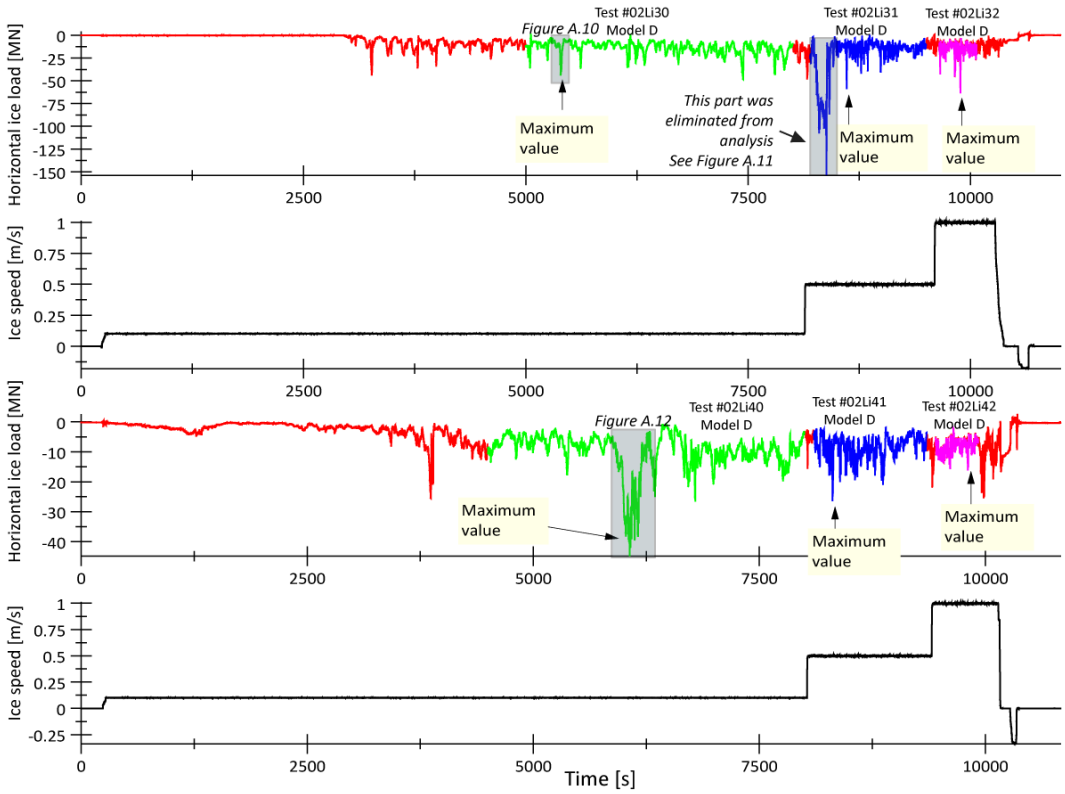

Figure A. 9 Signal selection and maximum value for Model D_F in managed ice

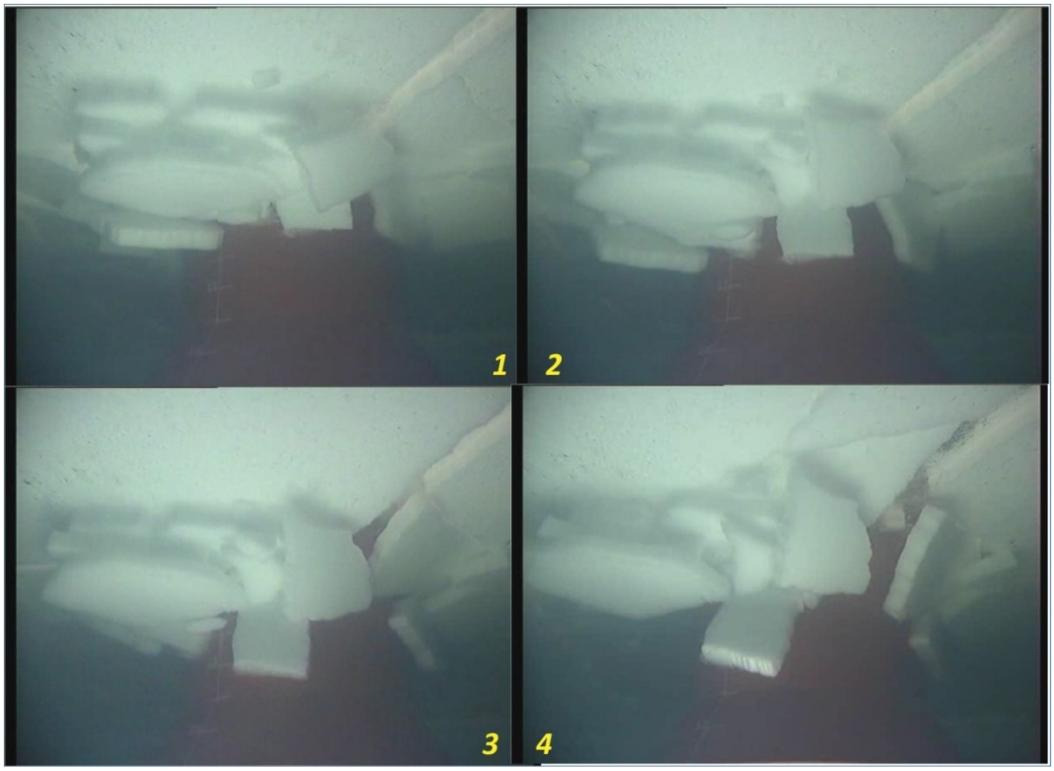

Figure A. 10 Loading process analysis of Model D_F in managed ice (large floes)

The “small” peak ice load in Test #02Li30 was indentified to be related to ice accumulation

and several times of ice breaking around the structure.

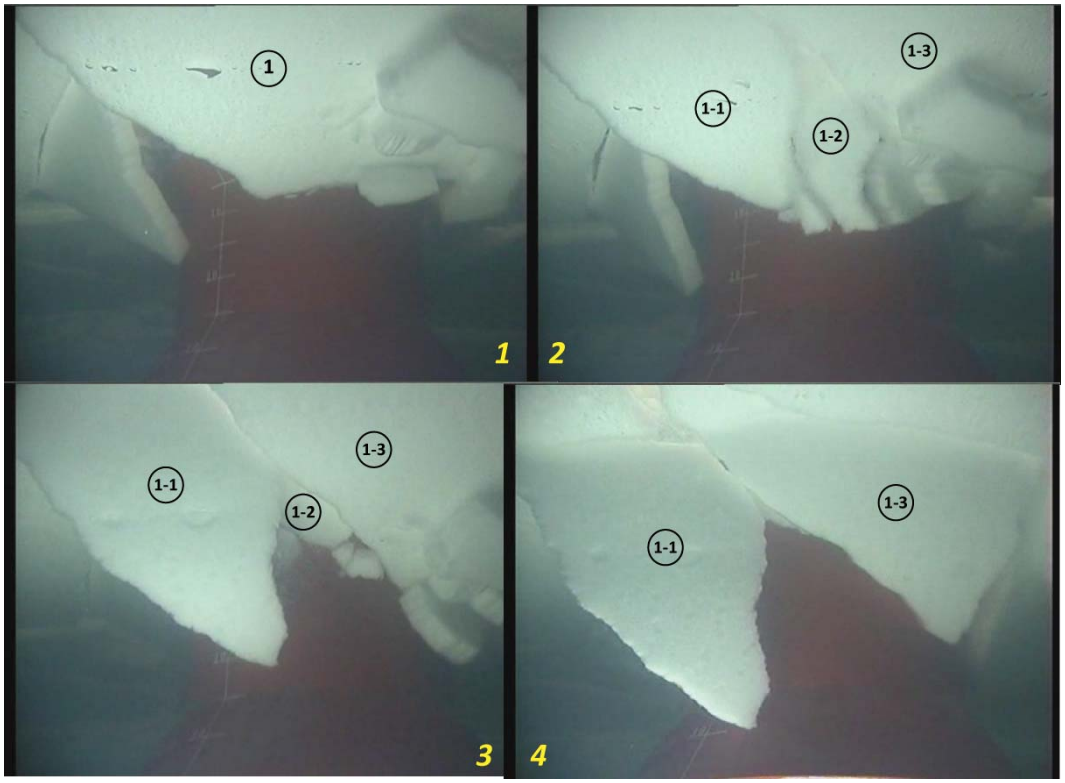

Figure A. 11 Loading process analysis of Model D_F in managed ice (large floes, ice speed 0.5 m/s)

Figure A. 11 displays how the extreme ice load appeared immediately after the structure accelerated from 0.5 m/s to 1 m/s. As can be seen from Figure A. 11, a very large block was rotated by Model D_F, and then broke into 3 pieces. This extremely large load was regarded as an artificial load since in nature, there is seldom any structure being accelerated like this. The consequence of such instant acceleration may lead to a fast rotating of a big ice floe encountered when the structure was at low speed.

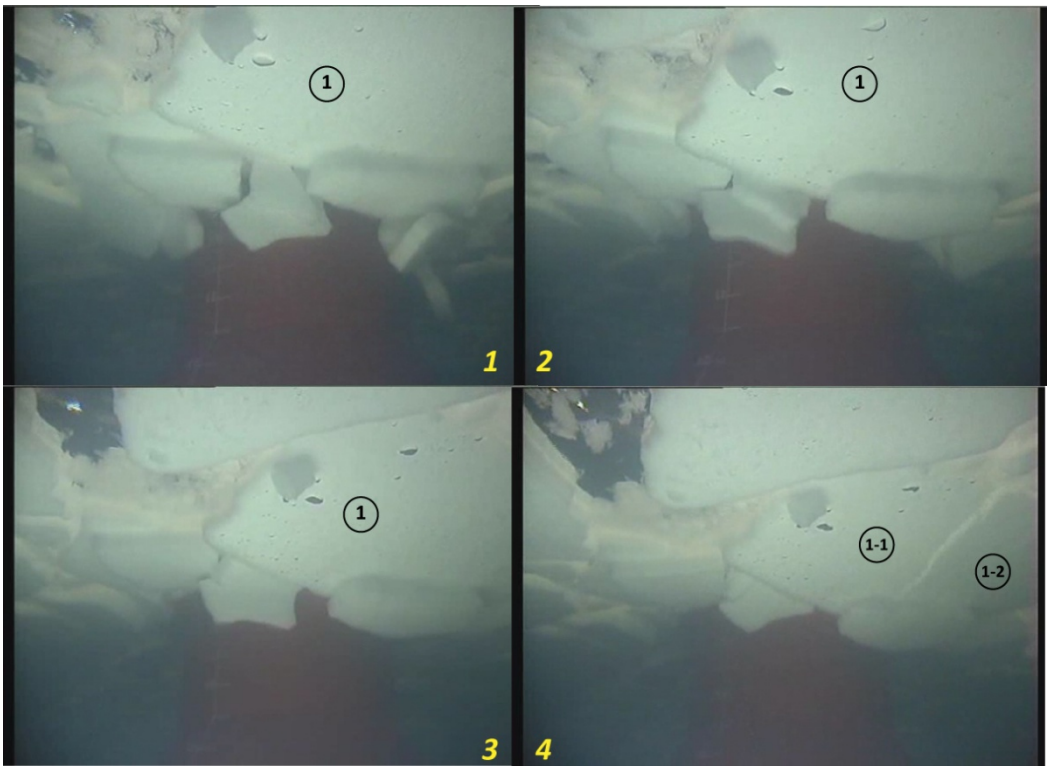

Figure A. 12 Loading process analysis of Model D_F in managed ice (small floes).

A relatively large ice floe (Number 1 in the figure) was found to be rotated by the structure and then was broken when the maximum load appeared.

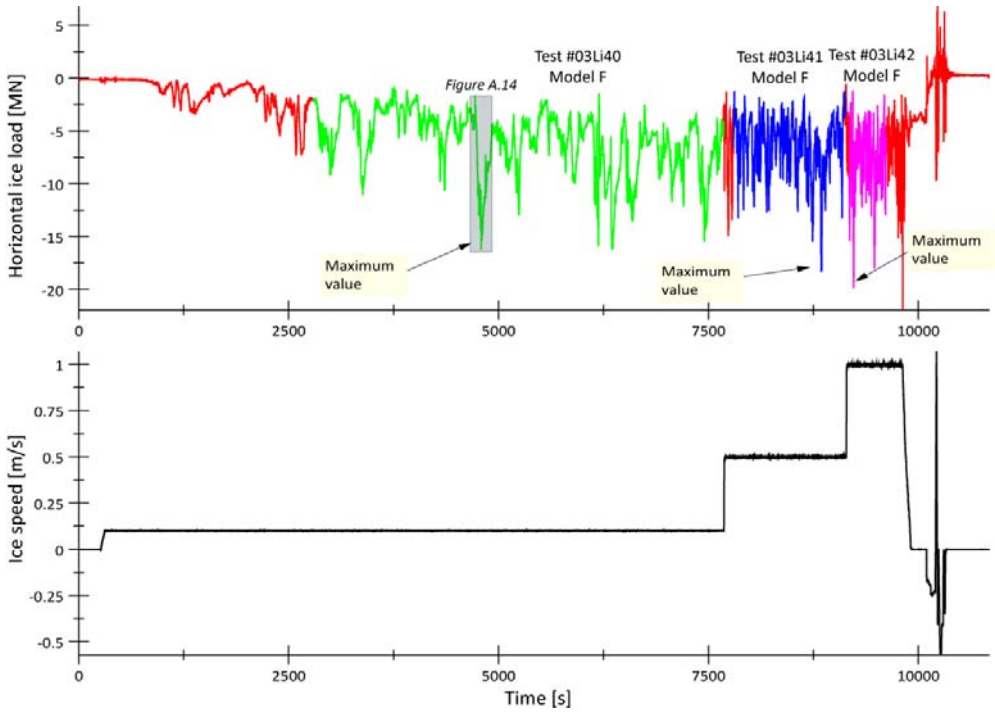

Figure A. 13 Signal selection and maximum value for Model F_F in managed ice

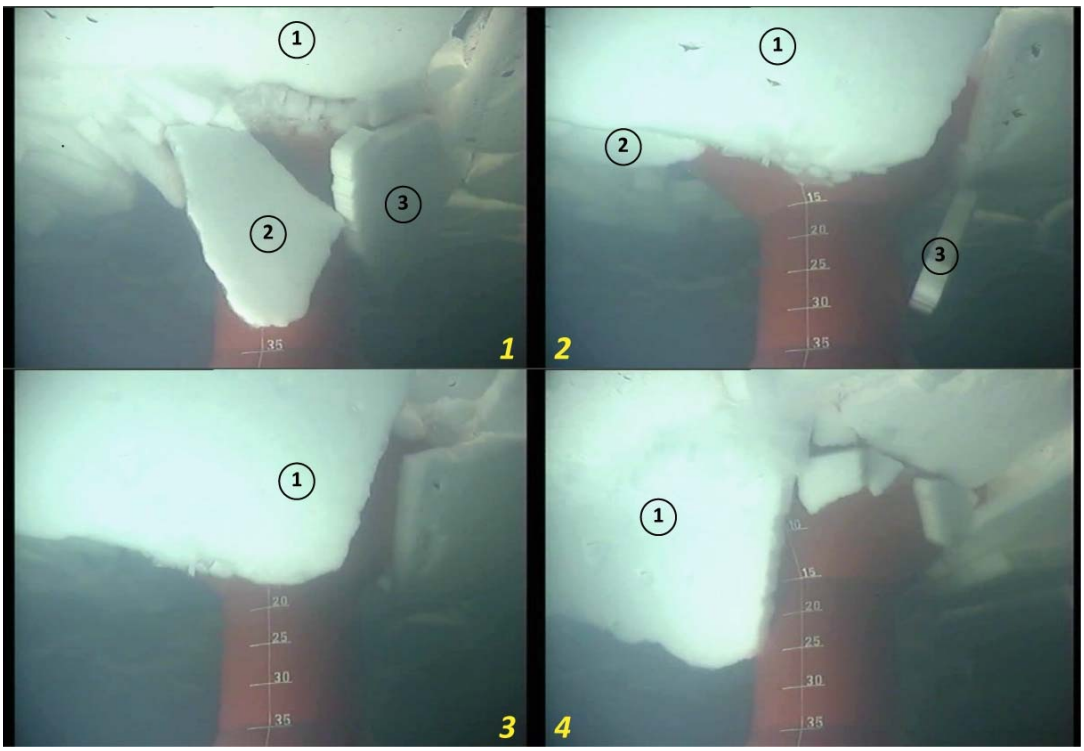

Figure A. 14 Loading process analysis of Model F_F in managed ice (small floes).

Similarly as before, when the maximum load was identified, a relatively large ice floe was found to be rotated and broken by the structure.

Based on all the above analysis, the following conclusions concerning the peak load could be given:

- In most cases, it is the relatively larger broken ice mass that induces the peak load.
- The duration of the peak load can to a certain degree tell the nature of the peak load:
  1) For a very short duration of the peak load, like an impulse, it could be inferred that the peak load was induced by the *ice breaking load*.(especially for ice breaks in the buckling failure mode)
  2) For a peak load duration which is quite close to a reasonable ice breaking length if multiplying the peak load duration with the ice speed, it could infer that the peak load was induced by the *ice rotating load*.
  3) For a peak load with an extremely long period in level ice, it could be inferred that the peak load was induced by the *ice accumulation load.*

Usually the appearance of the peak ice load is a combination of the above situations.

Appendix B: Input values for ridge load calculation

Model (Test #)	Model F_F (03Ri)	Model B_M (04Ri50)	Model B_M (05Ri50)	Model E_M (06Ri50)	Model E_M (07Ri50)
Keel depth [m]	6.804	18.5	18.5	18.5	18.5
Diameter [m]	50	30	30	50	50
Porosity [-]	0.2	0.2	0.2	0.2	0.2
phi [deg]	30	30	30	30	30
Cohesion [Pa]	5000	5000	5000	5000	5000
rhow [kg/m3]	1005	1005	1005	1005	1005
rhoi [kg/m3]	917.2	909.2	885.2	861.8	847.5
hc [m]	2.304	3	3	3	3
hr [m]	2.304	3	3	3	3
alfa [deg]	45	45	45	30	30
mu [-]	1.732	1.732	1.732	1.732	1.732
sigf [kPa]	792	684	468	324	648

Reference of Part II

HSVA, (2010), JIP Phase II, Ice Model Testing of Structures in Ice,Data Report, Report IO 442/10.

Kämäräinen, J. (2007), “Theoretical investigation on the effect of fluid flow between the hull of a ship and ice floes on ice resistance in level ice”, Doctoral Thesis.

Li Feng, Y. Qianjin, K. N. Shkhinek, Tuomo Kärnä, (2003), A Quanlitative Analysis of Breaking Length of Sheet Ice Against Conical Structure, POAC03, Dalian University of Technology, China.

Oddgeir Dalane, Sveinung, Løset, (2009), “JIP Phase I Report of Ice and conical structure interactions”

Ralston, T.D. (1977). Ice force design condiderations for conical structures. Proc. International Conference on Port and Ocean Engineering under Arctic Conditions (POAC 77), Memorial University of Newfoundland, Newfoundland, Canada, Vol. II, pp. 741-752..

Kotras, T.V., A. V. Baird, J. N. Naegle, (1983), “Predicting ship performance in level ice”, SNAME Transactions, Vol. 91, pp. 329-349.

Valanto, P. (2001). The Resistance of Ships in Level Ice. SNAME Transactions, Vol. 109, 2001, pp. 53 – 83.